Constitutive Modelling of Creep in a Long Fiber Random Glass Mat Thermoplastic Composite

by

Prasad Dasappa

A thesis
presented to the University of Waterloo
in fulfilment of the
thesis requirement for the degree of
Doctor of Philosophy
in
Mechanical Engineering

Waterloo, Ontario, Canada, 2008

DECLARATION

I hereby declare that I am the sole author of this thesis. This is a true copy of the thesis, including any required final revisions, as accepted by my examiners.

I understand that my thesis may be made electronically available to the public

<u>ABSTRACT</u>

Random Glass Mat Thermoplastic (GMT) composites are increasingly being used by the automotive industry for manufacturing semi-structural components. The polypropylene based materials are characterized by superior strength, impact resistance and toughness. Since polymers and their composites are inherently viscoelastic, i.e. their mechanical properties are dependent on time and temperature. They creep under constant mechanical loading and the creep rate is accelerated at elevated temperatures. In typical automotive operating conditions, the temperature of the polymer composite part can reach as high as 80°C. Currently, the only known report in the open literature on the creep response of commercially available GMT materials offers data for up to 24 MPa at room temperature. In order to design and use these materials confidently, it is necessary to quantify the creep behaviour of GMT for the range of stresses and temperatures expected in service.

The primary objective of this proposed research is to characterize and model the creep behaviour of the GMT composites under thermo-mechanical loads. In addition, tensile testing has been performed to study the variability in mechanical properties. The thermo-physical properties of the polypropylene matrix including crystallinity level, transitions and the variation of the stiffness with temperature have also been determined.

In this work, the creep of a long fibre GMT composite has been investigated for a relatively wide range of stresses from 5 to 80 MPa and temperatures from 25 to 90°C. The higher limit for stress is approximately 90% of the nominal tensile strength of the material. A Design of Experiments (ANOVA) statistical method was applied to determine the effects of stress and temperature in the random mat material which is known for wild experimental scatter.

Two sets of creep tests were conducted. First, preliminary short-term creep tests consisting of 30 minutes creep followed by recovery were carried out over a wide range of stresses and temperatures. These tests were carried out to determine the linear viscoelastic region of the material. From these tests, the material was found to be linear viscoelastic up-to 20 MPa at room temperature and considerable non-linearities were

observed with both stress and temperature. Using Time-Temperature superposition (TTS) a long term master curve for creep compliance for up-to 185 years at room temperature has been obtained. Further, viscoplastic strains were developed in these tests indicating the need for a non-linear viscoelastic viscoplastic constitutive model.

The second set of creep tests was performed to develop a general non-linear viscoelastic viscoplastic constitutive model. Long term creep-recovery tests consisting of 1 day creep followed by recovery has been conducted over the stress range between 20 and 70 MPa at four temperatures: 25°C, 40°C, 60°C and 80°C. Findley's model, which is the reduced form of the Schapery non-linear viscoelastic model, was found to be sufficient to model the viscoelastic behaviour. The viscoplastic strains were modeled using the Zapas and Crissman viscoplastic model. A parameter estimation method which isolates the viscoelastic component from the viscoplastic part of the non-linear model has been developed. The non-linear parameters in the Findley's non-linear viscoelastic model have been found to be dependent on both stress and temperature and have been modeled as a product of functions of stress and temperature. The viscoplastic behaviour for temperatures up to 40°C was similar indicating similar damage mechanisms. Moreover, the development of viscoplastic strains at 20 and 30 MPa were similar over all the entire temperature range considered implying similar damage mechanisms. It is further recommended that the material should not be used at temperature greater than 60°C at stresses over 50 MPa.

To further study the viscoplastic behaviour of continuous fibre glass mat thermoplastic composite at room temperature, multiple creep-recovery experiments of increasing durations between 1 and 24 hours have been conducted on a single specimen. The purpose of these tests was to experimentally and numerically decouple the viscoplastic strains from total creep response. This enabled the characterization of the evolution of viscoplastic strains as a function of time, stress and loading cycles and also to co-relate the development of viscoplastic strains with progression of failure mechanisms such as interfacial debonding and matrix cracking which were captured in-situ. A viscoplastic model developed from partial data analysis, as proposed by Nordin, had excellent agreement with experimental results for all stresses and times considered. Furthermore,

the viscoplastic strain development is accelerated with increasing number of cycles at higher stress levels. These tests further validate the technique proposed for numerical separation of viscoplastic strains employed in obtaining the non-linear viscoelastic viscoplastic model parameters. These tests also indicate that the viscoelastic strains during creep are affected by the previous viscoplastic strain history.

Finally, the developed comprehensive model has been verified with three test cases. In all cases, the model predictions agreed very well with experimental results.

ACKNOWLEDGEMENTS

I would like to express my sincere gratitude to my supervisor, Prof. Pearl Sullivan for her support, guidance, encouragement and patience during the project. I would also like to thank Dr. Duane Cronin for co-supervising and his help with the finite element analysis.

I am very grateful to Mr. Andy Barber for his assistance with the instrumentation and mounting of the strain gauges, Mr. Jim Baleshta for his assistance for the design modifications to the fixture used for creep tests, Mr. Wilhelm Norval for his assistance with tensile testing and Dr. Yuquan Ding for his technical assistance during the project.

I am thankful to Dr. Xinran Xiao and Dr. Peter H Foss of the Materials Processing Lab, General Motors Corporation, Warren, Michigan for providing the raw materials for the project and technical assistance.

I also thank my group mates (Composites and Adhesives Research Group) particularly Nan Zhou and Jonathan Mui for their help and support during this project.

TABLE OF CONTENTS

LIST OF TABLES

LIST OF FIGURES

xiii

xiv

NOMENCLATURE

A	Co-efficient of the Zapas and Crissman viscoplastic model
A_s	Cross-sectional area of the creep specimen
ANOVA	Analysis of Variance
a_σ	Vertical stress shift factor
a_{t_e}	Aging shift factor
a_T	Temperature shift factor
α	Coefficient of thermal expansion
β	Shape factor in Kohlrausch model
C	Parameters of the Zapas and Crissman viscoplastic model
C_1, C_2	Constants of the WLF equation
C_p	Specific heat capacity
D	Compliance (1/MPa)
D_0	Instantaneous compliance (1/MPa)
D_c	Constant in modified power law
D_i	Co-efficient of the Prony Series (modeling compliance)
D_l	Constant (Lai and Baker viscoplastic model)
D_p	Co-efficient of the power law
ΔD	Transient component of creep compliance
ΔH_c	Heat of cold crystallization
ΔH_f	Heat of fusion of 100% crystalline material
ΔH_m	Heat of fusion
δ	Phase lag
δ_{ij}	Kronecker delta ($i, j = 1, 2, 3$)
E	Relaxation modulus
E'	Storage modulus
E''	Loss modulus

E^*	Complex modulus
ε	Strain
$\dot{\varepsilon}$	Strain rate
ε_0	Instantaneous strain
ε_c	Creep strains
ε_r	Recovery strains
ε_R	$\varepsilon_c(t_r) - \varepsilon_r(t)$
ε_{ve}	Viscoelastic strains
ε_{vp}	Viscoplastic strains
g	Horizontal stress shift factor
g_0, g_1 and g_2	Non-linear parameters of the Schapery non-linear viscoelastic model
$g_{\sigma i}$	Non-linear parameter of the Schapery non-linear equation as a function of stress ($i = 0$, 1 or 2)
g_{Ti}	Non-linear parameter of the Schapery non-linear equation as a function of temperature ($i = 0$, 1 or 2)
$\hat{g}(\ )$	Function in the Zapas and Crissman viscoplastic model
GMT	Glass Mat Thermoplastic
Γ	Gamma function
k	Exponent in power law (constant)
k_s	Stiffness of the loading spring in creep fixture
L	Distance between the two inner bolt holes of the creep specimen
m	Exponent of time in Zapas and Crissman viscoplastic model
m_a	Mechanical advantage of the fixture
μ	Aging or shift rate
n	Exponent of time and stress in Zapas and Crissman viscoplastic model
n_l	Function of stress (Lai and Baker viscoplastic model)
N	Number of terms of the Prony series
η	Co-efficient of viscosity
p	Constant in modified power law

$\phi(\ )$	Function in the viscoplastic model
ψ , ψ'	Reduced time
σ	Stress (MPa)
σ_0	Constant stress applied during creep
$\sigma_{specimen}$	Stress level to be applied using the creep fixture
$\dot{\sigma}$	Stress rate
R	Thermal resistance of constantan disk
RSD	Relative Standard Deviation
t	Time
t_e	Aging time
t_r	Time at start of recovery
t_σ	Duration of creep tests
T	Temperature
$T_{\alpha*}$	Secondary glass transition temperature in polypropylene
T_g	Glass transition temperature
T_{ref}	Reference temperature
TTS	Time Temperature Superposition
τ	Variable of integration in linear and non-linear viscoelastic models
τ_c	Retardation time
τ_i	Retardation time in Prony series (Time constant)
τ_k	Relaxation time in Kohlrausch model
τ_{mpl}	Retardation time in modified power law
τ_r	Relaxation time
ν	Poisson's ratio
W_f	Weight fraction of fibre content
WLF	William, Landel and Ferry
ω	Angular frequency (radians/sec)
ξ	Variable of integration

CHAPTER 1

INTRODUCTION

1.1 Glass mat thermoplastic composites

Random glass mat thermoplastic (GMT) composites are polypropylene-based materials [1] reinforced with 20-50% glass fibers by weight. They are typically supplied as semi-finished sheets which are produced using methods such as melt impregnation, slurry deposition (similar to paper making) [2, 3] and double belt laminator [4, 5]. These semi-finished sheets are compression moulded [5] to obtain products of desired shape and size. The two main types of random GMT's, based on the fiber architecture, are:

- Chopped glass fiber mat GMT
- Continuous glass fiber GMT

(a)   (b)
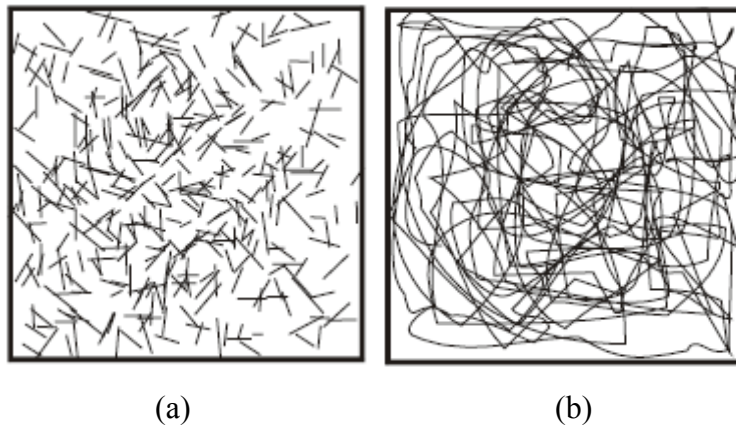
Figure 1.1 (a) Chopped glass fiber mat GMT (b) Continuous glass fiber mat GMT [6].

As the name suggests, the chopped glass fiber mat GMT consists of randomly oriented fibers of length varying between 20 to 75 mm, while the continuous glass fiber GMT consists of long fiber mat as shown in Figure 1.1 (b). The chopped fiber composites are characterized by good flow properties and are typically used for components with ribs and bosses. The long fiber composites exhibit good impact properties with low warpage during moulding and are used for large semi-structural parts [6, 7]. Other variations based on the fiber size and morphology (bundled and non-bundled fibers) are also available.

Figure 1.2 shows the fiber structure in an 80 mm x 80 mm square piece of Symalit GMT with two layers of continuous glass fibers.
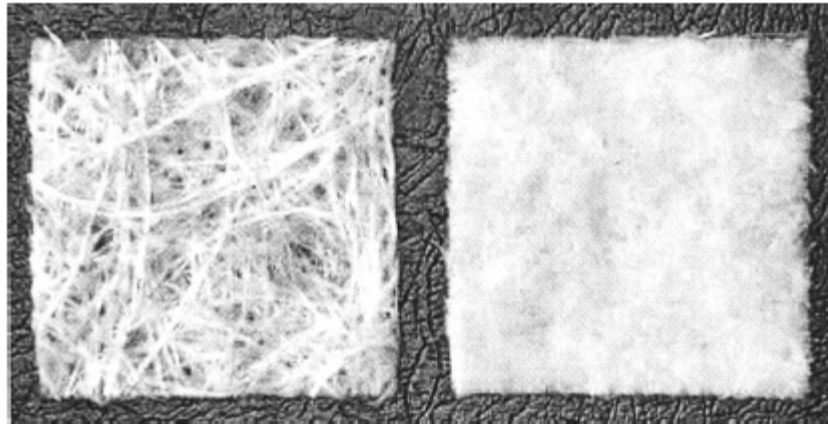
Figure 1.2 The fiber structure of GMT produced by Symalit with 30% glass fibers [8].

Over the past decade, the use of these composites in the automotive industry has increased substantially. This is primarily due to the faster processing time for these composites than that for sheet moulded components and injection moulded thermoplastics. Typically, it is possible to fabricate fairly large components with complicated geometries within 25 to 50 seconds [9]. Furthermore, improved GMT technologies are opening up new applications in the automotive market.

GMT composites offer other numerous advantages which have led to their increased usage such as superior strength-to-weight ratio, high impact resistance, good toughness and stiffness, ability to be recycled, retention of properties after recycling, corrosion and chemical resistance, dimensional stability and low cost per unit volume. These composites are usually used in applications where surface finish is not important. Particularly, automotive semi-structural parts such as door frames, bumper beams, load floors, seat frames, dash boards and front ends are common. They are also used for parts like battery trays, spare wheel covers and wells, instrument panels, under body panels, noise shields and side sills. Besides automotive applications, they are also used in applications like pallets, shipping containers, blower housings, helmets and instrument chassis [2, 6-10].

Figure 1.3 Typical GMT applications – Door frames, bumper beams, load floors, seat frames, dash board and battery trays [6].

1.2 Motivation for the present work

In most of the applications mentioned above, the parts are subjected to constant stresses over long durations. They are also subjected to thermal loads. It is well known that polymers creep under applied stresses and the extent of creep deformation is more significant at elevated temperatures. Although the applications are semi-structural, it is important that the molded GMT components are dimensionally stable over a long term. The creep behavior of GMT materials is yet to be studied in detail. The goal of the current work is therefore to characterize and model the creep behavior of a commercial long fiber GMT composite under thermo-mechanical loads.

The modeling of long-term creep of GMT composites is particularly useful since many of the potential applications are in the automotive industry where the component life expectancies exceed 10 years. Although full scale experimental testing for such long period of time is impractical, the ability to predict creep reliably is essential to avoid in-service failure. A common approach is to use short term test data to develop models for predicting creep deformations over long periods. Various accelerations schemes can be used for this purpose.

One of the major challenges in characterizing random GMT composites is the scatter in the properties. It has been found that some of the material property values such as modulus can vary by a factor of 2 over a ½ inch length. This is due to the inherent variability in the polymer matrix properties and non-uniform distribution of the glass fibers. Thus, it is necessary to apply statistical techniques and to design the experiments to separate the experimental scatter from the actual material behavior.

In many polymers and their composites, permanent viscoplastic strains have been observed during creep along with the recoverable viscoelastic strains. These strains are often associated with the damage mechanisms in the material such as cracks and fiber-matrix debonding. Although the presence of these viscoplastic strains has been known for over three decades, the knowledge of these viscoplastic strains is very limited. Since the

plastic strains are directly related to damage in the material, knowledge of viscoplastic behaviour of the material becomes important to determine the durability of the composite material.

1.3 Objectives and Scope

The main objective of the current work is to develop a semi-empirical constitutive model to describe the creep behaviour of a long fiber polypropylene GMT composite under mechanical and thermal loads. An extensive experimental program has been undertaken to achieve this objective. The experimental study has characterized the tensile creep response over increasingly higher stresses and temperatures. By analyzing the creep data, the linear and non-linear viscoelastic regimes for creep in the material are ascertained. At the outset of the study, the intent was to develop a generalized non-linear viscoelastic constitutive model but as will be demonstrated, a non-linear viscoelastic-viscoplastic model can better represent long term creep behaviour.

Broadly, the scope of this research work involves four parts:
1. Characterization of the GMT material thermo-physical and tensile properties
2. Modification and calibration of the creep fixture
3. Creep testing of the long fiber GMT composite material under combined thermal and mechanical loads and development of a non-linear viscoelastic-viscoplastic constitutive model, and
4. Characterization of viscoplastic strains

The characterization of material thermo-physical properties determined the following specific properties:
- modulus and tensile strength
- isotropy
- dependence of mechanical properties on temperature
- thermal properties and
- polypropylene crystallization kinetics

5

Wherever necessary, the tests were designed to measure the scatter in these property values using statistical techniques. Since the constitutive model relies heavily on reliable creep data, the execution of creep tests is the largest component of the work. An extensive creep testing program consisting of the various sets of creep tests outlined in the flow diagram given in Figure 1.4 has been undertaken in this research study.
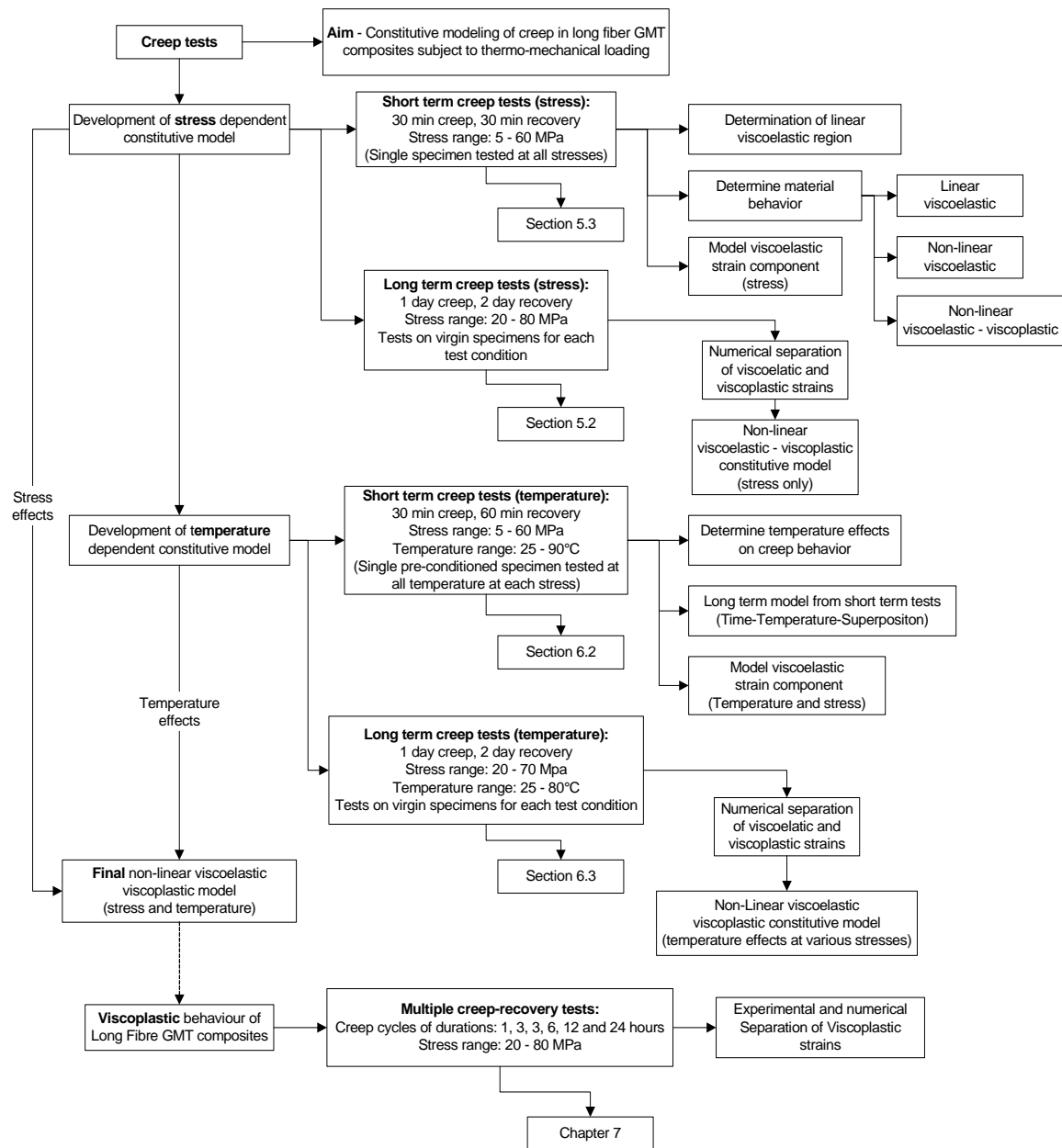
Figure 1.4 Flow diagram showing the creep tests undertaken to meet the study objective.

1.4 Presentation of Thesis

A detailed literature review of linear and non-linear viscoelastic constitutive models, viscoplasticity during creep in polymeric material, experimental methods, data reduction techniques and random glass mat thermoplastic materials is provided in Chapter 2. The experimental details of the various techniques used in this study are given in Chapter 3. The results of the various tests including Differential Scanning Calorimetry, Dynamic Mechanical Analysis and tension tests have been give in Chapter 4. The results of the creep tests are described in Chapters 5 to 7. Specifically, the results of the tests to determine the effect of stress on the creep properties of GMT composite are presented in Chapter 5 while the test results to determine the temperature effects are provided in Chapter 6. A detailed study of viscoplasticity during creep in GMT composite is provided in Chapter 7. The developed models are validated with three test cases in Chapter 8. Finally, the conclusions of this research work are presented in Chapter 9.

CHAPTER 2

LITERATURE REVIEW

2.1 Viscoelasticity in polymers

Polymeric materials exhibit a behaviour which is intermediate between that of elastic solids and viscous liquids when subjected to an external load. They show an initial elastic action upon loading, followed by a slow and continuous increase of strain at a decreasing rate. When the stress is removed, a continuously decreasing strain follows an initial elastic recovery. This behaviour is known as viscoelasticity, which is significantly influenced by the rate of straining or stressing. Viscoelastic materials are also called time-dependent materials as their response to an external excitation varies with time. Figure 2.1 compares the response of elastic, viscoelastic and a viscous material to an applied load.
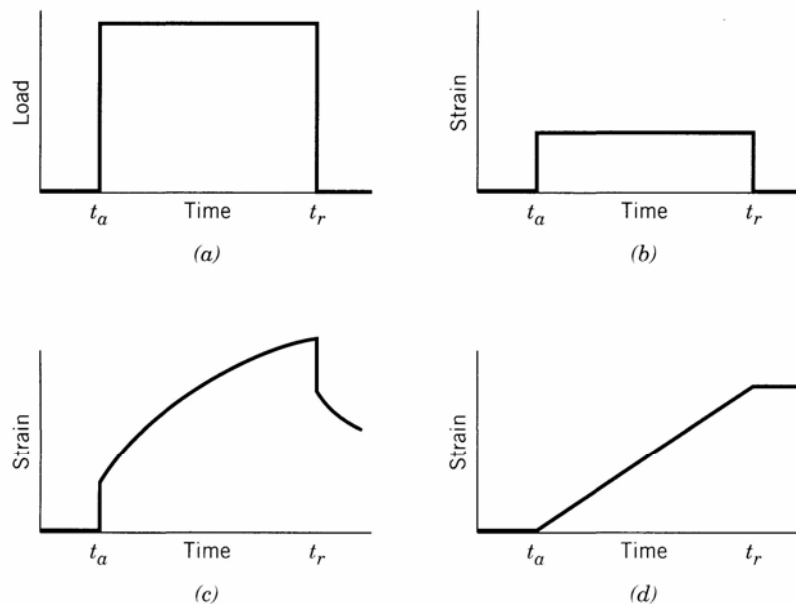
Figure 2.1 (a) load versus time – load applied instantaneously at time t_a and released at time t_r; (b) elastic response; (c) viscoelastic response; and (d) viscous response [11].

In addition to the stress and strain variables, the constitutive laws used to describe the viscoelastic behaviour of materials include time as a variable. Even under simple loading such as uni-axial creep, the shape of the strain-time curve may be complicated.

2.2 Creep and stress relaxation

The time dependent behaviour of materials may be studied by conducting creep-recovery and stress relaxation experiments.

Creep is a slow, continuous deformation of a material under constant stress. Unlike metals, polymers undergo creep even at room temperature. The creep response to a constant stress applied at time $t = 0$ is shown in Figure 2.2 (a).
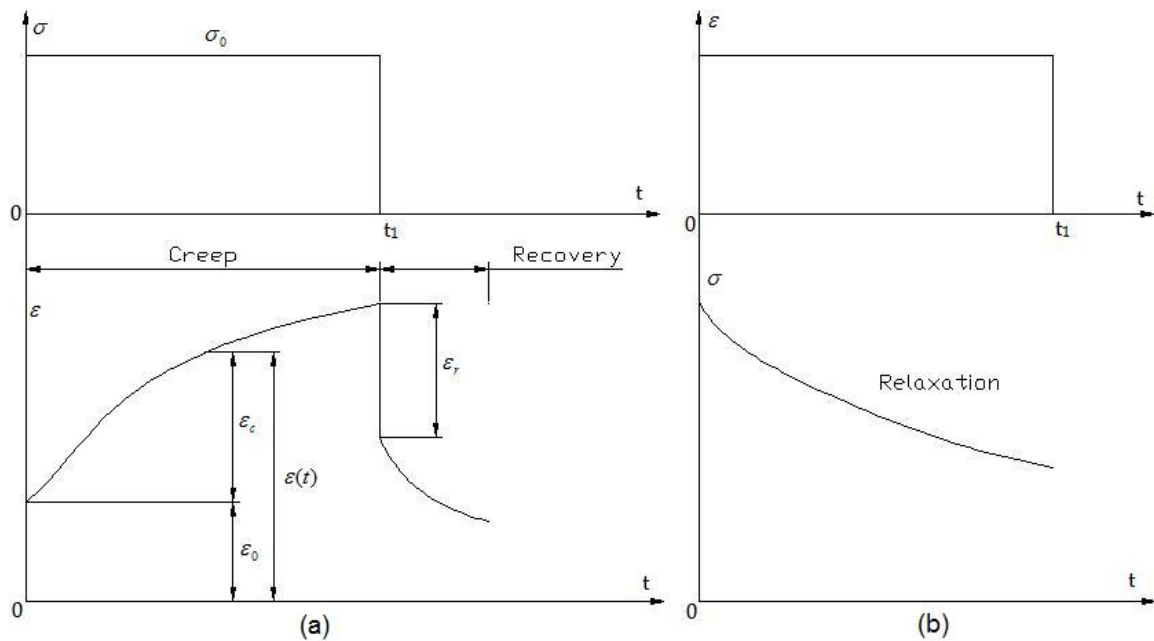
Figure 2.2 (a) Creep and Recovery (b) Stress relaxation.

An instantaneous strain (ε_0) proportional to the applied stress, is observed after the application of the stress and is followed by a progressive strain as shown in the figure. The ratio of the total strain ($\varepsilon(t)$) to the applied constant stress (σ_0) is called 'creep compliance' and is given by

$$D(t) = \frac{\varepsilon(t)}{\sigma_0} \tag{1}$$

In general, creep can be described in three stages: primary, secondary and tertiary. In the first stage, the material undergoes deformation at a decreasing rate, followed by a region

9

where it proceeds at a nearly constant rate. In the third or tertiary stage, it occurs at an increasing rate and ends with fracture. The total strain at any instant of time of a linear viscoelastic material is represented as the sum of the instantaneous elastic strain and creep strain, i.e., $\varepsilon(t) = \varepsilon_0 + \varepsilon_c$, and hence the creep compliance at any point of time is the sum of the instantaneous and the creep compliance, i.e., $D(t) = D_0 + \Delta D(t)$ where $\Delta D(t) = D(t) - D(0)$ is called the transient component of the compliance.

Following the creep stage, if the applied load is removed, a reverse elastic strain followed by recovery of a portion of the creep strain will occur at a continuously decreasing rate. The amount of the time-dependent recoverable strain during recovery is generally a very small part of the creep strain for metals, whereas for plastics, it may be a large portion of the time-dependent creep strain. Some plastics may exhibit full recovery if sufficient time is allowed for recovery. The strain recovery is also called delayed elasticity. This is illustrated in Figure 2.2 (a), when the applied stress, σ_0 is removed at time $t = t_1$.

Similarly, if a viscoelastic material is subjected to constant instantaneous strain, the initial stress developed in the material is proportional to the applied strain followed by a progressively decreasing stress with time. This behaviour is called stress relaxation as shown in Figure 2.2 (b). The ratio of the stress to the applied constant strain is called "relaxation modulus" given by

$$E(t) = \frac{\sigma(t)}{\varepsilon_0} \tag{2}$$

From a study of these time dependent responses of materials, the basic principles of governing time dependent behaviour under loading conditions other than those mentioned above may be established. In practice, the stress or strain history may be one of those described or a mixture, i.e., creep and relaxation may occur simultaneously under combined loading, or the load/strain history may be cyclic or have random variation.

2.3 Basic viscoelastic models

The behaviour of viscoelastic materials can be modeled by using elastic elements (springs), viscous elements (dashpots) and a combination of these basic elements in series or parallel. The following are some of the basic models which can be used to describe the stress-strain relationship for viscoelastic materials. Only the most common models are discussed here.

1. *Linear Spring and dashpot (Basic Elements)* - For a linear spring, the stress is proportional to the strain and the proportionality constant is called the Young's modulus, i.e., we have,

$$\sigma = E\,\varepsilon \tag{3}$$

   For a linear dashpot, the stress is proportional to the strain rate and the proportionality constant is called the coefficient of viscosity, η.

$$\sigma = \eta\frac{d\varepsilon}{dt} \tag{4}$$

2. *Maxwell model* – This model consists of a linear spring and dashpot in series. The total strain of this two-element model to an applied stress is the sum of the individual strains. Following this, the relation between the stress and the strain rates for this model is given by

$$\dot{\varepsilon} = \frac{\dot{\sigma}}{E} + \frac{\sigma}{\eta} \tag{5}$$

   The strain response of this model to a constant stress (σ_0) i.e., creep response is given by,

$$\varepsilon(t) = \frac{\sigma_0}{E} + \frac{\sigma_0}{\eta}t \tag{6}$$

11

Thus, the creep rate is constant with time and recovery is instantaneous (by $\frac{\sigma_0}{E}$ upon unloading) without any time dependence. There is also a residual of $\frac{\sigma_0}{\eta}t$ upon unloading as shown in Figure 2.3(b)
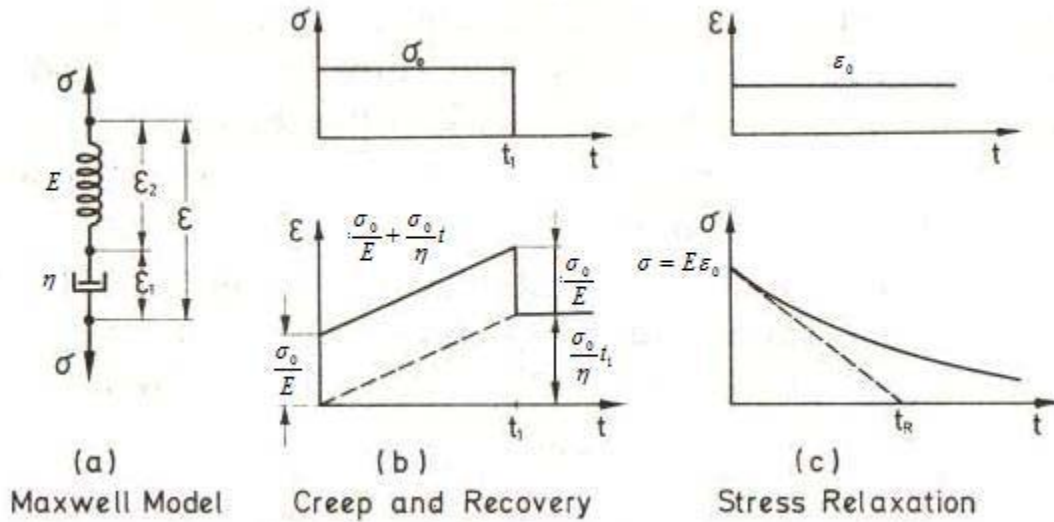
Figure 2.3 Maxwell model and its response [12].

The stress response of this model to a constant strain (ε_0) i.e., stress relaxation response is given by,

$$\sigma(t) = E\varepsilon_0 \exp\left(\frac{-Et}{\eta}\right) = E\varepsilon_0 \exp\left(\frac{-t}{\tau_r}\right) \qquad (7)$$

where $\tau_r = \frac{\eta}{E}$ is the relaxation time.

The Maxwell model and its response to constant stress and strain are given in Figure 2.3 (a), (b) and (c) respectively.

3. *Kelvin Model* – This model consists of a spring and dashpot in parallel. The total stress is the sum of the individual stresses in the two elements as shown in Figure 2.4. The relation between the stress and the strain rates for this model is given by,

$$\sigma = \eta\dot{\varepsilon} + E\varepsilon \qquad (8)$$

12

The strain response of this model to a constant stress (σ_0) i.e., creep response is given by,

$$\varepsilon(t)= \frac{\sigma_0}{E}\left[1-\exp\left(\frac{-Et}{\eta}\right)\right]= \frac{\sigma_0}{E}\left[1-\exp\left(\frac{-t}{\tau_c}\right)\right] \tag{9}$$

where $\tau_c =\dfrac{\eta}{E}$ is the retardation time.

The Kelvin model does not give time-dependent relaxation response.

(a)

Kelvin Model

(b)

Creep and Recovery
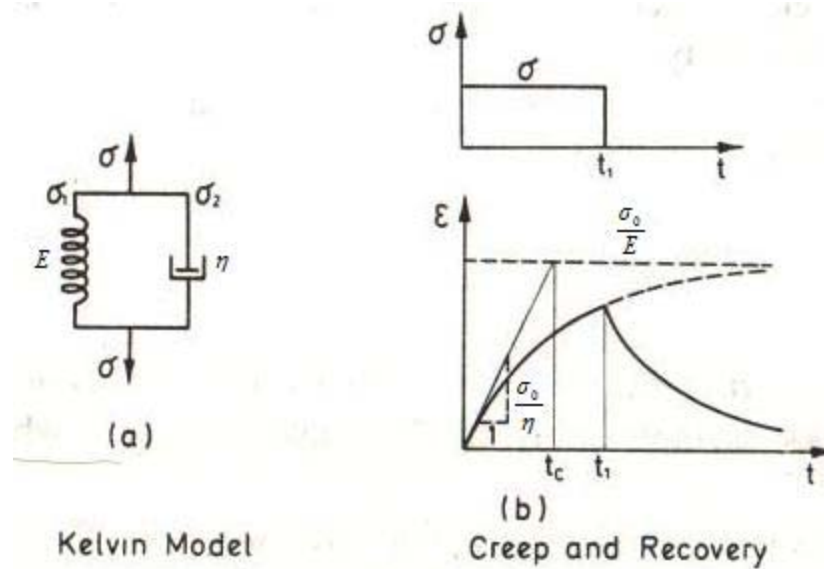
Figure 2.4 (a) Kelvin model (b) creep response (constant stress) [12].

4. *Generalized Maxwell model* – This model consists of many Maxwell models either in series or in parallel. When several Maxwell models are connected in series, the constitutive equation is given by,

$$\dot{\varepsilon}=\dot{\sigma}\sum_{i=1}^{N}\frac{1}{E_i}+\sigma\sum_{i=1}^{N}\frac{1}{\eta_i} \tag{10}$$

The response of this model is not much different from the earlier mentioned Maxwell model and hence is not significant.

When several Maxwell models are connected in parallel, the resulting model is capable of representing instantaneous elasticity, viscous flow, creep with various

13

retardation times and relaxation with various relaxation times. However, this model is more convenient when the strain history (stress relaxation) is known. Hence, the response of this model to a constant strain is given by

$$\sigma(t) = \varepsilon_0 \sum_{i=1}^{N} E_i \exp\left(\frac{-t}{\tau_r^i}\right) \tag{11}$$
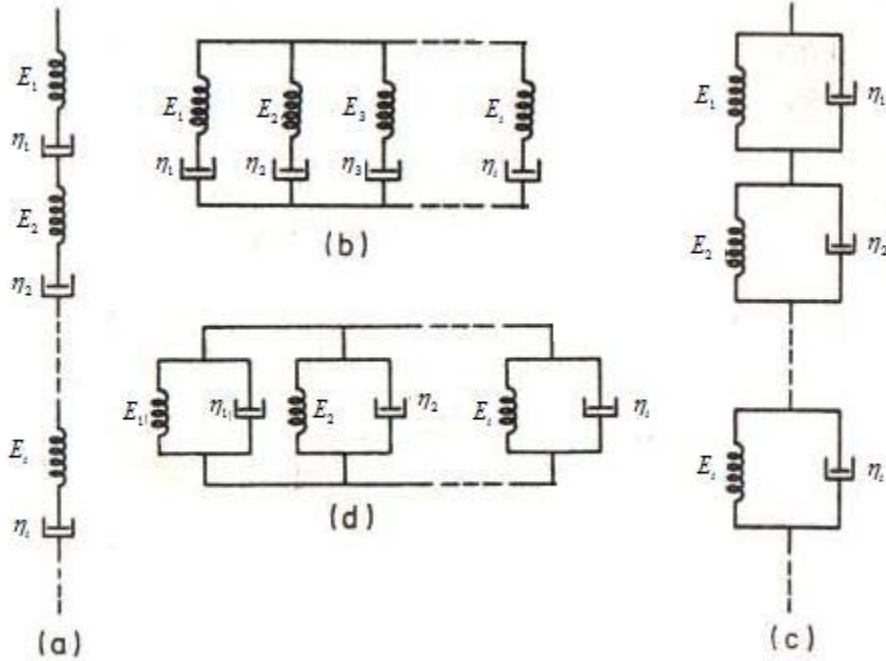
Figure 2.5 Generalized Maxwell in (a) series and (b) parallel, and
generalized Kelvin in (c) series and (d) parallel [12].

5. *Generalized Kelvin Model* –This model consists of many Kelvin models in series or in parallel. When several Kelvin models are connected in parallel, the constitutive equation is given by equation (12). Again, the response of this model is no different from the earlier mentioned Kelvin model and hence is not significant.

$$\sigma = \varepsilon \sum_{i=1}^{N} E_i + \dot{\varepsilon} \sum_{i=1}^{N} \eta_i \tag{12}$$

When several Kelvin models are connected in series the resulting constitutive equation is given by,

$$\varepsilon = \left(\sum_{i=1}^{N} \frac{1}{D\eta_i + E_i} \right) \sigma \qquad (13)$$

where $D = \dfrac{d}{dt}$ is the time differential operator.

This model is more convenient when the stress history is known i.e., creep. The creep response of this model is given by,

$$\varepsilon(t) = \sigma_0 \sum_{i=1}^{N} D_i \left(1 - \exp\left(\frac{-t}{\tau_c^i} \right) \right) \qquad (14)$$

where, D_i is the creep compliance.

Figure 2.5 shows the arrangement of the springs and dashpots in the various Generalized Maxwell and Kelvin Models.

There are several other combinations of the springs and dashpots possible like the Burger's model in which Maxwell and Kelvin models are considered in series, standard linear solid in which a Maxwell model is considered in parallel with another spring and so on.

2.4 Linear viscoelasticity

A viscoelastic material is said to be linear if,

1. The stress is proportional to the strain at a given time, i.e.

    $$\varepsilon[c\,\sigma(t)] = c\,\varepsilon[\sigma(t)] \qquad (15)$$

    This is shown in Figure 2.6 (a). This also implies that for a linear viscoelastic material, the creep compliance is independent of the stress levels [12]. Thus, the compliance-time curves at different stress levels should coincide if the material is linear viscoelastic.

2. The linear superposition principle holds. This implies that each loading step makes an independent contribution to the final deformation, which can be obtained by the

addition of these. This principle is also called "Boltzmann superposition principle". For a two step loading case given in 2.6 (b), the strain response is given by,

$$\varepsilon[\sigma_1(t) + \sigma_2(t - t_1)] = \varepsilon[\sigma_1(t)] + \varepsilon[\sigma_2(t - t_1)] \qquad (16)$$

Further, for multi-step loading, during which stresses σ_1, σ_2, σ_3 ….. are applied at times τ_1, τ_2, τ_3 …. the strain at time 't' is given by

$$\varepsilon(t) = \sigma_1 D(t - \tau_1) + \sigma_2 D(t - \tau_2) + \sigma_3 D(t - \tau_3) + …… \qquad (17)$$

where, $D(t - \tau)$ is the creep compliance.
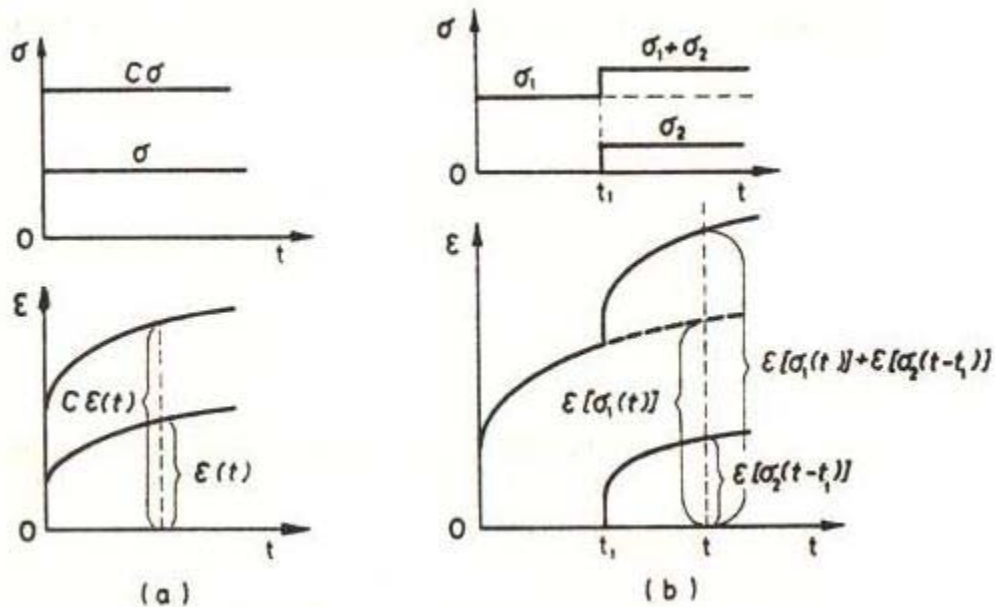
Figure 2.6 Linear viscoelastic material behaviour –
(a) Stress strain proportionality (b) Boltzmann superposition [12].

Typically in order to determine linear viscoelastic region, creep and recovery experiments are carried out. A suitable model is developed for the compliance using the creep portion of the experiment and using this model, the recovery strains are predicted. If the predicted and experimental recovery strains match, then linear superposition principle holds good and the material is linear.

Non-linearities in creep or relaxation behaviour can arise due to any of the variables: stress (creep), strain (relaxation), time and temperature. The maximum permissible

deviation from the linear behaviour of a material, which allows a linear theory to be employed with acceptable accuracy, depends on the stress distribution, the type of application and the level of experience. Many plastics behave linearly over short durations of loading, even at stresses for which considerable non-linearity is found over longer durations.

2.5 Integral representation of the linear viscoelastic constitutive equation

The response of a viscoelastic material to a multiple step load given by equation (17) can be generalized in the integral form (also known as Boltzmann superposition integral) as,

$$\varepsilon(t) = D_0\sigma + \int_0^t \Delta D(t-\tau)\frac{d\sigma}{d\tau}d\tau \tag{18}$$

The above integral is called the Hereditary or Volterra integral. The integral basically implies that the strain is dependent on the stress history of the material under consideration. The function $\Delta D(t-\tau)$ is called the kernel function of the integral. This function is the same in the case of non-linear viscoelastic models and hence will be described later.

2.6 Relating creep compliance and relaxation modulus

For purely elastic materials, modulus and compliance can be related by,

$$E(t) = \frac{1}{D(t)} \tag{19}$$

For viscoelastic material, equation (19) is not applicable. Based on the integral representation of viscoelastic materials given in equation (18), the relaxation modulus and the creep compliance are related by the convolution integral given by,

$$\int_0^t D(t-\xi)E(\xi)d\xi = t \ \text{ or } \int_0^t E(t-\xi)D(\xi)d\xi = t \tag{20}$$

17

However, it is to be noted that $D(0)E(0)=1$ (instantaneous) [13]. Analytical integration of equation (20) is possible only for simple forms of creep compliance. For example, if the compliance can be expressed by power law given by,

$$D(t)=D_p t^k \tag{21}$$

then, it can be shown that the relaxation modulus is given by,

$$E(t)=\frac{1}{D_p \Gamma(1+k)\Gamma(1-k)}t^{-k} \tag{22}$$

where, $\Gamma(x)=\int e^{-t}t^{x-1}dt$ is the gamma function

For complicated forms of creep compliance, numerical methods can be used. A variety of different methods of interrelating creep compliance and relaxation modulus based on the convolution given in equation (20) have been suggested by various researchers and are given in references [13 - 24].

A numerical integration technique for the conversion of creep compliance to the modulus by Hopkins *et al.* [13] is as follows:

Let $f(t)$ be the integral of relaxation modulus, $E(t)$ given by

$$f(t)=\int_0^t D(\xi)\,d\xi \tag{23}$$

This implies that $f(0)=0$ and $f'(\xi)=D(\xi)$.

Using the trapezoid rule for integration,

$$f(t_{n+1})=f(t_n)+\frac{1}{2}\big[D(t_{n+1})+D(t_n)\big]\big[t_{n+1}-t_n\big] \tag{24}$$

The convolution integral given in equation (20) can be rewritten as

$$t_{n+1}=\int_0^{t_{n+1}} E(\xi)\,D(t_{n+1}-\xi)\,d\xi \;=\;\sum_{i=0}^{n}\int_{t_i}^{t_{i+1}} E(\xi)\,D(t_{n+1}-\xi)\,d\xi \tag{25}$$

Each term in the summation given in equation (25) can be approximately written as,

$$\int_{t_i}^{t_{i+1}} E(\xi)\, D(t_{n+1} - \xi)\, d\xi = E(t_{i+\frac{1}{2}}) \int_{t_i}^{t_{i+1}} f'(t_{n+1} - \xi)\, d\xi$$

$$= -E(t_{i+\frac{1}{2}})\Big[f(t_{n+1} - t_{i+1}) - f(t_{n+1} - t_i) \Big] \tag{26}$$

where $t_{i+\frac{1}{2}} = \dfrac{(t_{i+1} + t_i)}{2}$

Substituting equation (26) in (25),

$$t_{n+1} = -\sum_{i=0}^{n-1} E(t_{i+\frac{1}{2}})\Big[f(t_{n+1} - t_{i+1}) - f(t_{n+1} - t_i) \Big] + E(t_{n+\frac{1}{2}}) f(t_{n+1} - t_n) \tag{27}$$

Solving for $E(t_{n+\frac{1}{2}})$, we get,

$$E(t_{n+\frac{1}{2}}) = \frac{t_{n+1} - \sum_{i=0}^{n-1} E(t_{i+\frac{1}{2}})\Big[f(t_{n+1} - t_i) - f(t_{n+1} - t_{i+1}) \Big]}{f(t_{n+1} - t_n)} \tag{28}$$

The relaxation modulus can thus be found out by using equation (28) and (24) alternatively with the first value at time $t = \frac{1}{2}$ given by,

$$E\left(\frac{1}{2}\right) = \frac{t_1}{f(t_1)} \tag{29}$$

2.7 Non-linear viscoelasticity

Linear viscoelastic principles have been widely used in the characterization of the mechanical behaviour of polymers. However, these principles are applicable only at low stresses. At high stresses the behaviour of polymers can be highly non-linear i.e., they do not follow equations (15), (16) or (17). Hence, application of the linear viscoelastic principles at these stresses would not be appropriate.

2.7.1 Basic principles and theoretical development

The non-linear constitutive law developed by Schapery [25-26] is most widely used for describing the behaviour of non-linear viscoelastic materials. This constitutive relation is

also widely used in the non-linear viscoelastic finite element methods. This constitutive equation which is very similar to the Boltzmann Superposition Integral (given by equation (18)) is based on thermodynamics and given by,

$$\varepsilon(t) = g_0 D_0 \sigma + g_1 \int_0^t \Delta D(\psi - \psi') \frac{dg_2 \sigma}{d\tau} d\tau \qquad (30)$$

where D_0 and $\Delta D(\psi)$ are the instantaneous and the transient components of compliance,

g_0, g_1, g_2 and a_σ are functions of stress,

ψ is the reduced time given by,

$$\psi = \int_0^t \frac{d\tau}{a_\sigma[\sigma(\tau)]} \quad (a_\sigma > 0) \text{ and } \psi' = \psi(\tau) = \int_0^\tau \frac{dt}{a_\sigma[\sigma(t)]} \qquad (31)$$

The terms g_0, g_1 and g_2 arise from the third and higher order dependence of the Gibb's free energy on the applied stress, while a_σ comes from the higher order effects in both entropy production and free energy. The term g_0 gives the stress and temperature effects on the elastic compliance and is a measure of the state dependent reduction/increase of stiffness. The term g_1 has a similar function operating on the transient creep compliance component, while g_2 gives the effect of load rate on creep and a_σ is the shift factor [26]. It must be noted that if $g_0 = g_1 = g_2 = a_\sigma = 1$, then equation (30) reduces to the Boltzmann superposition integral given by equation (18), which describes the linear behaviour. The advantage of this constitutive equation is that the same compliance function, which is used to describe the compliance in the linear viscoelastic materials, i.e., in the Boltzmann superposition integral, can also be used with this non-linear equation.

For a creep-recovery experiment with a stress history shown in Figure 2.2 (a), the creep response can be obtained by substituting constant stress σ_0 in equation (30) and noting that $\frac{dg_2 \sigma_0}{d\tau} = 0$ except for $t = 0$, the expression for creep reduces to,

$$\varepsilon_c(t) = \left[g_0 D_0 + g_1 g_2 \Delta D\left(\frac{t}{a_\sigma}\right) \right] \sigma_0 \qquad (32)$$

Further the recovery response can be given as,

$$\varepsilon_r(t) = g_2 \left[\Delta D\left(\frac{t_1}{a_\sigma} + t - t_1 \right) - \Delta D(t - t_1) \right] \sigma_0 \qquad (33)$$
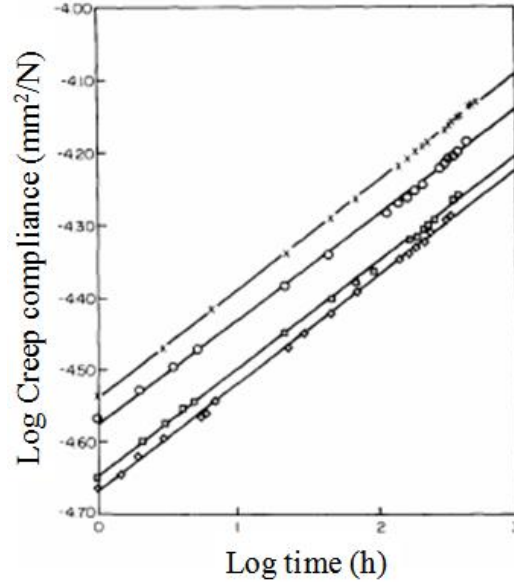
Figure 2.7 Creep compliance v/s time plotted on a log-log scale [27].

2.7.2 Data reduction and analysis to determine the parameters in Schapery non-linear model

The Schapery non-linear constitutive model given in Equation (30) contains a total of six parameters to be deduced from the experimental data which include a constant (D_0 – instantaneous compliance), a function of time (ΔD - transient compliance) and four functions of stress (g_0, g_1, g_2 and a_σ). These four material functions of stress can also depend on external factors like temperature and humidity. Hence, it is essential that the environmental conditions during the test be constant so that, they remain functions of stress alone.

Since the compliance, both instantaneous and the transient components, in the Schapery non-linear viscoelastic model is obtained in the linear viscoelastic region, the linear viscoelastic range of the material being characterized has to be determined. This can be done by plotting isochronous compliance-stress curves extracted at various time intervals

from the creep curve. For the material to be linear viscoelastic, the compliance-stress curve should be horizontal i.e., the compliance is constant with stress. Thus, the end of the linear viscoelastic region is marked by start of an increase in compliance with stress. Further, the Boltzmann superposition principle give by equation (17) has to be verified as well.

The instantaneous response (D_0) can be directly deduced from the experimental data. The ease with which the compliance can be found depends on the form of the compliance function chosen (based on experimental results). The transient component of the compliance can be modeled by various equations such as the power law - equation (34), modified power law - equation (35), Prony series - equation (11) and (14) and other more complicated forms (e.g., consisting of hyperbolic sine functions) depending on the type of material under consideration and the time period for which the constitutive equation should be applicable with the power law being the simplest one of them all. Whether or not the power law can be used to effectively describe the compliance can be found out by plotting the compliance-time curve on a log- log scale [27]. If the plot is a straight line, then the power law can be used to describe the material with the slope of the curve being the exponent of time and the y-intercept the coefficient (*D*). The log-log curve for glass fiber reinforced polyester, which follows the power law, is shown in Figure 2.7 [27]. The power law and its variants are usually insufficient for describing the compliance over a longer period and hence are rarely used in long-term models. However, they are widely used for short-term models owing to the simplicity of determining the parameters of the equation.

$$\Delta D(t) = D_p t^k \tag{34}$$

where, D_p and *n* are constants

Graphical and numerical methods can be used to obtain the parameters of the modified or general power law [26, 28] in equation (35). D_0 and D_c are shown in Figure 2.8, which shows the comparison between the power law and modified power law.

$$\Delta D(t) = D_0 + \frac{D_c - D_0}{\left(1 - \dfrac{\tau_{mpl}}{t}\right)^p} \tag{35}$$

where D, p, τ_{mpl}, D_0 and D_c are constants.
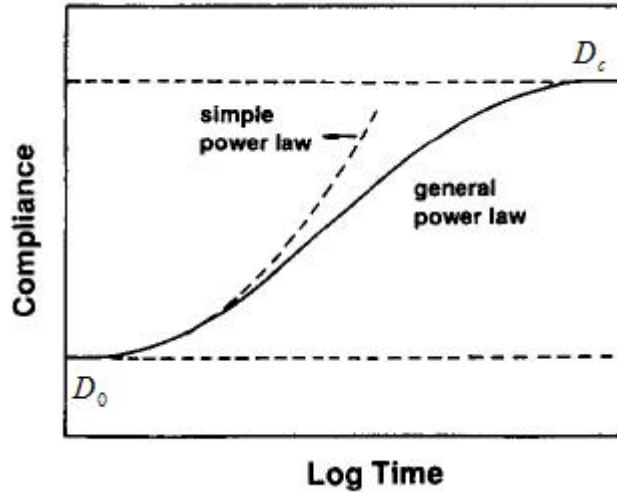
Figure 2.8 Power law and general power law [29].

Prony series consisting of exponential terms in the form given by equations (11) and (14) are most often used for modeling creep compliance in polymeric materials. Using an expression in the form of Prony series has the advantage in that adding additional terms to the series can extend the time over which the equation is applicable. This form is also more convenient for finite element implementation [30]. However, the methods of parameter deduction from the experimental data for Prony series are more complex than that for the power law. Numerical methods can be used to accurately determine the parameters of the Prony series. A review of the various numerical methods can be found in Chen [31]. The use of the weighted non-linear regression analysis for determining the Prony series is provided in detail.

Determining the non-linear parameters in equation (30) is not always simple. Typically, creep-recovery experiments are conducted to determine these parameters. The shift factor, a_σ can be obtained from a graphical shifting of the creep curves at the various

stress levels. The method will be described in greater detail in the next section. This yields the shift factors as a function of stress and a master curve. g_0 can be determined by comparing the instantaneous compliance in the linear and non-linear viscoelastic regions. g_2 can be determined by fitting the recovery data to equation (33) while g_1 can be determined by fitting the creep data to equation (32). The nonlinear parameters have to be found at the different stress levels using the above method. Finally, the non-linear parameters can be fit to suitable functions of stress using numerical methods.

A graphical method of determining the parameters of the non-linear viscoelastic equation has been provided by Lou *et al.* [32]. Graphical methods can often be quite tedious and are dependent on human judgement, which could lead to errors in parameter estimation. A numerical method based on least squares techniques to determine the non-linear parameters were proposed by Brueller [33]. The method involves an iterative procedure to determine the non-linear parameters, although complicated, can give accurate values.

2.7.3 Accelerated testing methods - long-term creep curves from short-term tests

The test methods to obtain the long term behaviour of materials from short term tests may be termed as accelerated test methods. Some of the commonly used methods include:
1. Time - Temperature superposition
2. Time - Stress superposition
3. Time - Elapsed time superposition

These are detailed in the following section.

1. *Time – Temperature Superposition (TTS):*

    This method is applicable to the thermo-rheologically simple polymers. The term thermo-rheologically simple implies that the effect of temperature on the compliance of these materials is to shift (or stretch) the time scale. This means that in these materials, when creep tests are carried out at higher temperatures, they simply predict the behaviour of the material over longer times at lower temperatures. The creep compliance at two temperatures T_1 and T_2 can be related by using the expression:

$$D(t, T_1) = D(t/a_T, T_2) \qquad (36)$$

where, a_T is the temperature shift factor given by the WLF equation [34-35] given by equation 54,

$$\log a_T = \frac{-C_1(T - T_{ref})}{C_2 + (T - T_{ref})} \qquad (37)$$

where, T_{ref} is the reference temperature usually taken to be the glass transition temperature (T_g), T is the temperature and C_1 and C_2 are constants.

It is to be noted that the concept of reduced time arises from the Time-Temperature superposition principle. This is clearly indicated by equation (36). This simply means that the creep which occurs at time increment dt at temperature T_1 is 'a_T' times slower/faster at temperature T_2 in a time increment $d\xi$.

The shift in the time scale is considered to be due to the change in the free volume, and hence is more pronounced in amorphous materials. However, it is much more complicated to apply in the case of semi crystalline polymers, and is usually not applicable for this class of materials [36-40].

This method can be applied only to determine the short-term behaviour of the materials or can be used to determine the long-term behaviour when the aging of the material is neglected during the course of the creep experiments in which case the results of the model could be terribly off from the actual behaviour.

Materials that do not have correspondence between temperature and compliance as mentioned above, are called thermo-rheologically complex materials for which TTSP cannot be applied. An excellent example of such a material is a composite material having two or more thermo-rheologically simple materials, in which each material is characterized by its characteristic shift function and the net effect of temperature on compliance need not correspond to either material [12].

2. *Time - Stress Superposition (TSSP):*

The time-stress superposition is based on the fact that stress has the same effect on materials as temperature does in thermo-rheologically simple materials. That is to say that stress has the effect of shifting the time scale and hence by performing the creep tests at higher stress levels; one can predict the behaviour at lower stress level over a longer time. This principle is illustrated in Figures 2.9 and 2.10.
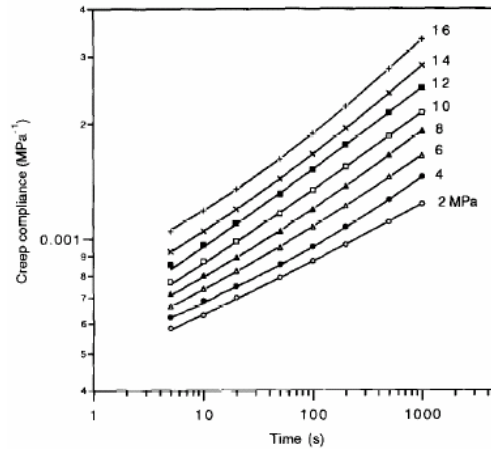
Figure 2.9 Momentary creep curves at stress levels between 2 to 16 MPa [36].
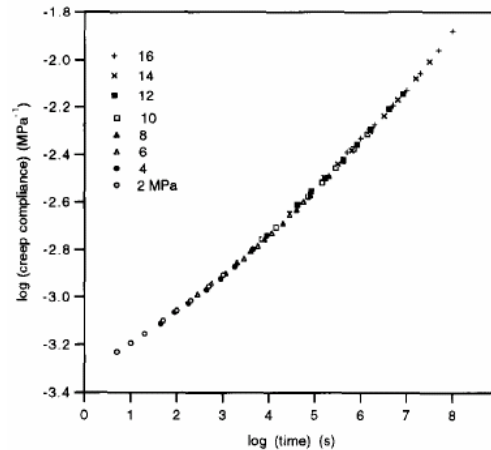
Figure 2.10 Master curve formed from the momentary curves in Figure 2.9 [36].

Analogous to the time-temperature-superposition principle, the creep compliance at two stress levels σ_1 and σ_2 can be related by,

$$D(t, \sigma_1) = g\, D(t/a_\sigma, \sigma_2) \tag{38}$$

Where, log g and log a_σ are the horizontal and vertical shifts respectively.

26

It can be seen from the Figure 2.10 that the compliance over a time period of up to 10^8 seconds has been estimated by using tests carried over time period of 1000 seconds as shown in Figure 2.9. In constructing the master curve a number of horizontal and vertical shifts have been applied to shift the compliance curves at different stress levels to a reference curve. Similar to that in TTS, the shift factor can be given by,

$$\log a_\sigma = \frac{C_1(\sigma - \sigma_0)}{C_2 + (\sigma - \sigma_0)} \qquad (39)$$

where, σ_0 is the reference stress and C_1 and C_2 are constants.

The above expression is similar to the one developed by Ferry and Stratton [42] on the basis of free volume theory.

Lai *et al.* [41] have successfully used the time stress superposition in the non-linear region of HDPE. They concluded that the principle is applicable over all stresses except at very low stresses for HDPE and at moderately high stresses beyond the linear range for PMMA.

3. *Time - Elapsed time superposition:*

This is also called the "Time-Aging time superposition principle". In this superposition method, short-term tests are carried out on specimens aged for different times. It is important to note that the test time (t) should be less than the physical age (t_e) of the material. This is to ensure that the physical aging effects can be separated out, as no or negligible aging of the material takes place during the test. These momentary curves at different aging times can then be shifted to obtain the master curve. The shift factor is given by,

$$a_{t_e} = \left(\frac{t_e + t}{t_e} \right)^\mu \qquad (40)$$

where, μ is the aging or shift rate given by $\mu = \dfrac{d \log a_{t_e}}{d \log t_e}$ which is the slope of the a_{t_e}

versus t_e curve plotted on the log-log sheet.

The momentary creep compliance can be described by using the 3-parameter Kohlrausch model given by,

$$D(t) = D_0 \exp(t / \tau_k)^\beta \tag{41}$$

where, D_0 is the initial compliance, t is the time, τ_k is the relaxation time and β is the shape factor.

Typically, the initial compliance of the material decreases with the aging time [43], i.e., the stiffness of the material increases with aging time. Further, for creep tests of times greater than the aging time, the creep compliance can be considered to be affected by the aging process. In this case, the reduced time (ψ) given by equation (42), has to be used [43, 44].

$$\psi = t_e \ln\left(\frac{t}{t_e} + 1\right) \quad \text{for } \mu = 1 \text{ and}$$

$$\psi = \frac{t_e}{1 - \mu}\left[\left(\frac{t}{t_e} + 1\right)^{1-\mu} - 1\right] \quad \text{for } \mu \neq 1 \tag{42}$$

where t_e is the aging time and t is the test time.

Using the reduced time given above in equation (42), long-term predictions can be obtained using short term tests.

Further acceleration can be obtained by aging at elevated test temperature in which case the shift parameter will be a function of temperature [45]. A more detailed description of this accelerated superposition scheme can be found in Brinson *et al.* [43]. This superposition principle has been applied for polypropylene by Skrypnyk *et al.* [46].

2.7.4 Extension to Schapery Non-linear model

The non-linear constitutive model given in equation (30) is a very general one and can be modified to extend its range of applicability. In doing so, additional variables might be required to account for different materials, loading and environmental conditions. For example, temperature effects can be modeled by considering the non-linear parameters to

be functions of temperature along with stress as illustrated by Peretz *et al.* [47-48]. In order to account for the effects of both temperature and stress, Peretz et al. [47-48] considered the non-linear material functions to be product of two terms which are given as follows:

$$a(\sigma,T)=a_\sigma(\sigma).a_T(T)$$

$$g_i(\sigma,T)=g_{\sigma i}(\sigma).g_{Ti}(T) \text{ with } i = 0, 1 \text{ or } 2 \tag{43}$$

where, $a_\sigma(\sigma)$ and $g_{\sigma i}(\sigma)$ are determined using the data at a reference temperature

$a_T(T)$ and $g_{Ti}(T)$ are determined using the data at a reference stress level.

The method of determining these non-linear functions is similar to that for the basic Schapery non-linear equation (30). Further, alternate form of equation (43), for instance sum of functions of stress and temperature is also possible; however this form in equation (43) is computationally advantageous. Other effects such as physical aging can also be included as illustrated by Skrypnyk *et al.* [46, 49].

2.7.5 Extension to multi-axial case

The constitutive model given by equation (30) considers only the uni-axial case. This can be generalized to include multi-axial loading by considering two independent functions instead of a single function $\Delta D(\psi)$ [50]. For an isotropic material, the stress strain relationship is given by,

$$\varepsilon_{ij} = (1+\nu(t))\{D\}\sigma_{ij} - \nu(t)\{D\}\sigma_{kk}\delta_{ij} \tag{44}$$

where, the operation $\{D\}\sigma$ is defined by the right hand side of equation (30), $\nu(t)$ is the time dependent Poisson's ratio of the material and δ_{ij} is the kroneker delta.

In most cases, the time dependence of Poisson's ratio is neglected [51] and hence the all the parameters of the creep model can be obtained from a uni-axial creep tests.

2.7.6 Application of the non-linear viscoelastic model to composite materials

In most of the studies on characterization of viscoelastic behaviour in polymeric composites, the same analysis scheme and constitutive laws used for neat polymeric

materials are used [47, 52-55]. At the same time, there are a number of other models developed using micromechanics analysis of composites which considers the matrix as viscoelastic and the fibers to be elastic [50, 56-57]. However, the former approach is considered in this work and hence micromechanical models will not be reviewed here.

2.8 Viscoplasticity
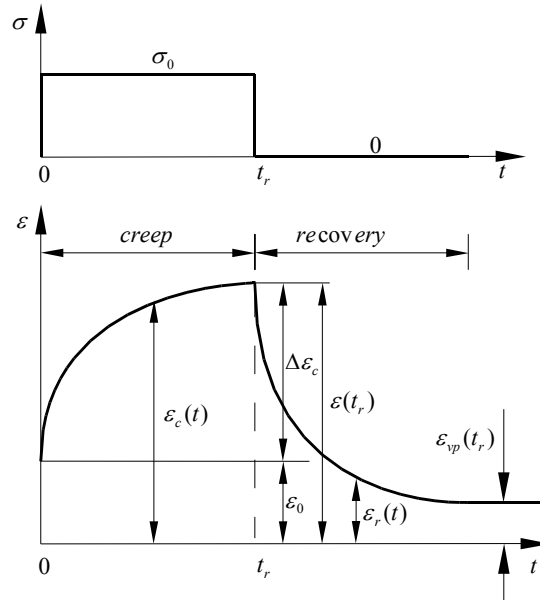
Figure 2.11 Typical Creep-recovery curves with viscoplastic strains.

It has been observed that creep strains in polymeric materials, particularly composite materials, are not completely recovered upon unloading, even after sufficiently long durations. This is illustrated in Figure 2.11 with $\varepsilon_{vp}(t_r)$ representing the viscoplastic strains. These un-recovered strains, which accumulate with time (under load) are commonly referred to as viscoplastic strains. The viscoplastic strains are due to the damage of the material such as matrix cracking, fiber-matrix debonding and matrix plasticity especially at higher stress levels [58]. In some of the earlier works on polymeric materials such as that by Lou *et al.* [32] and Peretz *et al.* [47-48], the creep test specimens were pre-conditioned by repeated loading and unloading (70 % of tensile strength for 10 cycles) prior to the actual tests in order to reduce the damage during the tests. Pre-conditioning the specimens was considered as a means of improving the repeatability of the creep tests. However, there is a lot of speculation whether the models developed

based on tests on pre-conditioned specimens is a representative of the actual behaviour of the material. To accurately describe the behaviour of the material, it is necessary to include both the recoverable viscoelastic strains and the non-recoverable viscoplastic strains in the constitutive model [52]. Thus, the total strains should be decomposed into,

$$\varepsilon(t) = \varepsilon_{ve} + \varepsilon_{vp} \tag{45}$$

where, ε_{ve} and ε_{vp} are the viscoelastic and viscoplastic strains respectively.

The viscoelastic strains (ε_{ve}) can be modeled by a linear viscoelastic model given by equation (18) or by a non-linear viscoelastic constitutive model such as the Schapery viscoelastic constitutive model given by equation (30) depending on the material response. The viscoplastic strains (ε_{vp}) are commonly modeled using the Zapas and Crissman model [59] given in equation (46).

$$\varepsilon_{vp} = \phi \left(\int_0^t \hat{g}(\sigma(\xi)) d\xi \right) \tag{46}$$

where, $\phi(\ )$ is a function which depends on the stress history ($\hat{g}(\sigma(\xi))$ with $\hat{g}(0)=0$). The above model was used to model the viscoplastic behaviour of ultra high molecular weight polyethylene [59] in which case the functional was considered in the form,

$$\phi \left(\int_0^t \hat{g}(\sigma(\xi)) d\xi \right) = \left(\int_0^t \hat{g}(\sigma(\xi)) d\xi \right)^n \tag{47}$$

with $\hat{g}(\sigma(\xi)) = C\sigma^m$

Also, $\varepsilon_{vp} = 0$, when $\sigma = 0$ or $t = 0$. Typically, single duration creep recovery experiments as shown in Figure 2.11 are carried out to determine the parameters of the non-linear viscoelastic-viscoplastic constitutive model. For such an experiment, the viscoplastic model during creep reduces to,

$$\varepsilon_{vp} = \left(C\sigma^m t \right)^n = A \left(\sigma^m t \right)^n \tag{48}$$

while that during recovery can be written as,

$$\varepsilon_{vp} = \left(C\sigma^m t_r \right)^n = A \left(\sigma^m t_r \right)^n \tag{49}$$

Substituting the Prony series into the non-linear viscoelastic model, the total strain, during creep in equation (45) reduces to,

31

$$\varepsilon_c(t) = \left(g_0 D_0 + g_1 g_2 \Delta D \left(\frac{t}{a_\sigma} \right) \right) \sigma_0 + A \left(\sigma_0{}^m t \right)^n$$

$$= \left(g_0 D_0 + g_1 g_2 \sum_{i=1}^{N} D_i (1 - e^{-t/\tau_i}) \right) \sigma_0 + A \left(\sigma_0{}^m t \right)^n \tag{50}$$

while the total strain during recovery can be given by,

$$\varepsilon_r(t) = \left(\Delta D \left(t - t_r + \frac{t_r}{a_\sigma} \right) - \Delta D \left(t - t_r \right) \right) g_2 \sigma_0 + A \left(\sigma_0{}^m t_r \right)^n$$

$$= \left(\sum_{i=1}^{N} D_i \left(e^{-(t-t_r)/\tau_1} - e^{-t/\tau_1} \right) \right) g_2 \sigma_0 + A \left(\sigma_0{}^m t_r \right)^n \tag{51}$$

The separation of the two strain components i.e., the viscoelastic and the viscoplastic strains in such experiments (single duration creep-recovery experiment) is not simple, as only the total strains are measured during the experiment and hence do not provide any data on the evolution of the plastic strains. A few numerical methods for separating these strains from the total creep strains using the data from single duration creep-recovery experiments have been proposed by Tuttle et al. [52], Lai et al. [53] and Zaoutsos et al. [54-55].]. In this research study, a new parameter reduction method has been proposed, which will be described in a later section.

The viscoelastic and viscoplastic strains can also be experimentally separated as demonstrated by Segard et al. [60], Nordin et al. [61] and Marklund et al. [62], which involves multiple creep-recovery experiments over single/varying durations and stresses. Segard et al. [60] showed that the time dependence of the viscoplastic strains can be determined by creep-recovery tests over two time intervals at a single stress level while stress dependence can be determined by conducting creep-recovery at two stress levels of a single duration. A similar but more general experimental and analytical framework for isolating the viscoplastic strains has been proposed by Nordin et al. [61]. The two sets of tests to determine the stress- and time-dependence of the viscoplastic strains are:

a. The first set of tests consists of performing creep tests of a fixed duration (t_σ) followed by recovery at the various stress levels of interest. The un-recovered strains

at the end of recovery in each of these tests can be considered as a good estimate of the total viscoplastic strains developed during the respective creep steps. From a plot of the viscoplastic strains versus stress on a log-log scale, an estimate of the product 'mn' and $\log A + n \log t_\sigma$ can be obtained as the slope of the curve and the y-intercept respectively $\left(\log(\varepsilon_{vp}) = (\log A + n \log t_\sigma) + mn \log(\sigma) \right)$.

b. The second set of tests consists of performing multiple creep tests of durations, $t_1, t_2, ..., t_r$ on a single specimen at a constant stress σ_t, with each test being followed by a recovery for a long time. If 'r' such cycles are carried out and assuming that the interruption between the tests does not affect the plastic strains, ε_{vp}^i then the total accumulated viscoplastic strains at the end of each cycle is given by,

$$\begin{aligned}
\varepsilon_{vp}^{1+2+....+r} &= \varepsilon_{vp}^1 + \varepsilon_{vp}^2 + ... + \varepsilon_{vp}^r \\
&= A \sigma^{mn} \left(t_1 + t_2 + ... + t_r \right)^n
\end{aligned}$$

(52)

From the plot of the total accumulated viscoplastic strain at the end of each cycle versus total time on the log-log scale, the exponent 'n' and $mn \log(\sigma_t) + \log A$ can be estimated as the slope and the y-intercept of the curve $\left(\log(\varepsilon_{vp}) = (mn \log(\sigma) + \log A) + n \log t_\sigma \right)$. Using these values and 'mn' obtained in step 1, 'm' and 'A' can be determined.

The above method has also been employed by Marklund *et al.* [62] to determine the viscoplastic strains in Flax/Polypropylene composites.

Other models to describe the viscoplastic strains are also available. Lai *et al.* [53] modeled the viscoplastic strains as,

$$\varepsilon_{vp}(\sigma, t) = \sigma D_l(\sigma) t^{n_l(\sigma)}$$

(53)

where, D_l is a constant, n_l is a function of stress

Chailleux *et al.* [63] has employed a similar model for Aramid fibers. However, since the material showed a threshold stress below which the viscoplastic strains were not significant, the Perzyna [64] model consisting of a viscous damper and a frictional slider in parallel as shown in Figure 2.12 was used. Recently, Schapery [65, 66] has proposed a non-linear viscoelastic-viscoplastic model based on thermodynamics. Further, it has been shown that for a uni-axial case, the viscoplastic model is equivalent to that proposed by Lai et al. [53]. The method for determining the parameters of the Schapery viscoelastic-viscoplastic model from experiments has been provided by Megnis *et al.* [67].
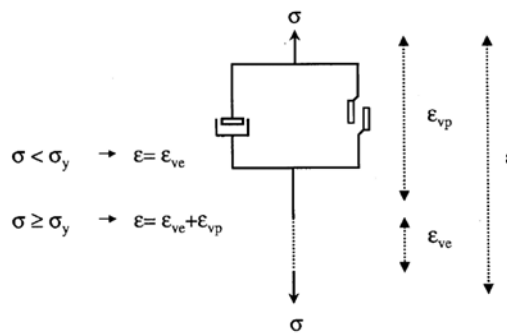
Figure 2.12 Viscoplastic model consisting of a frictional slider and viscous damper [63].

2.9 Random glass mat thermoplastic composites

A random glass mat thermoplastic composite is a semi finished composite sheet, which is heated and compression flow moulded. It consists of randomly oriented fibers, usually glass, embedded in a thermoplastic matrix with polypropylene being the most commonly used material to date. The fiber content is usually in the range of 20 % to 50 %. There are two different kinds of random GMT's based on the fiber architecture.

- Chopped glass fiber mat GMT
- Continuous glass fiber GMT

The chopped glass fiber mat GMT consists of fibers of length varying between 20 to 75 mm, while the continuous glass fiber GMT consists of mat of randomly oriented fibers as shown in Figure 1.1 (b). Figure 1.2 shows the fiber structure in an 80 mm x 80 mm square piece of Symalit GMT with two layers of continuous glass fibers.

GMT is typically available as sheets which are processed to obtain the parts of required shape and size. Melt impregnation (Figure 2.13) and slurry deposition (similar to paper making process) are two widely used methods in the manufacture of GMT [68]. Usually the glass mat is produced separately as shown in Figure 2.14, which is used to manufacture the GMT sheets as shown in Figure 2.13.
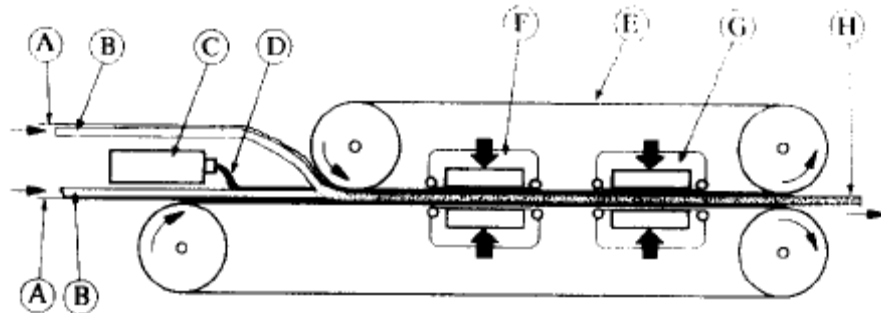
Figure 2.13 Manufacture of GMT by melt impregnation: (A) Thermoplastic resin films (B) Glass fiber mat (C) Extruder (D) Thermoplastic resin extrudate (E) Double belt laminator (F) Heating zone (G) Cooling zone (H) Finished sheet product [84].
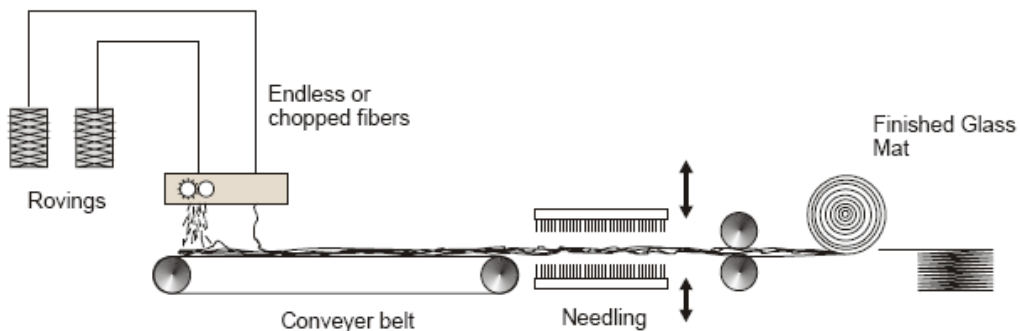
Figure 2.14 Glass fiber mat production process [1].

Compression moulding is one of the most widely used methods to produce components from GMT. However other methods such as solid phase thermoforming can also be used to process GMT [68].

The preheated GMT sheets are formed between the moulds by the application of pressure to produce the parts of required shape and size. Various methods are used to preheat the GMT sheets such as contact heating, radiation heating, hot air oven and infrared oven. A typical hot air oven is shown in Figure 2.15. The other heating methods are of similar

construction while the technology used for heating is different in each case. Figure 2.16 shows a typical compression moulding setup. The heated GMT sheets of required size are placed in the part cavity and a known pressure is applied on the top mould. Cooling of the mould is achieved by the temperature control lines. The part is removed from the mould using the ejector mechanisms. Advantages of compression moulding include short cycle times and ability to produce large parts. Typical cycle times for the polypropylene based GMT is about 25 to 50 seconds [9].
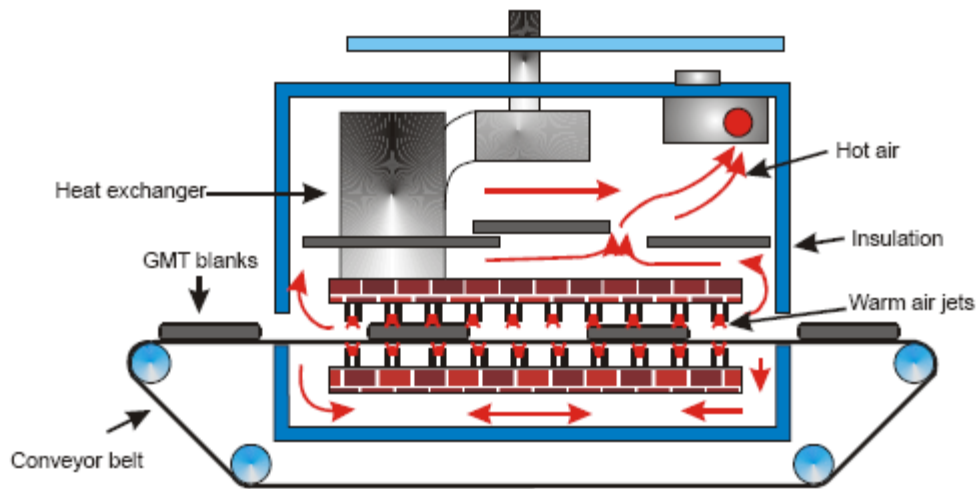
Figure 2.15 Hot air oven [10].
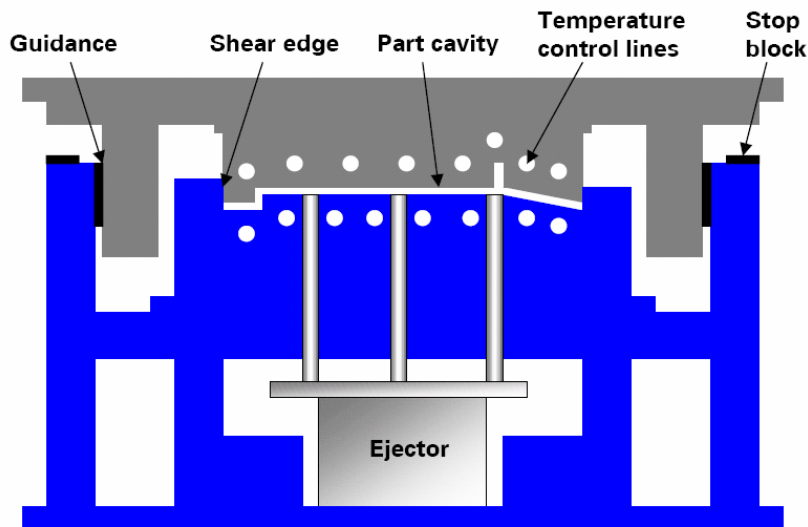
Figure 2.16 Compression moulding [7].

The various research efforts related to processing, tensile behaviour and creep modeling of GMT materials is presented below.

Processing:

It is well known that the mechanical properties of thermoplastics are strongly influenced by its processing history. For GMT composites, the effects of processing conditions are relatively well known: low mould temperatures significantly increase the residual stresses in the moulded component and deteriorates impact strength; lower blank temperature leads to lower tensile strengths [69]; and low stamping pressures and/or time under pressure increases the void content thereby reducing the strength of the material [70-71]. Void content of up to 5% has been found to have insignificant effect on the tensile properties [72], but the effects are more appreciable at higher values [71].

Residual stresses, crystallinity and temperature distribution in the material during compression moulding have been studied by Trend *et al*. [73]. Modelling of material flow during compression moulding process can be found in references [8, 74-76]. The flow of the material during the moulding process has a significant effect on the fiber content (volume fraction) and the fiber distribution of the moulded component. The specimens from plates having larger flow during moulding have considerably lower tensile strength in the flow direction due to the alignment of the fibers perpendicular to the flow direction [77]. Moreover, greater flow results in non-uniform tensile modulus and strength within the moulded plate with the specimens at the edge having higher values than those at the center due to flow-induced fiber orientation [4].

Tensile properties

In general, GMT mechanical properties are dependent on volume fraction; the tensile modulus increases linearly with the increase in fiber content but the tensile strength decreases after 20% fiber content due to poor fiber matrix bonding [78]. Furthermore, single fiber composites show better tensile properties than when the fibers are bundled together. Bundled fiber, however, have better impact properties [71, 9]. Recent work has

shown that the short fiber GMT exhibits higher tensile properties than the long fiber GMT but has greater directional dependence [79].

One of the major challenges in characterization of these composites is the scatter in the experimental data. It has been observed that the modulus of GMT can vary by a factor of two over half an inch of the material [80]. The variation in the tensile properties of GMT has been extensively studied by Stokes [80-83]. The average tensile properties directly correlated to the density distributions within the composite plate. Further statistical models for these properties have been developed by Busko *et al.* [84-86]. According to Stokes [80], specimen size effects have to be considered with caution in random mat materials. The tensile modulus has been found to be dependent on the gauge length of the specimen being tested and its value over any given length can be found by the harmonic mean of the moduli over smaller elements within this length of the specimen [80]. Even though specimen width does not considerably affect the mechanical properties, increasing the width of the specimen reduces the scatter in the data [4, 86].

Creep modeling:

Although the tensile properties of GMT materials have been studied extensively, there are only a handful of published studies on their tensile creep behaviour. Since polymeric matrices are innately viscoelastic, the time-dependent response of their composites needs to be better quantified to enable automotive part designers to design more confidently with these materials. Mathematical models capable of predicting creep response in these relatively complex materials are therefore required.

To date, the only published effort on modeling creep in GMT materials is that by Megnis, Allen and their co-workers. Megnis *et al.* [56] developed a micromechanics based model by representing the GMT material as a multi-layered symmetric and balanced composite laminate. The predictions for creep in GMT were based on pure polypropylene creep properties tended to underestimate the strains at longer times. It was, however, found that GMT exhibited fairly linear viscoelastic behaviour for stresses up to 24 MPa even though slight non-linearities were found in polypropylene at considerably lower stress levels.

Allen *et al.* [88] used the material data obtained experimentally by Megnis *et al.* [56] for finite element simulation of GMT materials. The finite element code for orthotropic viscoelastic behaviour to be used with commercial finite element software (ANSYS and ABAQUS) was developed using the algorithm developed by Zocher *et al.* [89]. The developed finite element code was verified by considering simulation of problems like uni-axial creep, creep of a tapered bar, bending in beams and a 3D case where an automotive sub frame was analyzed. The result of the uni-axial creep test simulation was in very good agreement with the experimental results. In the case of the creep of the tapered bar, the displacements were overestimated by about 10-20%. However, this error is comparable to the scatter in the experimental data. The creep analysis of a 3D automotive sub-frame shown in Figure 2.17 was also considered. The points marked in the figure give the points where the deformation was measured. Finite element analyses were carried out by considering the material both as isotropic and orthotropic. The creep deformations obtained from the finite element method were more than that the experimental results. The discrepancy between the experimental and the numerical results were attributed to the variabilities arising due to the moulding process such as variations in crystallinity and fiber distribution.
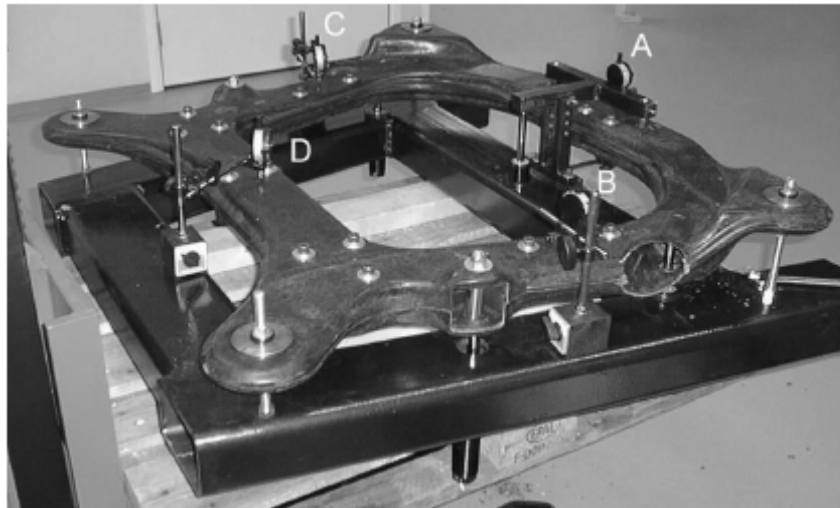
Figure 2.17 Creep of an automotive sub frame [88].

Despite several advantages mentioned earlier, GMT materials have certain disadvantages. As mentioned before, there is considerable amount of scatter in the experimental data. There is also considerable lofting of the material when it is heated to the forming

temperature as shown in the Figure 2.18. This is also known as deconsolidation and a detailed study on this can be found in Wolfrath *et al.* [90]. Deconsolidation is one of the reasons for poor surface finish of these composites [91].
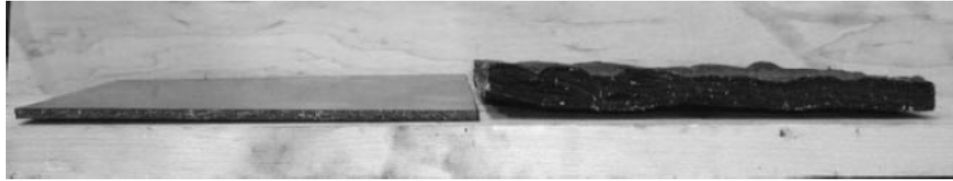
Figure 2.18 Lofting of GMT when heated to forming temperature
(before heating – left; after heating – right) [90].

CHAPTER 3

MATERIALS AND EXPERIMENTAL METHODS

3.1 Material Details

The material studied in this work is a polypropylene based random glass mat thermoplastic composite commonly known as 'GMT'. Two composite materials were studied simultaneously – one with chopped fiber glass mat and the other with endless or continuous fiber mat commercially known as D100-F40-F1 and G100-F40-F6 respectively both with 40 % fiber content. The scope of this work is focused on the G100 continuous (endless) fiber composite system. The material data sheet is given in Appendix A. The plaques for the experiments (test plaques) were produced by compression moulding at Polywheels Manufacturing Ltd, an industrial molding plant. The raw material (GMT plates) for compression moulding was in the form of 3.8 mm thick charge plates produced by Quadrant Plastics. The dimensions of the mould used for compression moulding was 390 mm x 390 mm (and hence the test plaque). Plates of thickness 3 mm and 6 mm were produced. The final dimensions of the GMT plates required for compression moulding were determined based on volume calculations regularly used at the compression molding plant.

To mould the test plaques, a hot air oven and compression moulding machine were used. The charge GMT plates were heated in an oven with three heating zones before moulding. The material was passed through the oven over a conveyor belt. Two heated GMT plates were heated, stacked one over the other and placed between the moulds to produce the 6-mm test plaques while only one heated GMT plate was sufficient to produce the 3-mm test plaques. The cavity in the mould was maintained at 60 °C while the core was maintained at 66 °C. A pressure of about 450 tonnes was applied for 40 seconds. Cooling water was passed through the mould to maintain the temperature of the cavity and the core. After a dwell time of 40 seconds, the plaques were removed manually and the flash (excessive material along the sides) was removed using a sharp edged knife. The total cycle time for production of one plaque was about 90 seconds

(including heating). A mark ('X') was made on the top left corner of the test plaque to identify the direction so as to ensure that all of the specimens from different plaque for tensile and creep testing could be machined in a consistent direction. Thirty test plaques of two thicknesses were produced at a stretch in one moulding batch run.

From matrix burn-off tests were carried out on the two materials to determine the fiber weight fraction following moulding. The burn-off tests consisted of heating a specimen of size 25 mm x 25 mm in a crucible covered by a steel mesh to 650°C and held at this temperature for 2 hours. For 5 specimens sampled from various locations of a plaque, the fiber weight fractions were determined to be 41 ± 3 % and 42 ± 3 % for the 3 and 6-mm material, respectively.

3.2 Experimental Methods

Although the primary purpose of this work is to characterize and model the creep response of the long fiber GMT material, additional tests to characterize the thermal and mechanical properties of the material were also carried out to. Overall, four different tests were performed to characterize the long fiber GMT material:

- Differential Scanning Calorimetry (DSC)
- Dynamic Mechanical Analysis (DMA)
- Creep testing
- Tensile test

3.2.1 Differential Scanning Calorimetry

Differential Scanning Calorimetry (DSC) is a thermal analysis technique used to measure heat flow associated with molecular transitions in materials as a function of time and temperature. The method is widely used to characterize polymers, pharmaceuticals, food, organic and inorganic chemicals.

DSC has many advantages, which contribute to its widespread usage, including fast analysis time, easy sample preparation, applicability to solids and liquids, wide temperature range and excellent quantitative capability.
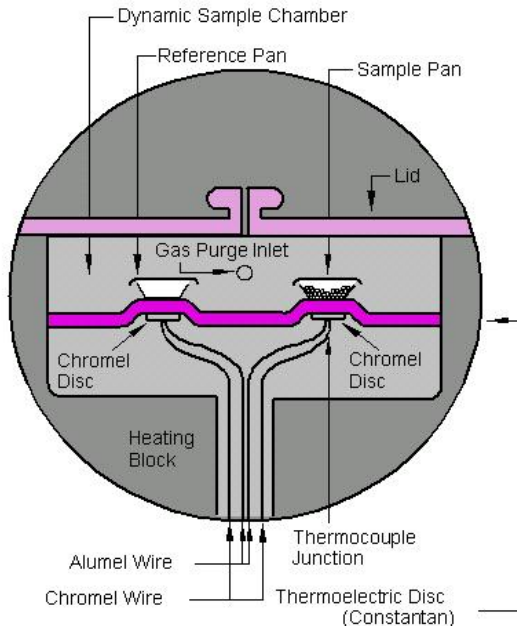
Figure 3.1 DSC cell schematic [92].

In DSC, the difference in heat flow between the sample and an inert reference is measured as a function of temperature as both the sample and the reference are subjected to a controlled environment of time, temperature and pressure. The most common instrument design is the heat flux design as shown in the Figure 3.1. In this design, a metallic disc (made of constantan alloy) is the primary means of heat transfer to and from the sample and reference. The encapsulated sample in a metal pan and the reference (an empty pan) sit on separate constantan disc platforms. As heat is transferred through the disc, the differential heat flow between the sample and the reference is measured by area thermocouples formed by the junction of the constantan disc and chromel wafers, which cover the underside of the platforms. These thermocouples are connected in series and measure the differential heat flow using the thermal equivalent of Ohm's law,

$$\frac{dQ}{dt} = \frac{\Delta T}{R} \qquad (54)$$

where, $\dfrac{dQ}{dt}$ = heat flow,

ΔT = the temperature difference between the reference and the sample

R = Thermal resistance of the constantan disc.

The chromel and alumel wires attached to the chromel wafers form thermocouples, which directly measure sample temperature. Purge gas is admitted to the sample chamber through an orifice in the heating block before entering the sample chamber. The result is a uniform, stable thermal environment, which assures baseline flatness and sensitivity. In DSC, the temperature regime seen by the sample and reference is linear heating or cooling at rates from as fast as 100°C/min to as slow as 0°C/minute (isothermal) [92].
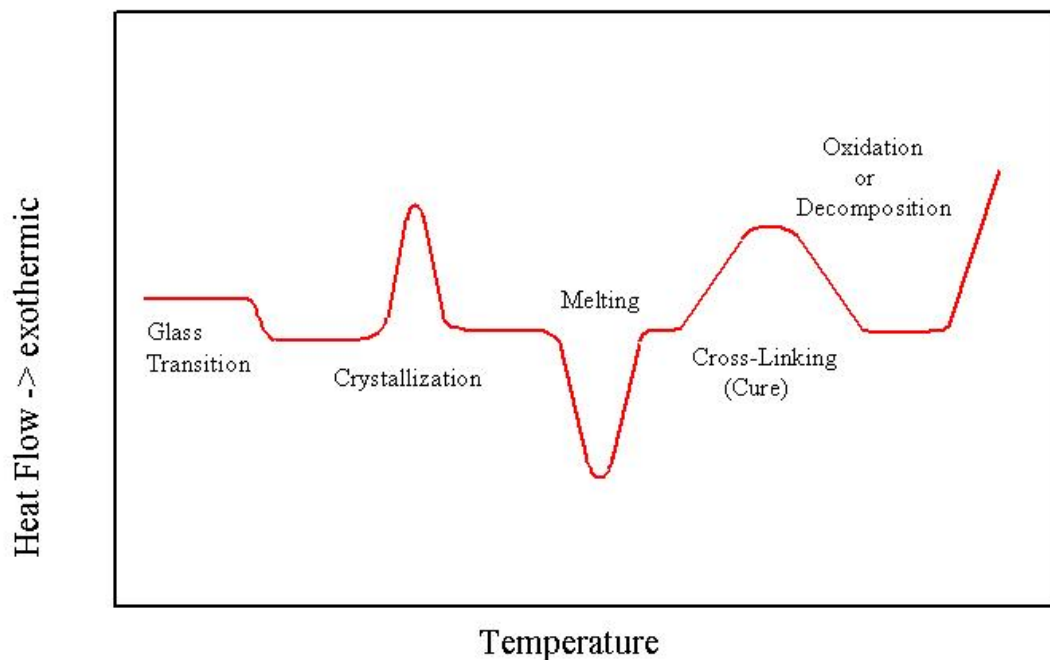
Figure 3.2 Typical output of DSC for the different transitions [92].

Using a DSC, various transitions in a polymeric material can be determined. The change in the signals for various transitions is shown in Figure 3.2. The glass transition, T_g, is associated with a large change in modulus as the polymer changes from rigid solid state to rubbery state. T_g of the material can be found by a shift in the heat flow curve. Crystallization and curing events which release energy are usually identified by the

presence of exothermic peak. Melting is identified by an endothermic peak as energy is absorbed by a polymeric material.

However, DSC has disadvantages as it does not have sufficient sensitivity, adequate resolution and mainly the ability to properly analyze complex transitions.

Many transitions are complex as they involve multiple processes like enthalpic relaxation which occurs during glass transition and crystallization of amorphous or meta-stable crystalline structures prior to or during melting. Enthalpic relaxation is an endothermic process and the magnitude of the heat, which a material absorbs during this process, depends on the thermal history of the material, and can sometimes cause the glass transition appear to be a melting transition. Another common problem encountered is the simultaneous crystallization and melting which makes it almost impossible to determine the initial crystallinity of a sample using the DSC. This is because DSC measures only the sum of all thermal events in the sample and thus when multiple transitions occur in the same temperature range, the output is confusing and can be easily misinterpreted.

This disadvantage can be overcome by using Modulated DSC (MDSC), which also measures the difference in heat flow between a sample and an inert reference as a function of time and temperature with the same heat flux cell design. However, in the MDSC mode, a different heating profile is applied to the sample and reference. Specifically, a sinusoidal modulation (oscillation) is overlaid on the conventional heating or cooling ramp to yield a profile in which the average sample temperature continuously changes with time but not in a linear fashion. Figure 3.3 shows the heating profile for a MDSC heating experiment. The net effect of imposing this complex heating profile on the sample is the same as running two experiments simultaneously on the material – one experiment at the traditional linear (average) heating rate and the other at a sinusoidal (instantaneous) heating rate. The actual rates for these two simultaneous experiments are dependent on three variables – heating rate, the period of modulation and the temperature amplitude of modulation.

The general equation, which describes the resultant heat flow at any point in a MDSC experiment, is

$$\frac{dQ}{dt} = C_p \frac{dT}{dt} + f(T,t) \qquad (55)$$

where $\dfrac{dQ}{dt} =$ total heat flow,

$C_p =$ Specific heat capacity,

$\dfrac{dT}{dt} =$ heating rate, and

$f(T,t) =$ heat flow from kinetic events (absolute temperature and time dependent)
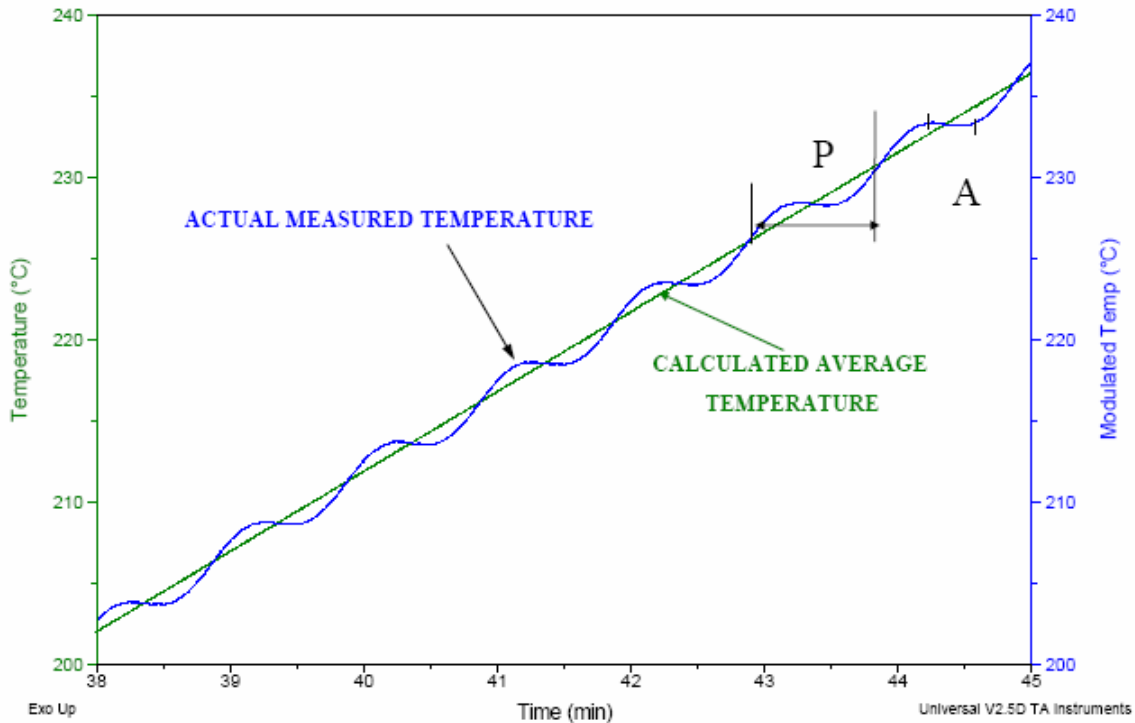
Figure 3.3 Heating profile in MDSC [92].

From the above equation, the total heat flow is the heat flow measured by the DSC which is composed of two components, one of which is a function of the materials heat capacity and rate of temperature change called the reversing heat flow (first term in equation (55))

46

and the other is a function of absolute temperature and time called the non-reversing heat flow.

MDSC determines the total as well as these two individual heat flow components to provide better resolution of complex transitions in materials. MDSC achieves this through the presence of two heating rates as seen by the material – the average heating rate which provides total heat flow information and the sinusoidal heating rate which provides the heat capacity information from the heat flow that responds to the rate of the temperature change. The reversing heat flow can be used to determine the glass transition and melting, while the non-reversing heat flow can be used to determine crystallization, melting, curing, decomposition and enthalpic relaxation.

Modulated DSC provides all of the same benefits as conventional DSC plus several additional benefits including separating complex transitions into more easily interpreted components, increased sensitivity for detection of weak transitions, increased resolution of transitions without loss of sensitivity, direct measurement of heat capacity and heat capacity changes from a single experiment along with determination of thermal conductivity and true initial crystallinity of polymers [92].

A typical MDSC experiment consists of heating the material from a temperature below the transition of interest to a temperature above its melting (for semi-crystalline materials). In order to determine the thermal characteristics of a material, heat-cool-heat experiments are conducted. This experiment can be used to determine polymer material characteristics, such as crystallinity, melting point and glass transition, which are directly dependant on thermal history. It also provides information regarding the characteristics of the material with a specified thermal history, i.e. when the material is cooled from its melting point to below its glass transition temperature. This would also provide information about the crystallization kinetics of the material. By cooling the material at different rates, the dependence of crystallinity on cooling rate can be determined.

3.2.2 Dynamic Mechanical Analysis

Dynamic Mechanical Analysis (DMA) is a technique that applies an oscillating force to a sample and analyzes the material's response to that force. From that oscillatory response, it is possible to quantify the material's tendency to flow (viscosity) and the material's ability to recover from deformation (elasticity).
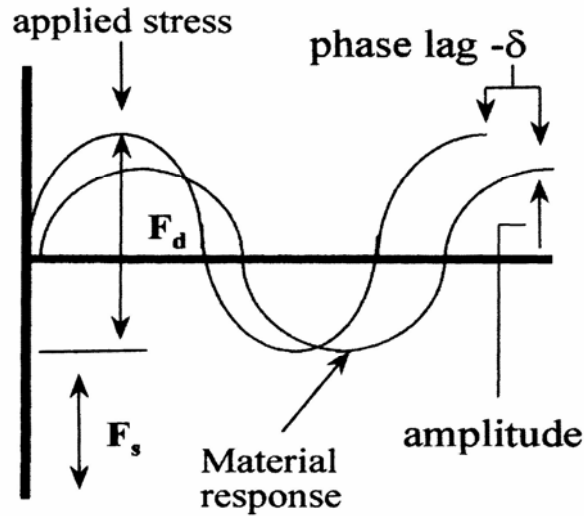
Figure 3.4 Response of a viscoelastic material for a sinusoidally applied stress [93].

Consider a sample being subject to a sinusoidally oscillating force [F_s – Static Force, F_d – Dynamic force] as shown in the Figure. 3.4. If the material is within the elastic limit, the sample will also deform sinusoidally. The response is reproducible. Within this range, the applied stress is given by,

$$\sigma = \sigma_0 \sin(\omega t) \qquad (56)$$

where, σ_0 is the maximum strain,

ω is the angular frequency (radians/sec) and

t is the time (sec)

For linear viscoelastic behaviour in equilibrium, the strain will lag behind the stress by a characteristic angle δ. The strain at time, t, is given by,

$$\varepsilon(t) = \varepsilon_0 \sin(\omega t + \delta) \qquad (57)$$

48

where, ε_0 is the maximum strain and

   δ is the phase lag

From the above two expressions, two terms called the storage modulus (E') and the loss modulus (E'') given by equations (58) and (59) can be determined,

$$E' = \frac{\sigma_0}{\varepsilon_0} \cos(\delta) \tag{58}$$

$$E'' = \frac{\sigma_0}{\varepsilon_0} \sin(\delta) \tag{59}$$

E' signifies the elastic behaviour and is proportional to the energy stored elastically and reversibly in the material, while E'' signifies the viscous behaviour of the material and is proportional to the energy transformed into heat due to the internal motions of the molecules and is irreversibly lost.
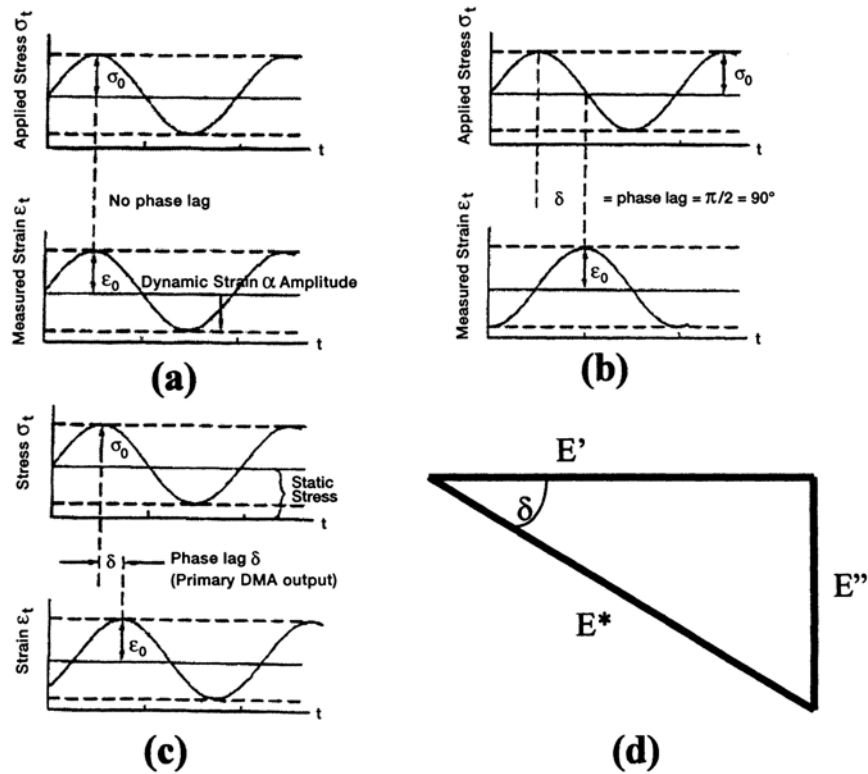
Figure 3.5 (a) Elastic response, (b) Viscous response, (c) Viscoelastic response, (d) relation between E', E'' and δ [94].

For an elastic material, the stress and the stain are in phase as shown in Figure 3.5 (a). This implies that the phase angle and the loss modulus are zero and hence the storage modulus is equivalent to the Young's modulus of the material.

For a viscous material we have,

$$\varepsilon(t) = \eta \frac{d\sigma}{dt} = \eta \omega \sigma_0 \cos(\omega t)$$
$$= \eta \omega \sigma_0 \sin(\omega t + \frac{\pi}{2})$$

(60)

Hence, the stress and the strain are out of phase by 90 degrees for a viscous material, as shown in the Figure 3.5 (b).

Finally, for a viscoelastic material, the stress and the strain are out of phase by δ and the values of δ lies between 0 and 90 degrees. The phase lag between stress and strain is shown in Figure 3.5 (c). The relation between the storage modulus (E'), loss modulus E'' and the phase angle δ is as shown in Figure 3.5 (d).

The tangent of the phase angle ($\tan(\delta)$) given by the ratio of the loss modulus to the storage modulus, is an important parameter obtained from DMA. This ratio also called damping indicates the ability of a material to lose energy to molecular rearrangements and internal friction [94].

$$\tan(\delta) = \frac{E'}{E''}$$

(61)

The term E^* in the Figure 3.5 (d) is called the complex modulus and is given by,

$$E^* = \sqrt{(E')^2 + (E'')^2}$$

(62)

Various clamps are available for use with the DMA such as the tension, compression, shear, single and double cantilever and three-point bend. Typically, for stiff materials three-point bending clamp shown in Figure 3.6 is used.
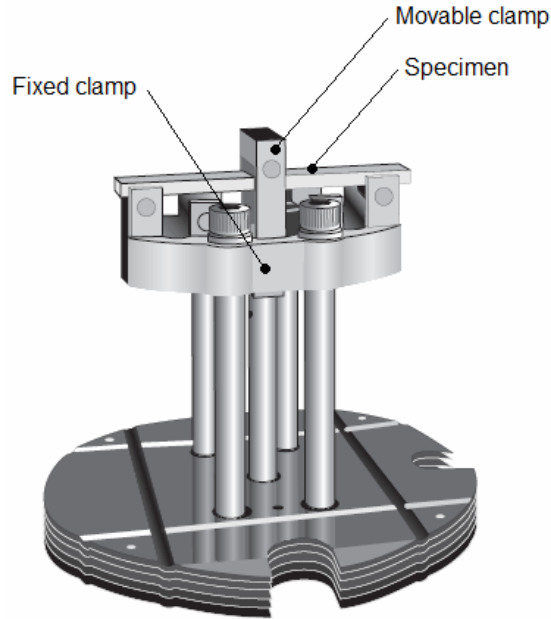
Figure 3.6 DMA – Three - point bending clamp [93].
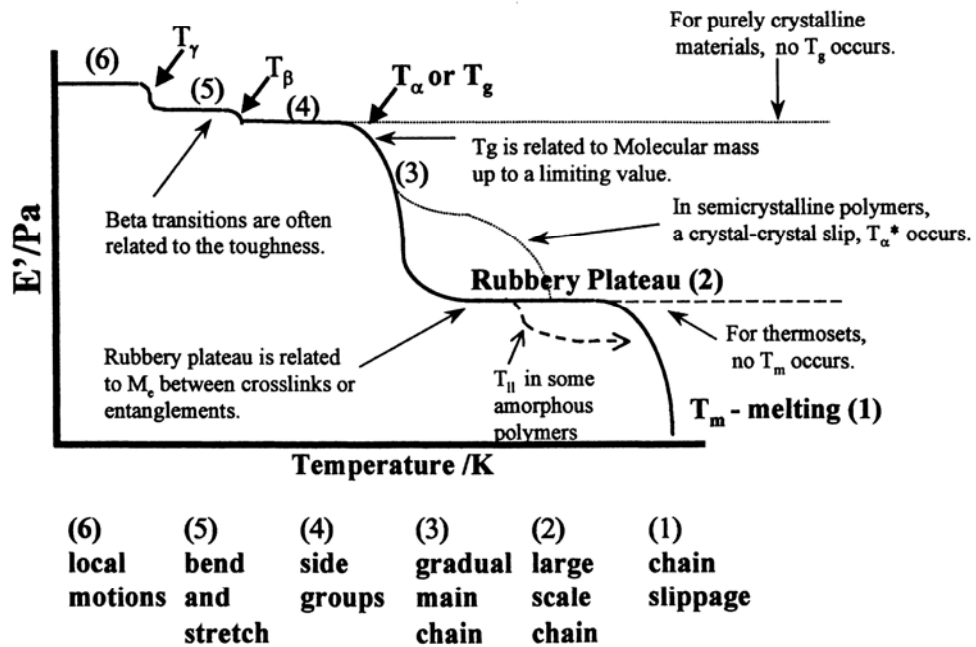
Figure 3.7 DMA temperature scan of a polymer [94].

DMA has numerous advantages over other thermal analysis techniques. The stiffness of a material is determined as the slope of the stress-strain curve from tensile testing at a fixed temperature. In case of polymers, the modulus depends on temperature and strain rate.

DMA gives the instantaneous modulus value each time a sine wave is applied and hence the variations of the modulus with temperature (or frequency) can be determined with a single test.

Polymers undergo transitions as the material is heated (or cooled) such as the glass transition. These transitions are important as the modulus changes when the material is heated (or cooled) past these transitions. DMA has the ability to detect these transitions. Figure 3.7 shows a temperature scan of a polymer, i.e., the polymer specimen is heated from a low temperature at a fixed rated while an oscillatory force is applied. It shows the various transitions (step change in the elastic or storage modulus) which a typical polymer would undergo as the temperature is increased.
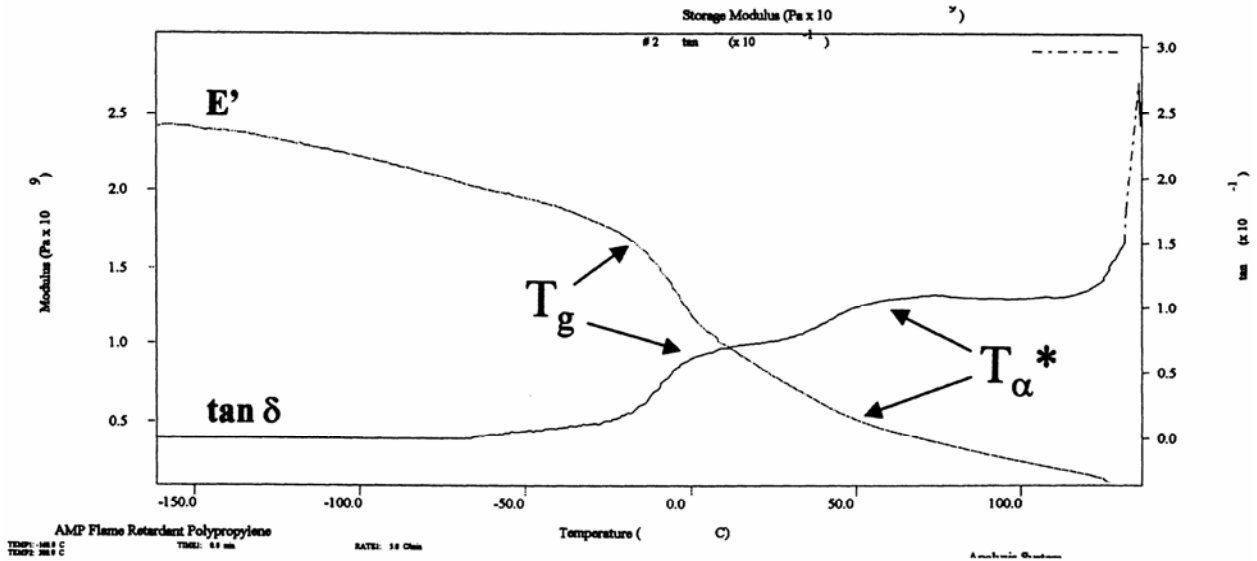
Figure 3.8 DMA temperature scan of polypropylene [94].

Some of the transitions, particularly those at lower temperature [e.g.: α, β transitions shown in Figure 3.7] are too small to be detected in other thermal analysis techniques like DSC or TGA, while they are readily detected in DMA. This is the case with polypropylene which undergoes two transitions as the material is heated from -50°C to 100°C. Figure 3.8 shows the typical DMA plot of polypropylene showing the variation of the storage modulus and the tan δ with temperature. The plot shows two transitions namely the glass transition (T_g) also known as 'α−transition' at a lower temperature range

of -10°C to 25°C and secondary glass transition called the α* transition [94] in the temperature range of 45°C to 90°C. Finally, the size of the specimen required for testing in a DMA is usually small.

3.2.3 Creep testing

As stated earlier, creep consists of loading a specimen under constant load. There are variety of creep testing equipment available based on the loading methods. One of the most common and simplest creep testing equipment uses dead weights to apply the required load. These weights are suspended at one end of the specimen while the other end is fixed. Systems with mechanical advantage using levers are also available. However, when dealing with multiple tests at high stresses, this type of creep testing setup is very inconvenient. More sophisticated and accurate methods use hydraulic (or pneumatic) drives to achieve the loading condition but are more expensive and complicated.

3.2.3.1 Description of the creep fixture
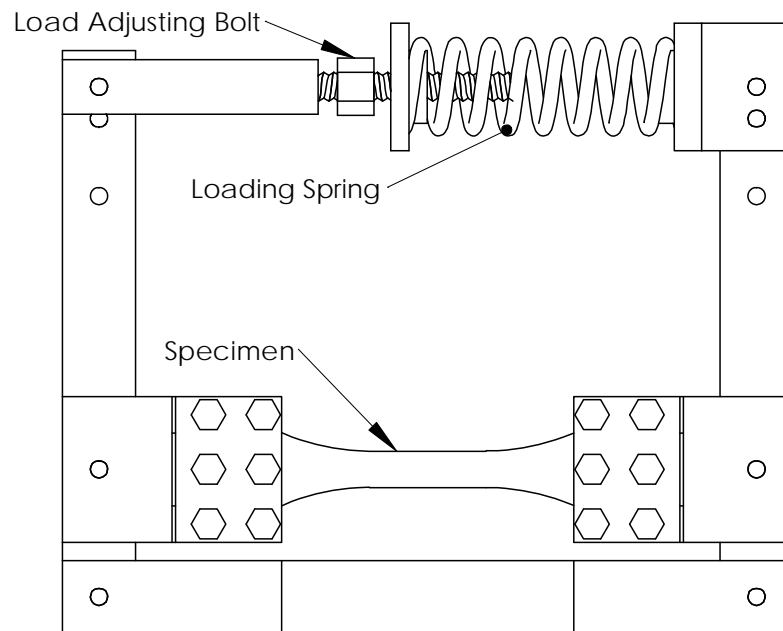
Figure 3.9 Creep fixture [95].

53

The creep testing fixture used in the present study is as shown in Figure 3.9. The fixture was designed by Houston *et al.* [95] for the Automotive Composites Consortium Group to study the environmental effects on the creep of polymeric composites (U.S patent # 5,798,463). The fixture is an all steel structure (304-SS) and uses a spring (material: chrome silicon) to apply the stress on the specimen. The fixture has a mechanical advantage with the magnification factor being '4'. Thus, a wide range of stresses can be applied using the fixture, with the maximum being 158 MPa for specimens with gauge length cross-sections of 12.70 mm x 3.2 mm.

According to the American Society for Testing and Materials (ASTM) [96], tensile specimen having geometry given in ASTM D638 [97] should be used. In this work, however, the creep specimen is a dog-bone shaped, Figure 3.10, which was designed to fit the fixture has been used. Specimens with uniform width can also be used.
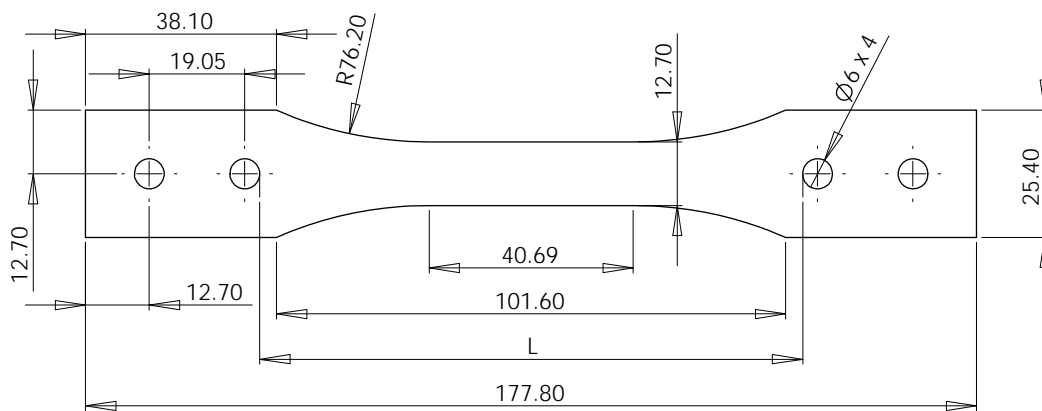
Figure 3.10 Creep specimen [95].

The setup procedures provided in the original fixture documentation [95] is as follows:
(i)   align the loading spring in the fixture.
(ii)   place the specimen along with the mounting plate cover on the grips so that the holes in the specimen, cover and the grips are aligned.
(iii)   tighten the bolts as shown in Figure 3.11 using a socket torque wrench to approximately 5.4 N-m. The load adjusting bolt is then turned to compress the spring to the test stress level. The amount by which the spring has to be compressed can be found out by using the relation,

$$\text{Spring deflection, } x = \frac{(\sigma_{specimen})\,(A_s)}{m_a * k_s} \tag{63}$$

where $\sigma_{specimen}$ is the test stress level,

A_s is the area of the specimen,

m_a is the mechanical advantage of the fixture ($m_a = 4$),

k_s is the stiffness of the loading spring (can be found out by a compression test on the spring)
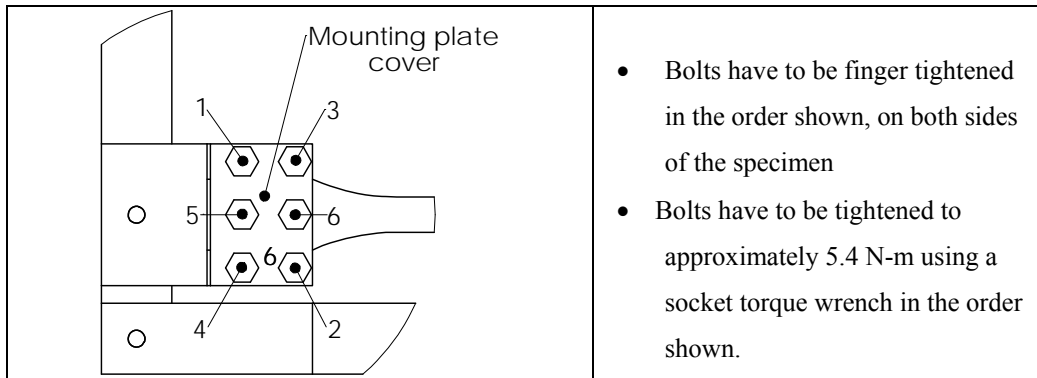
Figure 3.11 Steps for tightening fixture bolts [95].

The fixture should then be left undisturbed over the creep test duration. The distance 'L' as shown in Figure 3.10 should be measured before and after the creep tests.

3.2.3.2 Advantages of the creep fixture

This spring loaded creep fixture has numerous advantages, the foremost being its compactness. The fixture design is simple and hence inexpensive. They are relatively easy to use with smaller setup times. Multiple units can be built at low cost and can be used for simultaneous testing at different conditions. The entire fixture can easily fit into an environmental chamber (an oven in our case) and hence can be used to study the environmental effects on the creep characteristics. The fixture can be used over a wide range of stresses, covering the test range of most polymeric materials.

3.2.3.3 Disadvantages of the creep fixture:

The original creep fixture design also has a number of disadvantages:

1. One of the major disadvantages of this fixture is the relaxation of the load with creep. As mentioned earlier, the fixture has a mechanical advantage of '4' meaning that, if 100 N force is applied by the spring, then the net force acting at the specimen would be 400 N. However, if the specimen undergoes a deformation of 1 mm, the spring compression reduces by 4 mm and subsequently there would be a reduction in the load applied on the specimen. Hence, it has to be used with caution. The designers of the fixture suggest that if the spring deflection/compression decreases by 10% of the initial loading, the test has to be terminated. This is in contrast to the limit of 1% in accordance to the ASTM standards [96].

2. In a creep test, it is important to achieve instantaneous loading. According to ASTM standards [96], the loading and unloading has to be carried out rapidly and smoothly. It is preferred that the load be applied within 1 to 5 seconds. As mentioned earlier, the loading is achieved by turning the 'load adjusting nut' in the fixture. Higher the stress, greater the spring compression required which implies higher number of revolutions of the loading bolt and hence more the time taken to apply the load. Thus with the existing fixture design, it is not possible to apply the load in such short durations. Also the application of the load is intermittent due to the method of loading.

3. To determine the linear viscoelastic region in a polymer, Boltzmann superposition principle is used – according to which, recovery tests have be carried out. Also determination of the parameters of the non-linear viscoelastic equation requires performing recovery following creep. Recovery involves removing the applied stress instantaneously after the creep duration. However, with this fixture design, it is not possible to remove the applied load instantaneously.

4. The distance between the holes, 'L' as shown in Figure 3.10 is a critical parameter in the specimen. The specimen has to be machined accurately, especially the distance between the holes denoted by 'L' in Figure 3.10. Due to the mechanical advantage of the fixture, even slight changes in this dimension can notably affect the applied load.

3.2.3.4 Fixture modifications

As mentioned above, achieving rapid and smooth loading and unloading is an important characteristic of a creep fixture, which cannot be achieved with the original fixture design. Modifications to the creep fixture were needed to rectify the problem. While several design modification options were considered, only the actual changes to the fixture will be discussed here. Care was taken during the design of the modifications not to affect the existing functionality/design of the fixture.

Two changes were proposed and were successfully incorporated to the original fixture:

1. *Cam attachment*
   A cam attachment as shown in Figure 3.12 was designed to achieve rapid loading and unloading. The part drawings can be found in appendix B.
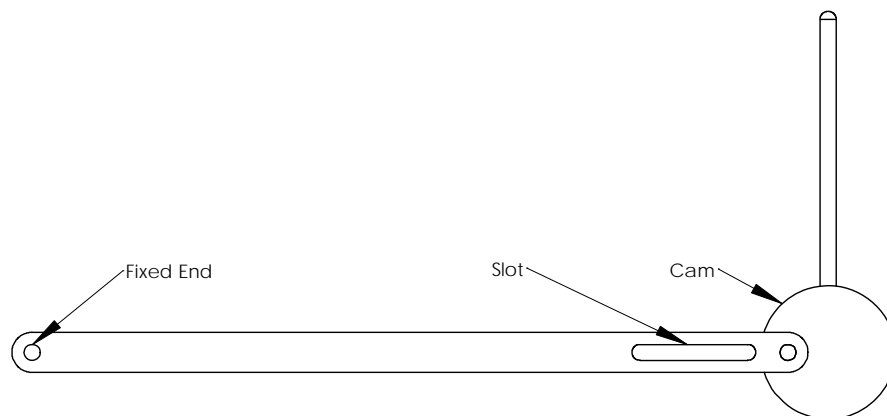
Figure 3.12 Cam assembly.
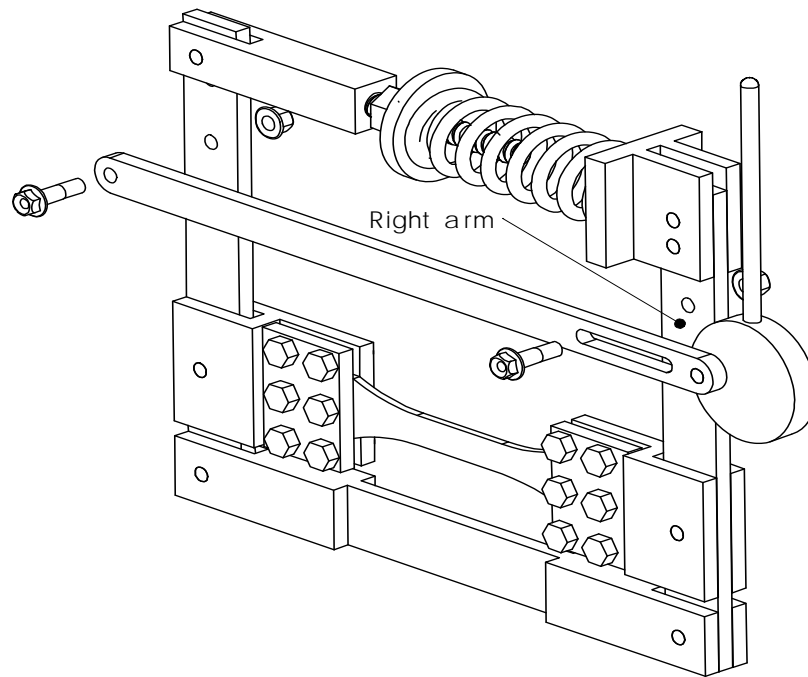
Figure 3.13 Exploded view of fixture and cam assembly.

The attachment consists of two parts – a holding bar and a cam. The holding bar has a hole at one end which is used to fix the bar to the fixture. It has a slot and a hole at the other. The cam is attached to this end of the bar as shown in Figure 3.12. The slot is provided to facilitate free movement of the right arm (as shown in Figure 3.14) of the fixture during loading and unloading. The bar can be attached to the fixture as in Figure 3.13. The unloaded and loaded positions of the fixture are illustrated in Figure 3.14(a) and (b) respectively.

During setup and recovery, there should not be any force acting on the specimen. This condition can be attained by turning the cam to the position shown in Figure 3.14 (a). In this position, the right arm of the fixture is perpendicular to the base of the fixture and all the force applied by the spring is transferred to the holding bar through the cam. Hence, there is no force acting at the grips in this position of the cam and the specimen can be fastened to the fixture.

(a) (b)
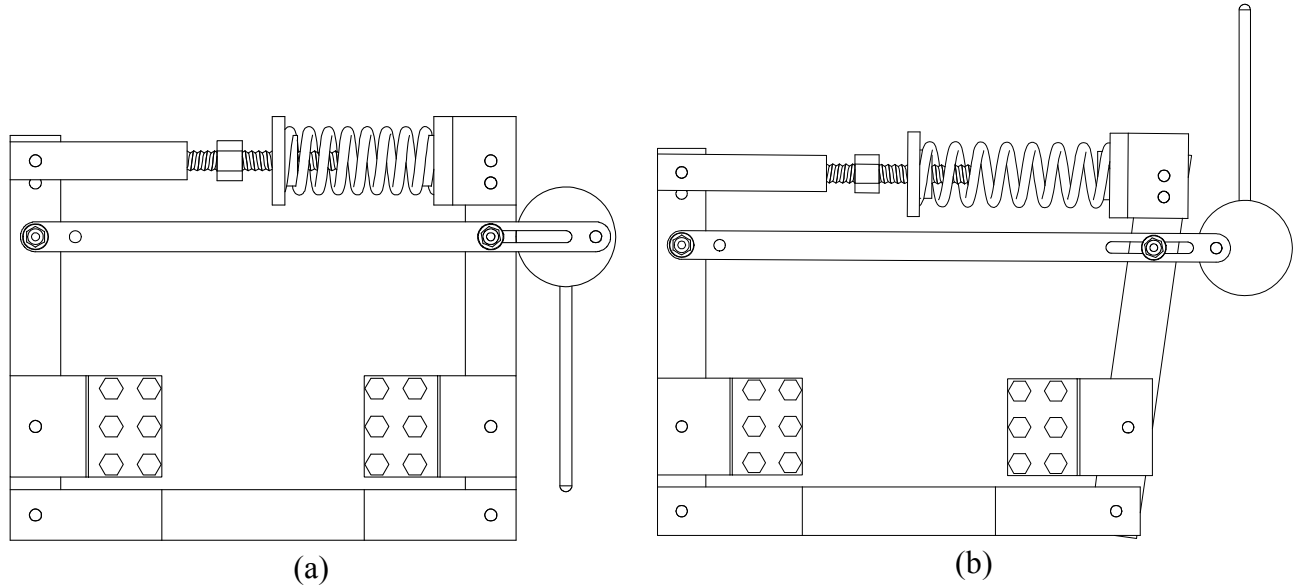
Figure 3.14 Cam positions during (a) setup and recovery (unloaded) (b) creep (loaded).

After setup, the cam can be released to the position shown in Figure 3.14 (b) to start the creep test. In this position, the force on the holding bar is released and is applied at the grips and hence the specimen. A locknut was used to ensure that the bolt holding the slot end of the bar is not over tightened. This end was lubricated to ensure smooth movement of the right arm of the fixture.

2. *Modifications to the right lever arm – addition of a slot*

While the cam attachment described above allows for instantaneous unloading, it does not however allow for the free movement of the specimen after unloading required for recovery, Figure 3.14 (b). To achieve this, a slot was machined from the existing hole on the right arm of the fixture. During machining, the left half of the original hole was left intact to ensure that the original functionality of the fixture is not affected. The original and the modified right arm of the fixture are as shown in Figure 3.15.

The sectional view 'A' of the fixture as shown in Figure 3.16 (a) during creep and recovery (or setup) of the original and modified fixtures are shown in Figures 3.16 (b), (c), (d) and (e). It can be seen from (c) and (e) that the machining of the slot does not change the original loading characteristics of the fixture. Furthermore, Figure 3.16

(d) shows that the addition of the slot provides the necessary clearance for the grips and hence specimen, to recover after removing the load.
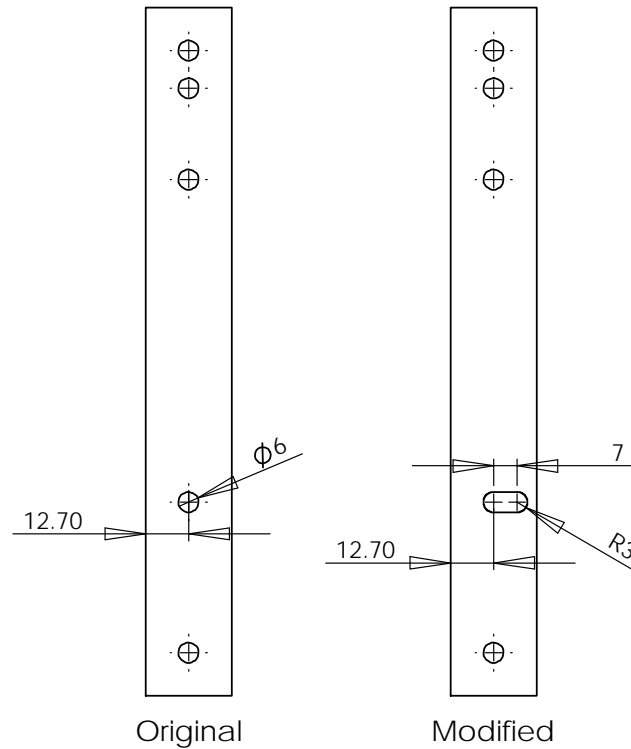
Figure 3.15 Original and modified right lever arm of the fixture.

It is obvious that even after the slot has been made, the specimen will have to recover against the weight of the grips. Using a load cell, it was found that the load reduces to zero when the cam is rotated to the recovery position, Figure 3.14 (a). Figure 3.17 shows a typical creep and recovery curve (30 minutes creep and 30 minutes recovery) of GMT specimen. The figure also shows the predicted curve based on Boltzmann superposition law. It can be seen that the strains return to zero at the end of recovery. Furthermore, there is excellent agreement between the experimental and predicted creep curves.
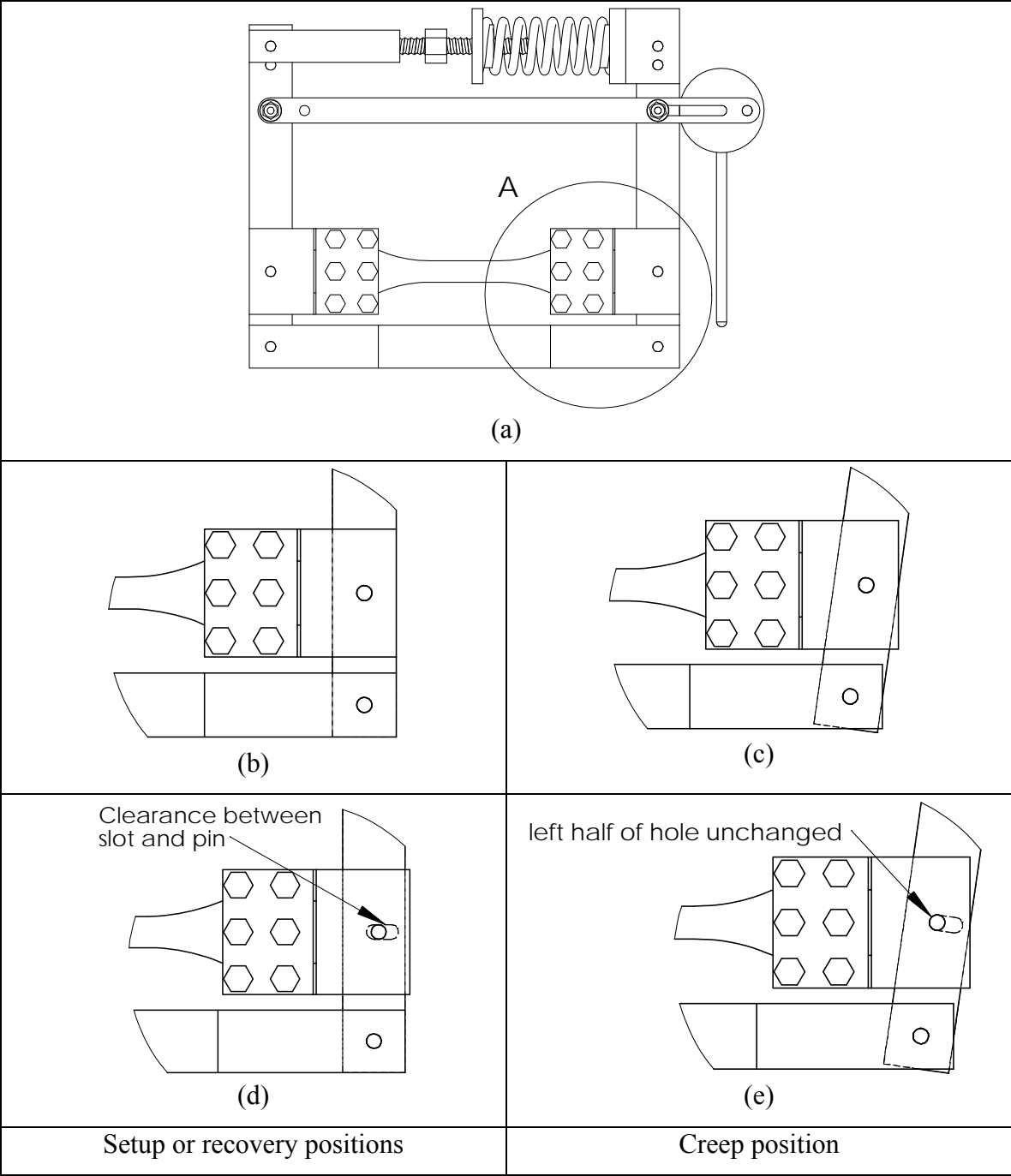
Figure 3.16 Positions of the original [(b) and (c)] and modified [(d) and (e)] fixture during recovery (or setup) and creep.

61
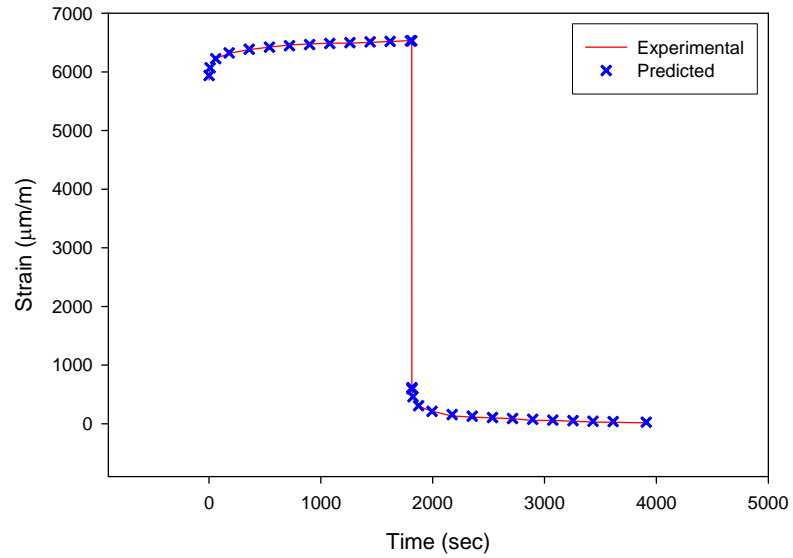
Figure 3.17 Experimental and predicted (Boltzmann superposition principle) creep and recovery curves.

3.2.3.5 Creep test setup

According to the setup details given in the documentation [95] for the fixture, the spring deflection has to be calculated using equation (63). The spring is then compressed by this amount using the load adjusting nut. However, certain measurements errors were associated with this loading procedure and led to poor repeatability. This was due to a number of factors including:

1. The reference point from which the spring deflection has to be applied could not be found accurately.
2. The documentation does not mention the location at which the spring deflection has to be measured. Two different locations 'A' and 'B', Figure 3.18, were considered, however neither of them provided satisfactory results. The measurements made at location 'A' were not accurate while that at 'B' were incorrect due to misalignment between the bottom holder and top holders (Figure 3.18). The spring inherently develops a curvature in the loaded position. This is because the top holder is connected to the right arm using two pins and does not

realign itself as the load is applied. Instead, it rotates as shown in Figure 3.19 (b), leading to misalignment between the two axes.
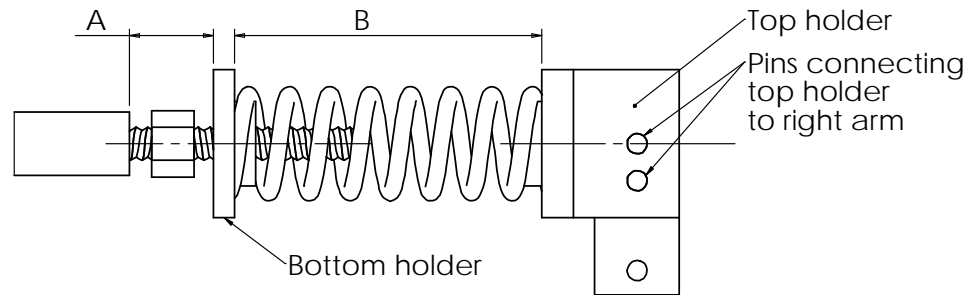
Figure 3.18 Measurement of spring deflection.
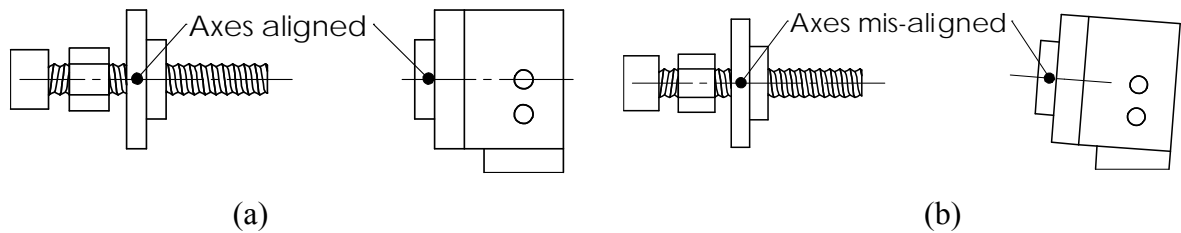
Figure 3.19 (a) No load position (setup) and (b) Load applied
(Spring excluded for clarity).

Instead of calculating the spring deflection and adjusting the loading bold, a direct load calibration procedure using a load cell was used to setup the creep fixture.

3.2.3.6 Load cell

A strain gauge based Honeywell load cell capable of measuring loads up-to 1000 lbs [approximately 4450 N] was used for calibrating the fixture. The specifications of the load cell are given in Appendix A. The load cell was general purpose unit and hence suitable attachments had to be designed for mounting onto the creep fixture. Figure 3.20 shows the load cell with its attachments. Individual part drawings of the load cell attachments are provided in the Appendix B. As mentioned earlier, the overall length (and the distance between the holes – 'L' shown in Figure 3.10) of the load cell is a critical parameter. Thus, to obtain an overall length of the load cell (with the attachments) as 177.80 mm (length of the specimen) while maintaining the alignment between the two

flat ends shown in Figure 3.20, a lock nut arrangement had to be provided. The attachment was machined from steel stock very similar to that of the creep fixture.
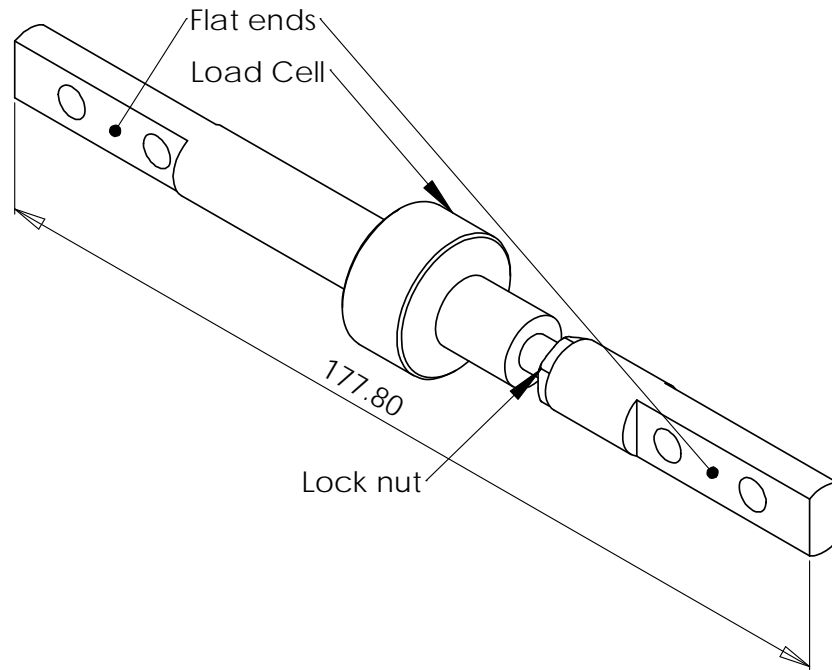
Figure 3.20 Load cell.

3.2.3.7 Creep fixture calibration

Each creep fixture was calibrated before every test using the load cell. The calibration procedure followed is given below:

1. The specimen dimensions are measured and the force required is calculated based on the required applied stress.
2. The cam is set to the setup position as in Figure 3.14 (a).
3. The load cell and the mounting plate cover are aligned over the grips and the bolts are tightened in the order shown in Figure 3.11.
4. The cam is now set to the creep position as shown in Figure 3.14 (b).
5. The loading adjusting bolt (Figure 3.9) is turned until the desired load is achieved.
6. The dimension 'A' shown in Figure 3.18 is noted (reference).
7. The cam is set back to the setup position and the load cell is carefully removed.

Once the creep fixture has been calibrated at the intended stress level, the specimen is mounted on the creep fixture and the load is then applied by rotating the cam to the creep position – Figure 3.14 (b). After the desired creep duration, the cam is set back to the recovery position. The recovery strains over the intended duration are then measured and finally, the specimen is removed from the creep fixture.

3.2.3.8 Strain measurement

All the creep specimens were strain gauged as per procedures recommended for polypropylene. The specifications of the strain gauge and the adhesive are given in Appendix A. Although polypropylene is difficult to adhere to, it was possible to mount the gauges consistently after some trial-and-error (especially with the type of adhesive used). The adhesive used was suitable over the temperature region of interest (operating limit < 95°C, maximum test temperature was 90°C). The strain was measured using a National Instruments Data acquisition system. The software for the data acquisition was developed using Labview [98]. The data acquisition system was capable of acquiring 32 channels of strain data.

3.2.3.9 Oven

All the creep tests were carried out in a temperature controlled environment provided by an oven. A horizontal air flow oven was used, which consists of a turbo blower used to re-circulate air over the heating element to provide fast and uniform heating over the entire volume of the oven. The temperature inside the oven is monitored by a microprocessor based feed back controller, using thermocouples inside the oven. The temperature in the oven was also monitored throughout the test using an external thermocouple. Typically four creep tests were carried out simultaneously for which, suitable trays to hold the creep fixtures inside the oven were designed.

CHAPTER 4

RESULTS AND DISCUSSION:
THERMAL ANALYSIS AND TENSILE TESTS

4.1 Differential Scanning Calorimetry

Two thermal analysis techniques used to characterize the physical properties of the GMT composites were Differential Scanning Calorimetry (DSC) and Dynamic Mechanical Analysis (DMA). Details of the experiments and results for both sets of tests are given in this section.

4.1.1 Experimental Details
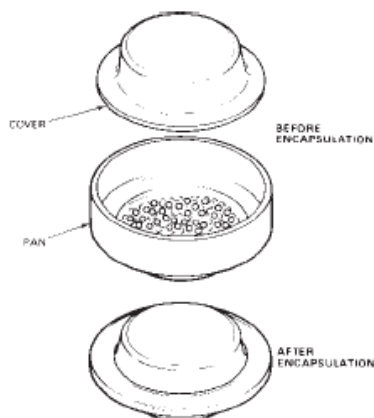
Figure 4.1 Hermetic pan for DSC [92].

Modulated Differential Scanning Calorimetry (MDSC) was carried out to determine the thermal transitions, crystallinity and the crystallization kinetics of the polypropylene matrix. The instrument was calibrated for the baseline, temperature and heat capacity to obtain the required instrument calibration parameters. The samples for the tests were cut from the center of the test plaque and encapsulated using a hermetic pan as shown in Figure 4.1 Care was taken during preparation of the sample to ensure that the mass of the sample material was between 12 to 13 milligrams and that the pan was properly sealed.

The MDSC experiment performed was a heat-cool-heat-cool-heat experiment. The material was heated from -30°C to 220°C at 5°C/min for all of the three heating stages of the experiment. Two cooling rates, 20°C/min and 10°C/min, were used to cool the material from 220°C to -30°C. The temperature was modulated at an amplitude of 1°C/min.Three trials were carried out with the specimen masses equal to 13, 12.7 and 13 mg, respectively.

4.1.2 Typical MDSC output

Figure 4.2 shows a typical plot of the MDSC temperature scan for the GMT composite (trial 1). The modulated scan provides the reversing, non-reversing and the total heat flow profiles.
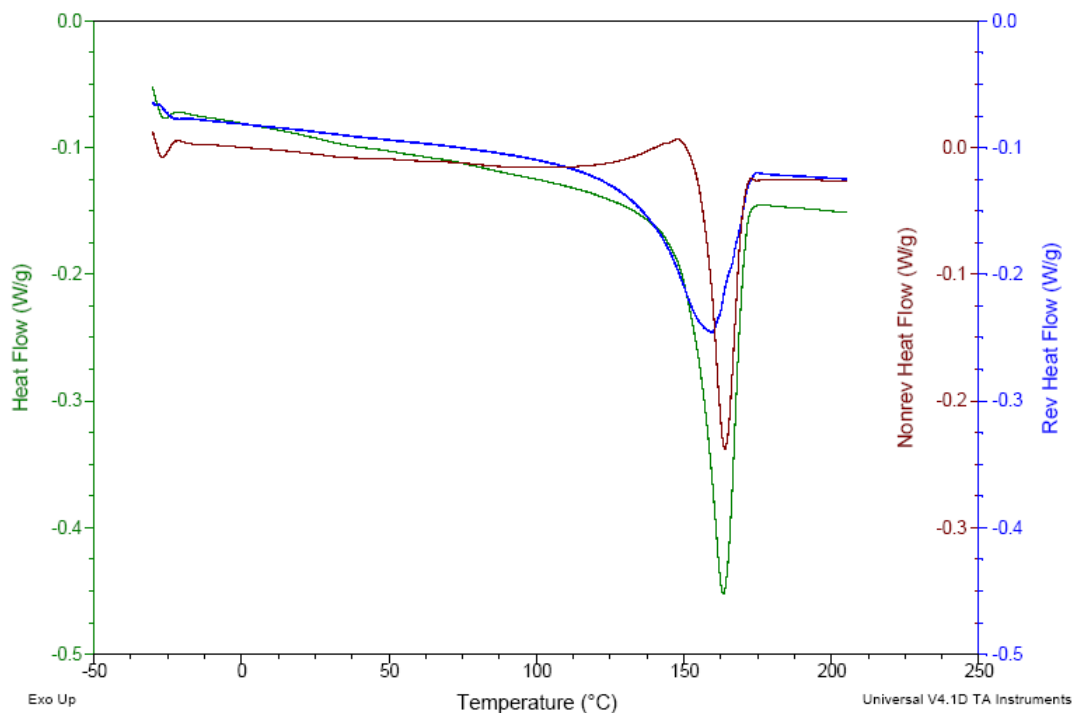
Figure 4.2 Typical MDSC scan for GMT composite.

The reversing heat flow shows a melting endotherm between 100 – 175°C while the non-reversing heat flow shows an exothermic event representing crystallization followed by a melting endotherm. The total heat flow, the sum of the two heat flows shows a single melting endotherm. There is no step change in any of the heat flows and hence glass

transition cannot be identified using MDSC. It is known that the glass transition temperature of polypropylene is approximately 0°C.

4.1.3 Melting point

The peak of the total heat flow curve is considered as the melting point of the material as shown in Figure 4.3. The melting points of the material for the three trials were 163.4°C, 164.0°C and 164.3°C with a mean of 164.0°C.
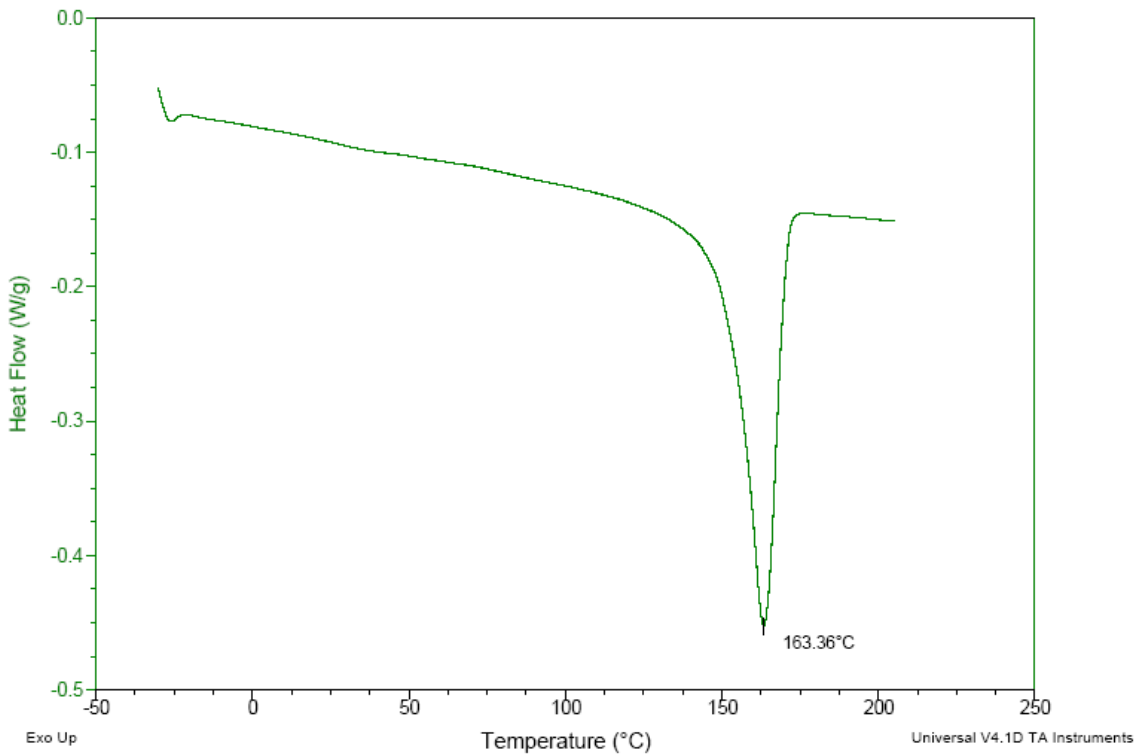
Figure 4.3 Endothermic peak showing the melting point of the material.

4.1.4 Degree of Crystallinity

The polypropylene crystallinity was determined by MDSC from the heat of fusion, which is the area under the melting transition. The degree of crystallinity (DOC) of the composite was calculated using the relationship proposed by Lee *et al.* [99],

$$\% DOC = \frac{\Delta H_m + \Delta H_c}{\Delta H_f (1 - W_f)} \times 100\% \tag{64}$$

where, ΔH_m is the heat of fusion (endothermic),

ΔH_c is the heat of cold-crystallization (exothermic),

ΔH_f is the heat of fusion for a 100% crystalline material,

W_f is the weight fraction of the fiber content.

Although the above expression was developed for DSC, it can also be used for MDSC by considering ΔH_m as the sum of the heat of fusions from the reversing and the non-reversing heat flow curves. From the non-reversing heat flow curve in Figure 4.2, it can be seen that the material undergoes crystallization as it melts. The area under this portion of the curve gives the heat of cold crystallization. Since the supplier does not provide information on the exact type of polypropylene used for the GMT, the heat of fusion (ΔH_f) for 100% crystalline isotactic polypropylene will be used for comparing %DOC. The reported value of isotactic polypropylene, the most common form, is 165 J/g [100].

The value of the weight fraction of the fiber content in the composite, W_f, was determined using thermo-gravimetric Analysis (TGA). Samples weighing about 30 mg of the GMT material were heated to about 450°C, at which the matrix decomposed. Since the glass fibers do not decompose or burn at this temperature, they remain in the TGA pan after the polypropylene matrix is burnt off. The TGA software calculates the weight fraction from the residual weight after the test. Three trials performed gave weight fractions of 38.60, 43.75 and 35% resulting in an average weight fraction of 39.12±4.4 %. For crystallinity calculations, the weight fraction of the material will be considered as 39.12% (0.391). The weight fraction determined from matrix burn off tests of samples of about 25 x 25 mm was slightly higher than the above value. However since the specimen size used for DSC and TGA are similar, the fiber weight fraction obtained from TGA has been employed for crystallinity calculations.

The heats of fusion in both reversing and non reversing heat flow curves and cold crystallization are shown in Figure 4.4. The area under the curve required to determine

the heat of fusion and crystallization was found using Universal Analysis Software v4.1D, developed by TA instruments.

The heats of fusion from reversing and non-reversing heat flow curves, the heat of crystallization and the crystallinity of GMT based on equation (94) are summarized in Table 4.1. The as-received crystallinity of the material ranges between 49.5 % - 54.2 %.
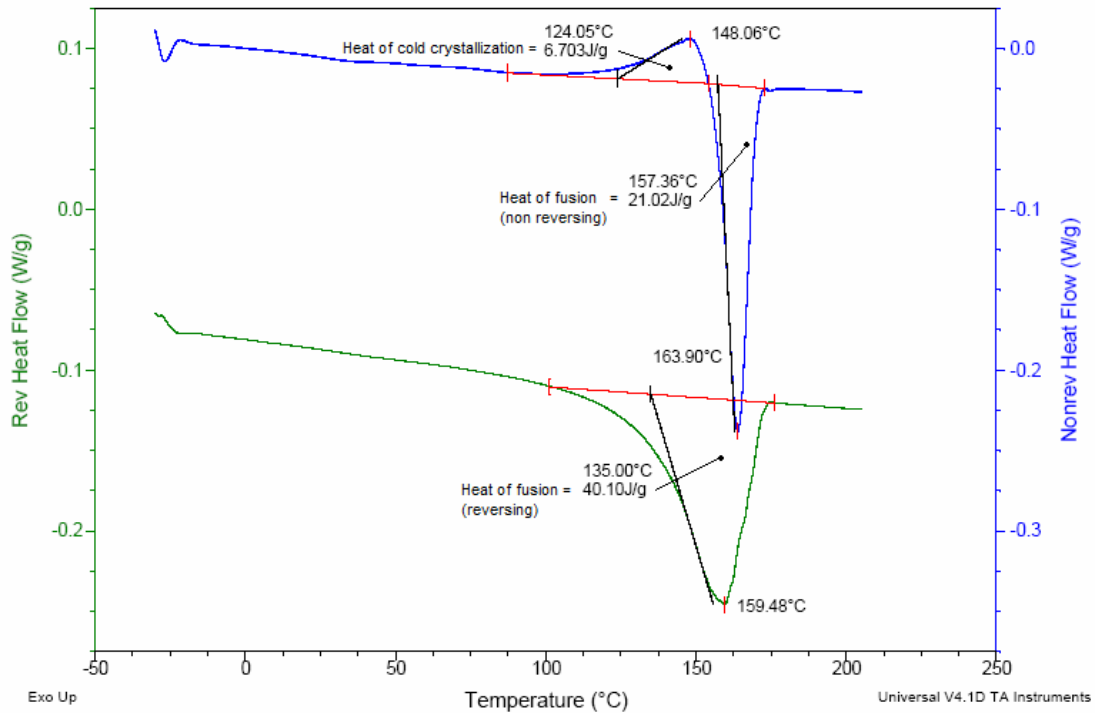
Figure 4.4 Heat of fusion and crystallization to determine initial crystallinity of GMT.

Table 4.1 Degree of crystallinity of long fiber GMT (base material).

Specimen	Heat of fusion (J/g)		Heat of cold crystallization (J/g)	% DOC
	Reversing	Non-reversing		
1	40.10	21.02	6.70	54.17
2	35.93	19.11	5.23	49.59
3	30.19	25.36	3.45	51.87

70

4.1.5 Crystallization kinetics of GMT

As mentioned earlier, the material was cooled at two cooling rates. Figures 4.5 and 4.6 show the heat flow curves obtained during cooling at 10°C/min and 20°C/min, respectively, for the three trials carried out. While both heat flow curves show a crystallization exotherm, the crystallization exotherm is wider at the higher cooling rate (20°C/min).

The temperatures at the peak of the crystallization exotherm for cooling at 10°C/min are 117.57°C, 117.11°C and 117.51°C and that at 20°C/mn are 112.08°C, 110.99°C and 111.20°C. This indicates that the peak of crystallization exotherm shifts towards lower temperature as the cooling rate is increased.
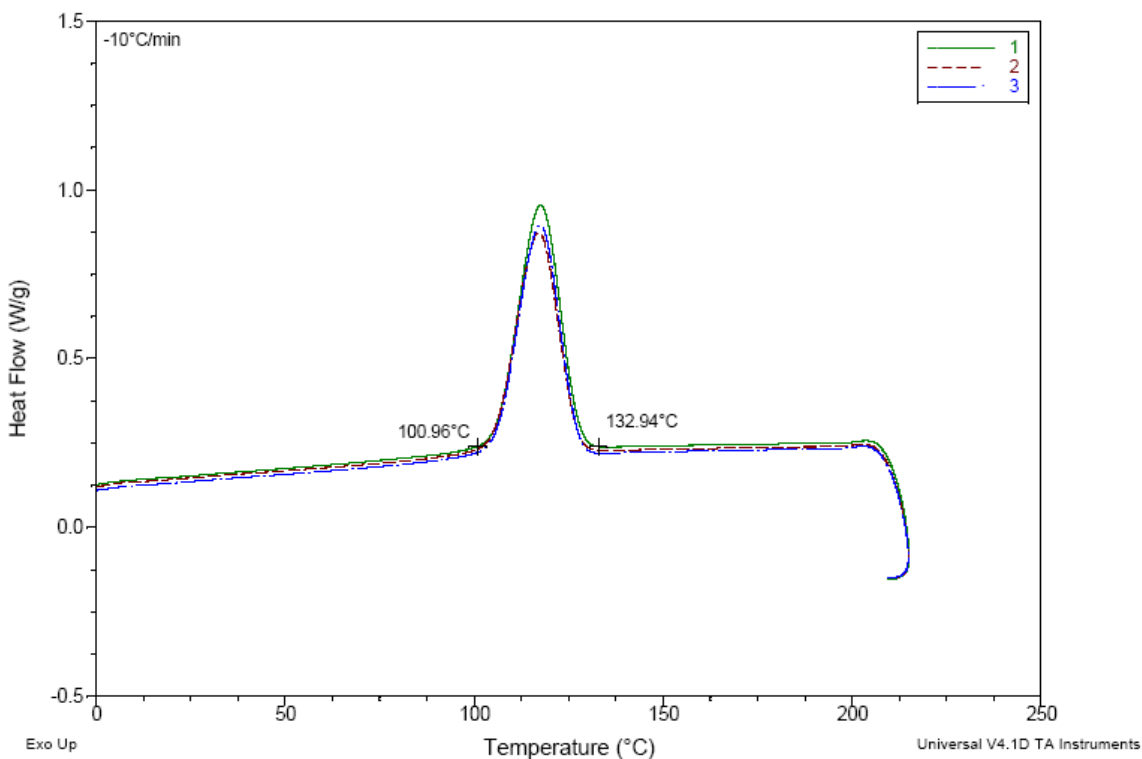
Figure 4.5 Heat flow curve obtained at cooling rate of 10°C/min.
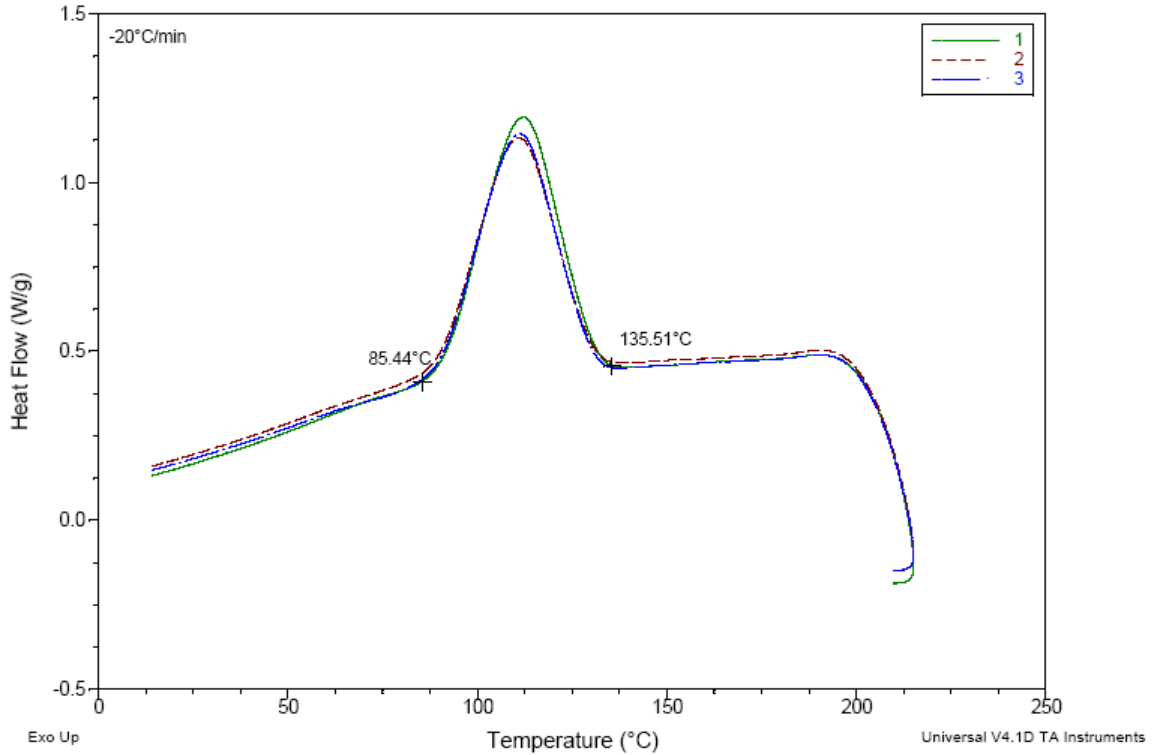
Figure 4.6 Heat flow curve obtained at cooling rate of 20°C/min.

Table 4.2 Calculated % DOC obtained at two cooling rates (during cooling).

Specimen	Heat of crystallization (J/g)		% DOC	
	-10°C/min	-20°C/min	-10°C/min	-20°C/min
1	58.07	56.41	57.81	56.16
2	52.45	50.3	52.21	50.07
3	54.73	53.11	54.48	52.87

The heat of crystallization and crystallinity levels obtained for the above cooling curves are given in Table 4.2. The % DOC is obtained using equation (64) by considering $\Delta H_m = 0$. The heat of crystallization of specimen 1 is higher than that of the other two indicating slightly lower fiber content in this sample.

After cooling the specimen, an MDSC scan was carried out to determine the characteristics with known thermal history. The total, reversing and the non-reversing

heat flows of the sample at base/as-received state and that after cooling at 10°C/min and 20°C/min, respectively, are given in Figure 4.7. Changes in the shape and the location of the melting endotherm can be observed. There is a shift in the melting temperature. The melting points of the as-received and those after the two cooling scans are shown in Figure 4.8. It can be seen that the melting point of the as-received material is higher than those of the other two conditions. Moreover, the melting point of the specimen after cooling at 20°C/min is higher than that cooled at 10°C/min indicating that the melting temperature increases with cooling rate. This behaviour has also been observed in other semi-crystalline polymers such as polyethylene [101].
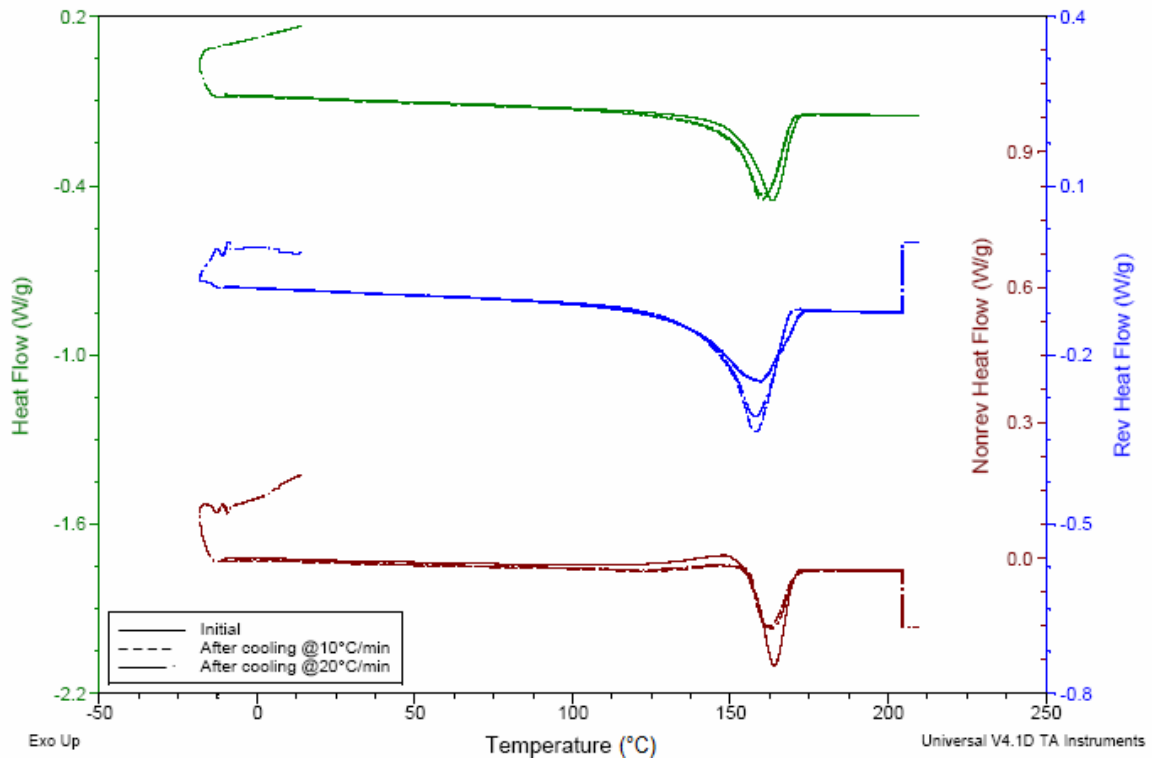
Figure 4.7 Heat flow of the base material and after cooling at 10°C/min and 20°C/min.

Table 4.3 gives the heats of fusion and cold crystallization and % DOC after cooling at the two rates obtained from the MDSC temperature scan. As expected, the degree of crystallinity decreases with the increase in cooling rate. Further, the heat of crystallization for the material cooled at 10°C/min is lower than that cooled at 20°C/min. Further, the % DOC obtained from the cooling (during crystallization) and the heating cycles (during

melting) (Tables 4.2 and 4.3 respectively) are almost equal (heating % DOC slightly less than cooling %DOC).
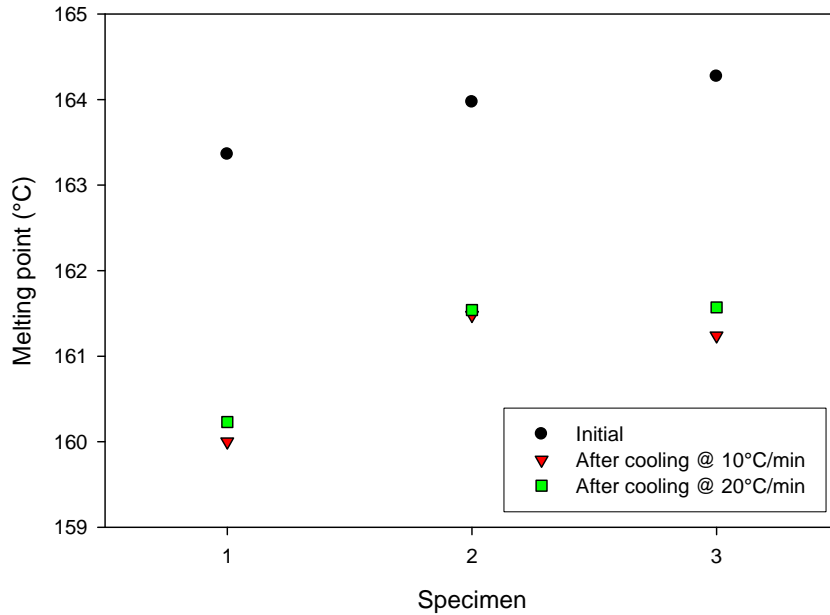
Figure 4.8 Melting point of the base material and after
cooling at 10°C/min and 20°C/min.

Table 4.3 % DOC of GMT after cooling at two cooling rates (from the heating cycle).

Specimen	Heat of fusion (J/g)		Heat of cold crystallization (J/g)	% DOC
	Reversing	Non-reversing		
After cooling at 10°C/min				
1	46.91	13.25	2.215	57.68
2	36.12	16.1	0.985	51.00
3	40.88	13.54	1.241	52.94
After cooling at 20°C/min				
1	38.5	20.8	6.368	52.69
2	36.24	18.86	5.191	49.68
3	30.58	24.94	3.967	51.32

The % DOC of the base material and that obtained after cooling at the two rates are shown in Figure 4.9. The % DOC of the base material for two trials falls in between that

74

obtained at the two cooling rates but is closer to that obtained at 20°C/min for one trial. This implies that the base material was most probably cooled between 15°C/min to 20°C/min during compression moulding.
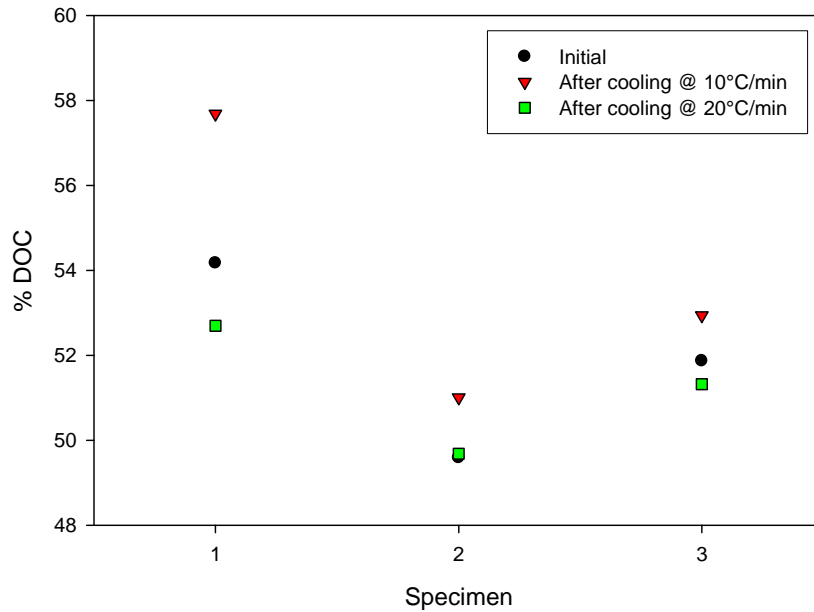
Figure 4.9 %DOC of the as-received and after cooling at two different cooling rates.

4.2 Dynamic Mechanical Analysis

4.2.1 Experimental Details

The second thermal analysis technique used was Dynamic Mechanical Analysis (DMA). DMA was carried out to determine the variation of the modulus with temperature, transitions in the material and the isotropy of the material. The instrument was calibrated following the instructions for load and clamp calibration. As the material was relatively stiff, a three-point bending clamp, as shown in Figure 3.6, was used. The distance between the two supports was 50 mm and the load was applied at the center of this span. A rectangular specimen with a nominal length of 60 mm and width 12.8 mm was used. DMA specimens were prepared by waterjet machining of 3 mm thick GMT moulded plaques. Specimens were cut in three directions as shown in Figure 4.10. Two specimens in each direction were tested.
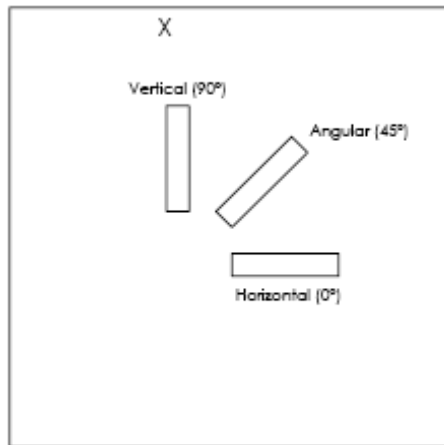
Figure 4.10 Three orientations of DMA samples tested.

The oscillatory frequency for DMA testing was 1 Hz for all of the tests. The amplitude of the oscillations for these tests was determined using a strain sweep experiment. A strain sweep experiment consists of measuring the dynamic properties of the material at strains of various amplitudes for a given frequency. The plot of the storage modulus versus amplitude can be used to determine the amplitude within the linear viscoelastic region and the force limit of the instrument. A strain sweep was carried out over an amplitude

76

range of 10 – 280 μm at increments of 10 μm. Amplitudes above 125 μm could not be applied as the equipment reached its force limit, i.e., 18 N. Figure 4.11 shows a plot of storage modulus versus amplitude. As shown, the variation of storage modulus between 30 μm and 100 μm is less than that below 30 μm. Using amplitudes at the lower end of the range may lead to test instabilities. Moreover, the instrument may not be able to reach the set amplitude (for higher amplitudes) during a cooling test since the polymer stiffness is expected to increase at sub-ambient temperature. By considering both factors, the most suitable amplitude for our tests was 80 μm.
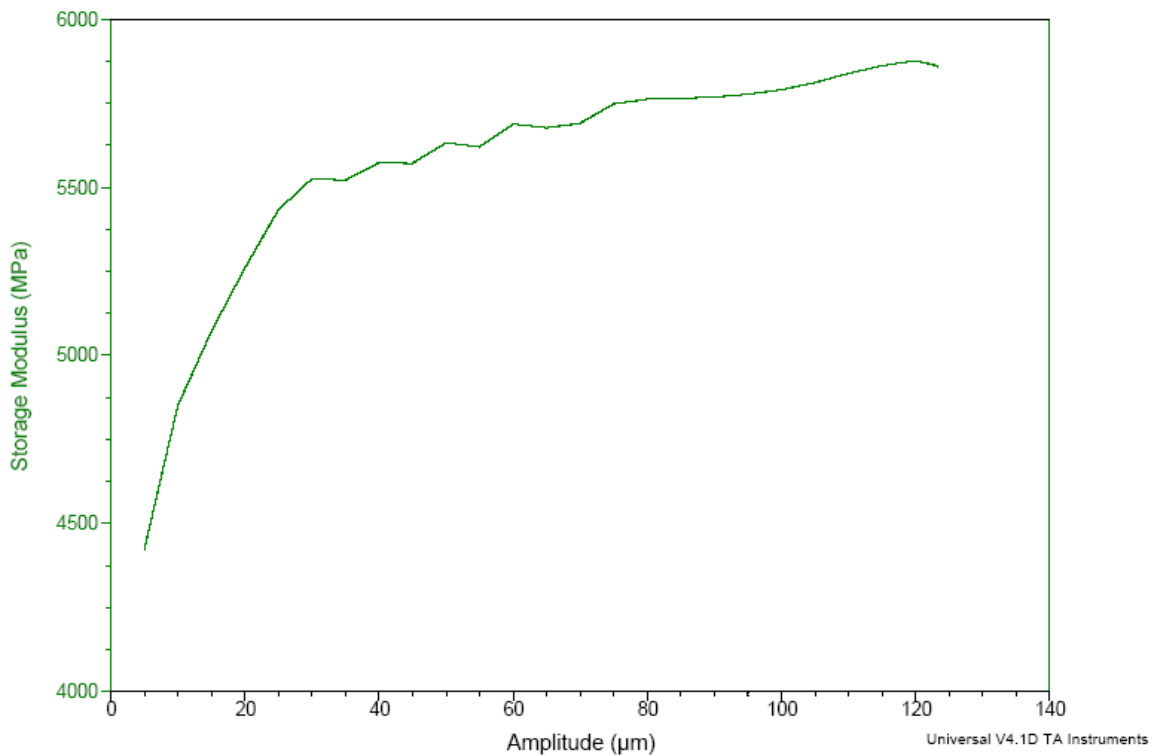
Figure 4.11 Strain sweep – Storage modulus versus test amplitude.

Using the above mentioned test parameters, a DMA temperature scan was carried out at constant frequency. The GMT specimen was mounted on the three-point bending clamp after measuring the dimensions and a holding force of 0.1 N was applied to hold the specimen in position. The specimen was then cooled from room temperature (25°C) to -50°C at 2°C/min after which it was heated again at 2°C/min to 155°C, with an applied force at all times. The cooling was achieved using liquid nitrogen. Since the

polypropylene melting point from MDSC tests was found to be approximately 165°C, the maximum test temperature was limited to 155°C.

4.2.2 Typical DMA profile

Figure 4.12 shows a typical DMA profile for the long-fiber GMT with the variation of storage modulus and tan δ shown. The variation of the storage modulus and tan δ is slightly different for the cooling and heating ramps.
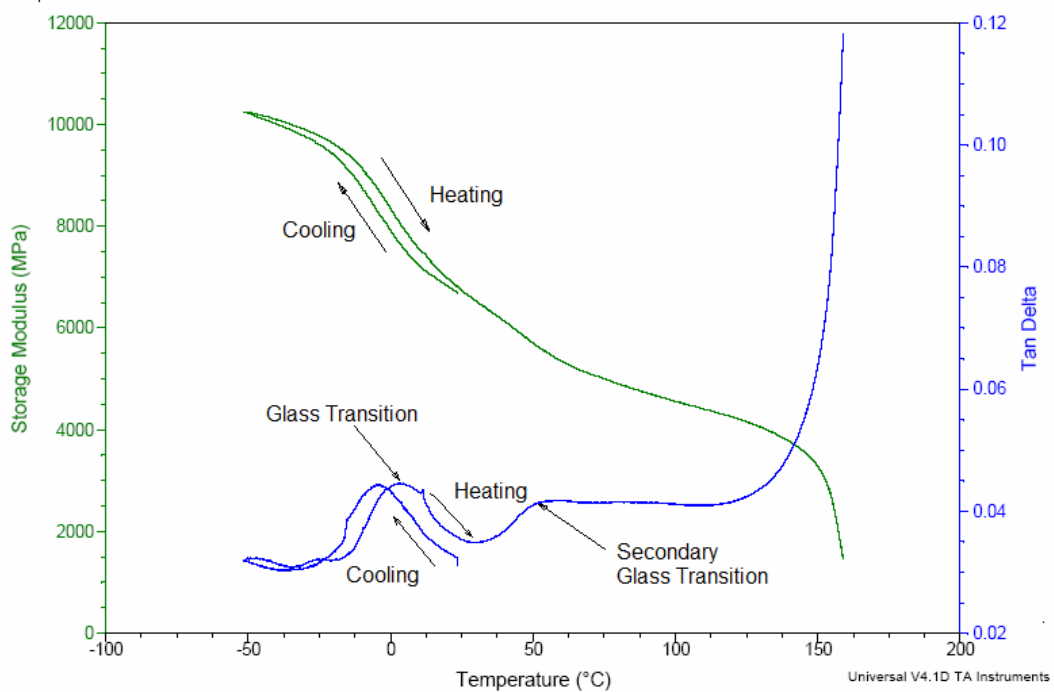
Figure 4.12 Typical DMA profile for long fiber GMT (90° cut specimen).

4.2.3 Transitions in GMT

Transitions in polymers can be identified by the presence of peaks in a plot of tan δ versus temperature. From Figure 4.13, it can be seen that the tan δ curve shows two distinct transitions with the first transition between -30°C to 25°C which is associated with the glass (α) transition. The second transition between 30°C to 60°C is referred to as the α* transition [100]. Our measured curves were very similar to that for polypropylene shown in Figure 3.8. Accordingly, the temperatures for the glass transition (T_g) and

78

secondary/sub transition temperatures ($T_{\alpha*}$) [94] will be assigned as 3.6°C and 60.5°C, respectively, for the sample shown in Figure 4.13. It is noted that while the glass transition could not detected from the MDSC tests, it is very clear from the DMA output. Also, these transitions are characteristic of the polypropylene matrix and not the fiber since glass fiber is very stable at this temperature range.
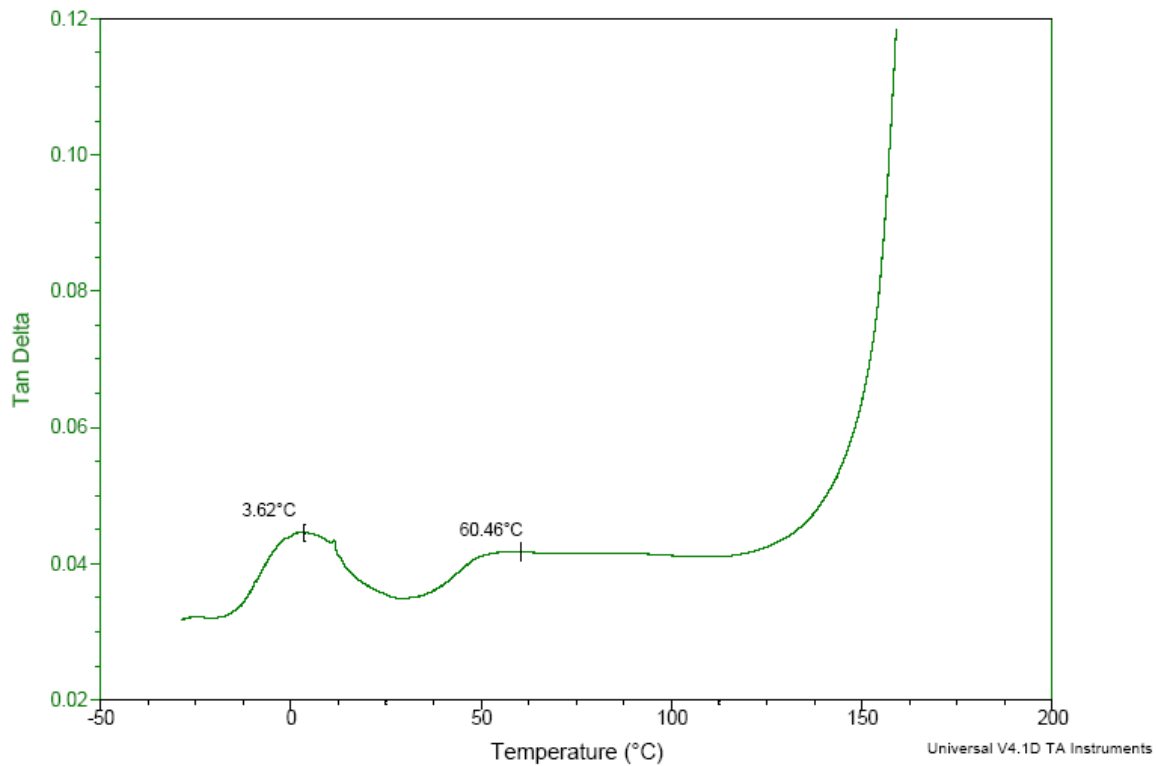
Figure 4.13 Plot of tan δ versus temperature showing glass transition and secondary/α* temperatures (90° cut specimen).

Table 4.4 shows the T_g obtained during cooling and heating and $T_{\alpha*}$ for 6 tests carried out at the three cut orientations. The average T_g for the cooling and heating curves are -2.57°C and 3.49°C respectively and average $T_{\alpha*}$ is 61.34°C. The T_g obtained during cooling has greater consistency than that found during heating. Also, the shape of the tan δ curves during cooling are smoother than that obtained during heating as can be seen from Figures 4.14 and 4.15.

79

The α^* transition is due to the slippage between the crystallites and the α^* temperature (T_{α^*}) is sensitive to the processing conditions [94]. Based on this, the variation in T_{α^*} can be attributed to the difference in processing conditions of the specimens even though they were from the same test plaque. A plausible explanation is the existence of a cooling gradient across the test plaque during moulding which is commonly observed in the moulding of large surface areas.

Table 4.4 Glass transition and secondary α* glass transition temperatures.

Trial No	Orientation	Glass transition 'Tg' (°C)		α* transition (°C)
		Cooling	Heating	
1	0°	-2.04	4.86	49.3
2		-3.17	4.4	48.59
3	45°	-1.95	4.29	74.32
4		-2.55	4.86	60.64
5	90°	-1.85	-1.08	74.71
6		-3.83	3.62	60.46
	Mean	**-2.565**	**3.49**	**61.34**
Standard Deviation		**0.79**	**2.29**	**11.45**
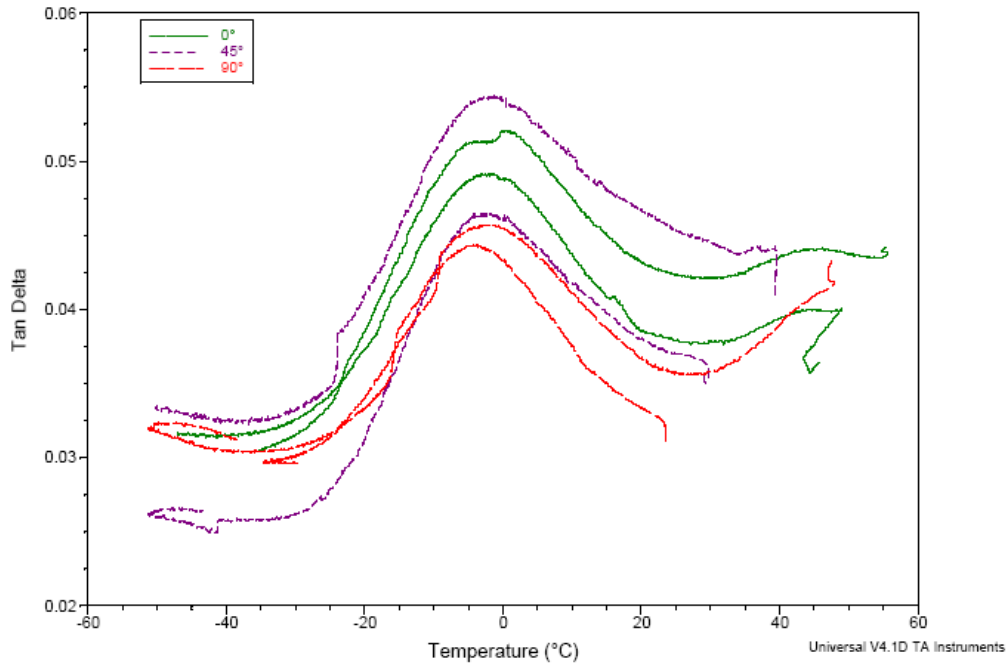
Figure 4.14 Overlay of tan δ curves obtained during cooling from room temperature to -50°C.

80
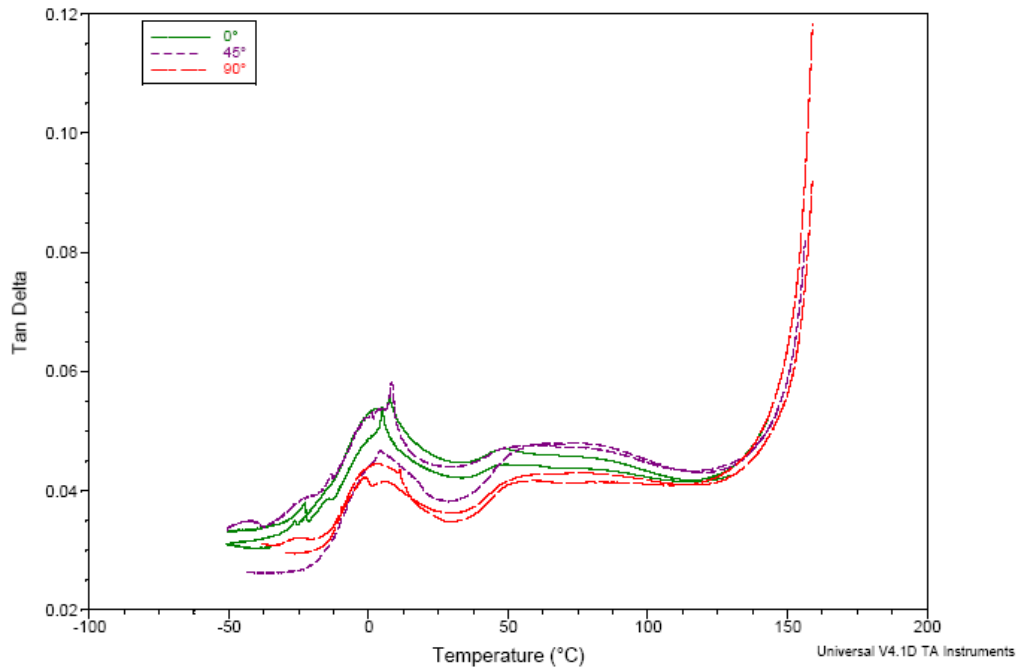
Figure 4.15 Overlay of tan δ curves obtained during heating from -50°C to 150°C.

4.2.4 Variation of modulus with temperature

The typical variation of modulus with temperature for GMT is shown in Figure 4.16. In Figure 4.16, the variation of modulus with temperature for three different specimen orientations is superimposed. It can be seen that the storage modulus decreased by about 6000 MPa (50 – 60% as that of the storage modulus at -50°C) as the material is heated from -50°C to 150°C [Storage modulus decreases by about 30% when heated from 25°C to 80°C while it increases by 50% when cooled from 25°C to -30°C]. There is also considerable scatter in the modulus values of specimens at the same orientation. The effect of the orientations on the storage modulus will be considered in the next section.

Figure 4.17 show the variation of storage modulus, derivative of storage modulus with respect to temperature and tan δ with temperature. By plotting the derivative of the storage modulus, it is possible to differentiate three distinct zones:

81

1. $-50°C < T < T_g$: the rate of decrease of storage modulus increases with temperature,

2. $T_g < T < T_{\alpha*}$: the rate of decrease of stiffness decreases with temperature, and

3. $T_{\alpha*} < 140°C$: the storage modulus decreases at a constant rate.

After 140°C, there is a rapid decrease in the storage modulus, Figure 4.17. Despite the scatter in the storage modulus and its variation due to orientation of the specimens, the derivative of the storage modulus for all of the six specimens follow a similar trend (Figure 4.18) indicating that the variation of the storage modulus with temperature is independent of the orientation and depends only on the matrix phase.
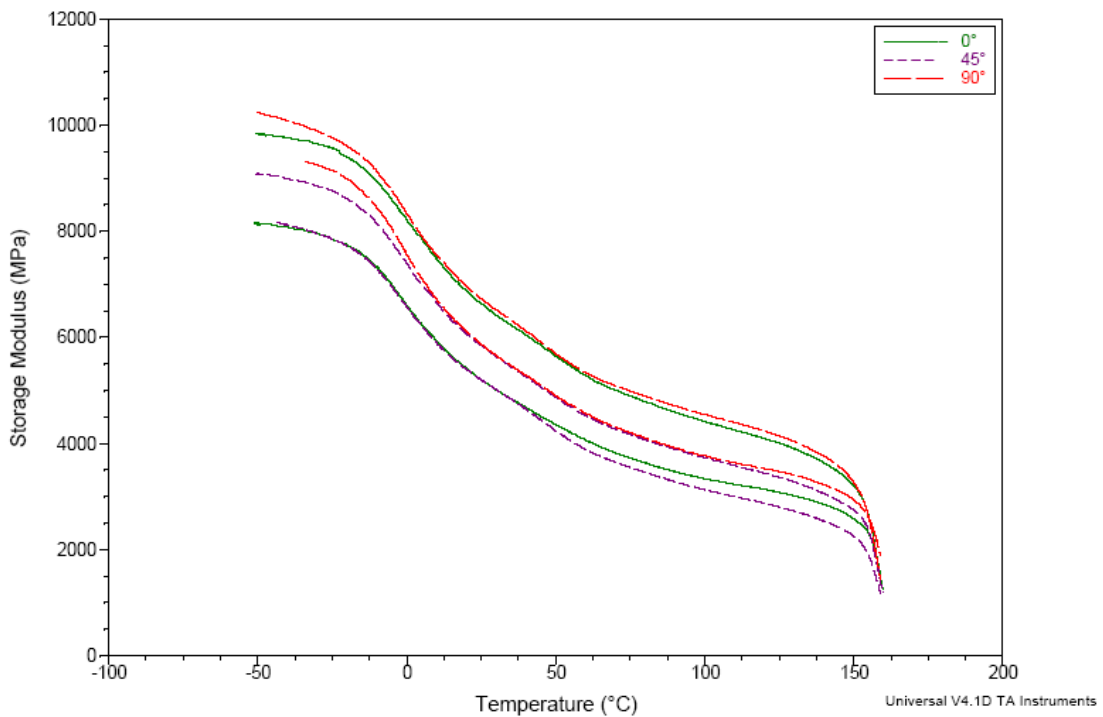
Figure 4.16 Variation of storage modulus with temperature and orientation.
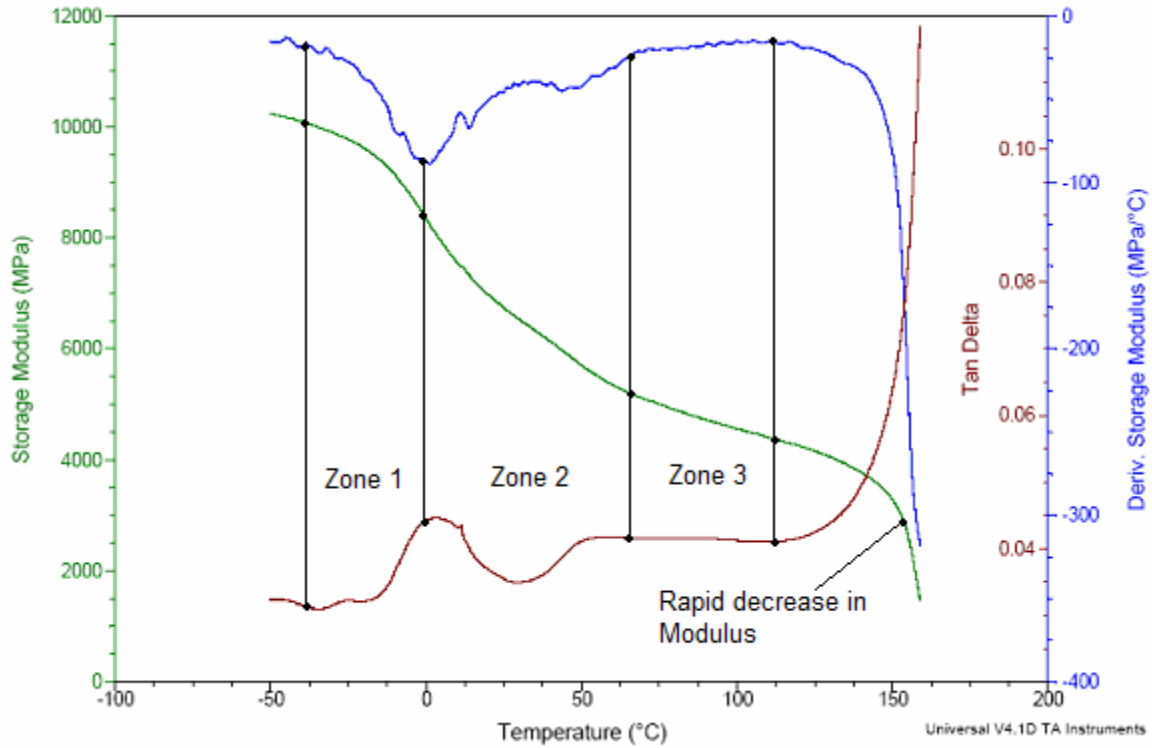
Figure 4.17 Typical variations of storage modulus, tan δ and rate of change of storage modulus with temperature.
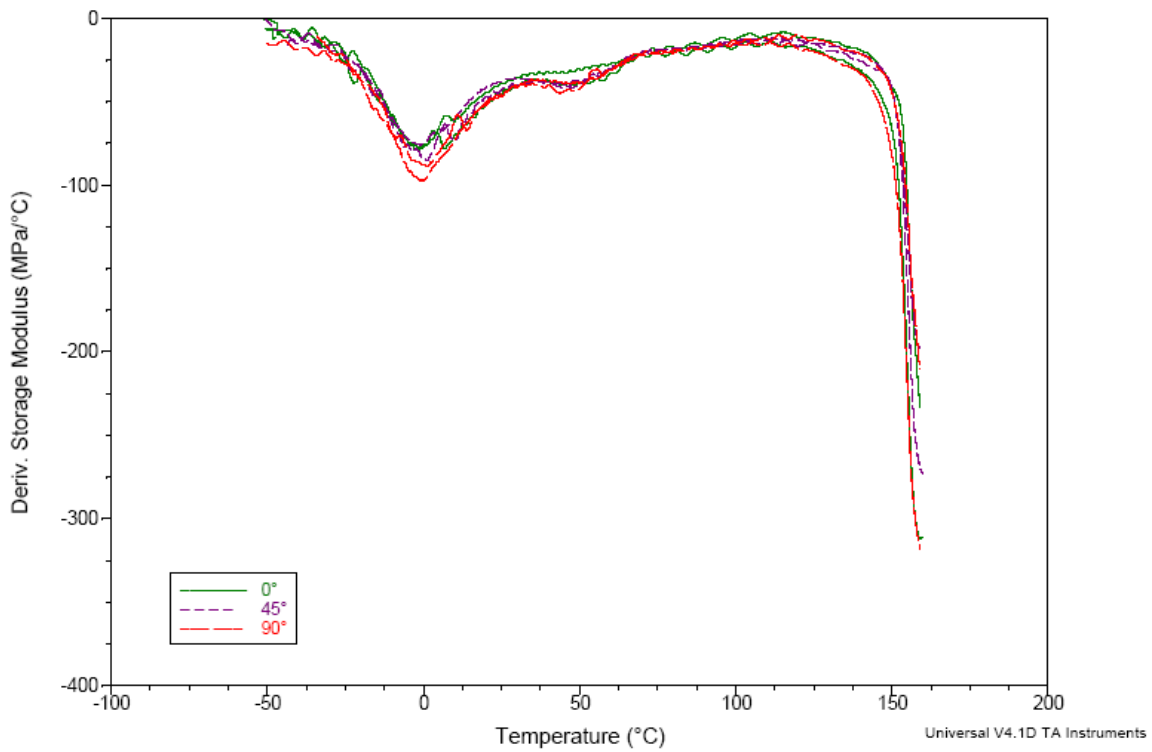
Figure 4.18 Overlay of rate of change of storage modulus with temperature for specimens cut at three different orientations.

4.2.5 Effect of specimen orientation

Figure 4.19 shows the variation of the storage modulus with the orientation at three temperatures. It is clear that the storage modulus does not vary significantly with the specimen orientation. A statistical analysis of the data inferred the same. However, it is not possible to draw conclusions on the effect of orientation on the material modulus as the sample size used for the DMA tests is small. The effect of the orientation on the modulus and tensile strength will be studied using tensile test results in the next section.
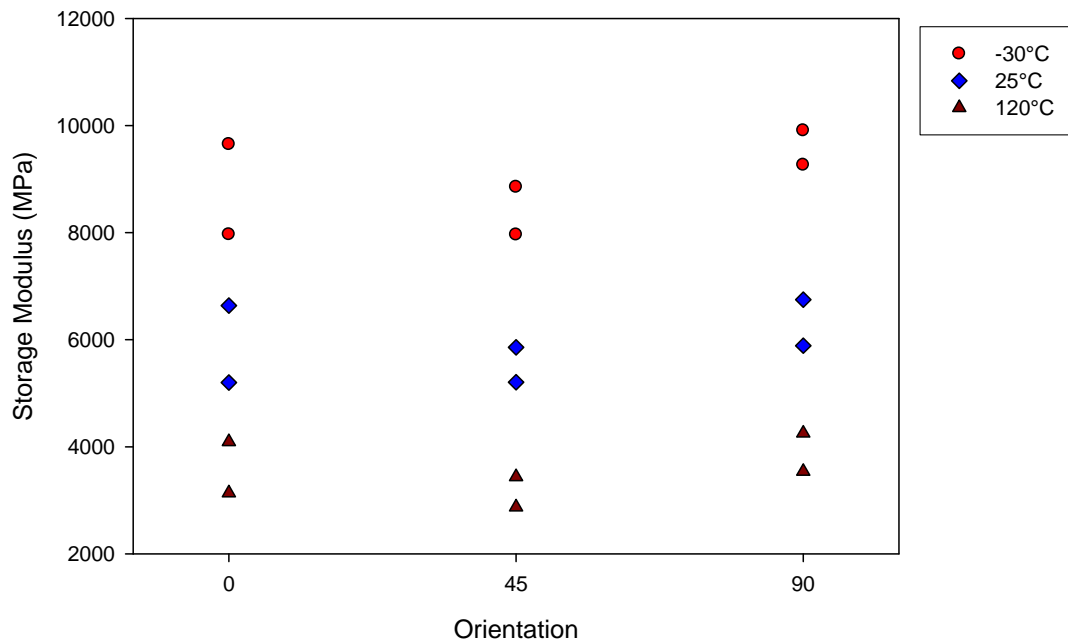
Figure 4.19 Variation of storage modulus with specimen orientation.

4.3 Tensile tests

4.3.1 Experimental details

(a)

(b)

(c)
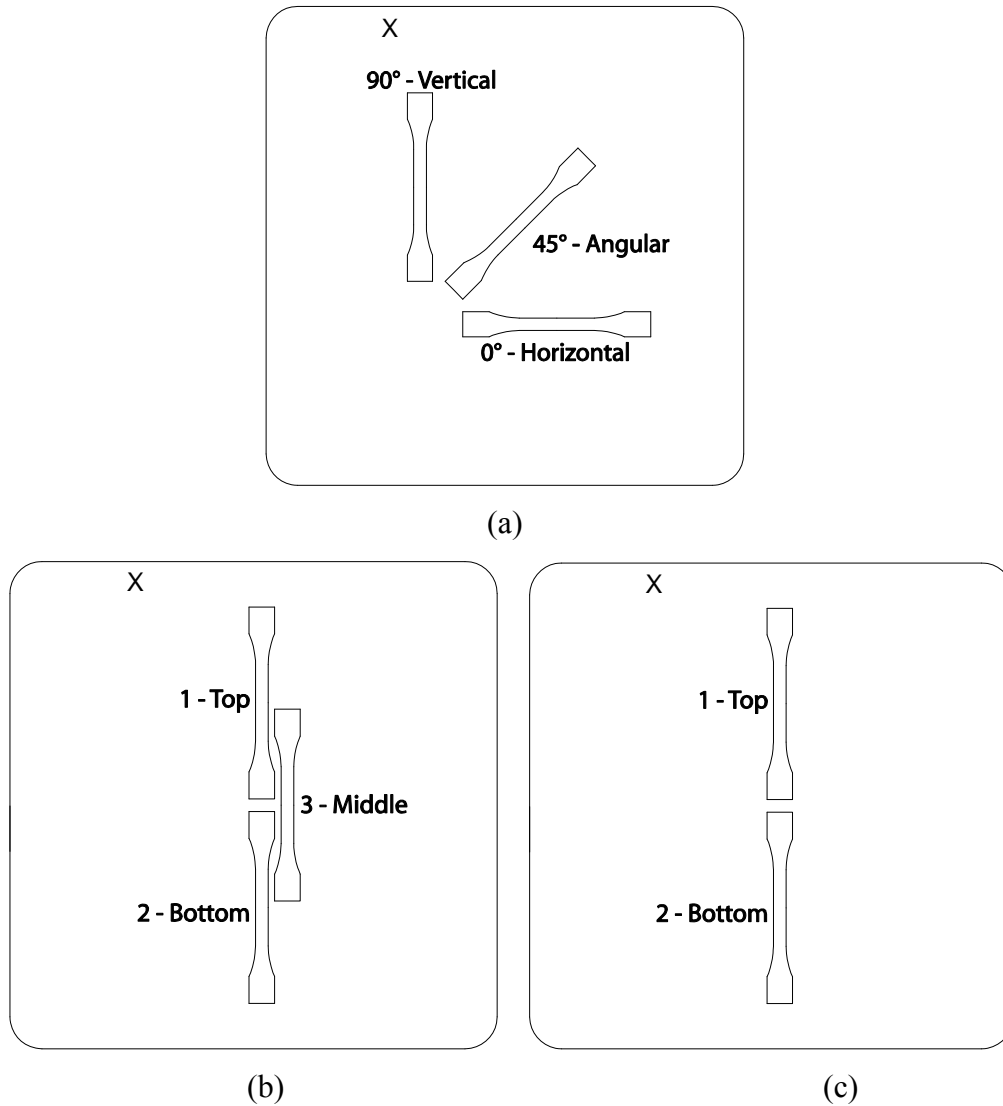
Figure 4.20 Specimen locations for tensile tests to determine (a) variability between plaques for 3-mm GMT (b) variability between plaques for 6-mm GMT (c) effect of orientation.

Tensile tests were carried out to obtain the mechanical properties namely, Young's modulus and the tensile strength of the long fiber GMT. These tests were also performed to estimate the variability in the mechanical properties within and between test plaques. A set of specimens were also tested to determine the dependence of modulus and tensile strength on the specimen machined direction.

Specimens from the center region of five test plaques in the 90° direction as shown in Figure 4.20 (a) were tested to determine the variability within and between the plaques. Three specimens for 3 mm thick GMT and two specimens for 6 mm thick GMT, shown in Figures 4.20 (b) and (c) respectively were tested per plaque. Further, six specimens in the other two orientations, i.e., 0° and 45°, shown in Figure 4.20 (a) were tested to investigate the isotropy of the plaque.

Tests were conducted on the GMT material from plaques having two different thicknesses, i.e. 3 mm and 6 mm, in accordance to the ASTM D638M-93 standard [103]. The type I geometry given in the ASTM standard is reproduced in Figure 4.21. All specimens were machined using waterjet machining (tolerance – ±0.1 mm). A clearance of 1.5 inches (38.1 mm) was allowed on all sides of the test plaque and hence the specimens were machined only from the centre of the test plaque. As part of the statistical design, tests were carried out in random order on a screw-driven tensile testing machine of capacity up to 15,000 kg. During the test, the cross head was moved at a rate of 5 mm/min. An extensometer of gauge length 50.80 mm was used to measure the axial deformation.
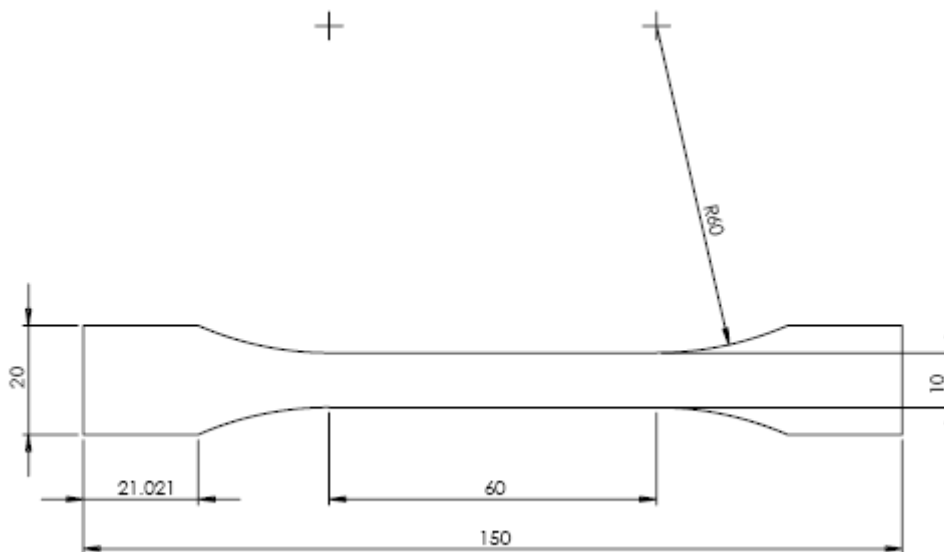
Figure 4.21 Tensile specimen – Type I in accordance to ASTM D638M–93 [103].

4.3.2 Tensile test results

a. Typical stress-strain curve

A typical stress-strain curve of the long-fiber GMT composite is shown in Figure 4.22. As seen from the plot, the stress-strain curve is not linear. The portion of the curve up to 0.25% strain corresponding to a stress of about 20 MPa was found to be linear using the commercial graphing and statistical software Sigmaplot V9 and was hence used to determine the Young's modulus. The stress at failure was considered as the tensile strength of the specimen.

The Analysis of Variance (ANOVA) statistical technique was used to analyze the modulus and tensile strength data using Minitab R14, a commercial statistical package. A brief review of ANOVA and the statistical terms used has been provided in Appendix C.
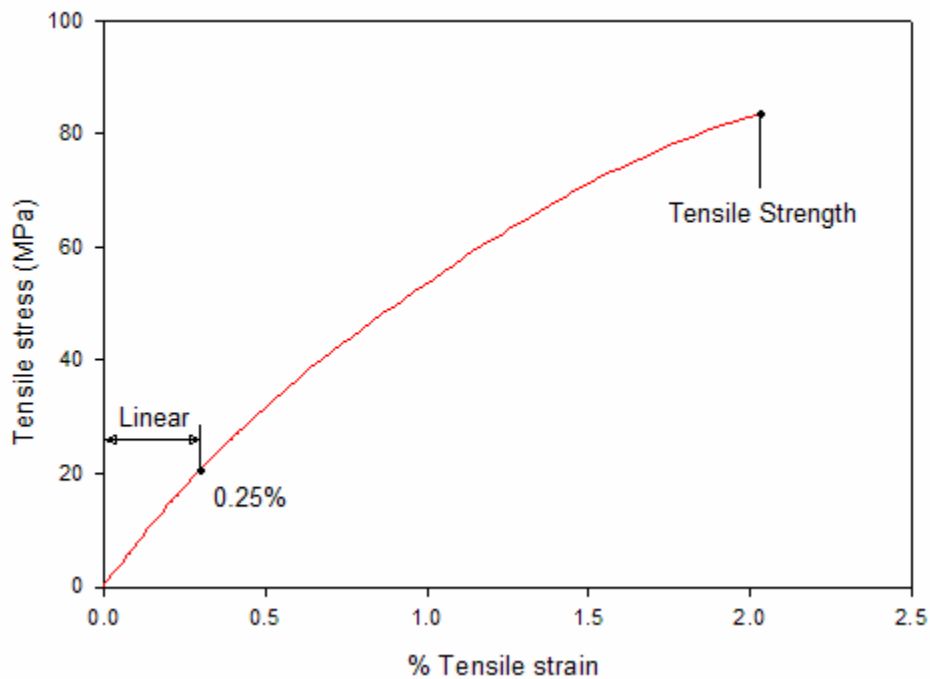
Figure 4.22 Typical stress-strain curve for long-fiber GMT.

b. Variability within and between plaque variability:
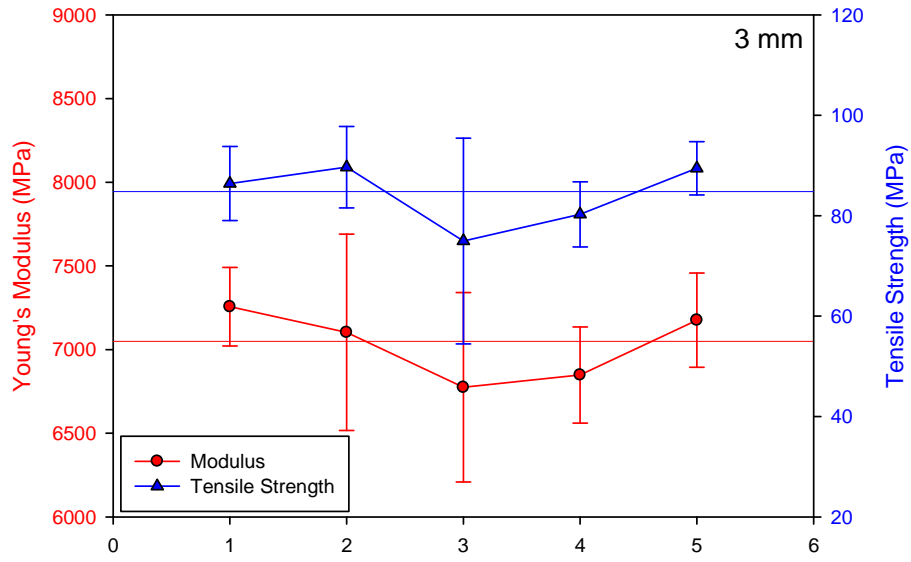
(a)
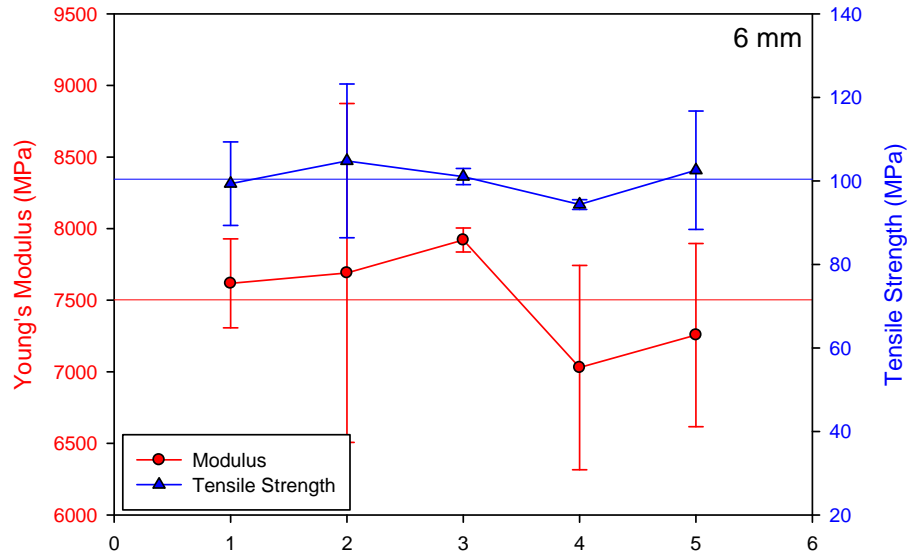
(b)

Figure 4.23 Variation of Young's modulus and tensile strength data between plaques
(a) 3 mm and (b) 6 mm thick GMT.

The variation of the mean Young's modulus and tensile strength values with the test
plaques for the 3- and 6-mm thick GMT are shown in Figures 4.23 (a) and (b)
respectively. As expected, there are variations in the tensile properties both within and

between plaques. The variations however are much lower than those given in reference [80]. The variability in the modulus within the plaque for the five plaques tested was between 4-8% for the 3 mm thick GMT and 4-10% for the 6 mm think GMT. It has to be noted that only two specimens per plaque were tested for the 6 mm thick GMT. The data for the two materials was analyzed using Analysis of Variance (ANOVA) to determine the effect of two factors, i.e., plaque (between plaques effect) and location (within plaque effect) on the two tensile properties. From the statistical analysis (p-values from ANOVA), it was found that the mean modulus and tensile strength variations with both location and plaque were insignificant ($p > 0.05$) for both the materials. Thus, statistical analysis indicates that both the modulus and tensile strength obtained from various plaques are comparable, which validates the use of multiple plaques for creep characterization of this material.

[Note on statistical analysis: Typically, for studies like the one under consideration, statistical inferences are given at 95% level of significance. The p-values, which are the levels of significance at which the hypotheses (whether the means of the output at the various levels of a factor are equal) being tested can be rejected will be used for statistical comparison. If the p-value is less than 0.05 then it indicates that the hypotheses can be rejected, and it can be concluded that the mean of the output at the various levels differ. If p-value is greater than 0.05 then it will be concluded that the hypotheses i.e., means of the output at the various levels are same. A brief review of the statistical concepts is provided in appendix C.]

c. Effect of specimen orientation

The Young's modulus and tensile strength for three orientations studied are shown in Figure 4.24 (a) and (b) for the 3- and 6-mm thick GMT, respectively. For the 90°, the test results from part (a) given above were used. ANOVA showed that both materials exhibit directional dependence.
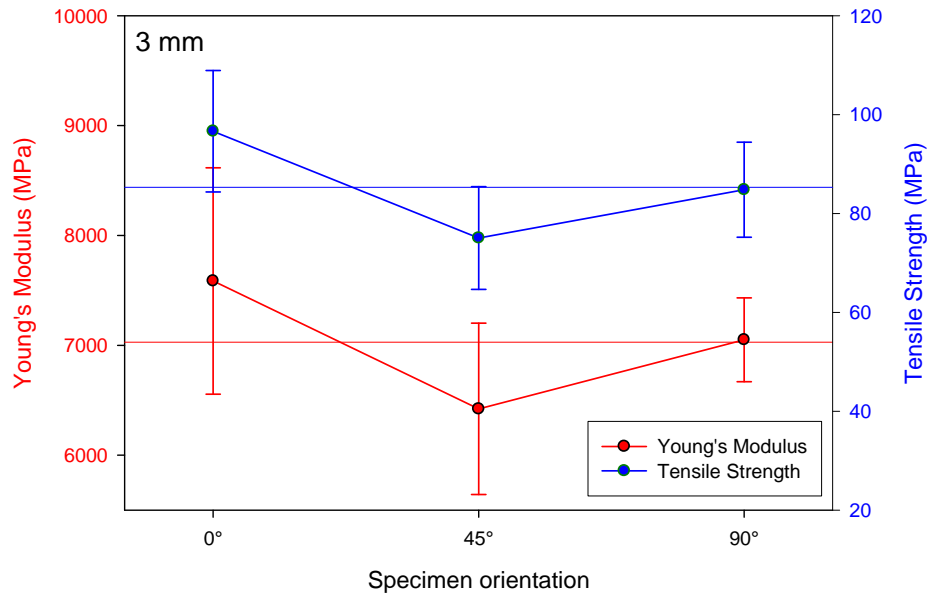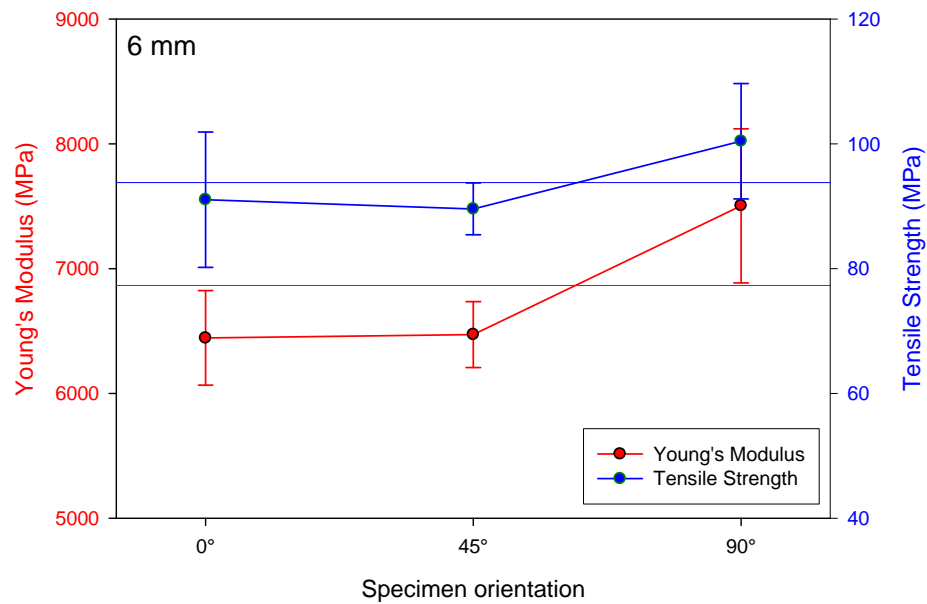
Figure 4.24 Effect of specimen orientation for (a) 3 mm and (b) 6 mm thick GMT.

The tensile properties of the 6-mm thick GMT in two directions (0° and 45°) are very similar while that in the third direction is considerably higher. This could be due to the flow during the moulding causing alignment of fibers in this direction (90°) leading to higher property values. In case of the 3-mm thick GMT, the tensile properties in 0° and 90° seem very similar as shown in Figure 4.24 (a), although the scatter in the 0° is higher.

Further statistical analysis showed the tensile properties variations in these two directions (0° and 90°) are insignificant. The coverage of the charge GMT plates before moulding of the 3-mm thick GMT was higher than that in the 6-mm thick GMT. Hence the flow during moulding the 3-mm thick GMT was considerably lower, leading to more uniform properties.

d. Comparison of tensile properties of 3-mm and 6-mm thick GMT

For consistency, all creep tests were carried out on specimens cut from the vertical (90°) direction, Figure 4.20 (a). The results in section (b) given above were used to obtain the average properties for the two materials which are summarized in Table 4.5. The tensile properties given in Table 4.5 were obtained as an average of 15 and 10 specimens for the 3- and 6-mm thick GMT respectively. The property values for the 6 mm thick GMT are higher than the 3-mm thick GMT due to the higher fiber weight fraction of the 6-mm thick GMT as was found from the matrix burn off tests. The weight fraction for the 3-and 6-mm thick GMT was found as 40 ± 2 % and 42 ± 3 % respectively.

Table 4.5 Average tensile properties for the two thicknesses.

Material	Young's Modulus (MPa)	% RSD	Tensile strength (MPa)	% RSD
3 mm	7050 ± 382	5.4	84.80 ± 9.6	11.3
6 mm	7503± 618	8.2	100.41 ± 9.24	9.2

Note: % Relative Standard Deviation, % $RSD = \dfrac{Standard\ Deviation}{Mean} \times 100$ (65)

4.4 Chapter summary

The main conclusions from two thermal analysis techniques, MDSC and DMA, and tensile testing of the composite material are as follow:

(1) Calorimetry showed that the melting point of the GMT composite is approximately 164.0°C. The crystallinity of the polypropylene matrix is between 49-54%. When the cooling rate was varied from 10 to 20°C/min, the crystallinity of the material decreased but the melting point increased. From the controlled cooling experiments, it can be estimated that the material was cooled at a rate between 15 to 20°C/min during moulding of the test plaques.

(2) Dynamic mechanical analysis showed that the T_g and α^* transitions for this material occur at 3.49°C and 61.34°C respectively. The variation of the storage modulus with temperature has been determined. The reduction in moduli within the temperature range 25 – 80°C for creep testing in this work is fairly significant.

(3) Tensile testing performed on the two materials showed that the variability in the tensile properties of the 3-mm thick GMT to be lower than that in the 6-mm thick GMT material. From statistical analysis it has been found that the mean tensile properties obtained from different plaques are similar. Furthermore, the tensile properties of the 3-mm thick GMT showed lower directional dependence than the 6-mm thick GMT. The tensile properties of the 6-mm thick GMT in one direction (90°) were higher than the other two directions due to the flow of the material during moulding. Finally, the tensile properties of the 6-mm thick GMT have been found to be higher than the 3-mm thick GMT due to the higher fiber weight fraction in the former material.

CHAPTER 5

RESULTS AND DISCUSSION:

EFFECT OF STRESS ON CREEP IN GMT MATERIALS

5.1 Creep tests overview

Creep testing constitutes the major work of this research study. The purpose is to determine the effect of thermal and mechanical loads on creep in long fiber GMT materials over a wide range of stresses and temperature. At the start of the experimental program, non-linear viscoelastic behaviour was expected especially at higher stresses and also with temperature. However, after preliminary experiments, the material was found to exhibit non-linear viscoelastic-viscoplastic behaviour. Hence, the experimental program was aimed at determining the effects of stress and temperature on both viscoelastic and viscoplastic strains. Furthermore, the viscoplastic strains have been investigated in detail. The focus of this work is to characterize the 3-mm thick GMT. However, the stress effects on the creep behaviour of 6-mm thick GMT have been considered to determine the effect of thickness on the creep behaviour. The tests carried out on the 3 mm thick GMT is summarized in Figure 1.4 and Table 5.1. A total of nearly 500 creep tests of varying durations, stresses and temperatures have been conducted to characterize the creep in the long fiber GMT composite. The relatively large sampling for each test condition is necessary because of the known high experimental scatter exhibited by GMT materials.

The short-term tests (both stress and temperature) listed in Table 5.1 are preliminary tests to determine if stress and temperature have an effect on the creep behaviour. In these tests, the material variability is minimized by repeatedly testing a single specimen over the entire range of stresses and temperatures. Furthermore, it has to be noted that although models have been developed based on short-term tests in both chapters 5 and 6, the sole purpose of short-terms tests is to determine the general effects of stress and temperature on the viscoelastic component of creep response. The viscoplastic strains

developed in these short-term tests are expected to be minimal. As will be seen later, it also illustrates the simplification of the parameter estimation methods when viscoplastic strains are not considered. Finally, the long-term tests given in Table 5.1 provide both viscoelastic and viscoplastic behaviour of the material and hence the complete general models are developed from the results of these tests.

Table 5.1 Creep tests carried out on the 3-mm thick GMT material.

Effect	Test	Test duration (hours)		Stress		Temperature		No of Repeats
		Creep	Recovery	No of levels	Range	No. of levels	Range	
Stress effect	Short	0.5	0.5	14	5 to 60 MPa	1	25°C	6
	Long	24	48	7	20 to 80 MPa	1	25°C	4
Temperature Effect	Short	0.5	1	4	20 to 60 MPa	14	25 to 90°C	3
	Long	24	48	5	20 to 70 MPa	3	40°C to 80°C	3
Viscoplastic strains	-	1, 3, 3, 6, 12 and 24	3, 9, 9, 18, 36 and 72	7	20 to 80 MPa	1	25°C	4

In this chapter, the results of the creep tests carried out to determine the effect of stress on the creep behaviour of the material is presented. Due to the scatter in the material properties, two separate creep test schemes have been employed:

1. Short-term creep tests – 30 minutes creep followed by 30 minutes recovery
2. Long-term tests – 1 day creep followed by 2 day recovery

In this entire thesis, "short-" and "long–term" tests will be the terminology used to differentiate between the above two test schemes. In creep characterization, long-term tests are usually much longer than 1 day. The details of the experiments and the results are given in the following sections.

5.2 Short term creep tests

As stated in references [80-83], scatter in the properties is an inherent characteristic of the material. Hence, short term tests were carried out to capture the behaviour of the material

while minimizing the effects of inherent variability in the material. This is achieved by conducting creep tests at multiple stress levels on a single specimen. The aim of the short term tests was to identify the linear viscoelastic region of the material. It is noted that the constitutive model developed using the short term data does not consider damage accumulation of the material.
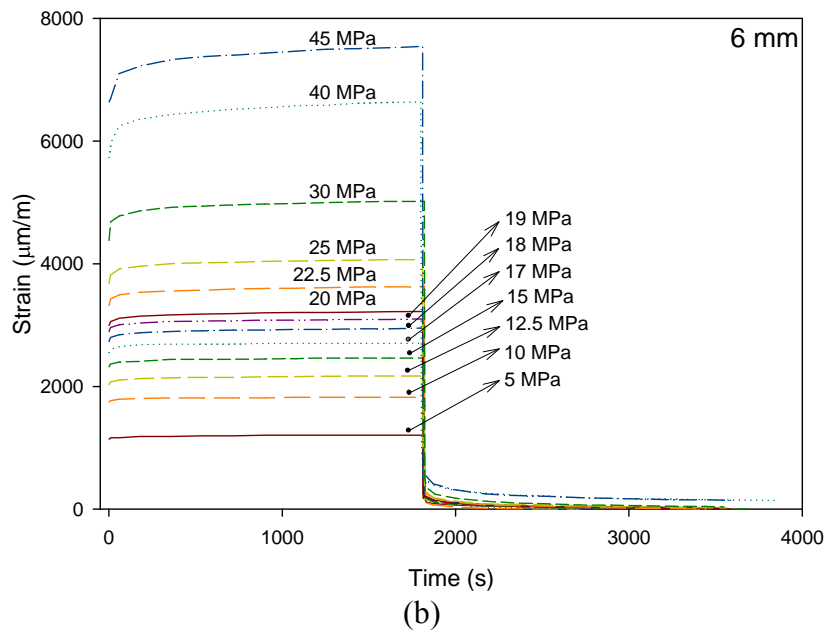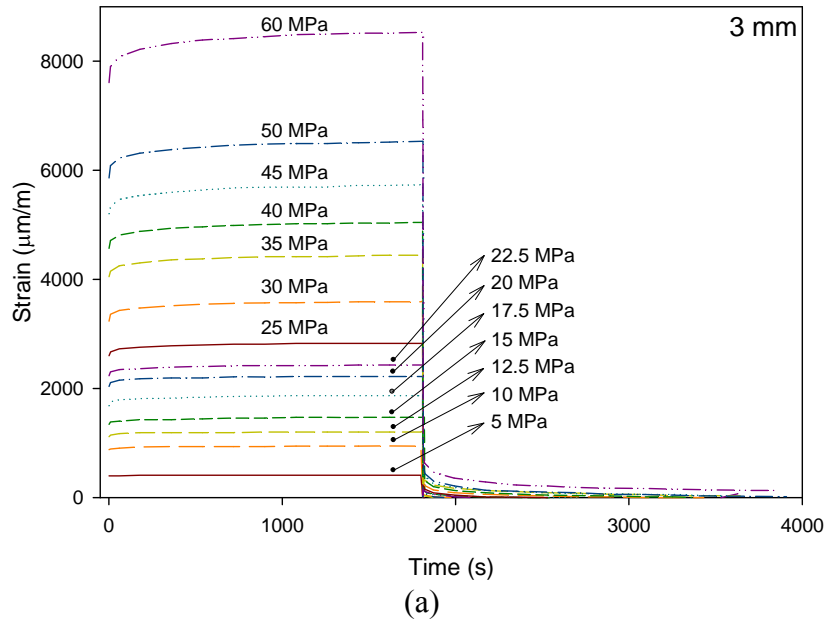
Figure 5.1 Typical creep curves from short term tests for (a) 3-mm (b) 6-mm thick GMT.

5.2.1 Experimental details

The short term creep tests consisted of 30 minutes creep followed by 30 minutes recovery for each stress level considered. Creep tests at 14 stresses over the stress range of 5 to 60 MPa (5, 10, 12.5, 15, 17.5, 20, 22.5, 25, 30, 35, 40, 45, 50 and 60 MPa) have been considered for the 3-mm thick GMT. However at loads greater than 3.5 KN, instantaneous loading and unloading could not be achieved due to the fixture load limitation. Hence, the maximum stress for the 6- mm thick GMT was limited to 45 MPa. The 6-mm thick GMT material has been tested at 13 stress levels - 5, 10, 12.5, 15, 17, 18, 19, 20, 22.5, 25, 30, 40 and 45 MPa. A single specimen was repeatedly used at all the stress levels to minimize the error due to material variability. The tests were replicated six times with each replicate carried out on separate specimens. Specimens for such tests are normally pre-conditioned [e.g. 32] by repeated loading and unloading for a fixed number of cycles prior to the testing to minimize the effects of material damage. However, the specimens used in this work were not pre-conditioned but care was taken to ensure minimal residual strains at the end of recovery. It was observed that creep strains were completely recovered at lower stress levels, and furthermore the residual strains at higher stress levels were small.

Typical creep-recovery curves from the short-term tests for the two materials are shown in Figures 5.1 (a) and (b) using single specimens for each thickness. The stress levels tested for the two materials are shown in the respective figures. Small magnitudes of un-recovered strains are observed at the end of recovery especially at higher stress levels. These un-recovered strains are usually referred to as the viscoplastic strains (ε_{vp}) shown in Figure 2.11. Also, as a single specimen was repeatedly tested at all the stress levels, any un-recovered strains from one creep-recovery test was reset to zero before the start of the next test. The scatter in the creep properties was about 7 % which is evident in Figures 5.2 (a) and (b) showing the variation instantaneous strains with stress for the six specimens. The scatter in the data at stresses below 15 MPa were slightly higher due to the rigidity of the fixture, which reduces the calibration accuracy at lower loads. The data at these low stress levels were not considered for further analysis.

96
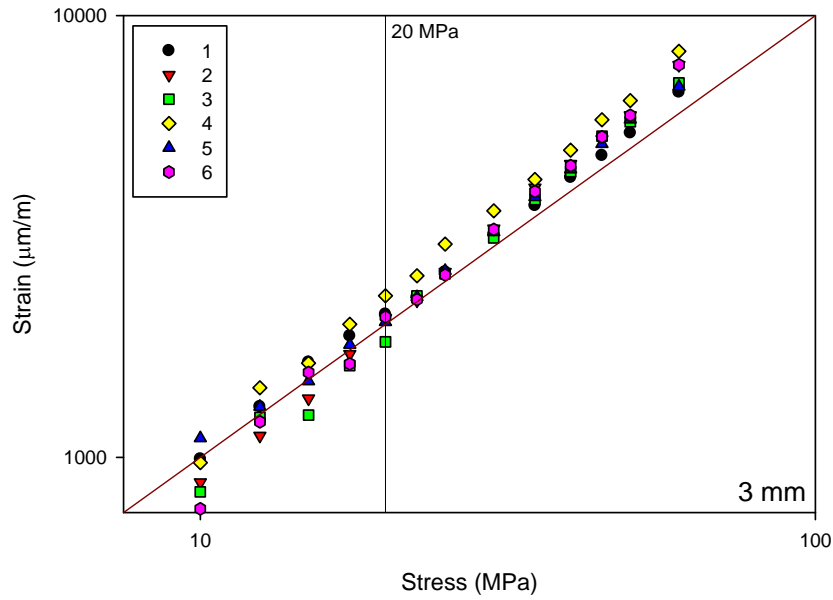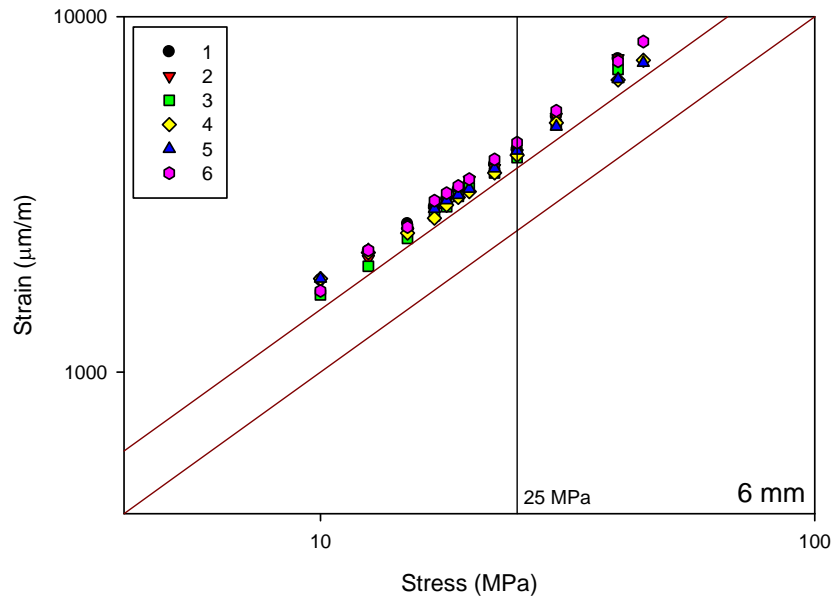
Figure 5.2 Instantaneous strains from creep tests of (a) 3 mm (b) 6 mm
thick GMT on a log-log scale.

5.2.2 Tests of linearity

The determination of the linear viscoelastic region is one of the most important aspects in
the characterization of polymeric materials and their composites. Typical techniques for

determining the linear viscoelastic region have been described earlier in section 2.4. Given the large scatter in GMT material behaviour, it is prudent to apply more rigorous analyses for assessing the linearity region for this material. Accordingly, three of the techniques will be applied to analyze the linearity of GMT creep data:

a. Proportionality of creep strain with stress at various times
b. Equality of compliance at various stress levels
c. Boltzmann superposition principle

(a) Stress-strain proportionality

The stress strain proportionality is one of the primary requirements for linearity in viscoelastic materials. Non-linearities can not only arise due to stress, but also due to time. Certain materials behave as linear viscoelastic materials at lower stresses over short durations, while considerable non-linearity can be detected at the same low stresses over longer durations [12]. Hence, it is important to check the proportionality of the strain with stress at various time intervals.

Figures, 5.2 (a) and (b) show a plot of instantaneous strains versus stress on a log-log scale extracted from the creep tests for the 3- and 6-mm thick materials respectively. The plot also shows the scatter in the experimental data. The 6-mm thick GMT material seems more linear over the smaller stress range considered. The instantaneous strain-stress curves deviate from the 45° diagonal (linear case) at about 20 MPa and 25 MPa for the 3- and 6-mm thick GMT material respectively, indicating the start of non-linear behaviour. A similar trend was found from the tensile stress-strain curves.

Note: The check for stress-strain proportionality $\left(\varepsilon = c\sigma\right)$ i.e., by determining the deviation from the 45° diagonal on a log-log scale is based on the fact that for a linear relationship between stress and strain, the slope of the stress-strain curve on log-log scale would be 1 $\left(\log\varepsilon = \log c + (1)\log\sigma\right)$. A slope of 1 indicates the inclination of the line is 45° (slope = tan(θ)). For a non-linear relationship, the slope would be different. For

example, in case of a second order relationship, $\varepsilon = c\,\sigma^2$, the slope would be 2 $\left(\log \varepsilon = \log c + \left(2\right) \log \sigma \right)$ which corresponds to a line at angle 63.43°.
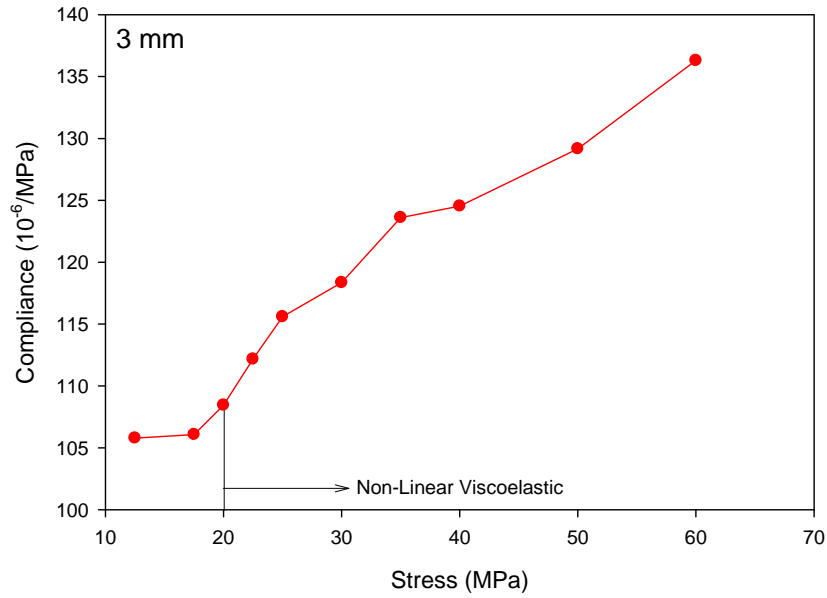
(a)
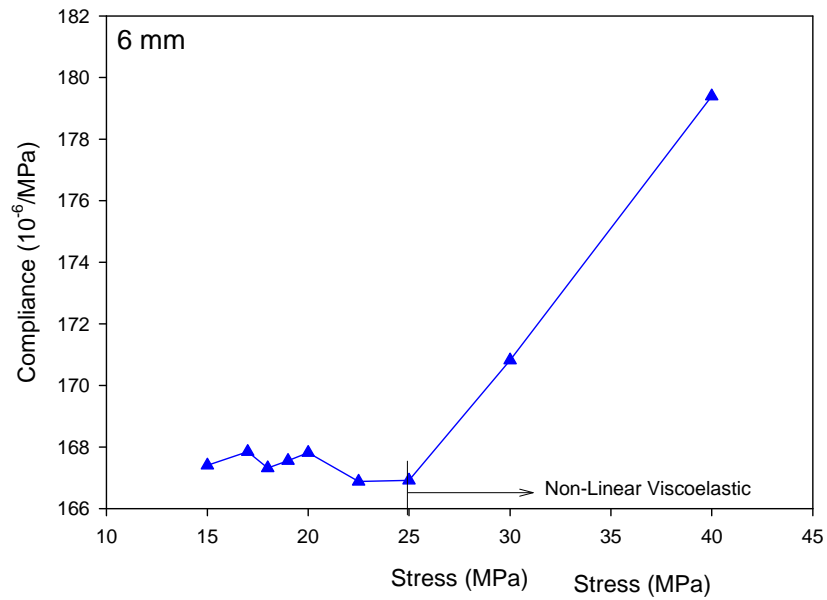
(b)

Figure 5.3 Variation of average compliance after 30 minutes creep with stress for (a) 3-mm (b) 6-mm thick GMT.

(b) Equality of compliance:

This is a direct consequence of the proportionality criterion given above. It implies that within the linear viscoelastic region, the compliance at any stress level at a given time is a constant. However, the advantage over the stress-strain proportionality criterion is that statistical analysis can be used to make inferences on the equality of compliance with stress. ANOVA is a very useful statistical tool for validating this condition, i.e., it can be used to determine the equality of the mean compliances at the various stress level while considering the variability in the data. The average compliance at the end of creep extracted from 6 tests at each of the various stress levels for the 3- and 6-mm thick GMT are shown in Figures 5.3 (a) and (b) respectively. It can be seen that the compliance starts increasing at about 17.5 MPa and 25 MPa for the 3-mm and 6-mm thick GMT respectively.

ANOVA was carried out on the two data sets, i.e., at two time intervals – instantaneous and that after 30 minutes creep for the both the materials. The p-values obtained from the statistical analysis were less than 0.05 (Appendix D) indicating that the compliance does change with stress. Further statistical analysis indicated that the compliance up to 20 MPa for the 3 mm thick GMT and 25 MPa for the 6 mm thick GMT are statistically equal and hence represents the linear viscoelastic range for the two materials. Although the increase in the compliance with stress is evident in Figure 5.3 for both the materials, statistical analysis of the data is important. This is because the results of the statistical analysis indicates that the increase in compliance is significant even when the material variability is taken into account (For all of the above statistical analysis, the statistical assumptions that the errors are normally and independently distributed were verified and were found to be satisfactory in each of the cases.) Viscoelasticity being inherent property of the polymer matrix, the 6 mm thick GMT consisting of higher fiber weight fraction has a wider linear viscoelastic region.

(c) Superposition

The superposition of the creep and recovery is an extension of the Boltzmann Superposition law given earlier. It involves comparing the experimental and predicted recovery curves. The recovery curves are predicted by a model developed from the creep portion of the experiment. An extrapolated creep curve is also obtained for the total duration of the experiment (creep time + recovery time). The data for the two curves are then added to obtain the total curve, as shown in Figure 5.4.
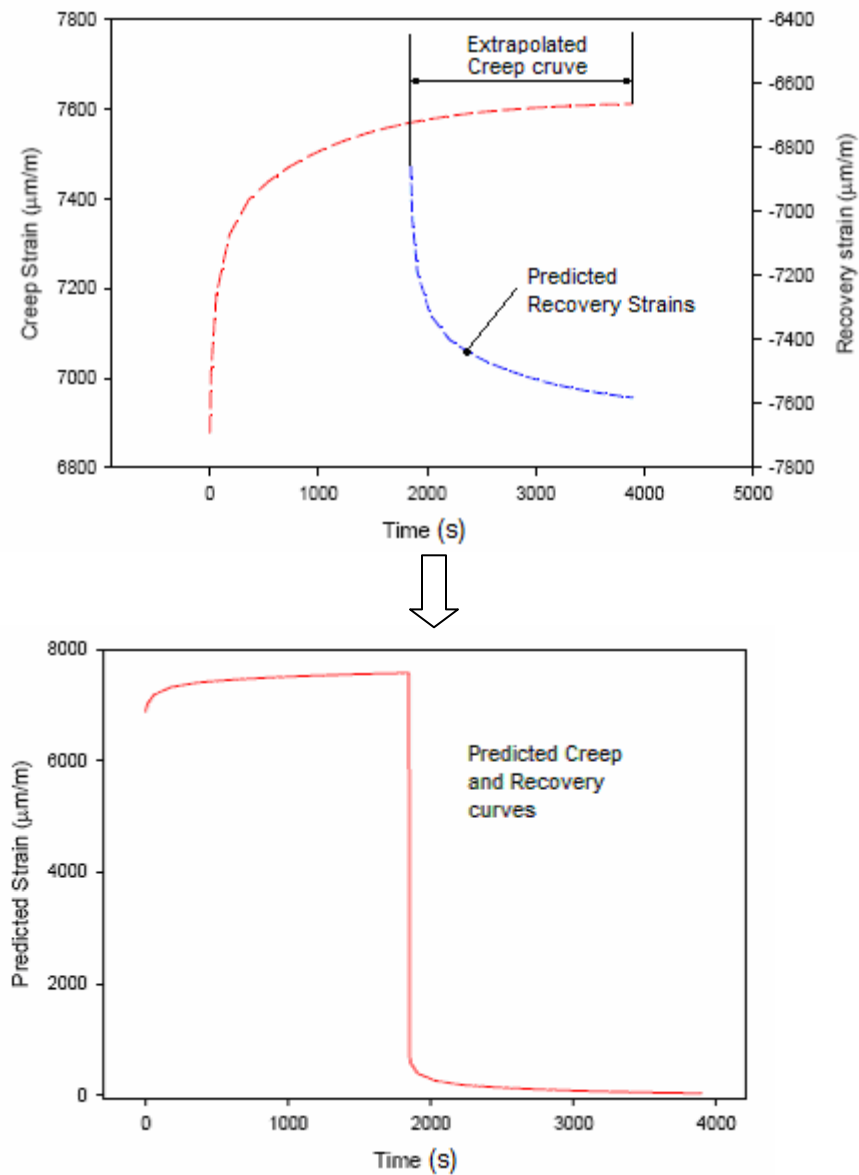
Figure 5.4 Illustration of the Boltzmann superposition method.

$$\Delta D(t) = \sum_{i=1}^{n} D_i (1 - e^{-t/\tau_i})$$
(66)

Creep-recovery experiments were carried out to verify linearity using the superposition principle. Since from the previous two sections, 20 MPa and 25 MPa have been found to mark the end of the linear viscoelastic region for the 3 mm and 6 mm thick materials respectively, the data at these stress levels for each trial were considered for verification of the Boltzmann superposition principle. The creep curves at these stress levels were fitted to a 3 term Prony series ($n = 3$) given in equation (66). This model was then used to predict the creep and recovery curves at the other stress levels.
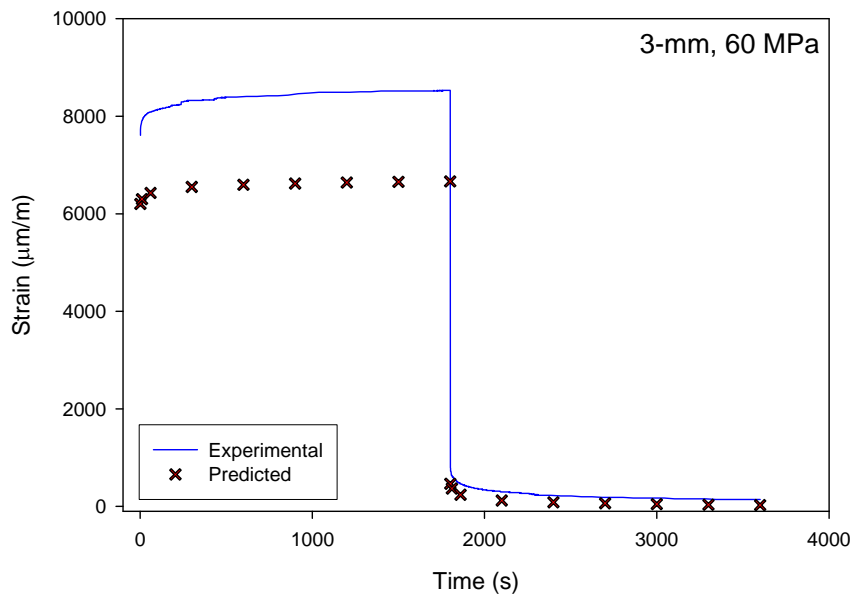
Figure 5.5 Comparison of experimental with the predicted strains at 60 MPa using Boltzmann superposition principle for the 3-mm thick GMT.

A typical creep-recovery prediction obtained at 60 MPa for the 3-mm thick GMT composite using the model obtained from the respective 20 MPa data following Boltzmann superposition principle is shown in Figure 5.5. As expected, the model under-predicts the creep strains while the recovery behaviour is over predicted. The under-prediction of the creep strains indicate that the compliance at 60 MPa is much higher than that at 20 MPa and hence the difference. The over-prediction of the recovery strains is due to the un-recovered plastic strains in the experimental data. This indicates that a non-linear viscoelastic viscoplastic model is required to efficiently model the creep behaviour

in these materials. Similar results were obtained at the other stress levels for both the materials i.e., under-prediction of the creep strains and over-prediction of the recovery strains. The difference between the predicted and experimental curves increased with stress indicating an increase in the non-linear behaviour with stress.

The average permanent strains obtained as the total un-recovered strains at the end of recovery at the various stress levels for the two materials are plotted in Figure 5.6. The average residual strains for the 6-mm thick material was higher than that in the 3 mm thick GMT with a non-linear variation. As mentioned earlier, these plastic strains have been associated with damage accumulation mechanisms such as fiber-matrix debonding, matrix cracking, fiber rupture and matrix plasticity [56, 58]. It has to be noted that the plastic strains given in Figure 5.6 are not an absolute indication of the amount of permanent deformation in the material, as a single specimen was used to test over the entire range of stress levels. It has been found that the plastic strains developed in a virgin specimen loaded at the same stress level is much higher than that shown in Figure 5.6.
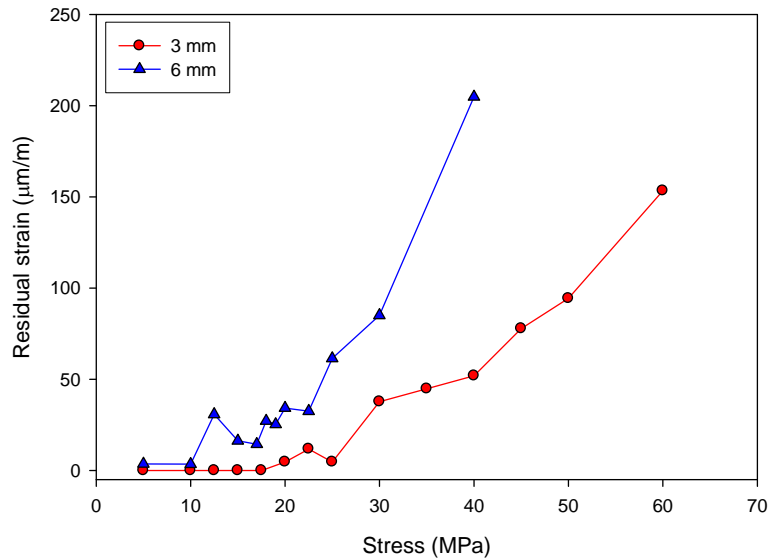
Figure 5.6 Average plastic strains developed during 30 minutes creep at various stress levels for the two GMT thicknesses.

5.2.3 Model development

It is evident that plastic strains are accumulated during creep and therefore, a non-linear viscoelastic-viscoplastic constitutive model is more appropriate to model the behaviour of these materials. However, since the magnitude of the plastic strains over the durations considered are a small compared to the overall creep strains, these short term creep tests can be used to obtain a good representative model for the viscoelastic behaviour of the material. Hence a non-linear viscoelastic constitutive model has been developed from this data set. The model developed here is important as it gives a good estimate of the non-linearity parameters in the constitutive law and can be used to verify the parameters obtained from a different experimental scheme presented in the next section. This is necessary as the material exhibits large scatter in properties.

The non-linear viscoelastic constitutive model in equation (32) has four non-linearity parameters - a_σ, g_0, g_1 and g_2. Considering the scatter in the data and to simplify the parameter estimation process, a_σ has been considered as one. The following procedure was employed to obtain the three non-linear parameters.

1. The model for compliance was obtained as a 3-term Prony series in the linear viscoelastic region of the material, i.e., at stress levels of 20 MPa and 25 MPa for the 3- and 6-mm thick GMT respectively. The model parameters obtained as an average of 6 trials are given in Table 5.2. The time constants were pre-selected as $\tau_i = 10^i$ to simplify the curve fitting process.

2. An estimate of the non-linear parameter g_1 can be obtained by using equation (67) as given in references [54,55].

$$g_1 = \frac{\Delta\varepsilon_c - \varepsilon_{vp}}{\Delta\varepsilon_c - \Delta\varepsilon_0 - \varepsilon_{vp}} \qquad (67)$$

where, $\Delta\varepsilon_0$ is the difference between the instantaneous loading and unloading strains, ε_{vp} is the total un-recovered plastic strain at the end of recovery and $\Delta\varepsilon_c$ is the creep strain (viscoelastic strains).

g_1 models the difference in the loading and unloading behaviour of the material and it is evident from equation (67) that if $\Delta\varepsilon_0 = 0$, then $g_1 = 1$ [32,54,55]. The typical instantaneous strains during loading and unloading plotted in Figure 5.7 for the 3-mm material show no difference in these strains in almost all of the cases and hence g_1 found from equation (67) was very close to one (>0.99). Similar results were found in case of 6-mm thick GMT at stresses lower than 30 MPa. At 40 MPa, there was slight difference in these strains (due to the slightly higher plastic strains), however still yielded g_1 close to one. Based on these observations, g_1 was considered to be '1' for both materials.
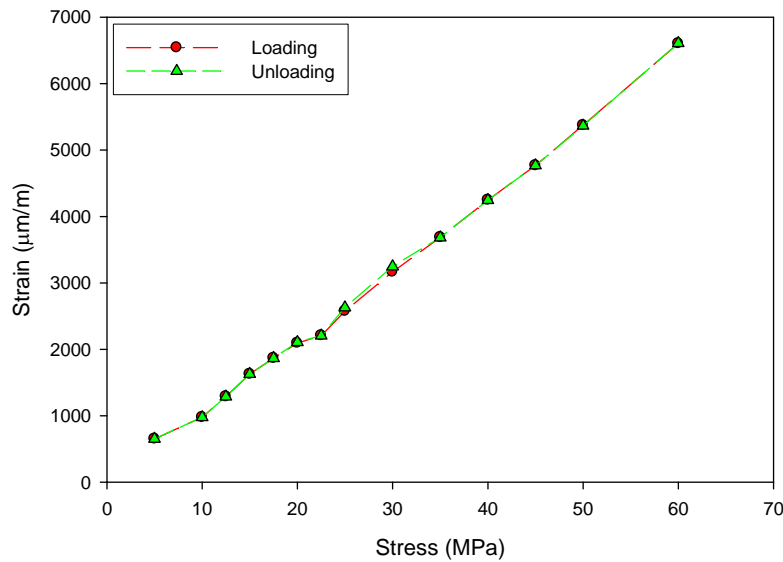
Figure 5.7 Instantaneous loading and unloading strains for the 3 mm thick GMT.

3. Since the plastic strains developed in these tests are small compared to the total creep strains, the instantaneous creep response can be determined directly from the experimental creep curves. g_0 can be obtained as the ratio of the instantaneous creep

response at any given stress level to that in the linear viscoelastic region. It has to be noted that when the magnitude of the plastic strains are higher, the instantaneous elastic response cannot be directly extracted from the experimental creep curves, as mentioned above. This is because part of the plastic strain is developed at the instant of loading which cannot be directly separated from the elastic response in single creep-recovery experiments.

4. The non-linear creep response for a creep-recovery experiment shown in Figure 2.11 is given by,

$$\varepsilon_c(t) = \left(g_0 D_0 + g_1 g_2 \sum_{i=1}^{N} D_i (1 - e^{-t/\tau_i}) \right) \sigma_0 \tag{68}$$

g_2 can be obtained by fitting equation (68) to the creep curves at stresses in the non-linear viscoelastic region of the material, since all the other parameters of the equation have been determined in the previous steps.

Table 5.2 Average Compliance Model parameters for the two materials.

Time constants (sec)		Parameters	3 mm	6 mm
-	-	D_0 (x 10^{-6} MPa)	103.35	152.09
τ_1	10	D_1	2.25	4.39
τ_2	100	D_2	2.28	4.78
τ_3	1000	D_3	3.52	7.04

The above procedure was used to obtain the non-linear parameters for all the six trials carried out for both materials. The non-linear parameters g_0 and g_2 obtained for the various trials were similar and were found to vary linearly with stress. Average values of these parameters (from the six trials) obtained for the 3- and 6-mm thick GMT are plotted in Figure 5.8 (a) and (b) respectively. The non-linear parameters have been curve fit to linear functions of stress. g_0 and g_2 as linear functions of stress for the 3-mm thick GMT was found as:

$$g_0 = \begin{cases} 1, & \sigma \le 20\,MPa \\ 0.9139 + \left(4.6503 \times 10^{-3}\right)\sigma, & \sigma > 20\,MPa \end{cases}$$

$$g_2 = \begin{cases} 1, & \sigma \le 20\,MPa \\ 0.9411 + 0.0128\,\sigma, & \sigma > 20\,MPa \end{cases} \tag{69}$$
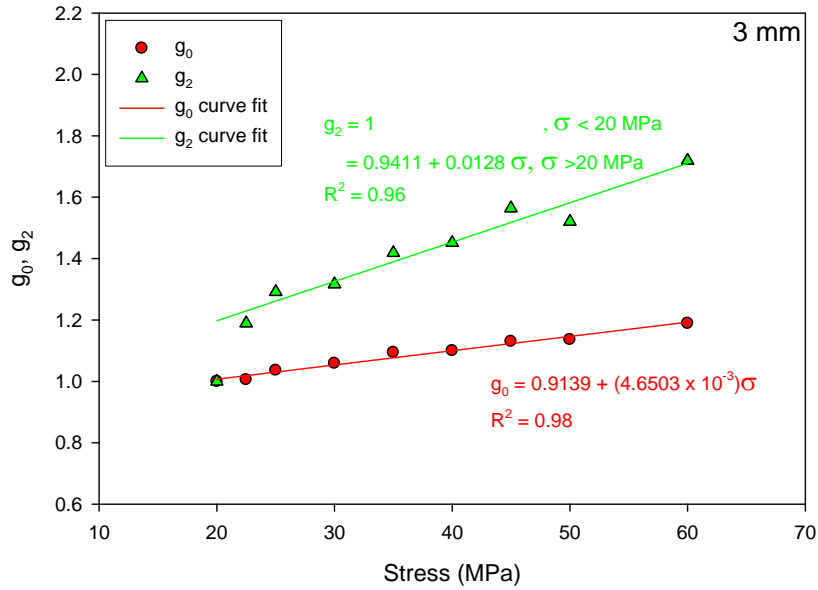
(a)
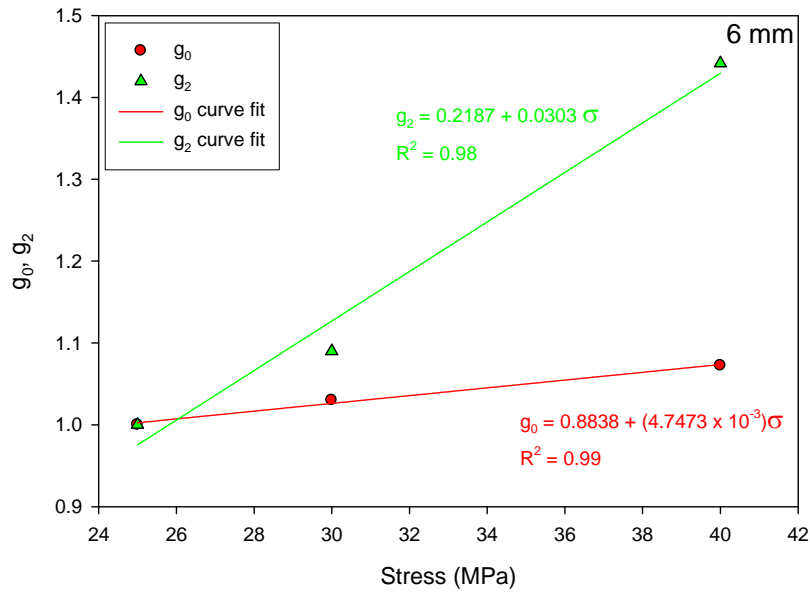
(b)

Figure 5.8 Non-linear viscoelastic parameters for the (a) 3-mm (b) 6-mm thick GMT.
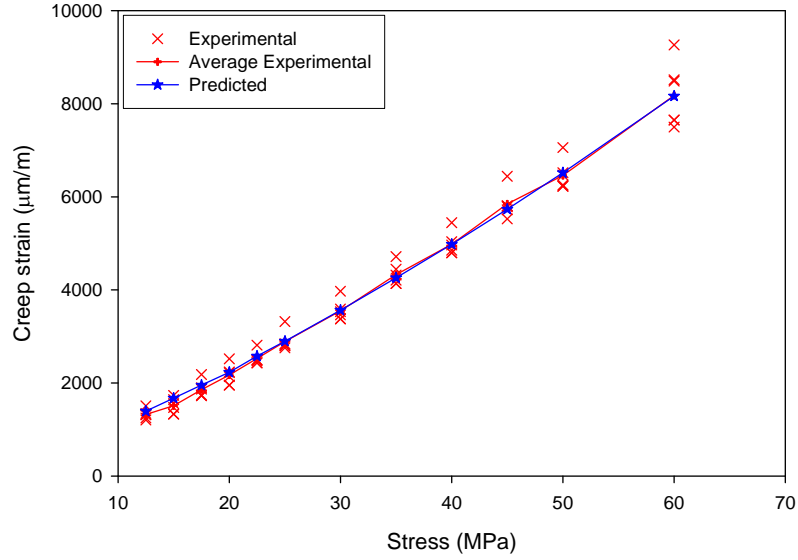
Figure 5.9 Comparison of the predicted creep strains at the end
of 30 minutes creep with the experimental strains for the 3 mm thick GMT.

g_0 and g_2 as linear functions of stress obtained for the 6-mm thick GMT was found as:

$$g_0 = \begin{cases} 1, & \sigma \leq 25\,MPa \\ 0.8838 + \left(4.7473 \times 10^{-3}\right)\sigma, & \sigma > 25\,MPa \end{cases}$$
$$g_2 = \begin{cases} 1, & \sigma \leq 25\,MPa \\ 0.2187 + 0.0303\sigma, & \sigma > 25\,MPa \end{cases} \tag{70}$$

5.2.4 Model Predictions

Overall, the models developed for each material predicted the creep strains very well as shown in Figure 5.9 which shows a comparison of the predicted creep strains for the 3 mm thick GMT with the experimental and the average experimental value (of 6 trials). The average parameters as given in Table 5.2 and equations (69) and (70) can predict the creep strains well within a variability of about 7 % for the two materials. Further, the models developed slightly over-predict the recovery strains in all the cases, especially at higher stresses due to the plastic strains as shown in Figure 5.10 (lower strains indicate over-prediction). It is therefore necessary to add a viscoplastic component to the constitutive model to account for the accumulative plastic strains. The models which

have been developed from short-term tests are expected to provide good predictions over relatively short durations especially at lower stress levels when the plastic strain development is minimal.
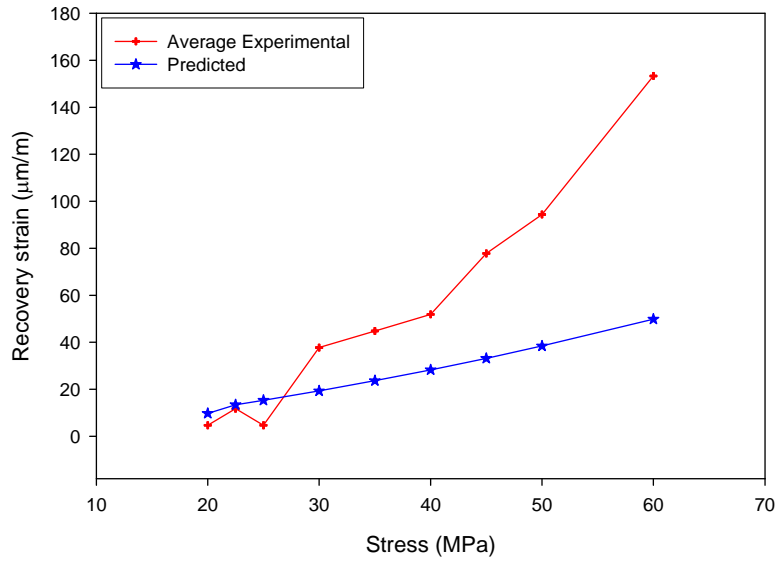
Figure 5.10 Comparison of the predicted strains after 30 minutes of recovery with the experimental at the various stress levels for 3-mm thick GMT.

5.3 Long term creep tests

From the short term test results presented in the previous section, it is clear that the long fiber GMT composite exhibits non-linear viscoelastic viscoplastic behaviour. However, since a single specimen was repeatedly tested at all the stress levels considered, the viscoplastic strains observed in the short term tests are less than the actual values. In order to obtain a general non-linear viscoelastic viscoplastic model, creep-recovery tests over a longer duration has been carried out. Creep tests consisting of one day creep followed by two day recovery over a stress range of 20 MPa to 80 MPa were conducted in increments of 10 MPa. These tests were replicated 4 times with each test carried out on separate randomly selected virgin specimens. The results of creep tests and development of a non-linear viscoelastic viscoplastic constitutive model of only the 3-mm thick GMT composite has been presented here.

5.3.1 Creep test results
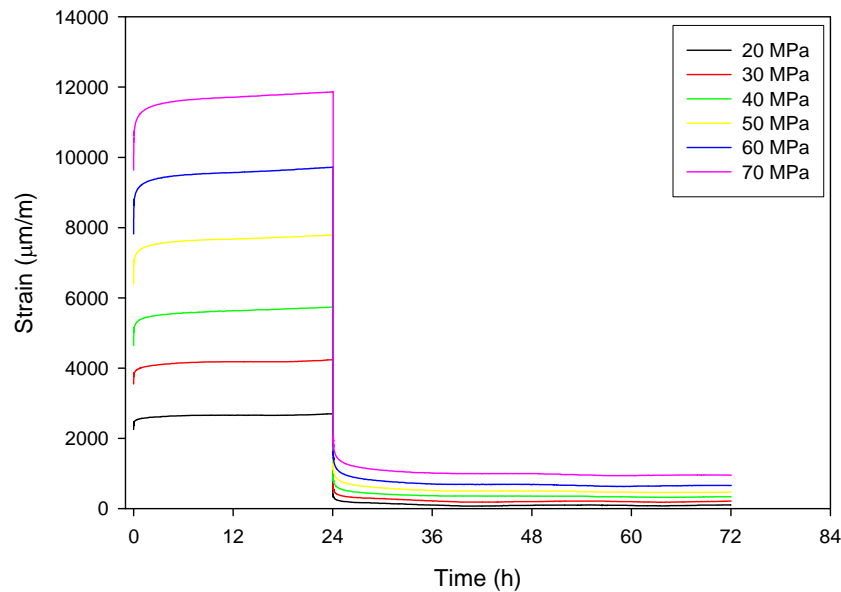
Figure 5.11 Average creep-recovery curves (1 day creep and 2 day recovery).

Figure 5.11 shows the average creep-recovery curves obtained at each of the six stress level increments between 20 and 70 MPa obtained. These curves were obtained as an

average of the four creep-recovery tests carried out at each stress level. The specimens were allowed to recover for two days following one day creep. Un-recovered strains at the end of 2 day recovery have been observed at all stress levels with the magnitude increasing with stress. It can be seen from Figure 5.11 that the rate of recovery is relatively fast during the first 12 hours after unloading but becomes negligible beyond that. Hence, the un-recovered strains after two-day recovery can be considered as a good estimate of the viscoplastic strains developed over one-day creep. This value will be referred to as the experimental viscoplastic strains. Figure 5.12 shows a non-linear increase in the average experimental viscoplastic strains accumulated over one-day of creep especially at stresses above 50 MPa. As mentioned earlier the development of these permanent strains has been associated with progressive accumulation of micro-damage in the material through mechanisms such as matrix cracking, fiber rupture and fiber-matrix debonding [56].
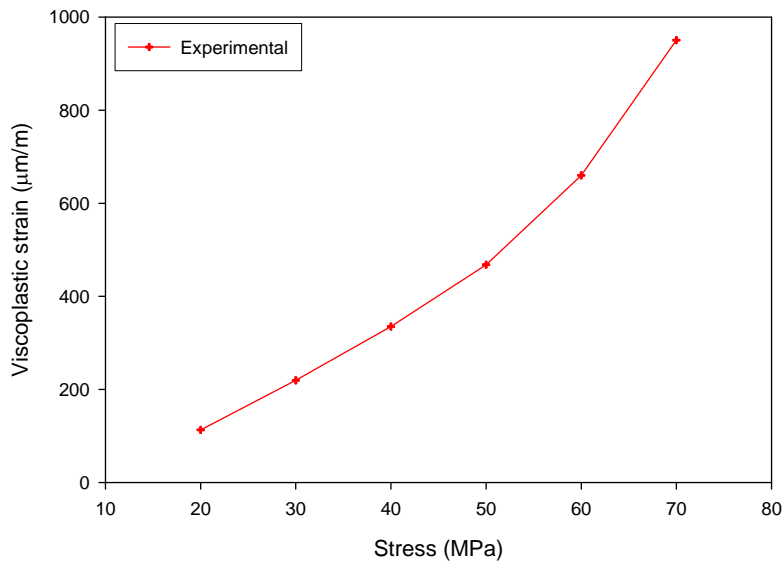
Figure 5.12 Average experimental viscoplastic strains developed during
1 day creep at the various stress levels.

Figure 5.13 shows a plot of the instantaneous strains, ε_o (as shown in Figure. 2.2(a)) versus stress. The average scatter in these tests was found to be about 7.5%. The standard deviation of the strains from 4 replicates over the creep duration was consistent, indicating that the variability is mostly in the instantaneous response of the material. Data

scatter is an inherent property of random mat materials because of their random fiber distribution and various levels of induced damage in the material following instantaneous loading.
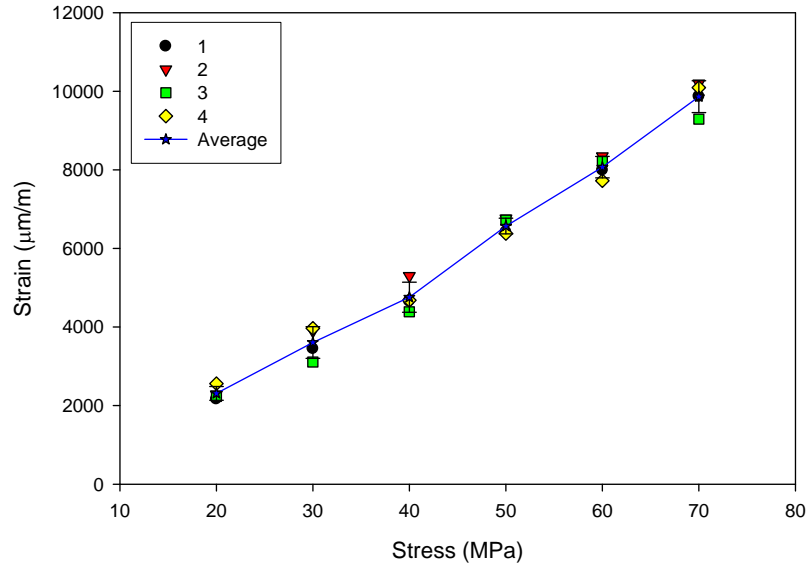
Figure 5.13 Instantaneous strains from creep tests at 6 stress levels.
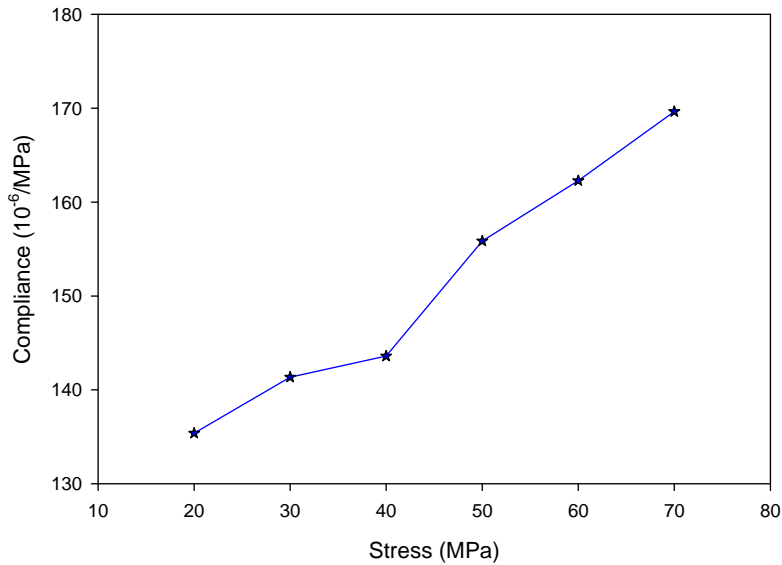
Figure 5.14 Average compliance at the end of 1 day of creep.

The average compliance from the four tests carried out at each stress level obtained from the creep strains at the end of 1 day creep is plotted in Figure 5.14. A linear increase in creep compliance with stress with the exception of the anomalous behaviour at 40 MPa

due to relatively larger data scatter at that load can been observed. Furthermore, statistical analysis, ANOVA has been employed to determine whether the use of a non-linear viscoelastic model can be justified considering the scatter in the experimental data. As with the short term tests, ANOVA was used to check the equality of the mean compliances at the various stress levels. The p-values obtained from ANOVA of the compliance at two time intervals, instantaneous and after one-day creep, were less than 0.05 indicating that the material compliance is dependent on the stress. Hence the material has to be modelled using a non-linear viscoelastic model.
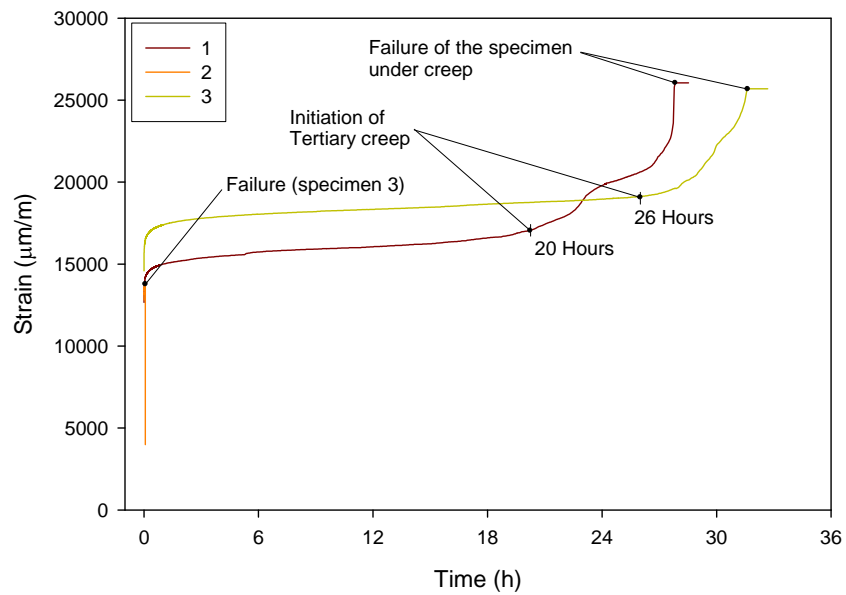
Figure 5.15 Creep curves at 80 MPa exhibiting primary, secondary, tertiary creep and finally failure.
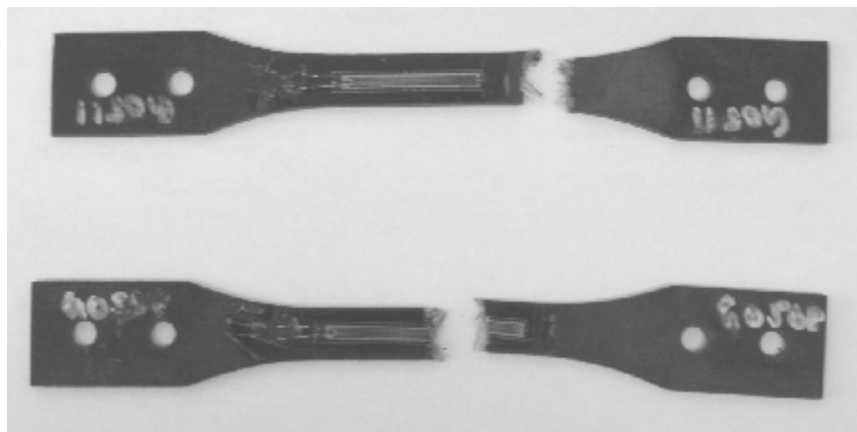
Figure 5.16 Failure of creep specimens at 80 MPa.

For tests performed at the highest stress level, i.e. 80 MPa, the variability in creep behaviour near the failure stage was rather high for the four specimens tested. As illustrated in Figure 5.15, one failed after 6 minutes of creep, two failed after 28 and 32 hours, respectively, exhibiting distinct tertiary creep zones while the last specimen did not show any signs of initiation of tertiary creep. Since the intent of the project is to develop models in the secondary creep region, the data at 80 MPa was not considered for analysis or constitutive modeling. The failed specimens are shown in Figure 5.16

5.3.2 Constitutive model

To model the creep in long fiber GMT composites, the total strains have to be decomposed as given in equation (45). The stress history during a creep-recovery experiment shown schematically in Figure 2.11 can be given as,

$$\sigma(t) = \begin{cases} \sigma_0, & 0 \le t \le t_r \\ 0, & t \ge t_r \end{cases} \tag{71}$$

The creep and the recovery strain response during the stress history given in equation (71) i.e., during the times $0 \le t \le t_r$ and $t \ge t_r$ respectively are given by equations (50) and (51) respectively. From the short-term test (induced damage is minimal) results presented in the previous section, the instantaneous creep and recovery strains were found to be equal (for which $g_1 = 1$). Since the short term tests provide a good estimate of the viscoelastic behaviour of the material, the same trend can be expected in the long term tests as well. Hence, the non-linearity parameter g_1 can be considered as one [32]. To further simplify the data reduction process and considering the scatter in the data, the stress shift factor a_σ was assumed to be one. Under these conditions ($g_1 = 1$ and $a_\sigma = 1$), the Schapery non-linear viscoelastic model reduces to the form of Findley's non-linear viscoelastic model [104]. Substituting Prony series expression in equation (66) for the transient creep compliance and using $g_1 = a_\sigma = 1$, the creep and recovery strains can be written as,

$$\varepsilon_c(t) = \left(g_0 D_0 + g_2 \sum_{i=1}^{N} D_i (1 - e^{-t/\tau_i}) \right) \sigma_0 + A \left((\sigma_0)^m t \right)^n \tag{72}$$

114

$$\varepsilon_r(t) = \left(\sum_{i=1}^{N} D_i \left(e^{-(t-t_r)/\tau_i} - e^{-t/\tau_i} \right) \right) g_2 \sigma_0 + A\left((\sigma_0)^m t_r \right)^n \qquad (73)$$

Reducing the viscoelastic model to the Findley's non-linear model implies that the dependence of the instantaneous response on stress is modeled by g_0 while dependence of the transient creep strains or the time dependent response is modeled by g_2.

5.3.3 Method for parameter estimation

As mentioned in the previous chapter, single duration creep-recovery experiments only provide a final value of the viscoplastic strains developed during creep as only the total strains are measured. No information regarding the evolution of the viscoplastic strain is obtained. However, it is possible to numerically separate the viscoplastic strain response from the total creep strains.

The equation for creep strains given in Equation (72) requires 15 constants and two stress dependent non-linear functions (considering a 5 term Prony series for the linear creep compliance). To estimate the model parameters of the Findley's non-linear viscoelastic combined with Zapas and Crissman viscoplastic model employed, the following procedure was adopted:

1. An estimate of the permanent strain $\varepsilon_{vp}(t_r)$ can be obtained as the total un-recovered strain after very long recovery durations (usually 2 to 3 times the creep duration).

2. Using these values of $\varepsilon_{vp}(t_r)$, $\varepsilon_r(t) - \varepsilon_{vp}(t_r)$ can be calculated from experimental data at various stress levels. From equation (73) it can be shown that ,

$$\varepsilon_r(t) - \varepsilon_{vp}(t_r) = \left(\sum_{i=1}^{N} D_i \left(e^{-(t-t_r)/\tau_1} - e^{-t/\tau_1} \right) \right) g_2 \sigma_0 \qquad (74)$$

115

3. $\varepsilon_r(t) - \varepsilon_{vp}(t_r)$ data from creep-recovery test at a stress in the linear viscoelastic region is fit into equation (74) by considering $g_2 = 1$, to obtain the parameters of the Prony series. The time constants τ_i can be pre-selected to simplify the curve fitting process [56].

4. $\varepsilon_r(t) - \varepsilon_{vp}(t_r)$ data from tests at stresses in the non-linear viscoelastic region are curve fit to equation (74) using the parameters of the Prony series from step 3, to determine g_2 at each stress level considered.

5. In order to eliminate the plastic strain from the equation, the strain $\varepsilon_R(t) = \varepsilon_c(t_r) - \varepsilon_r(t)$ is calculated from the experimental data [53]. Using equations (72) and (73), it can be shown that,

$$\varepsilon_R(t) = \varepsilon_c(t_r) - \varepsilon_r(t) = \left(g_0 D_0 + g_2 \sum_{i=1}^{N} \left(D_i \left(e^{t_r/\tau_i} - 1 \right) \left(e^{-t_r/\tau_i} - e^{-t/\tau_i} \right) \right) \right) \sigma_0 \tag{75}$$

6. $\varepsilon_R(t)$ calculated at a stress in the linear viscoelastic region is curve fit to equation (75) to determine D_0 ($g_0 = 1$).

7. Similarly, $\varepsilon_R(t)$ calculated at stress levels in the non-linear viscoelastic region is curve fitted to equation (75) to determine g_0 at each stress level considered by using D_0 from step 6.

8. Since all the parameters of the viscoelastic model in equation (72) have been determined, the parameters of the viscoplastic model can be obtained by fitting equation (72) to the creep curves. Another way would be to estimate the viscoplastic strains by subtracting the predicted viscoelastic strains from the experimental creep strains [53] and the resulting curves are then fit to equation (48) to obtain the parameters of the viscoplastic model.

116

In the above method, the viscoplastic strains are estimated using the non-linear viscoelastic model predictions. Hence, it is critical that a representative viscoelastic model is developed, as slight variations can cause errors in the calculation of the plastic strains.

5.3.4 Non-linear viscoelastic viscoplastic model

The estimation of parameters in the constitutive model was carried out using the average of four creep-recovery tests conducted at each stress level. Two different models were considered to model the compliance – simple power law (equation (34)) and Prony series. In case of power law (not given here), curve fits to both $\varepsilon_r(t) - \varepsilon_{vp}(t_r)$ (step 4) and $\varepsilon_R(t)$ (step 7) yielded good initial predictions however tend to diverge from the experimental data at longer times ($R^2 > 0.95$ was obtained in most cases). Prony series yielded better fits to the experimental data with R^2 values greater than 0.99 in most of the cases and hence was considered for the model. A 5- term Prony series was considered to model the compliance and the time constants of the model were pre-selected as $\tau_i = 10^i$ seconds. The parameters of the Prony series used to model the linear viscoelastic compliance are given in Table 5.3. The non-linear parameters obtained are plotted in Figure 5.17. It can be seen that the g_0 increases linearly with stress (with the exception of that at 40 MPa). Moreover, g_2 was found to be one for stresses up to 30 MPa and increases linearly thereafter.

Table 5.3 Coefficients and time constants of Prony series
model of linear viscoelastic creep compliance.

Time constants (sec)		Coefficients (10^{-6} MPa)	
-	-	D_0	110.67
τ_1	10	D_1	3.23
τ_2	100	D_2	4.64
τ_3	1000	D_3	5.27
τ_4	10000	D_4	5.13
τ_5	100000	D_5	1.49
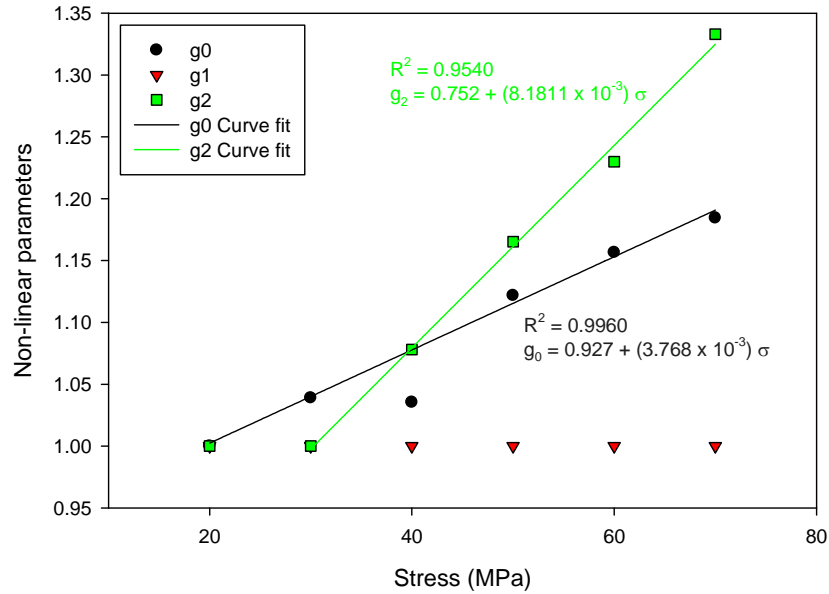
Figure 5.17 Non-linear parameters of the Schapery non-linear viscoelastic model.
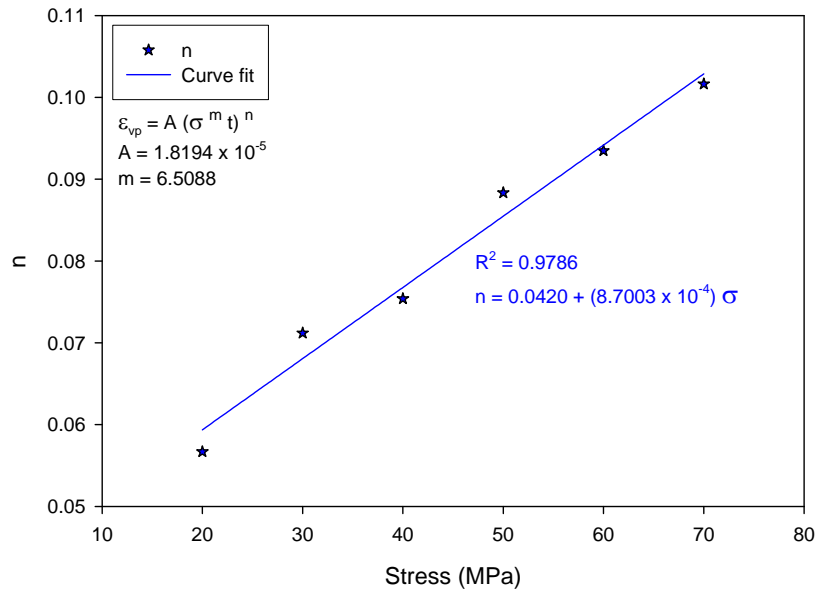
Figure 5.18 Parameters of the viscoplastic constitutive model.

g_0 obtained from the long term tests (Figure 5.17) are similar in magnitude to that obtained from the short term tests (Figure 5.8 (a)) while g_2 obtained from the short term tests (Figure 5.8 (a)) are much higher than those from the long term tests (Figure 5.17).

This difference might be due to the difference in durations of the two tests schemes (30 minutes and 1 day) as g_2 operates on the transient component of the creep data.

Using the model parameters thus obtained, the viscoplastic strains were determined by fitting equation (72) to the average creep curves. In order to obtain a general model for all the stress levels, two of the three parameters ($A = C^n$ and *m*) were considered to be constants as the average value of the parameters obtained from an initial curve fit. The creep curves were fitted to equation (72) to obtain '*n*' as a function of stress as shown in Figure 5.18.

Finally, the non-linear parameters - g_0 and g_2 of the viscoelastic constitutive model and '*n*' of the viscoplastic constitutive model were fit to linear models as shown in Figures 5.17 and 5.18 respectively. These linear models of stress are given in equations (76) and (77). The parameters of the linear viscoelastic compliance given in Table 5.3 together with equations (76) and (77) form the final non-linear viscoelastic viscoplastic constitutive model.

Non-linear parameters of the viscoelastic model:

$$g_0 = 0.927 + (3.768 \times 10^{-3})\,\sigma$$

$$g_2 = \begin{cases} 1, & \sigma \leq 30\,\text{MPa} \\ 0.752 + (8.1811 \times 10^{-3})\,\sigma, & \sigma > 30\,\text{MPa} \end{cases} \tag{76}$$

Viscoplastic model:

$$A = C^n = 1.8194 \times 10^{-5}$$

$$m = 6.5088 \tag{77}$$

$$n = 0.0420 + (8.7003 \times 10^{-4})\,\sigma$$

5.3.5 Model predictions
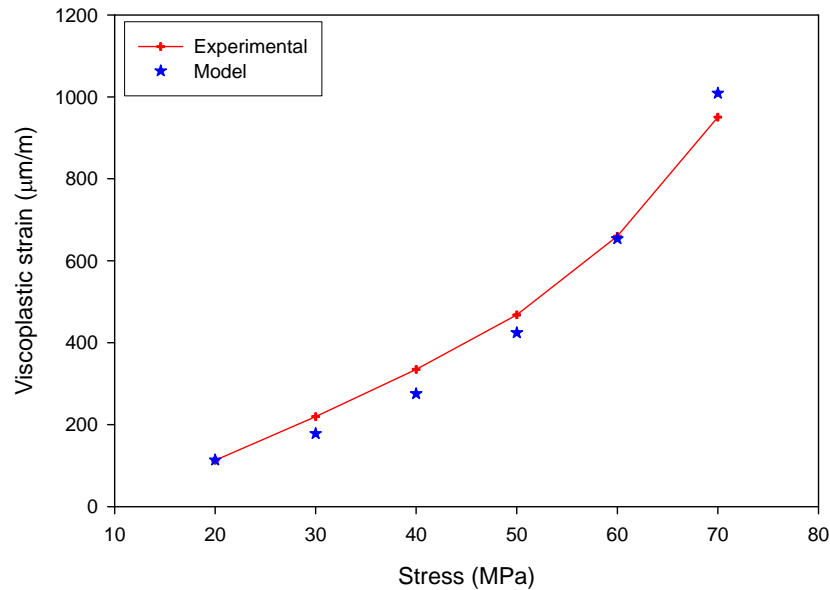
Figure 5.19 Average Experimental and predicted un-recovered plastic strains after 2 day recovery following 1 day creep.

A comparison of the viscoplastic strains predicted using the model in equation (77) with the experimental values is shown in Figure 5.19. The model under-predicts the viscoplastic strains at stresses between 30 and 50 MPa and over-predicts at 70 MPa. The predicted viscoplastic strains during creep and recovery are shown in Figure 5.20. The viscoplastic strains are only developed under load and hence the viscoplastic strains are constant during recovery. Figure 5.21 shows the three strain components i.e., elastic, viscoelastic and viscoplastic as predicted using the model along with the total strains and the experimental creep curves. It can be seen that the magnitude of the viscoplastic strains is comparable (>50%) with the viscoelastic strains and hence form a major portion creep. The creep and recovery predictions are compared with the experimental values in Figures 5.22 and 5.23 respectively. The creep curves at 70 and 40 MPa are over-predicted while that at the other stress levels are in good agreement with the experiment. The non-linear viscoelastic model is sensitive to the values of g_0 as it affects the instantaneous response, which is greater than either the viscoelastic or the viscoplastic response as shown in Figure 5.21. Since equation (76) slightly over-estimates the non-linear

parameter, g_0, (Figure 5.17), the overall strains at certain stress levels are also over-predicted. The recovery strains predicted at the two extreme stress levels – 20 and 70 MPa are very good. At the intermediate stress levels, the model developed slightly over-predicts the initial recovery behaviour but gives good predictions at longer times.
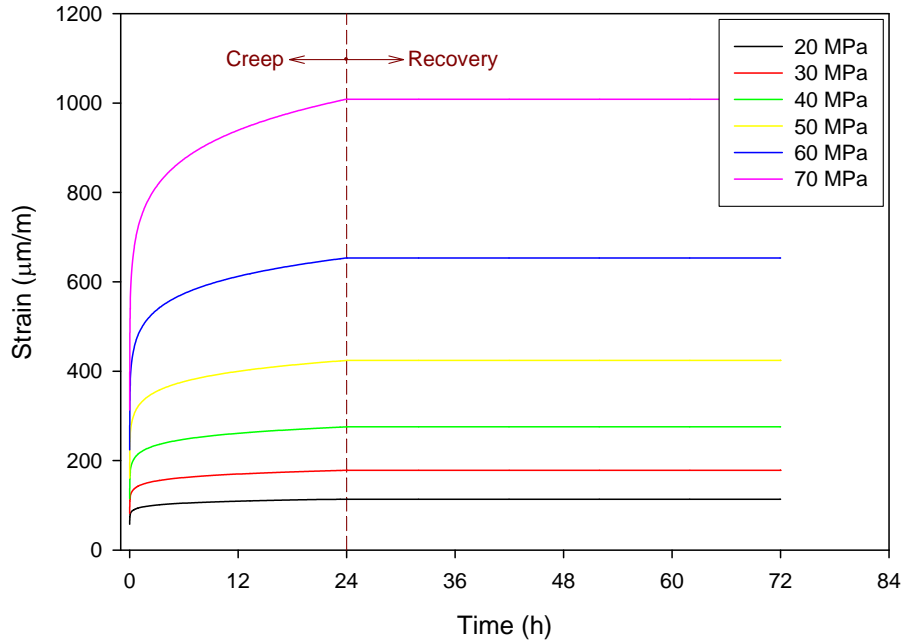
Figure 5.20 Predicted plastic strains during creep and recovery.
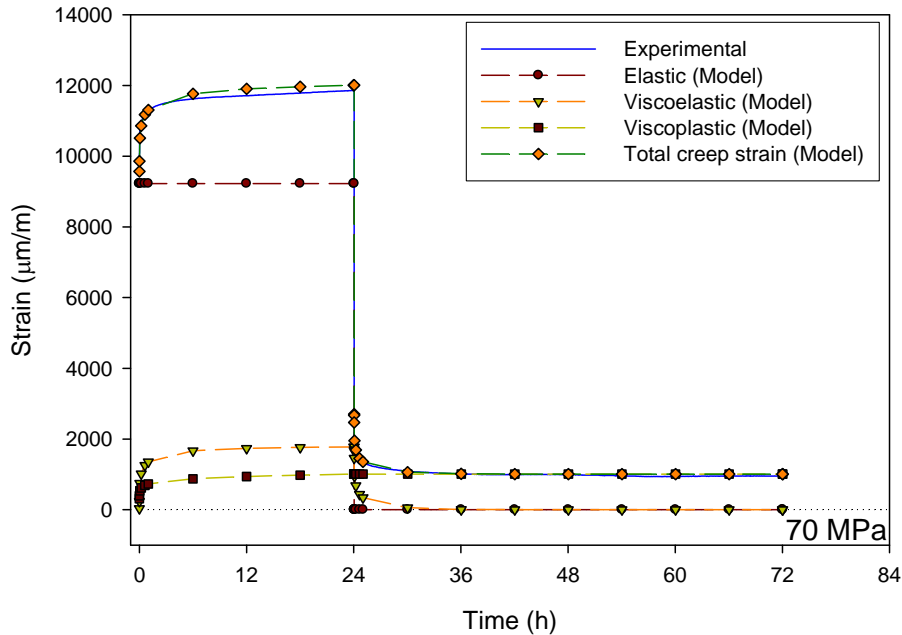
Figure 5.21 Average experimental, elastic, viscoelastic
and viscoplastic strains at 70 MPa.
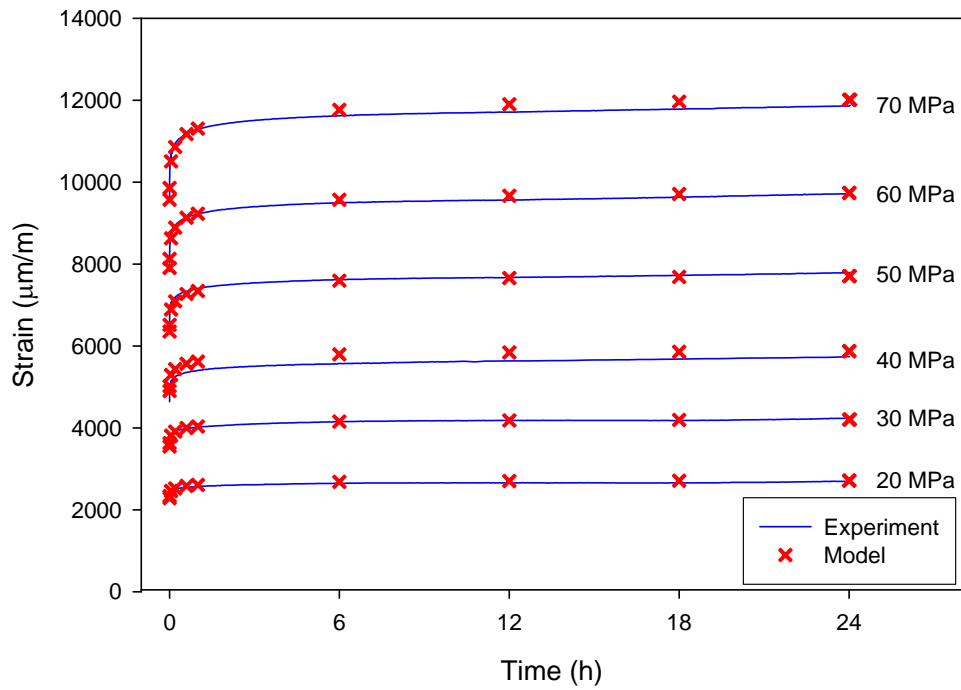
Figure 5.22 Comparison of the non-linear viscoelastic viscoplastic model prediction with the experimental creep strain.
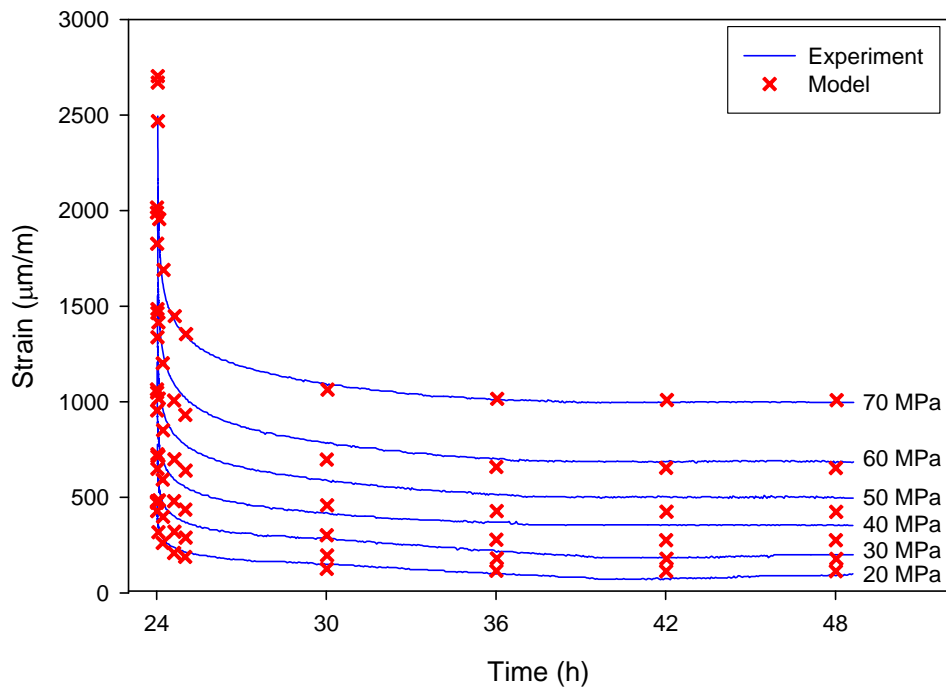
Figure 5.23 Comparison of the non-linear viscoelastic viscoplastic model prediction with the experimental recovery strain.

Finally, the total creep strain predictions after 1-day creep for the various stress levels are compared with the experimental values in Figure 5.24. It can be seen that the slight differences in the model predictions in Figures 5.22 and 5.23 are not significant especially when the scatter in the material creep properties is considered.
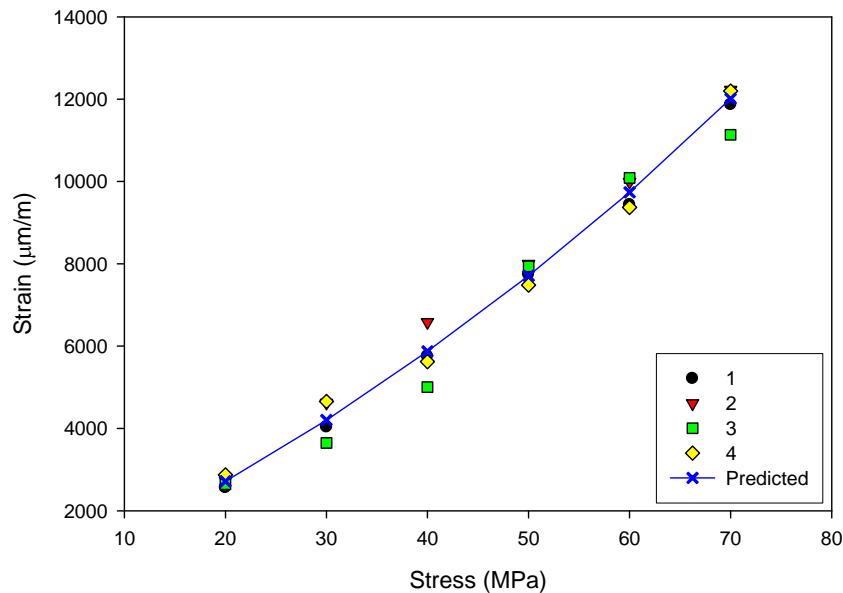
Figure 5.24 Comparison of predicted total creep strains after 1 day creep with the experimental values.

5.4 A note on Prony series

In the previous section on the short term creep tests, it was mentioned that a model in the form of Prony series was used to predict the recovery strains using the Superposition principle. According to the superposition principle, the creep data was extrapolated to a duration equal to the creep and recovery i.e., the model obtained from 30 minutes creep was used to obtain creep predictions over 60 minutes. Hence, it is essential to know the characteristics of the Prony series and its extrapolation capability over this duration.

A 3-term Prony series will be considered to illustrate the characteristics of the equation. The contribution of each term of the Prony series and the total of the 3-term Prony series given in equation (66) (n=3) for unit co-efficients (D_0, D_1, D_2 and D_3) with relaxation

times of 10, 100 and 1000 respectively are shown in Figure 5.25. It can be seen that the first and second terms of the Prony series increase with time and finally attain the maximum value. The terms remain constant at the maximum value i.e., the value of the co-efficient (one in this case). It can be observed that both the first and second terms attain the maximum value after a time equal to 5-6 times the relaxation time. The third term shows a similar trend. Similar characteristics can be expected for a Prony series with larger number of terms.
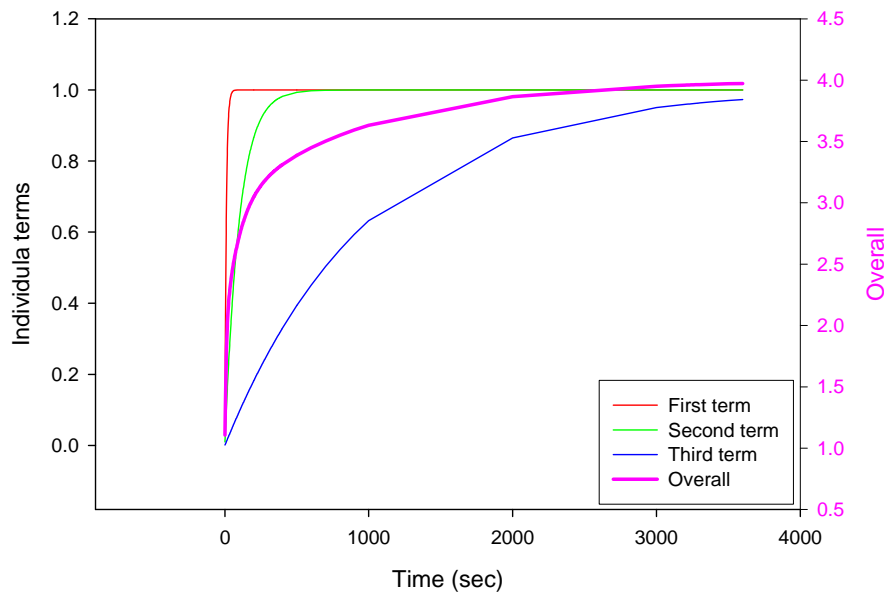
Figure 5.25 Contribution of individual terms of the Prony series.

To determine how well the Prony series extrapolates the creep response, 4 curves from the long term tests (24 hours creep) were selected at random. The data up to the first 30 minutes was used to obtain the parameters of a 3-term Prony series. This model was then used to predict the compliance after 60 minutes and compared with the experimental curves. The experimental and predicted values are shown in Figure 5.26. As can be seen, the predicted curves underestimate the compliance after about 2200 seconds, however very slightly. The compliance predictions after 1 hour creep are about 0.6 % less than the experimental.

124
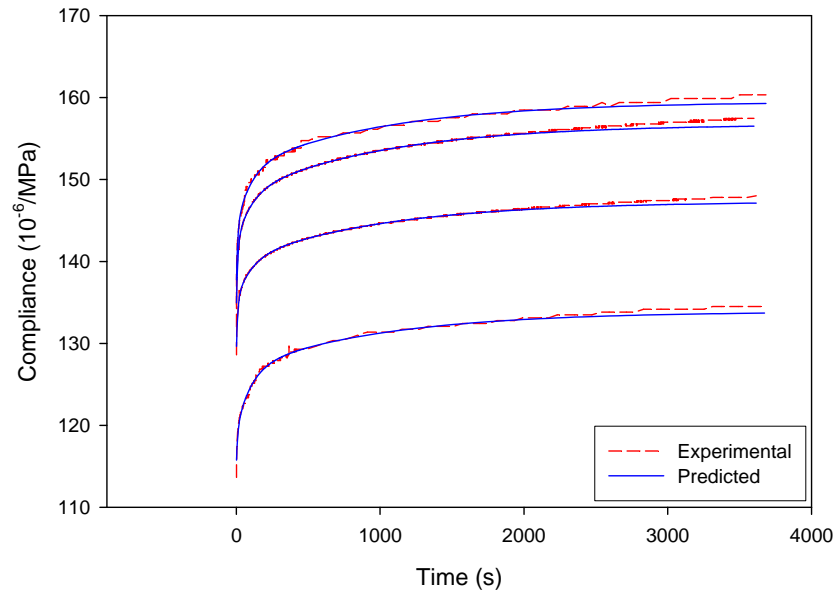
Figure 5.26 Comparison of the predictions obtained from a
3 term Prony series with the experimental.

5.5 Chapter conclusions

The main conclusions of this chapter are:

- From three linearity tests carried out on the short term creep test data, the linear viscoelastic range seemed to depend on the fiber weight fraction. It was found that the 6-mm thick GMT with a higher fiber weight fraction was linear viscoelastic up to 25 MPa while that for the 3-mm thick GMT was only up to 20 MPa. Non-linear viscoelastic constitutive models developed from the short-term creep data have provided fairly good creep predictions over relatively short durations. However, plastic strains tend to develop during creep over time which necessitates the addition of a viscoplastic component to the constitutive model.

- From long term tests of 1 day creep followed by recovery conducted on the 3-mm thick GMT over a stress range of 20 to 80 MPa, it was found that the material exhibits non-linear viscoelastic viscoplastic behaviour. A model for predicting viscoelastic-viscoplastic creep-recovery behaviour of a long-fiber glass mat thermoplastic composite has been developed. Findley's non-linear viscoelastic model coupled with Zapas and Crissman viscoplasticity model has been used to describe the creep behaviour of the material. A simplified data reduction method has been employed to determine the parameters of the constitutive model. Creep predictions of the developed model are in good agreement with the experimental values while the recovery strains are slightly over-estimated at many stress levels. However, the final predictions are well within the scatter range of the material which is about ±7.5%.

CHAPTER 6

RESULTS AND DISCUSSION:

EFFECT OF TEMPERATURE ON CREEP IN GMT MATERIALS

6.1 Overview

Temperature has a strong influence on the mechanical properties of polymeric materials. As seen from the DMA results presented in Section 4.2, the storage modulus of the material reduces by 30% as the temperature is increased from 25°C to 80°C. Semi-structural automotive components made from GMT composites are subjected to temperature variations during service. For example, in a hot climate under direct sun, the temperature of some of the components can rise to over 80°C. Hence, the characterization of GMT composites under thermo-mechanical loads is important to ensure confidence in component design. This chapter will present results of the following analysis:

a. Development of long-term creep model from short term tests using Time-Temperature-Superposition

b. Determination of temperature-dependent non-linear viscoelastic parameters and

c. Determination of temperature-dependence of viscoplastic strains

As before, in consideration of the scatter in the material properties, two separate creep test schemes have been employed:

1. Short term creep tests – 30 minutes creep followed by 60 minutes recovery

2. Long term creep tests – 1 day creep followed by 2 day recovery

Results from these test schemes will be described in the following sections.

6.2 Short term creep tests

As with the short term tests carried out to determine stress effects on GMT creep in the previous chapter, the short-term tests presented in this section were carried out to capture

the temperature dependence of the creep properties while minimizing the effects of inherent variability in the material.

Short-term creep tests consisting of 30 minutes creep followed by 60 minutes recovery were conducted. Tests at five stress levels between 20 and 60 MPa in increments of 10 MPa and 14 temperature levels between 25 and 90°C in intervals of 5°C have been performed. Scatter in the material properties is a problem with random fiber mat composites. Hence, to eliminate the material variability and to isolate the effect of temperature on the creep behaviour, a single specimen was tested at all the 14 temperature levels consecutively at each stress level. It has been found that the thermal exposure over the temperatures and durations considered here does not degrade the material properties [105], i.e., physical aging or thermal degradation has not been detected at 90°C over 11 days. Furthermore, to improve the confidence of the obtained data, tests at each stress level were repeated at least 3 times using separate specimens and average curves obtained from these tests were used for analysis. Tests at 60 MPa were performed only once since this test condition tends to induce high plastic strains.

The creep tests were carried out inside an oven. Before each creep-recovery test, the oven temperature was increased to the desired value and the fixture with a mounted specimen was held at this temperature for 15 minutes. This was to ensure that both the fixture and the specimen are at the same temperature as the oven. Before starting a new creep-recovery test, any residual viscoplastic strains from the previous test was reset to zero.

6.2.1 Pre-conditioning treatment

From the results presented in the previous section, it is clear that plastic strains are developed during creep in GMT composites. The magnitude of the viscoplastic strains accumulated for all the stresses up to 70 MPa is significant (5 – 10 % of the instantaneous strain and is greater than 50% of the viscoelastic strains). Intuitively, temperature will also affect the accumulation of viscoplastic strains in these materials but the extent of this effect is not clear. Hence, to minimize the formation of viscoplastic strains during the

tests (especially at higher temperatures), all the specimens used for the creep tests were pre-conditioned. Pre-conditioning is commonly adopted to reduce scatter in the data.

Creep specimens were pre-conditioned at room temperature using the same creep fixture. Pre-conditioning consisted of conducting 15 creep-recovery cycles of about 15 second duration (each) at room temperature at a stress of 50 MPa (~60% of the UTS) for specimens tested between 20 and 50 MPa. The specimen used for the creep test at 60 MPa was pre-conditioned at 60 MPa. Figure 6.1 shows the typical strains observed during pre-condition. As seen, a rapid increase in plastic strains was observed up to the 5th cycle while the increase in the plastic strains beyond this was small. Following the pre-conditioning, the creep fixture was recalibrated to the force corresponding to the stress required for the creep test. The specimen was then subjected to 2 cycles of 15 minutes creep followed by 15 minutes recovery and 1 cycle of 30 minutes creep followed by 60 minutes recovery at room temperature (~22°C). These three creep-recovery cycles were conducted to eliminate any viscoplastic strains which might be developed at the test stress. However, the plastic strains developed during these tests were minimal indicating the effectiveness of pre-conditioning in reducing viscoplastic strains during the creep tests.
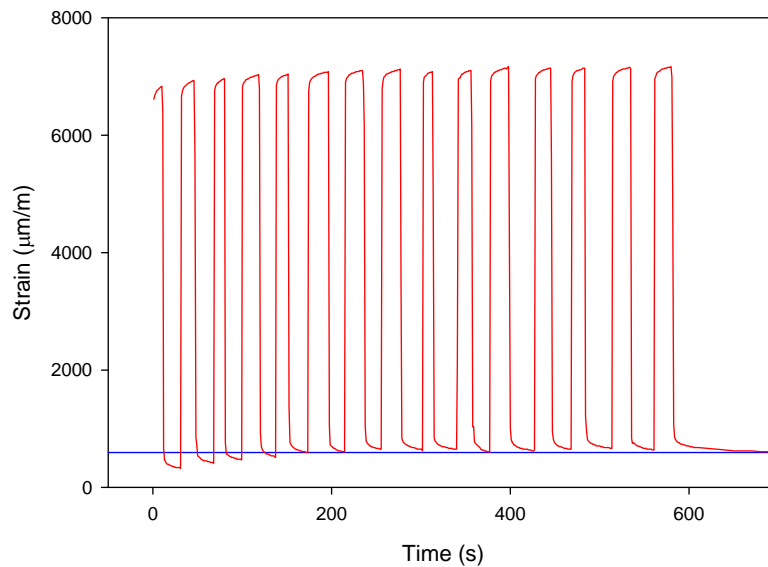
Figure 6.1 Pre-conditioning of creep specimens.

6.2.2 Coefficient of thermal expansion

Before starting each creep-recovery test, the fixture and the specimen were soaked at the set temperature for 15 minutes. The strains before and after heating the specimen were recorded along with the temperature. The thermal strains obtained from these tests are plotted with both absolute temperature and relative temperature in Figure 6.2. Using 25°C as the reference temperature, T_{ref}, the thermal strains were fitted to a model of the form given in equation (78). The coefficient of thermal expansion, α, was found to be 11.9365×10^{-6} /°C. A rather large scatter of about 25% was observed in the value of the thermal strains. The data plotted in Figure 6.2 was obtained as an average of 14 tests.

$$\varepsilon_{TE} = \alpha (T - T_{ref}) = \alpha \; \Delta T \tag{78}$$
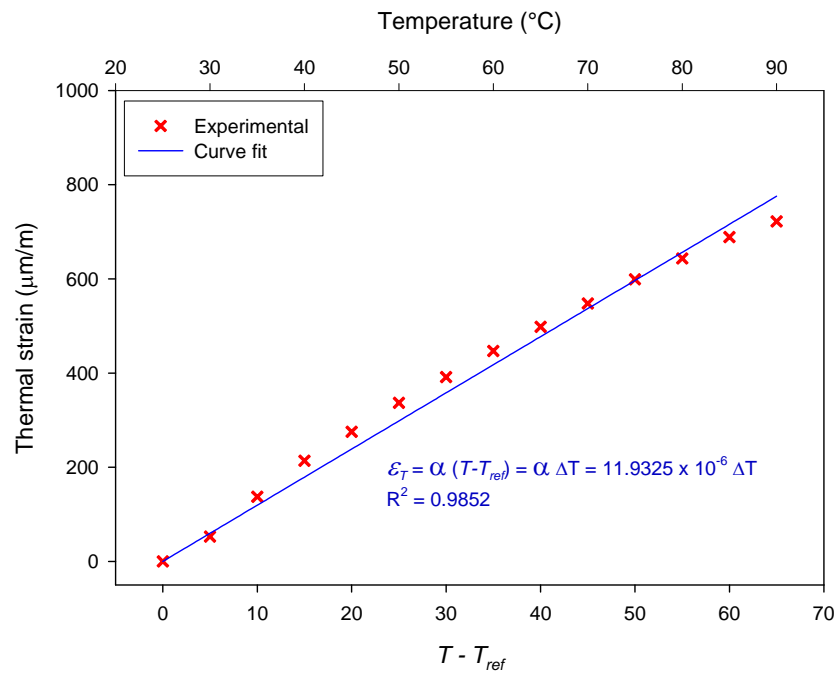
Figure 6.2 Thermal strains measured for GMT composite.

6.2.3 Creep test results

Figures 6.3 to 6.7 show the average isothermal creep-recovery curves obtained at the 14 temperature levels for stresses ranging from 20 to 60 MPa respectively. An overlay of the creep-recovery curves at the five stress levels for the temperatures considered is plotted

in Figure 6.8. These figures show that the creep-recovery behaviour over the 20 – 50 MPa stress range is fairly similar with creep strains increasing at similar rates with temperature. However the creep rate is much higher at 60 MPa than at the lower stresses especially for temperatures higher than 50°C. The variability in the data at room temperature was about 8 % with slightly higher scatter at higher temperatures mostly due to variability caused by thermal expansion. In all of the creep-recovery curves in Figures 6.3 to 6.7, the strains due to thermal expansion have been deducted from the raw data.
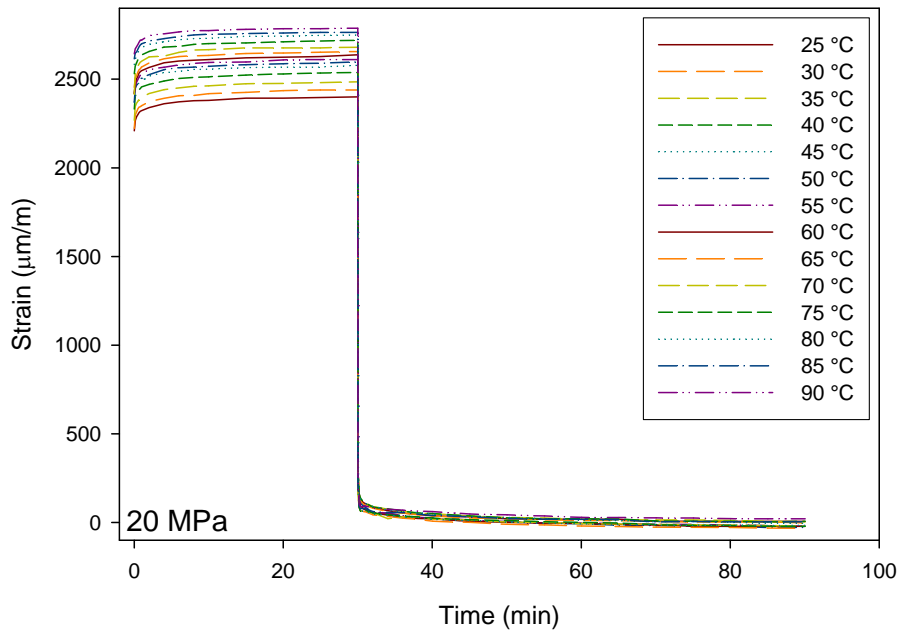
Figure 6.3 Creep-recovery curves over the various temperatures at 20 MPa.
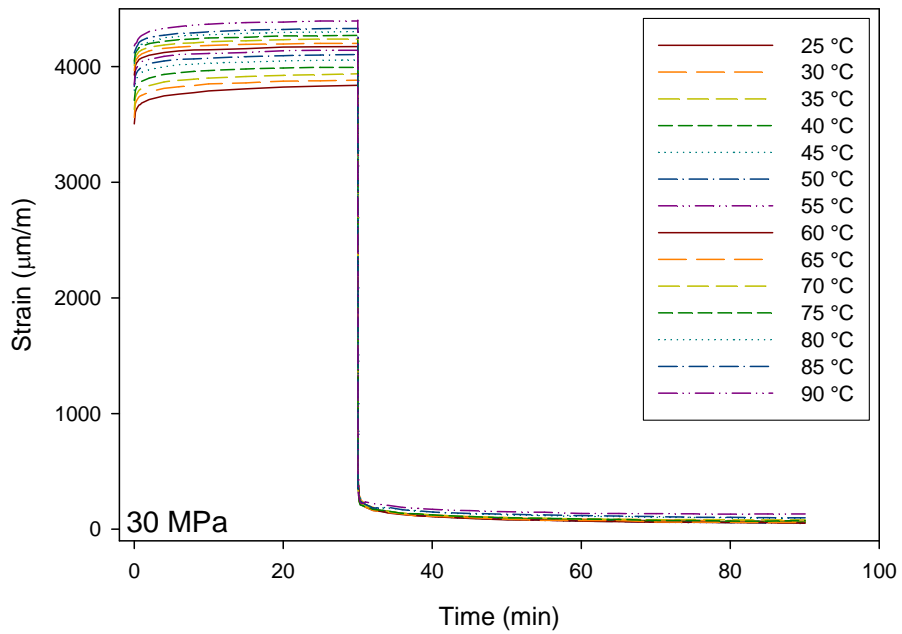
Figure 6.4 Creep-recovery curves over the various temperatures at 30 MPa.
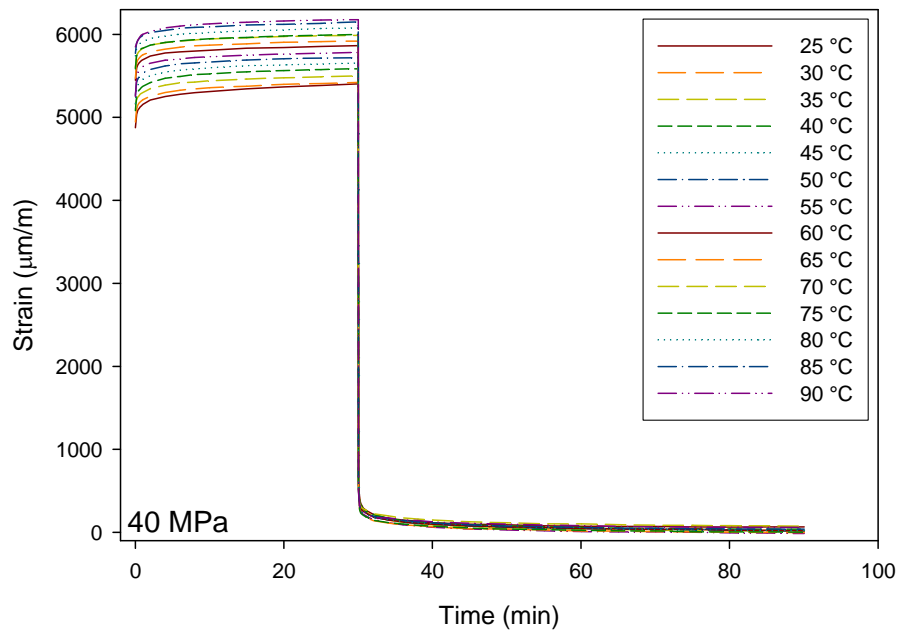
Figure 6.5 Creep-recovery curves over the various temperatures at 40 MPa.
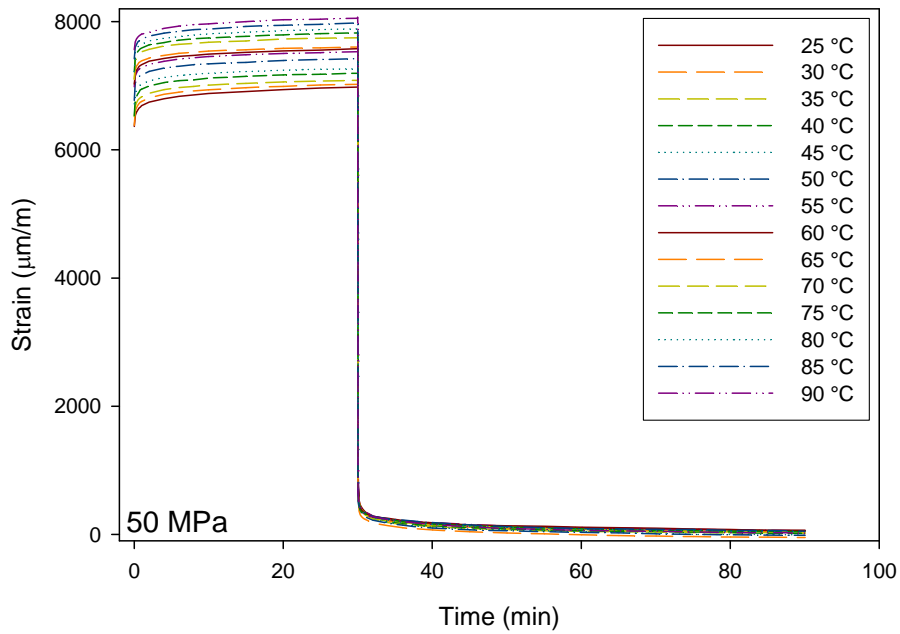
Figure 6.6 Creep-recovery curves over the various temperatures at 50 MPa.
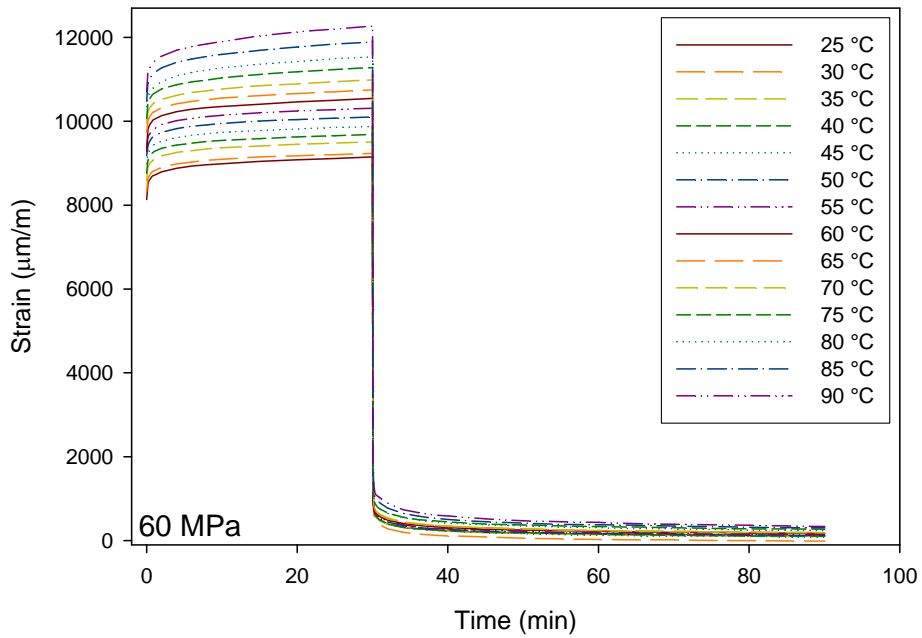
Figure 6.7 Creep-recovery curves over the various temperatures at 60 MPa.
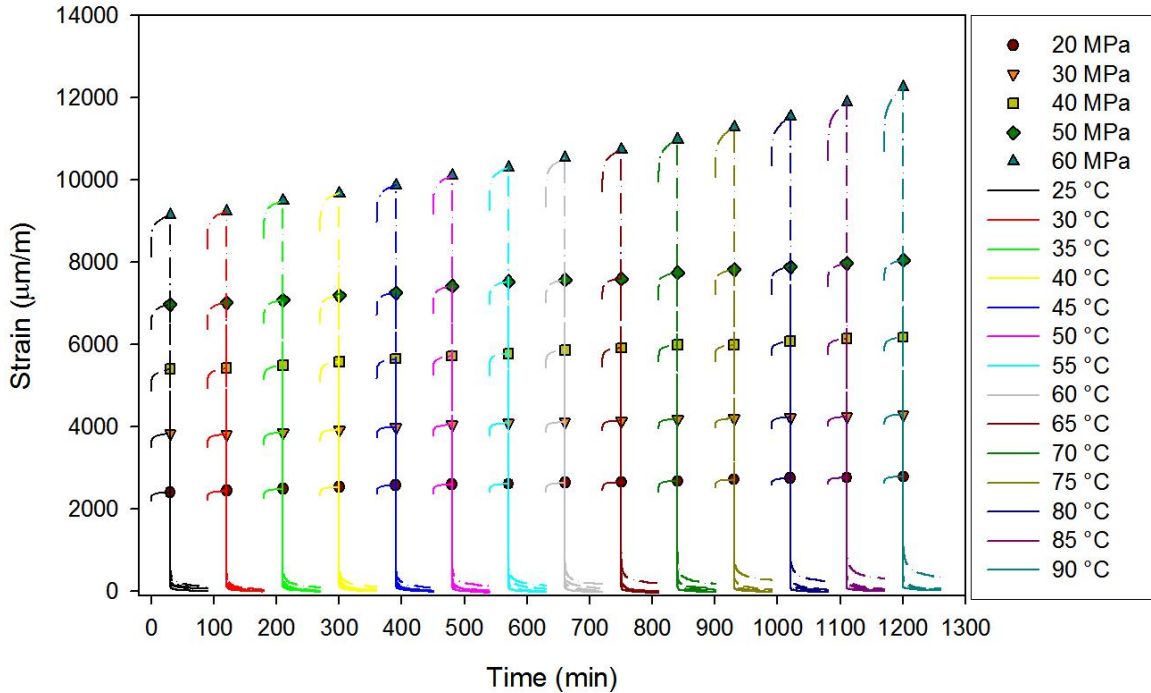
Figure 6.8 Overlay of creep recovery curves over the 14 temperatures
at stresses between 20 and 60 MPa.

Figure 6.9 (a) shows the variation of average compliance (instantaneous) with stress at the various temperature levels. The compliance increases linearly with stress at lower temperatures and becomes increasingly non-linear with stress at higher temperatures especially at stresses above 40 MPa. Figure 6.9 (b) shows the variation of compliance at the end of creep with temperature at the various stress levels. The compliance increases almost linearly with temperature at all stress levels. The compliance versus temperature curves up to 50 MPa (with the exception of the 30 MPa curve after 60°C which is probably due to scatter) are almost parallel to each other indicating similar temperature dependence of the creep behaviour at these stress levels. The increased slope of the compliance-temperature curve at 60 MPa shows increased temperature dependent non-linearity. The creep strains (only the transient component) developed over 30 minutes under load with temperature at the various stress levels is plotted in Figure 6.10. Creep strains decreased slightly with increasing temperature up to 50 MPa but the reverse occurred at 60 MPa.
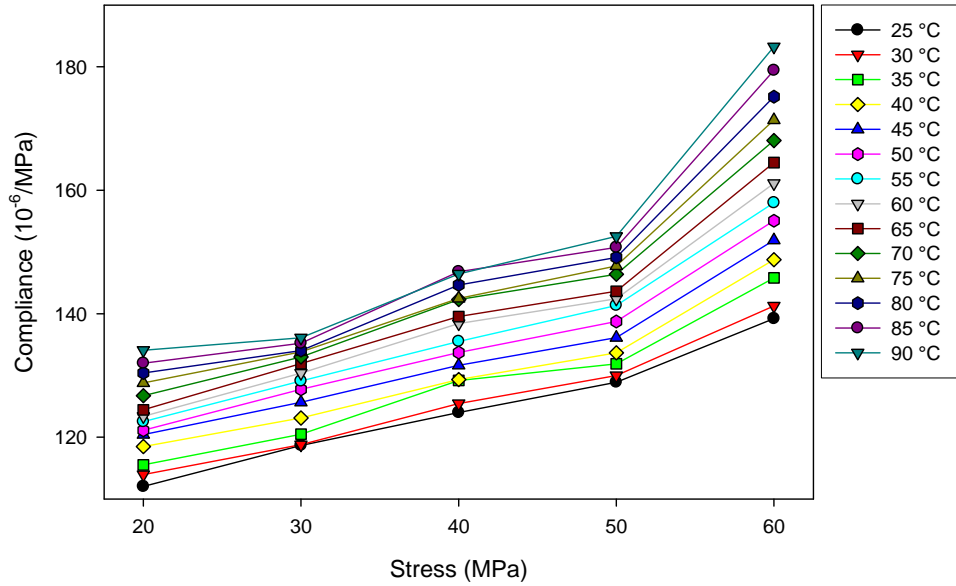
(a)
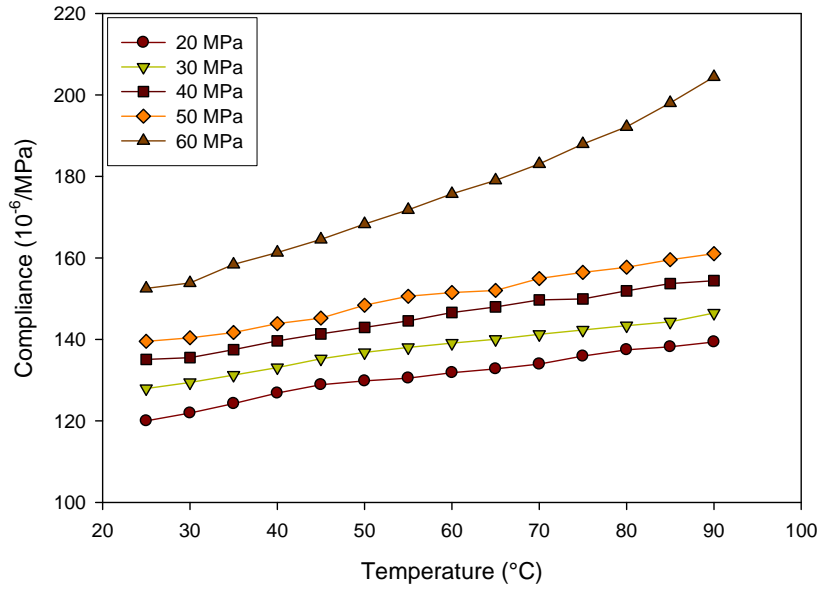
(b)

Figure 6.9 Variation of (a) Instantaneous compliance with stress at the various temperatures (b) compliance at end of creep with temperature at various stresses.
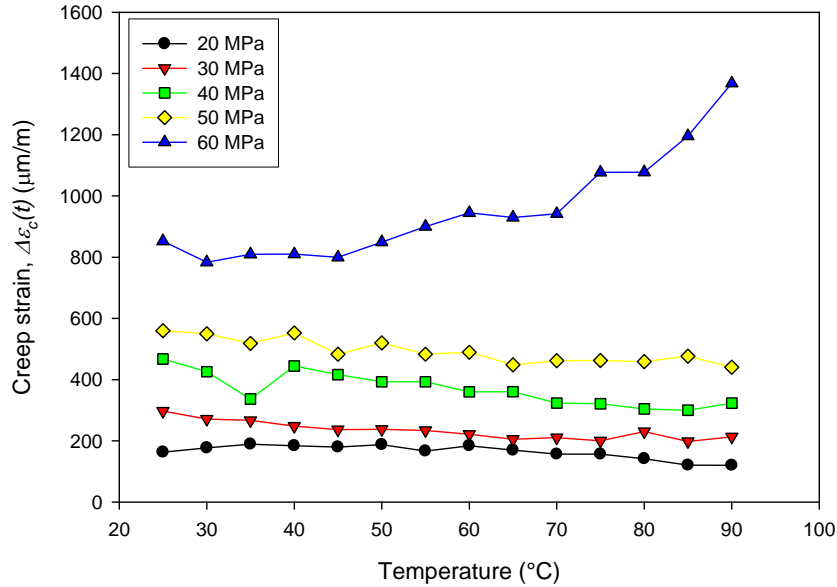
Figure 6.10 Variation of creep strain, $\Delta\varepsilon_c(t)$ in Figure 2.11, over a 30-minute creep duration plotted against temperature for increasing stresses.
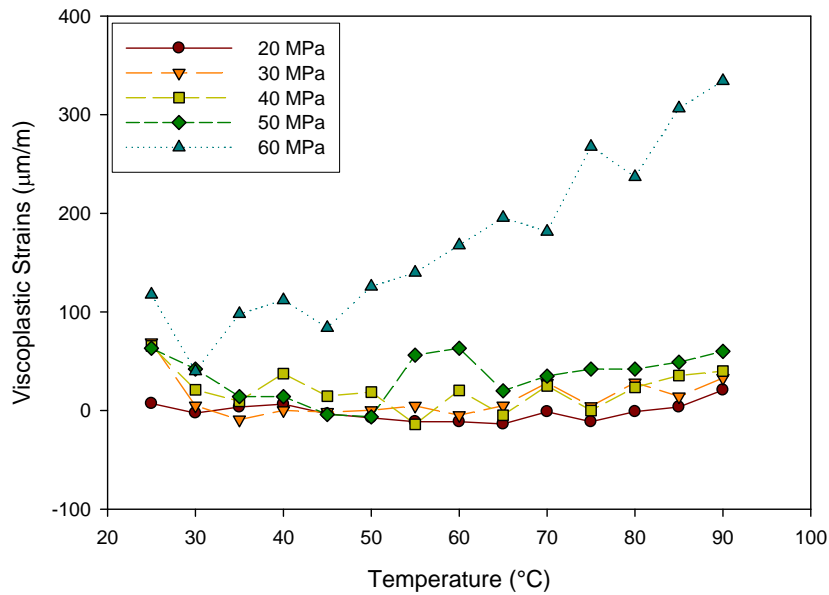
Figure 6.11 Average viscoplastic strains developed at the various applied stresses and temperatures.

The presence of un-recovered plastic strains at the end of recovery especially at higher temperatures and stresses is evident from creep recovery curves plotted in Figure 6.8. The average viscoplastic plastic strains developed during the creep tests with varying temperatures at stresses between 20 and 60 MPa are plotted in Figure 6.11. These strains

136

are the un-recovered strains at the end of 1 hour recovery. It can be seen that the magnitude of viscoplastic strains below 50 MPa is similar and fairly low for the temperatures tested. At 60 MPa, however, much higher viscoplastic strains are observed and they increase with temperature. This implies that the accumulation of viscoplastic strains is also temperature-dependent. It has to be noted that the viscoplastic strains plotted in Figure 6.11 was obtained from creep-recovery tests on pre-conditioned specimens and hence does not indicate the magnitude of plastic strains which would have been developed in a virgin specimen that is subjected to the same test conditions.

6.2.4 Time temperature superposition

One of the main objectives of conducting the short-term tests and using a single specimen for tests at all 14 temperature levels was to obtain data for Time-Temperature Superposition (TTS). The use of a single specimen ensures that the scatter in the data between tests at the various test temperatures is minimized. Moreover, testing pre-conditioned specimens ensure that there are only viscoelastic strains during creep loading as TTS cannot be applied for viscoplastic strains.
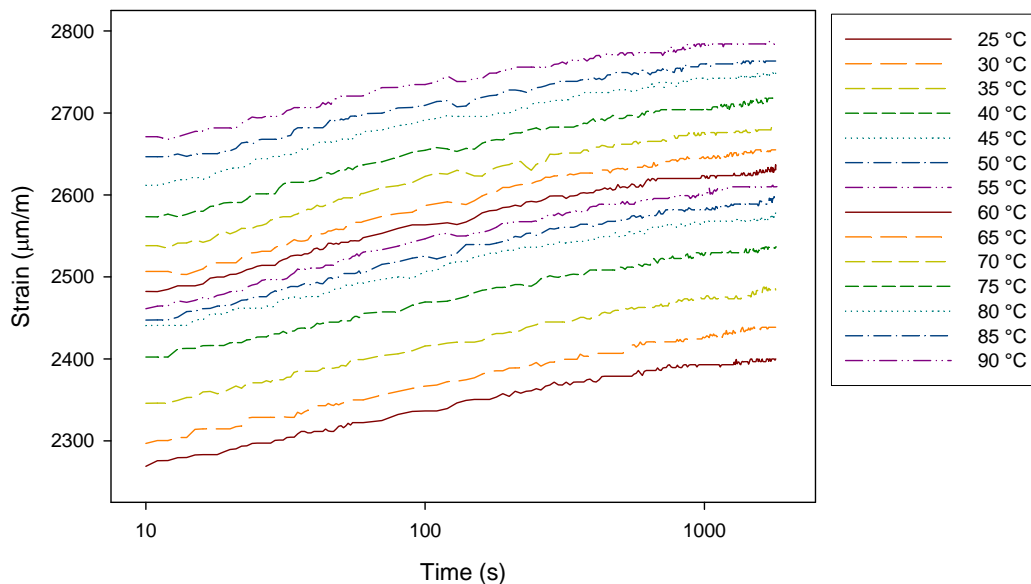
Figure 6.12 Creep curves at temperatures between 25 and 90°C
at 20 MPa on log-time scale.

137
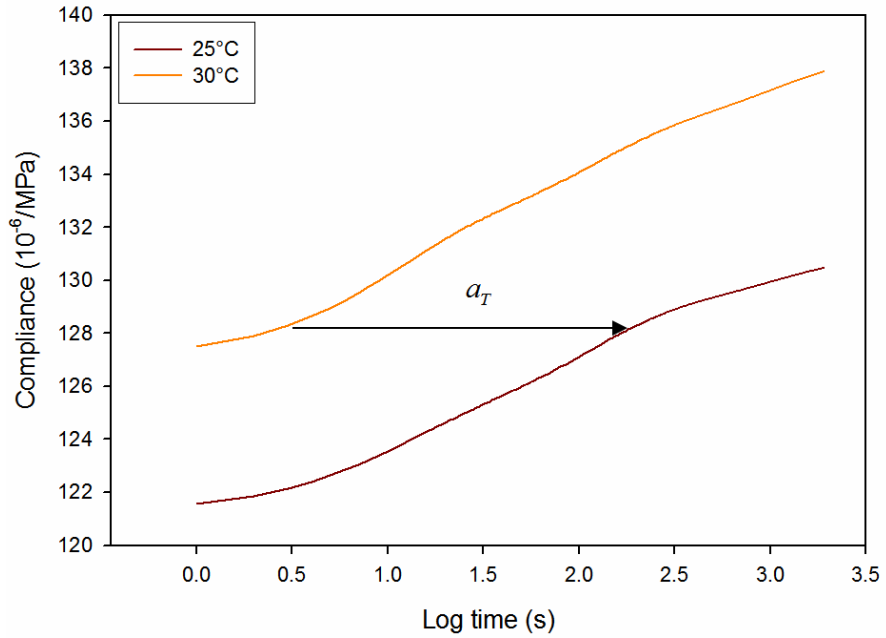
Figure 6.13 Illustration of the Time-Temperature superposition.
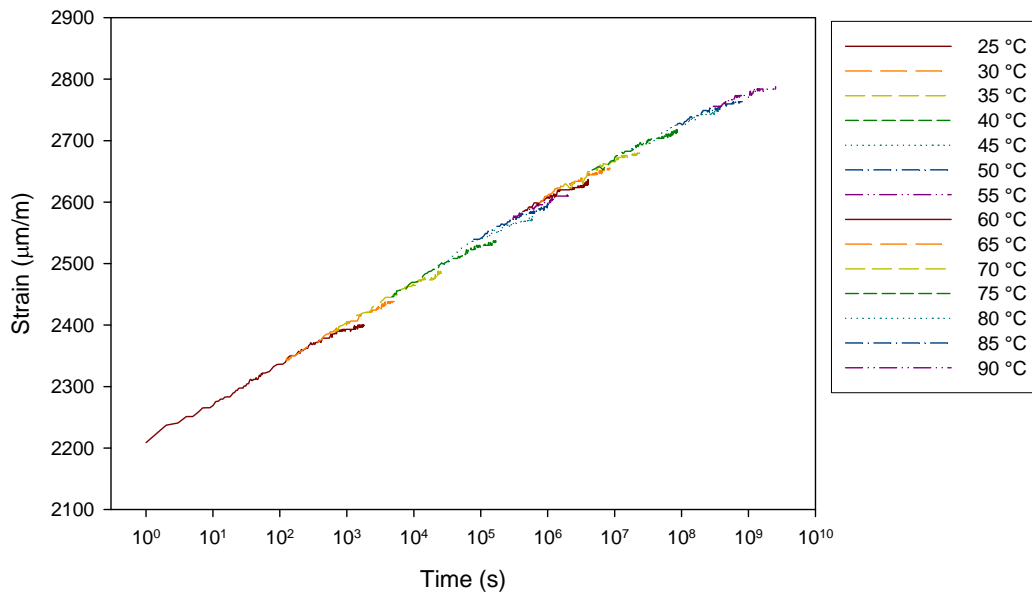
Figure 6.14 Creep curves after Time-Temperature superposition
on log time scale, reference temperature, T_{ref} = 25 °C.
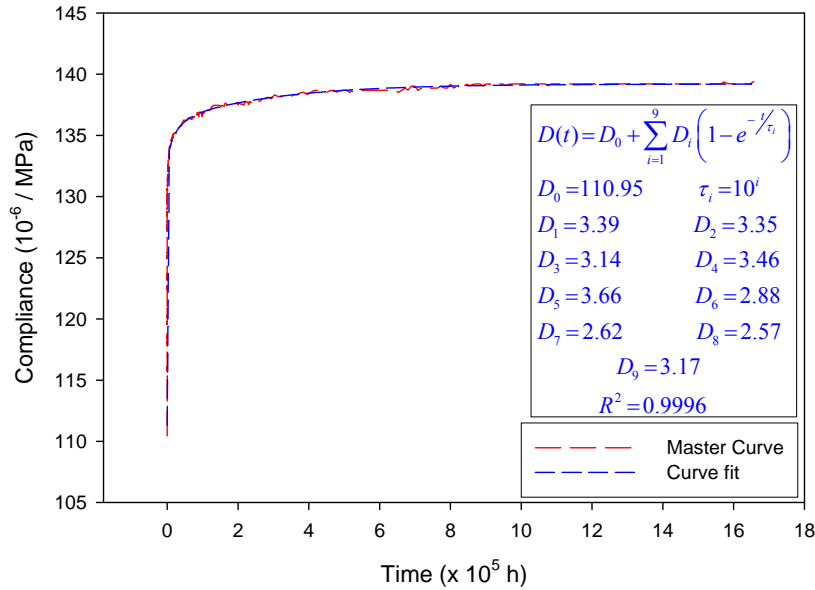
Figure 6.15 Final master curve and curve fit to 9-term Prony series.

Results presented in the previous section showed that the material is linear viscoelastic up to 20 MPa at room temperature. Hence, TTS can be carried out on the creep curves obtained at the various temperature levels at 20 MPa. The creep curves obtained at the 14 temperature levels between 25 and 90 °C are plotted in Figure 6.12 on a logarithmic time scale. These curves were obtained as an average of four trials carried out on separate pre-conditioned specimens. Time-temperature superposition involves shifting the curves in Figure 6.12 horizontally towards the curve at reference temperature, T_{ref}, as illustrated in Figure 6.13. The 25°C curve was used as the reference curve. The superimposed curves obtained after shifting the other curves to the reference is plotted in Figure 6.14. Finally, the master curve obtained from TTS is plotted in Figure 6.15. The master curve obtained can provide creep compliance predictions up to 16 x 10^5 hours (>185 years) at room temperature. However, it has to be noted that the duration of the predictions decreases with the increase in temperature. The master curve in Figure 6.15 has been fitted to a 9 term Prony series using commercial curve fitting software, Sigmaplot[®]. To simplify the curve fitting process, the time constants τ_i were pre-selected as 10^i seconds during curve fitting. As shown in Figure 6.15, very good fit with R^2 greater than 0.99 was obtained with the Prony series. The parameters of the Prony series model are given in Table 6.1.

139
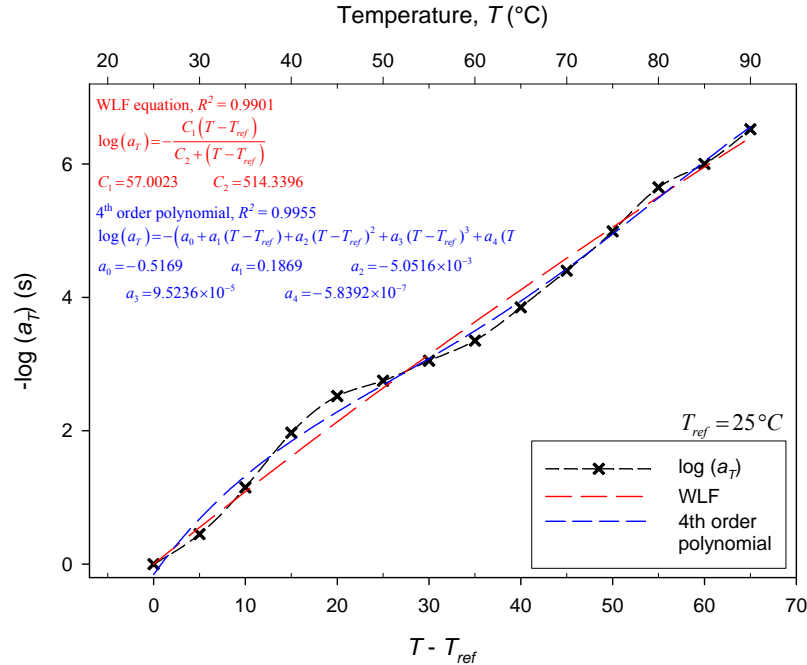
Figure 6.16 Shift factors with reference temperature, T_{ref} = 25°C.

The shift factors (log (a_T)) obtained from TTS are plotted against the absolute temperature, T and relative temperature, T - T_{ref} in Figure 6.16. The shift factor shows a minor inflection near 45°C but if this was ignored, the shift factors vary almost linearly with temperature. The inflexion can be explained by the polypropylene secondary glass transition. From the DMA results plotted in Figure 4.12, two transitions are clearly seen in the tan(δ) plot with temperature. The first is the glass transition temperature (α) with a peak around 0°C and the secondary glass transition (α^*) between 35 and 60°C. The DMA results correspond with the observed inflexion in the shift factor-temperature curve, Figure 6.16.

The shift factors were curve fitted to the WLF equation (37) as shown in Figure 6.16 which resulted in a good fit given by R^2 values of greater than 0.99. However, the WLF equation is fairly linear as compared to the experimental curve and is unable to follow the curvature of the shift factor-temperature curve due to inflexion observed around 45°C. For an even better fit, a fourth order polynomial of the relative temperature as given in equation (80) has been obtained to model the shift factors.

$$\log\left(a_{T}\right)=-\frac{57.0023\left(T-T_{ref}\right)}{514.3396+\left(T-T_{ref}\right)} \tag{79}$$

$$\log\left(a_{T}\right)=-\left(-0.5169+0.1869\left(T-T_{ref}\right)-5.0516\times10^{-3}\left(T-T_{ref}\right)^{2}+\right.$$
$$\left.+9.0516\times10^{-5}\left(T-T_{ref}\right)^{3}+5.83926\times10^{-7}\left(T-T_{ref}\right)^{4}\right) \tag{80}$$

(a)

(b)
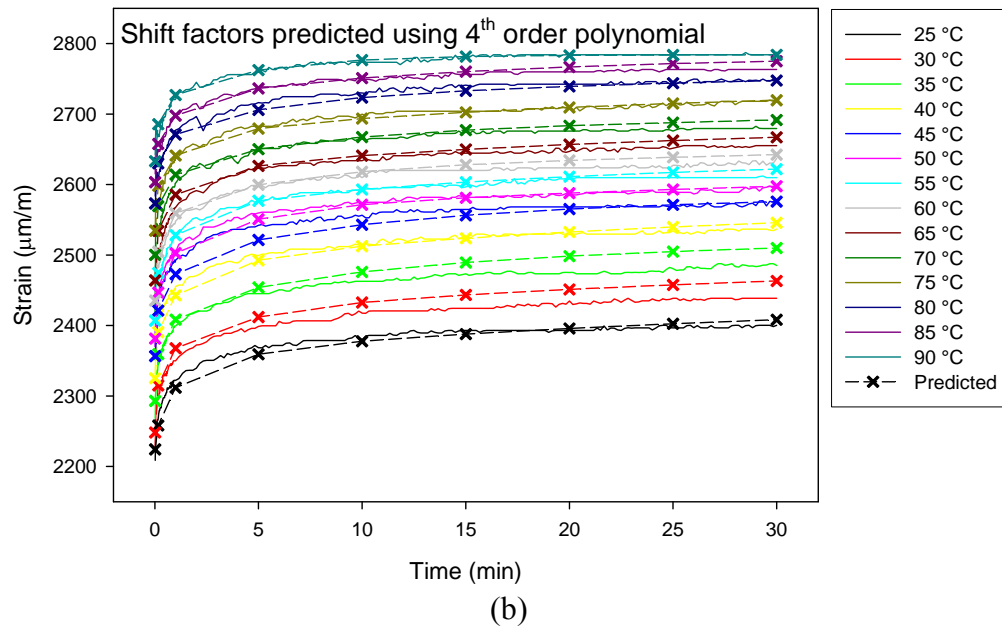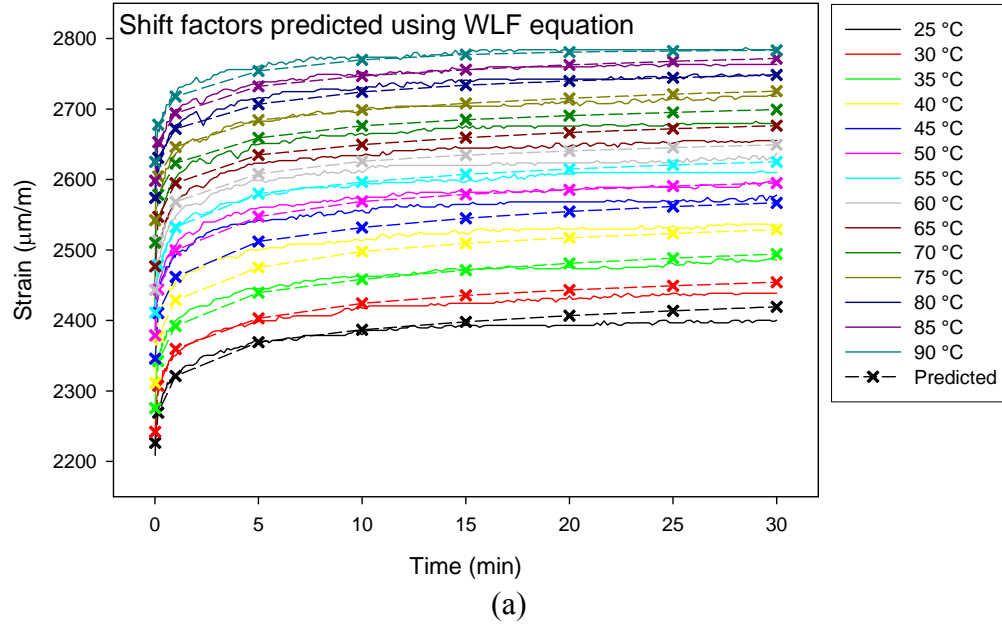
Figure 6.17 Experimental and predicted creep curves using shift factors
obtained from (a) WLF equation (b) 4th order polynomial.

The predicted creep curves at the various temperatures obtained from the master curve using the shift factors from the WLF eqauation (79) and fourth order polynomial in equation (80) are plotted along with experimental creep curves in Figures 6.17 (a) and (b), respectively. The predictions obtained from the fourth order polynomial are slightly better. However, considering the scatter of about 8% seen in the material properties, the WLF equation seems fitting to the constitutive model.

6.2.5 Non-linear viscoelastic model development

In order to include the effects of temperature in non-linear viscoelastic model, the non-linear parameters have to be considered as a function stress and temperature as given in equation (43). As in the previous chapter, $g_1 = a_\sigma = 1$ has been considered. Substituting Prony series for compliance, with $g_1 = 1$, $a=a_T$ and equation (43) for the non-linear parameters, the creep strains can be written as,

$$\varepsilon_c(t) = \left(g_{\sigma 0} g_{T0} D_0 + g_{\sigma 2} g_{T2} \sum_{i=1}^{N} D_i (1 - e^{-t/(a_T \tau_i)}) \right) \sigma_0 \tag{81}$$

The following procedure which is similar to that in section 5.2.3 has been employed to determine the parameters of the non-linear viscoelastic model in equation (81):

1. A reference temperature, T_{ref} was chosen as 25°C and Time-Temperature Superposition was carried out on the series of creep curves at the various temperatures obtained at a 20 MPa (stress in the linear viscoelastic region). The resulting master curve was fit to the Prony series to obtain the parameters given in Table 6.1. Also, the shift factors obtained were curve fit to the WLF equation.

2. Considering the relatively small magnitude of the plastic strains developed in these tests, the instantaneous response can be directly obtained from the experimental creep curves.

3. $g_{\sigma 0}$ can be obtained as the ratio of the instantaneous creep response at any stress level to that in the linear viscoelastic region at the reference temperature i.e., 25 °C.

142

4. $g_{\sigma 2}$ can be obtained by fitting equation (81) to the creep curves at the reference temperature (25°C). It has to be noted that at the reference temperature $g_{T0} = g_{T2} = 1$.

5. Since part of the non-linear effects due to temperature is modeled by the shift factors from TTS, g_{T0} cannot be directly deduced similar to $g_{\sigma 0}$ as in step 3. Both g_{T0} and g_{T2} can be obtained by fitting equation (81) to the creep curves at the various temperature levels for each stress level using the respective values of $g_{\sigma 0}$ and $g_{\sigma 2}$ obtained in steps 3 and 4 and the shift factors obtained from TTS in step 1.

Table 6.1 Parameters of the Prony series fit to the TTS master curve at 20 MPa.

Equation		$D(t) = D_0 + \sum_{i=1}^{9} D_i \left(1 - e^{-t/\tau_i}\right)$	
Time constants, τ_i (sec)		10^i	
Coefficients (10^{-6}/MPa)			
D_0	110.95	D_1	3.39
D_2	3.35	D_3	3.14
D_4	3.46	D_5	3.66
D_6	2.88	D_7	2.62
D_8	2.57	D_9	3.17

6.2.6 Non-linear viscoelastic model

The stress dependent non-linear parameters are plotted in Figure 6.18 (a). $g_{\sigma 0}$ was found to vary linearly with stress and a linear function of stress has been fitted to the data as given in equation (82). $g_{\sigma 2}$ is independent of stress up to 30 MPa at one and then the values increase linearly up to 50 MPa. The value of $g_{\sigma 2}$ at 60 MPa is slightly higher than expected (from previous experiments results). This is most probably due to the plastic strains developed during the tests at 60 MPa, which are considerably higher than that at the lower stress levels. Since these plastic strains have not been excluded and have been modeled as the viscoelastic strains, the slightly higher value of $g_{\sigma 2}$ might be due to this. $g_{\sigma 2}$ has been fit as a cubic function of stress as given in equation (83). If the values of $g_{\sigma 2}$

at 60 MPa are excluded, the $g_{\sigma 2}$ can be modelled as a linear function of stress up to 50 MPa as shown in Figure 6.18 (a) and equation (84).
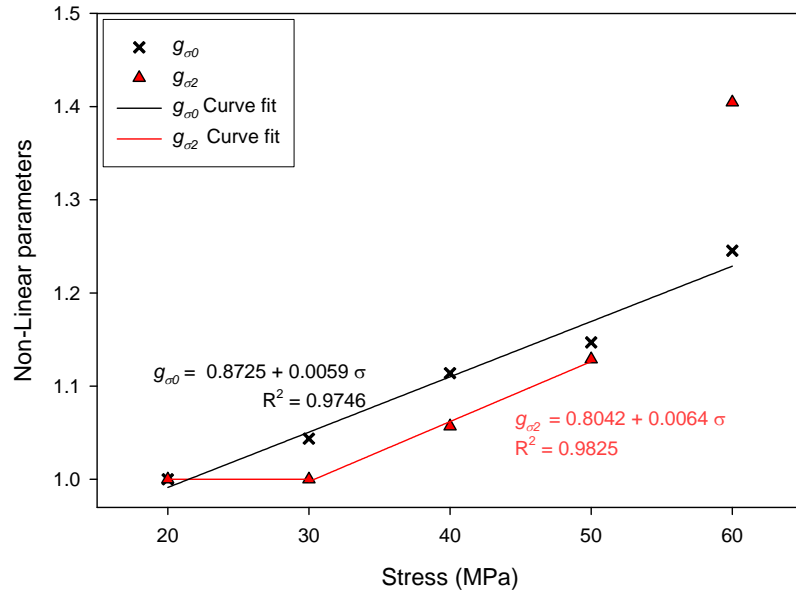
(a)
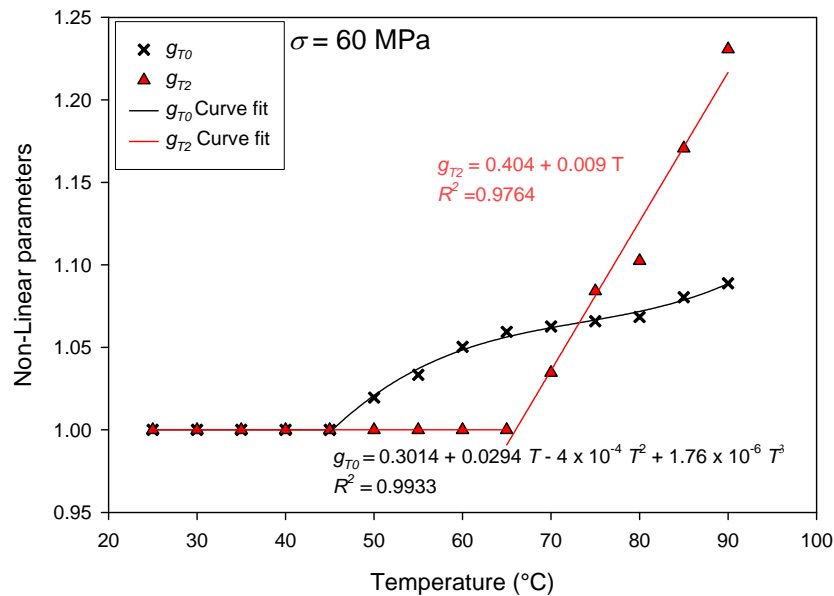
(b)

Figure 6.18 (a) Non-linear parameters $g_{\sigma 0}$ and $g_{\sigma 2}$ with stress with curve fit (b) Non-linear parameters g_{T0} and g_{T2} as a function of temperature at 60 MPa.

$$g_{\sigma 0} = \begin{cases} 1, & \sigma \le 20\text{MPa} \\ 0.8725 + 0.0059\sigma, & \sigma > 50 \text{ MPa} \end{cases} \qquad (82)$$

$$g_{\sigma 2} = \begin{cases} 1, & \sigma \le 30\text{MPa} \\ -0.9696 + 0.1484\sigma - 3.7019 \times 10^{-3}\sigma^2 + 3.1472 \times 10^{-5}\sigma^3, & \sigma > 30\text{MPa} \end{cases} \qquad (83)$$

or

$$g_{\sigma 2}(\sigma) = \begin{cases} 1, & \sigma \le 30\text{MPa} \\ 0.8042 + 0.0064\sigma, & \sigma \le 50 \text{ MPa} \\ 1.4045, & \sigma = 60 \text{ MPa} \end{cases} \qquad (84)$$

Both the non-linear functions of temperature, g_{T0} and g_{T2} were found to be almost equal to 1 for stresses up to 50 MPa. Slight variations followed no particular trend. Hence to simplify the model, both g_{T0} and g_{T2} were considered as equal to 1 up to 50 MPa. This implies that the non-linear effect of temperature up to 50 MPa can be effectively modeled using just the shift factors found from TTS (at 20 MPa). It does not, however, imply that the creep behaviour at these stress levels is identical as there is still an effect from the stress dependent non-linear functions. g_{T0} and g_{T2} obtained at 60 MPa are plotted in Figure 6.18 (b). As shown in Figure 6.18 (b), g_{T0} and g_{T2} at 60 MPa were found to be equal to 1 up to 45°C and 65°C, respectively. Beyond 45°C, g_{T0} increased sharply up to 60°C, and the slope is reduced thereafter up to 80°C. Typically, the decrease in the slope of the g_{T0}–temperature curve means a reduction in the rate of increase of instantaneous strains with temperature as g_{T0} models the non-linearity in the instantaneous response. However, in this case, the reduction is a consequence of modeling the master curve obtained from TTS using Prony series. Each term in the Prony series in equation (66) reaches an asymptotic value after a duration of about 5 times the time constant (τ_i) as shown in Figure 5.25. For example, if the time constant of the first term of the Prony series, $D_i(1 - e^{-t/\tau_1})$ is 100 seconds then at time t = 500 seconds, the effective value of the term is about 0.993 D_i, with negligible increases in the value thereafter. The effect of using the shift factors from TTS is to increase or decrease the time constant (τ_i) with temperature. Thus, in cases where the creep curves at higher temperature are shifted to lower temperature at longer times (to the right), the shift factors from TTS reduce the

time constants (τ_i) with temperature. An immediate effect of this is that as temperature increases, the first few terms of the Prony series reach their asymptotic values instantaneously and remain almost constant thereafter. The number of terms reaching this asymptotic value instantaneously increases with temperature. With this effect of the shift factors, the instantaneous strains are no longer modeled by just D_0 and g_0, as the first few terms of the Prony series which are expected to model the transient or time-dependent response now include part of the instantaneous response. This effect is very significant at higher temperatures (higher shift factors) and stresses (higher value of the non-linear parameter $g_{\sigma 2}$). It can be seen from Figure 6.18 (b) that the value of g_{T2} increases after 65°C which is about the temperature when there is a reduction in the slope of the g_{T0}-temperature curve. Finally the slope of the g_{T0}-temperature curve increases beyond 80°C indicating an increased effect of temperature on the instantaneous response. The variation of g_{T0} with temperature at 60 MPa beyond 45°C has been modeled as a cubic function of temperature.

At 60 MPa, g_{T2} was again found to be very close to 1 over an extended temperature range up to 65°C. As with the temperature dependent non-linear parameters (g_{T0} and g_{T2}) at lower stresses (20 – 50 MPa), the slight deviation from one followed no particular trend. Hence g_{T2} at 60 MPa was approximated to be equal to 1 up to 65°C. Beyond 65°C, g_{T2} was found to vary almost linearly with temperature. This together with $g_{\sigma 2}$ shows that the creep at 60 MPa is much higher than that at lower stress levels and is further accelerated by temperature. Also, the effect of the glass mat reinforcement reduces at 60 MPa especially beyond 45°C. With the above data, it can be suggested that the material should not be used for stresses higher than 60 MPa especially when the temperature is greater than 45°C. The variation of the temperature dependent non-linear functions at 60 MPa is summarized in equation (85) which has been obtained by curve fitting a total of 70 creep curves.

$$g_{T0} = \begin{cases} 1, & \sigma \leq 50\,\text{MPa}, 25°\text{C} < \text{T} \leq 90°\text{C} \\ 1, & \sigma = 60\,\text{MPa}, 25°\text{C} < \text{T} \leq 45°\text{C} \\ 0.3014 + 0.0294\,\sigma - 4 \times 10^{-4}\,\sigma^2 + 1.76 \times 10^{-6}\,\sigma^3, \\ & \sigma = 60\,\text{MPa}, 45°\text{C} < \text{T} \leq 90°\text{C} \end{cases}$$

$$g_{T2} = \begin{cases} 1, & \sigma \leq 50\,\text{MPa}, 25°\text{C} < \text{T} \leq 90°\text{C} \\ 1, & \sigma = 60\,\text{MPa}, 25°\text{C} < \text{T} \leq 65°\text{C} \\ 0.404 + 0.009\,\sigma, & \sigma = 60\,\text{MPa}, 65°\text{C} < \text{T} \leq 90°\text{C} \end{cases} \qquad (85)$$

Overall, it was observed that the quality of the curve fits at stresses below 50 MPa were good with R^2 values greater than 0.95 in most of the cases. This was before some of the parameters were rounded off to 1 to simplify the model. The approximation is expected to only affect the instantaneous response rather than the shape of the curves. At 60 MPa, the curve fits up to 60°C were fairly good. Above 60°C, however, the model could not keep up with the increasing creep rates especially at longer times even though the model fit reasonably well at lower times. As explained earlier, this is partly due to the effects of using Prony series for the master curve since the Prony series predicts a part of the instantaneous response at higher temperatures. As shown in Figure 6.10, the time-dependent creep response ($\Delta D(t).\sigma$) at stresses below 50 MPa decreased slightly beyond 70°C (due to the softening of the polypropylene matrix which causes the glass fibers to carry a greater share of the load). This effect is modelled by the shift factors. However, at a higher stress level (60 MPa), the transient creep response actually increases with temperature especially at temperatures beyond 75°C. This implies that g_{T2} should be high at these temperatures at 60 MPa. However, if g_{T2} increases, the instantaneous response modeled by the transient portion of the model increases simultaneously due to the effect of the shift factors and Prony series mentioned above. This in turn limits the value of g_{T2} during curve fitting and hence limiting the quality of the curve fit.

Finally, it has to be noted that the viscoplastic strains have not been modeled above as the magnitude of these strains are relatively small due to the use of pre-conditioned specimens and shorter duration of the tests. The viscoplastic strains are in fact fairly

significant especially at higher stresses and temperatures as will be shown in the next section.
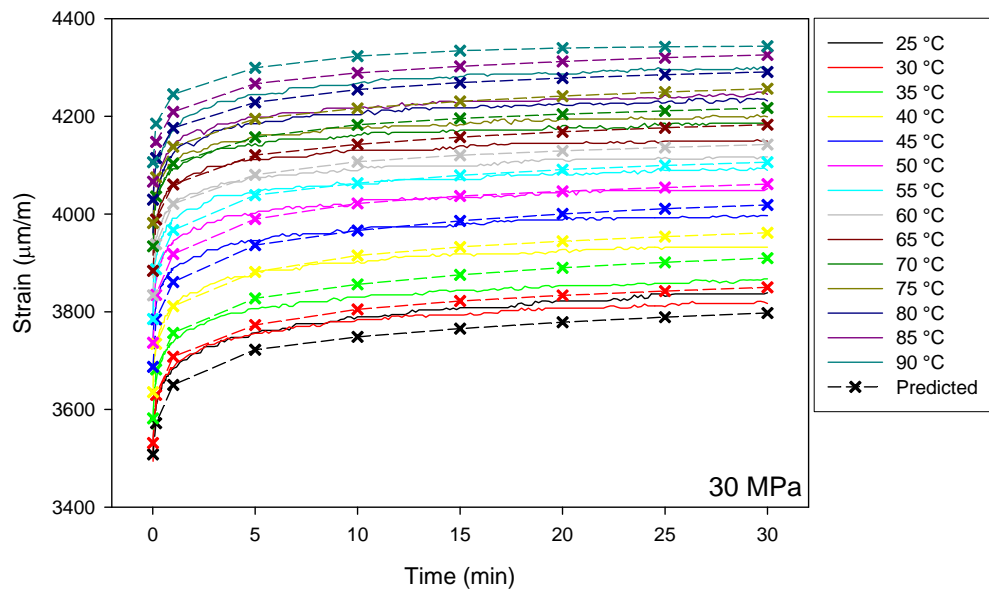
Figure 6.19 Experimental and predicted creep curves at 30 MPa.
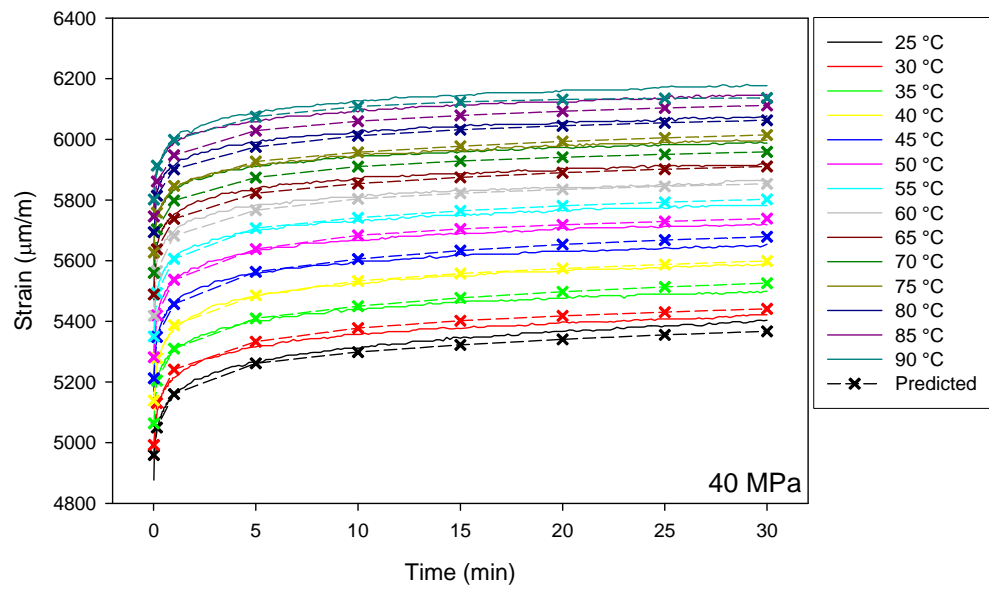
Figure 6.20 Experimental and predicted creep curves at 40 MPa.
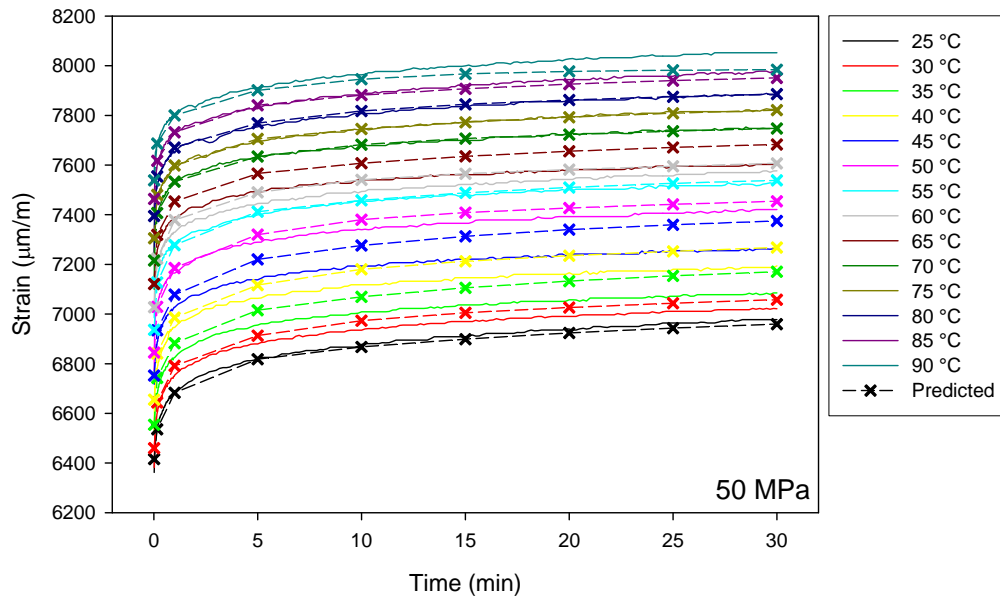
Figure 6.21 Experimental and predicted creep curves at 50 MPa.
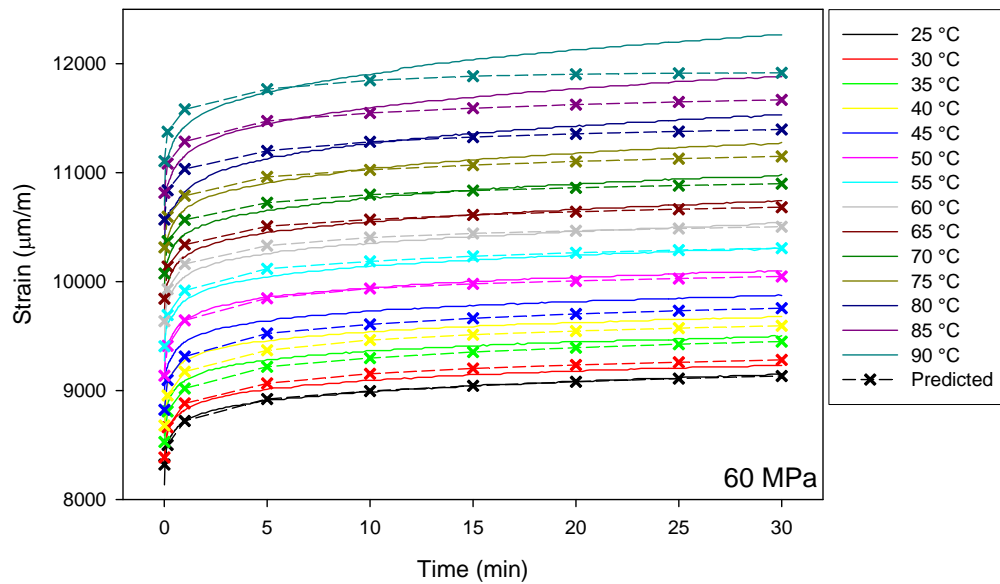
Figure 6.22 Experimental and predicted creep curves at 60 MPa.

6.2.7 Model predictions

The predictions of the non-linear viscoelastic model using non-linear viscoelastic parameters in equations (82) to (85), Prony series in Table 6.1 and shift factors from the WLF equation (79) at stresses between 30 to 60 MPa are compared with the experimental

creep curves in Figures 6.19 to 6.22 respectively. At 30 MPa, the predictions are fairly good but only at the intermediate temperatures. Even though the predictions for the other temperatures are not as good, the shapes of the predicted curves are fairly close to the experimental curves and the difference is mostly in the instantaneous response. The creep curves at 40 and 50 MPa are predicted very well at most temperature levels. At 60 MPa, the predictions up to 70°C are very good. However, at temperatures above 70°C, the creep curves are flatter and fail to keep up with the increasing creep rates with temperature. Similar behaviour is seen in creep predictions at both 40 and 50 MPa at 90°C. As mentioned earlier, this was observed during curve fitting and hence was expected. It should be noted that a total of 70 curves have been fitted to obtain the model and is very difficult to obtain a model that would satisfy every one of them. Furthermore, some inaccuracies in the predicted creep curves in Figures 6.19 to 6.22 are caused by the differences in the non-linear parameters predicted using equations (82) and (85). Figure 6.23 compares the experimental strains after 30 minutes creep with the model predictions. It is quite clear that the model predictions are well within the experimental scatter. Finally, the recovery curves at all stress and temperature levels are fairly well predicted with the difference being the small magnitude of plastic strains.
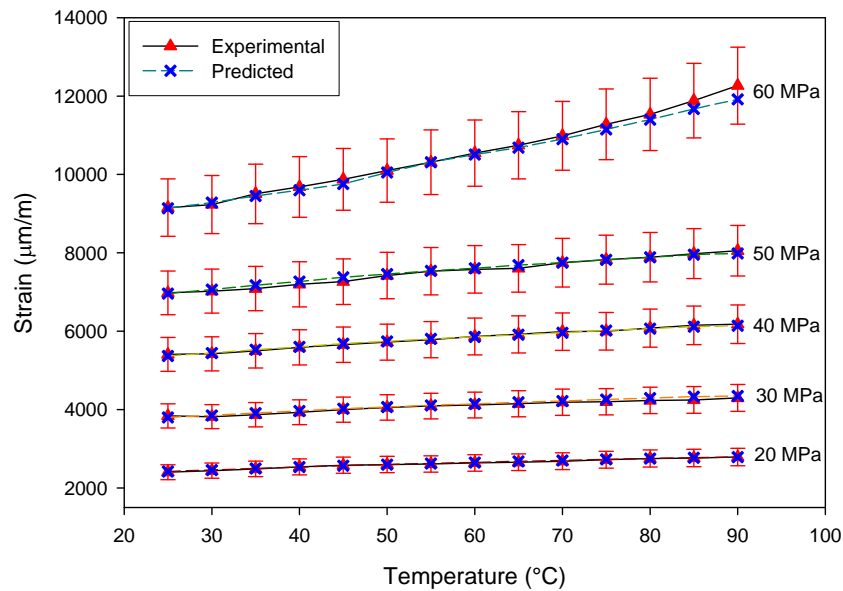
Figure 6.23 Comparison of the experimental and predicted strains after
30 minutes of creep at the various stress and temperatures.

6.3 Long term creep tests

The short term creep tests presented in the previous section provided an overview of the temperature dependence of the creep behaviour in long fiber GMT composites. However, since pre-conditioned specimens were employed and multiple tests were carried out on a single specimen, the overall creep response was lower than the actual due to the reduced viscoplastic strains. Furthermore, the effect of multiple loading cycles (since a single specimen was tested at all temperatures) especially at higher stresses and temperatures is not known and could affect the creep behaviour. Hence, to obtain a general non-linear viscoelastic viscoplastic constitutive model, creep-recovery tests using virgin specimens over a longer duration over a wide range of temperatures and stresses have been conducted. The results of these tests are presented in this section.

Creep recovery tests similar to that presented in section 5.3, consisting of 1 day creep followed by recovery for 2 days have been conducted at three temperatures: 40, 60 and 80°C. Five stress levels were considered: 20, 30, 50, 60 and 70 MPa. These tests were replicated at least 3 times on separate strain gauged, randomly selected virgin specimens. The test setup was similar to that of the short term tests. After calibration of the fixture at the required stress level, the specimen was mounted on the fixture and placed inside an oven. Before loading, the oven temperature was increased to the test temperature and the specimen and fixture were soaked at the test temperature for 15 minutes.

6.3.1 Creep test results

The average creep-recovery curves at the various stresses obtained at the three temperatures – 40, 60 and 80°C are plotted in Figures 6.24, 6.25 and 6.26 respectively. The creep rate at 70 MPa at 60°C as well at stresses beyond 30 MPa at 80°C are very high. The creep response at all stresses and temperatures below these is similar to that at room temperature shown in Figure 5.11, i.e., it shows secondary creep with moderate creep rates. The creep curves obtained at 70 MPa and 80°C from the three trials conducted are plotted in Figure 6.27. As shown, all three specimens tested failed before

24 hours. Two of the specimens (specimens 1, 3) failed gradually exhibiting tertiary creep behaviour while one of the specimens (specimen 2) failed abruptly after 10 hours.
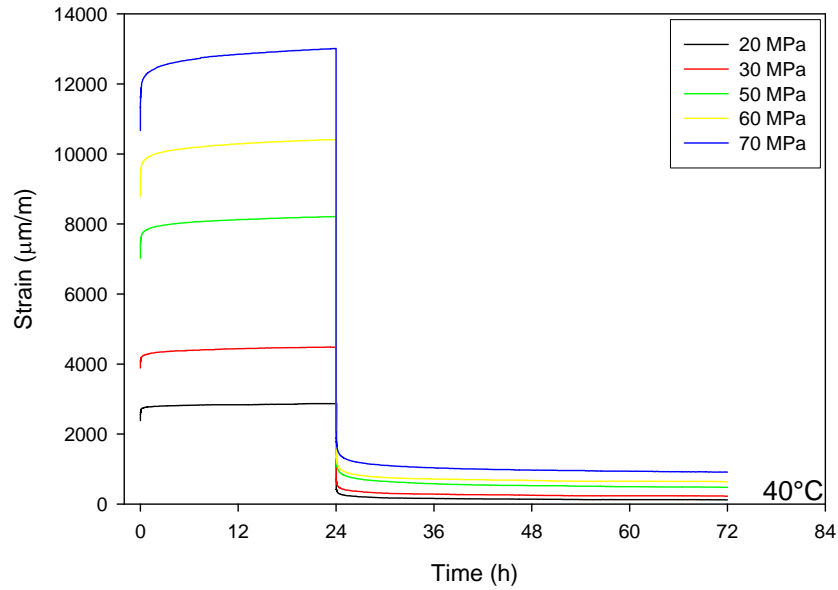
Figure 6.24 Creep recovery curves at the various stress levels at 40°C.
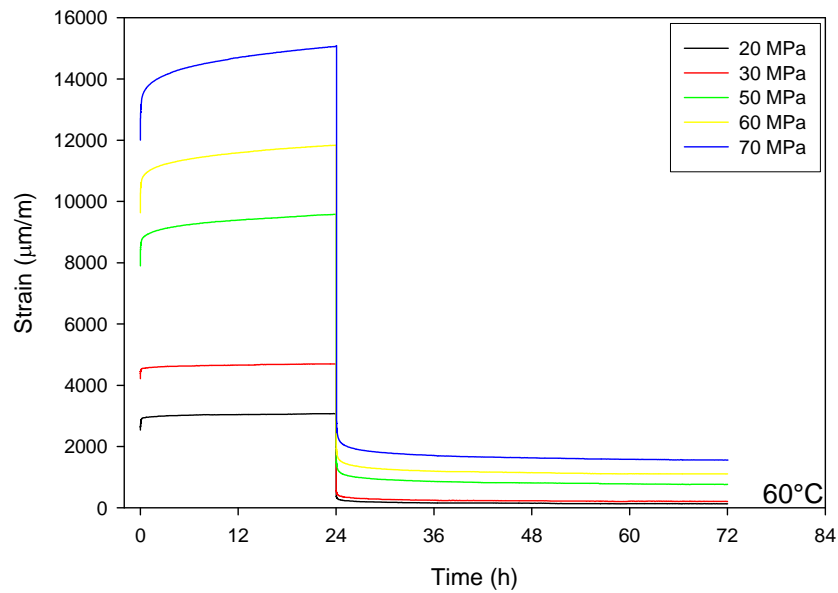
Figure 6.25 Creep recovery curves at the various stress levels at 60°C.
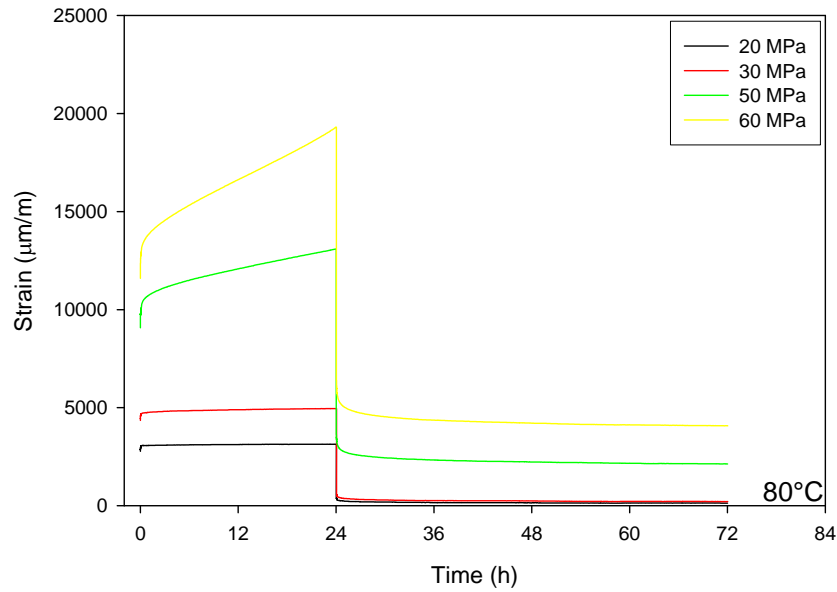
Figure 6.26 Creep recovery curves at the various stress levels at 80°C.
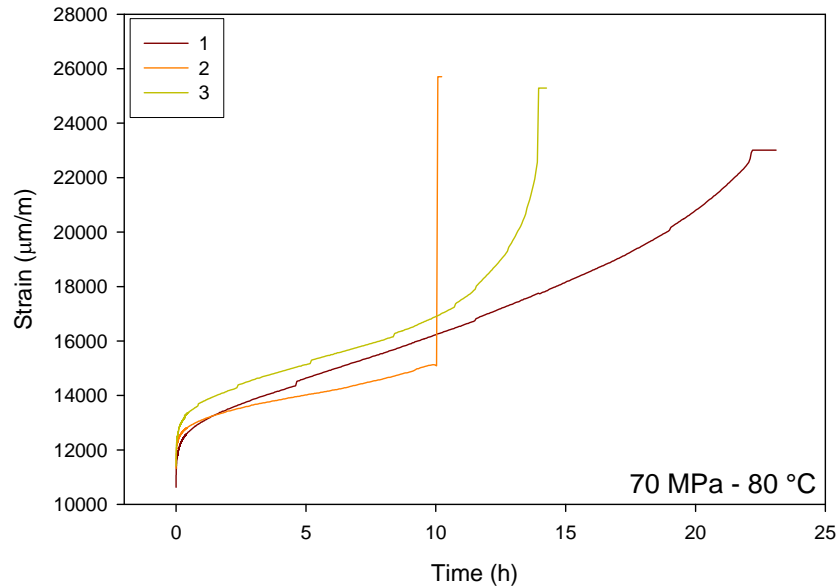
Figure 6.27 Creep curves obtained from three trials at
70 MPa stress and at a temperature of 80°C.

Figure 6.28 shows the variation of the instantaneous strains, i.e., strains upon loading with stress, at the various temperatures considered. The slope of the curves increases with temperature indicating an increase in compliance with temperature. Increasingly non-linear strain-stress behaviour is observed as the test temperature is increased especially at stresses above 30 MPa. The increase in non-linearity with temperature is further proved

153

by the non-linear increase in the slope of the compliance (obtained at the end of one day creep) stress curves plotted in Figure 6.29. A variability of about 8.5 % has been observed based on the instantaneous strains. Similar to the short term tests, the variability increased slightly with temperature due to the additional variability from the thermal strains (thermal expansion).
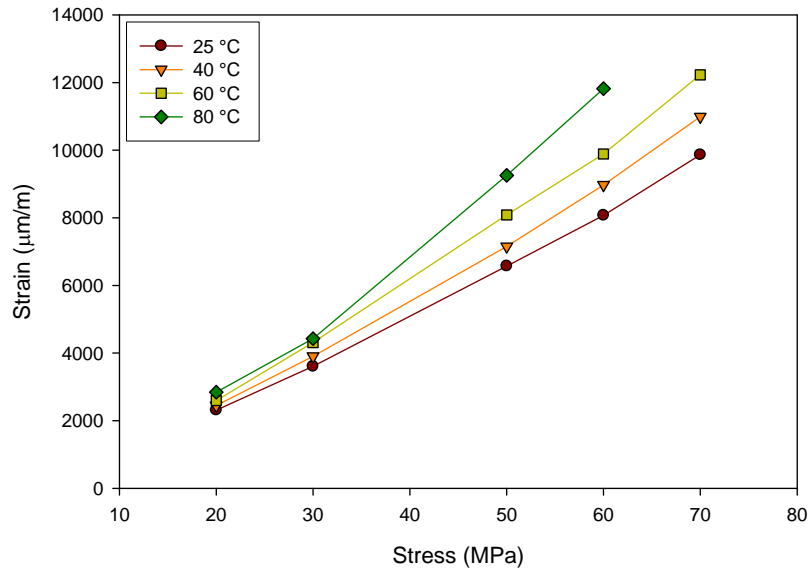
Figure 6.28 Variation of the instantaneous strains with stress and temperature.
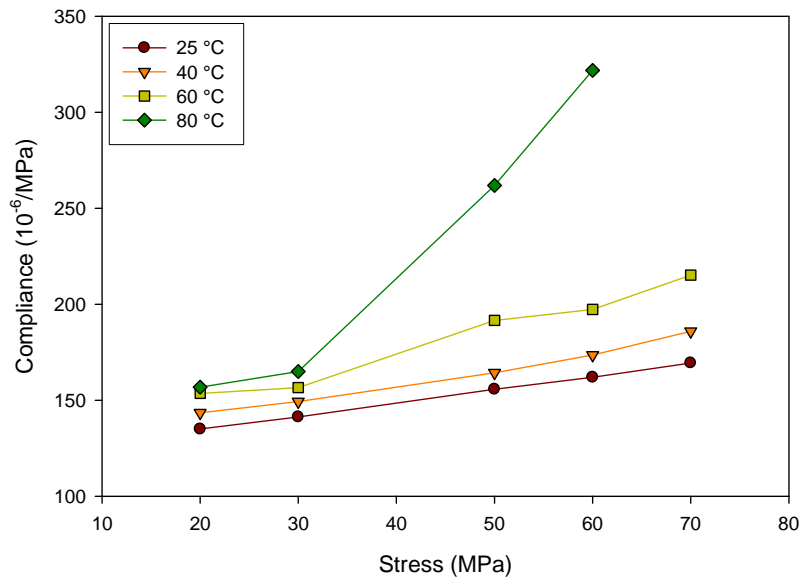
Figure 6.29 Variation of compliance at the end of one day
creep with applied stress and temperature.

6.3.2 Viscoplastic strains

The increasing levels of the un-recovered strains at the end of recovery with stress in the creep-recovery curves are evident in Figures 6.24 to 6.26. The un-recovered strains or the viscoplastic strains at the end of 1 day creep at the stresses and temperatures considered are plotted in Figure 6.30. The data at 25°C is obtained from the results presented in the previous chapter (Figure 5.12). It can be seen that the viscoplastic strains at room temperature (25°C) and 40°C are almost equal at all stress levels. This indicates that the damage mechanisms in the material up to 40°C are similar. Furthermore, the viscoplastic strains are independent of temperature below 30 MPa. For a given temperature, stress has a strong influence on the development of viscoplastic strain, especially beyond 30 MPa.
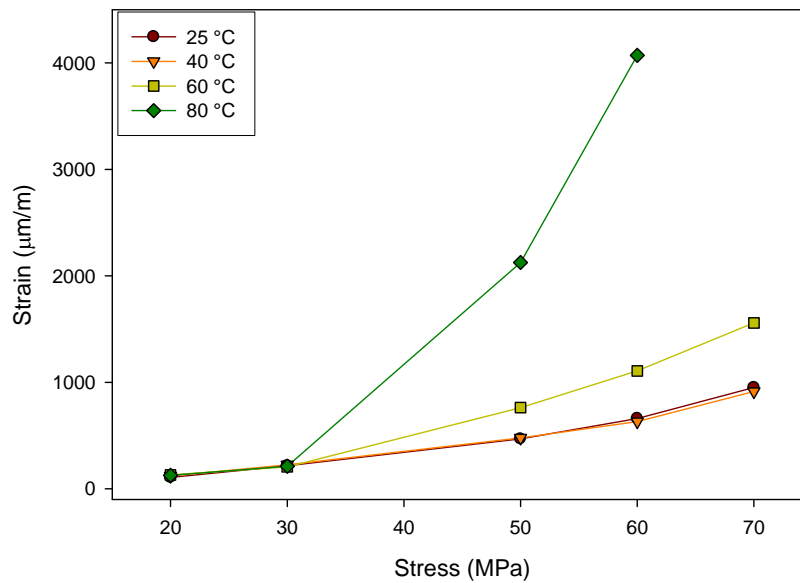
Figure 6.30 Variation of viscoplastic strains with stress
at the various temperatures.

The viscoplastic strains developed at 60 °C at stresses above 30 MPa are higher than that at lower temperatures. Also, there is a drastic increase in the viscoplastic strains at 80 °C over 30 MPa. Interestingly, this increase in viscoplastic strains observed at these temperatures corresponds with the increase in the transient creep response observed in Figures 6.25 and 6.26. For example, the variation of the creep strains ($\Delta\varepsilon_c$ in Figure 2.11) and the viscoplastic strains with temperature at 60 MPa are plotted in Figure 6.31. It can

be seen that both the creep strain, $\Delta\varepsilon_c(t)$ (and hence creep rate) and viscoplastic strain behave similarly with temperature. These results strongly suggest that the total creep response in the material is directly associated with the development of viscoplastic strains. Furthermore, the viscoplastic strains constitute 30 – 40 % of the creep strains with greater contribution at the higher temperatures. It is prudent to point out that part of the viscoplastic strains plotted in Figure 6.31 is developed upon loading.
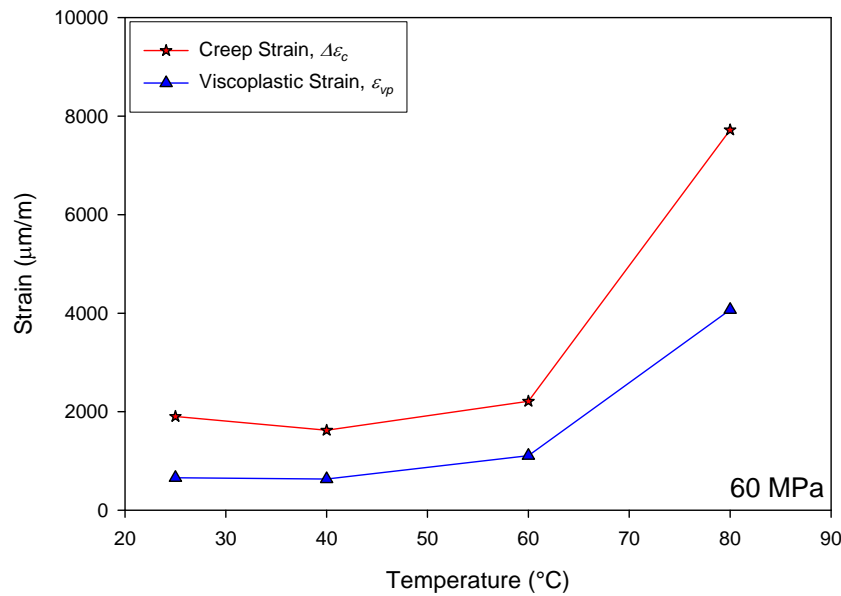
Figure 6.31 Comparison of the creep strains with viscoplastic strains
at various temperatures for 60 MPa stress.

The viscoplastic strains in GMT materials have been found to be developed due to fiber-matrix debonding and transverse cracking during creep loading in the material [106]. However, it is suspected that the higher viscoplastic strains at 60 - 80°C and at stresses between 60 and 70 MPa are further exacerbated by matrix plastic yielding and softening along with the above damage mechanisms.

6.3.3 Method to determine non-linear viscoelastic viscoplastic model

The method presented in Section 5.3.3 has been extended to separate the viscoelastic strains and hence to obtain the non-linear parameters of the viscoelastic model as

functions of stress and temperature as given in equation (43). Following equation (43), nonlinear viscoelastic viscoplastic model during creep and recovery can be written as,

$$\varepsilon_c(t) = \left(g_{\sigma 0}(\sigma) g_{T0}(T) D_0 + g_{\sigma 2}(\sigma) g_{T2}(T) \sum_{i=1}^{N} D_i (1 - e^{-t/\tau_i}) \right) \sigma_0 + A\left((\sigma_0)^m t \right)^n \quad (86)$$

$$\varepsilon_r(t) = \left(\sum_{i=1}^{N} D_i \left(e^{-(t-t_r)/\tau_i} - e^{-t/\tau_i} \right) \right) g_{\sigma 2}(\sigma) g_{T2}(T) \sigma_0 + A\left((\sigma_0)^m t_r \right)^n \quad (87)$$

Again, $g_1 = a_\sigma = 1$ has been considered to simplify the data reduction method. The method employed to obtain the non-linear parameters and the viscoplastic model is summarized below.

1. An estimate of the permanent viscoplastic strains $\varepsilon_{vp}(t_r)$ at all the stress and temperatures of interest can be obtained as the total un-recovered strain after very long recovery durations (usually 2 to 3 times the creep duration).

2. Using these values of $\varepsilon_{vp}(t_r)$, $\varepsilon_r(t) - \varepsilon_{vp}(t_r)$ can be calculated from experimental data at various stress levels. From equation (87) it can be shown that ,

$$\varepsilon_r(t) - \varepsilon_{vp}(t_r) = \left(\sum_{i=1}^{N} D_i \left(e^{-(t-t_r)/\tau_i} - e^{-t/\tau_i} \right) \right) g_{\sigma 2}(\sigma) g_{T2}(T) \sigma_0 \quad (88)$$

3. $\varepsilon_r(t) - \varepsilon_{vp}(t_r)$ data from creep-recovery test at a stress in the linear viscoelastic region at room temperature is fit into equation (88) by considering $g_{\sigma 2} = g_{T2} = 1$, to obtain the parameters of the Prony series. The time constants τ_i can be pre-selected to simplify the curve fitting process [56].

4. $\varepsilon_r(t) - \varepsilon_{vp}(t_r)$ data from tests at stresses in the non-linear viscoelastic region at room temperature are curve fit to equation (88) while considering, $g_{T2} = 1$ using the parameters of the Prony series from step 3, to determine $g_{\sigma 2}$ at each stress level considered.

157

5. $\varepsilon_r(t) - \varepsilon_{vp}(t_r)$ data from tests at stresses in the non-linear viscoelastic region at higher temperature (or temperatures other than room temperature considered) are curve fit to equation (88) using the parameters of the Prony series from step 3 and $g_{\sigma 2}$ from step 4 to determine g_{T2} at each temperature considered for the various stress levels.

6. In order to eliminate the plastic strain from the equation, the strain $\varepsilon_R(t) = \varepsilon_c(t_r) - \varepsilon_r(t)$ is calculated from the experimental data [53]. Using equations (86) and (87), it can be shown that,

$$\varepsilon_R(t) = \varepsilon_c(t_r) - \varepsilon_r(t) = \left(g_{\sigma 0}(\sigma) g_{T0}(T) D_0 + g_{\sigma 2}(\sigma) g_{T2}(T) \sum_{i=1}^{N} \left(D_i \left(e^{t_r/\tau_i} - 1 \right) \left(e^{-t_r/\tau_i} - e^{-t/\tau_i} \right) \right) \right) \sigma_0$$

(89)

7. $\varepsilon_R(t)$ calculated at a stress in the linear viscoelastic region is curve fit to equation (89) to determine D_0 ($g_{\sigma 0} = g_{T0} = 1$).

8. Similarly, $\varepsilon_R(t)$ calculated at stress levels in the non-linear viscoelastic region at room temperature is curve fitted to equation (89) using $g_{T0} = 1$ and D_0 from step 6 to determine $g_{\sigma 0}$ at each stress level.

9. In order to determine g_{T0}, $\varepsilon_R(t)$ calculated at stress levels in the non-linear viscoelastic region at higher temperatures (or temperatures other than room temperature considered) is curve fitted to equation (89) using $g_{\sigma 0}$ for the respective stress from step 8 and D_0 from step 6 to determine g_{T0} at each stress level considered by using D_0 from step 6.

10. Since all the parameters of the viscoelastic model in equation (89) have been determined, the parameters of the viscoplastic model can be obtained by fitting equation (89) to the creep curves at the various stresses and temperatures considered.

Another way would be to estimate the viscoplastic strains by subtracting the predicted viscoelastic strains from the experimental creep strains [53] and the resulting curves are then fitted to equation (48) to obtain the parameters of the viscoplastic model.

6.3.4 Alternate method to estimate viscoplastic strains

From the above method, it can be seen that the parameters of the viscoelastic model, i.e., the Prony series parameters, are obtained at room temperature in the linear viscoelastic region, while only the non-linear parameters are varied at the other stresses and temperatures (in the non-linear viscoelastic region). In the case of the long fiber GMT composite, since g_1 was found to be 1, only the parameters $g_0(\sigma,T) = g_{\sigma 0}(\sigma)g_{T 0}(T)$ and $g_2(\sigma,T) = g_{\sigma 2}(\sigma)g_{T 2}(T)$ were considered in the viscoelastic model (Findley's model). This implies that g_0 and g_2 model the non-linear effects of stress and temperature on the instantaneous and the transient components of the creep compliance (obtained in the linear viscoelastic region). It is obvious that varying g_2 scales the magnitude of the creep strain based on stress and/or temperature (increases creep strain or the transient creep response with an increase in g_2) and has rather limited control over the shape of the creep curve. However, in most of the polymeric materials, the shape of the creep-curves varies with stress and temperature, with the change in the shape increasing with temperature. Hence, although equations (86) and equations (87) may have modeled the overall magnitudes of instantaneous and transient creep components fairly well, the shape of the predicted curve may not be accurate.

The above observation is not a major shortcoming when modeling just the non-linear viscoelastic response, as the overall creep is still reasonably predicted. However, in cases where the viscoplastic strains have to be separated, the inability to model the difference in the shapes of the creep curves becomes important, as the magnitudes of the viscoplastic strains are relatively small. Any difference in the shape of the predicted and experimental viscoelastic strains affects the viscoplastic strain-time curve as it is obtained from the predicted non-linear viscoelastic model parameters (step 10). It has to be noted that this only affects the shape of the viscoplastic strain-time curve obtained rather than

the final magnitude of the viscoplastic strains (as the method uses the final magnitude of viscoplastic strains or the total unrecovered strains, to determine the model parameters).

In order to address the above, an alternate method for separating the viscoplastic strains is provided here. The method is based on the assumption that the creep-recovery curves at each stress level are linear viscoelastic with respect to its own stress level. Hence, a separate Prony series is used to model each creep curve (at various stress and temperatures) and hence decouples the viscoelastic and the viscoplastic strains. It is obvious that for a non-linear viscoelastic material, a different set of D_0 and parameters of Prony series for each of the creep curves at the stress and temperature levels considered will be obtained. This method not only simplifies the curve fitting process but also improves the accuracy of the curve fits and hence provides a good estimation of viscoplastic strains. The creep and recovery response without the non-linear parameters are given by equations (90) and (91) respectively.

$$\varepsilon_c(t) = \left(D_0 + \sum_{i=1}^{N} D_i (1 - e^{-t/\tau_i}) \right) \sigma_0 + A\left((\sigma_0)^m t \right)^n \tag{90}$$

$$\varepsilon_r(t) = \left(\sum_{i=1}^{N} D_i \left(e^{-(t-t_r)/\tau_1} - e^{-t/\tau_1} \right) \right) \sigma_0 + A\left((\sigma_0)^m t_r \right)^n \tag{91}$$

The following methodology has been employed to analyze the creep-recovery curves at each stress and temperature level in order to separate viscoplastic strains.

1. An estimate of the permanent strain $\varepsilon_{vp}(t_r)$ can be obtained as the total un-recovered strain after very long recovery durations (usually 2 to 3 times the creep duration) for each stress and temperature considered.

2. Using these values of $\varepsilon_{vp}(t_r)$, $\varepsilon_r(t) - \varepsilon_{vp}(t_r)$ can be calculated from experimental data at various stress levels. From equation (91) it can be shown that

$$\varepsilon_r(t) - \varepsilon_{vp}(t_r) = \left(\sum_{i=1}^{N} D_i \left(e^{-(t-t_r)/\tau_1} - e^{-t/\tau_1} \right) \right) \sigma_0 \tag{92}$$

160

3. $\varepsilon_r(t) - \varepsilon_{vp}(t_r)$ data for each creep-recovery test at the various stress and temperatures of interest is fit to equation (92) to obtain the parameters of the Prony series i.e., D_i and τ_i. The time constants τ_i can be pre-selected to simplify the curve fitting process [56].

4. In order to eliminate the plastic strain from the equation, the strain $\varepsilon_R(t) = \varepsilon_c(t_r) - \varepsilon_r(t)$ is calculated from the experimental data [53]. Using equations (90) and (91), it can be shown that,

$$\varepsilon_R(t) = \varepsilon_c(t_r) - \varepsilon_r(t) = \left(D_0 + \sum_{i=1}^{N} \left(D_i \left(e^{t_r/\tau_i} - 1 \right) \left(e^{-t_r/\tau_i} - e^{-t/\tau_i} \right) \right) \right) \sigma_0 \qquad (93)$$

5. Experimentally determined $\varepsilon_R(t)$ at the various stress and temperatures considered are fit to equation (93) using the Prony series parameters from step 3, to determine the D_0

6. Since all the parameters of the viscoelastic model in equation (90) have been determined, the parameters of the viscoplastic model can be obtained by fitting equation (90) to the creep curves.

It has to be noted that the above method is only valid when $g_1 = 1$. Also the above method only provides the viscoplastic model. The method given in the previous section has to be used to determine the non-linear viscoelastic parameters.
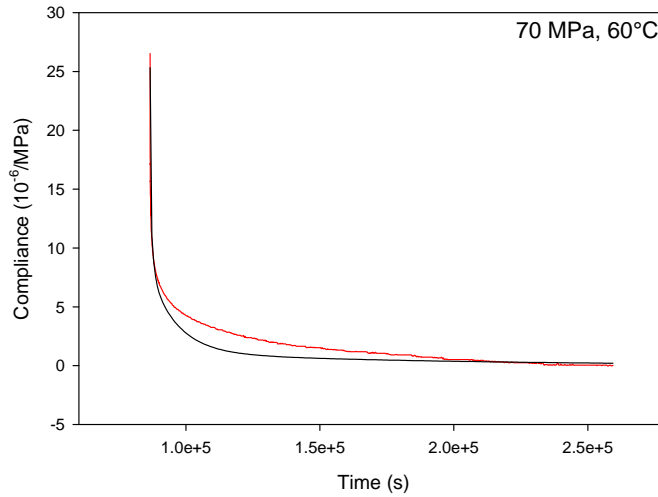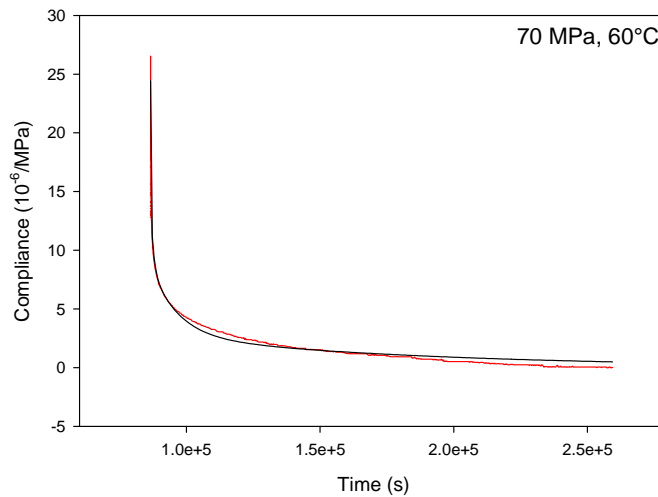
Figure 6.32 Curve fits to $\varepsilon_r(t) - \varepsilon_{vp}(t_r)$ to (a) equation (88) and
(b) equation (92) at 70 MPa and 60°C.

The fits to recovery data (with viscoplastic strain removed) of equations (88) (non-linear viscoelastic model) and equations (92) (linear viscoelastic model) are illustrated in Figures 6.32 (a) and (b) respectively. The inability of the non-linear viscoelastic model to exactly follow the recovery curve can be seen in Figure 6.32 (a). The difference however is small compared to the total creep strains. It is suggested that the above method has to be used only when the viscoplastic strain evolution needs to be determined accurately.
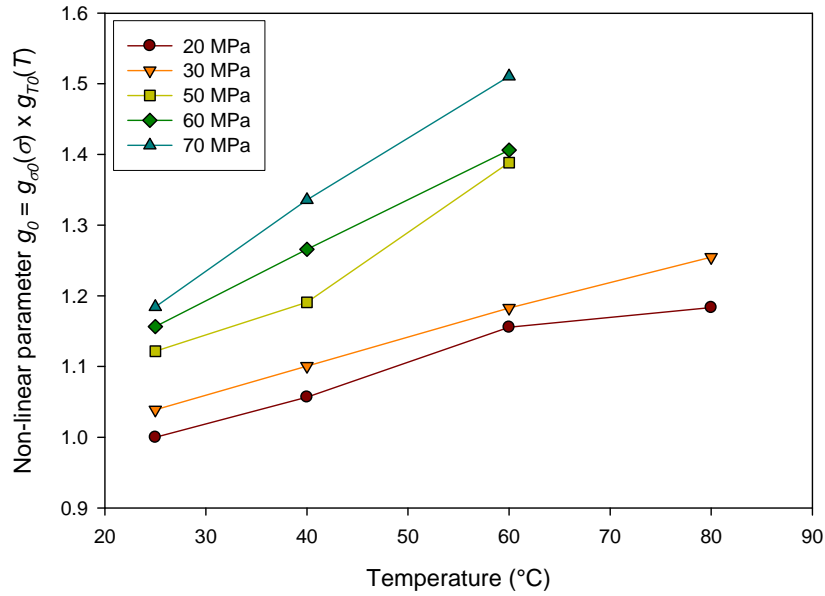
Figure 6.33 Variation of Non-linear parameter $g_0(\sigma, T) = g_{\sigma 0}(\sigma)g_{T0}(T)$ with temperature at the various temperature levels.
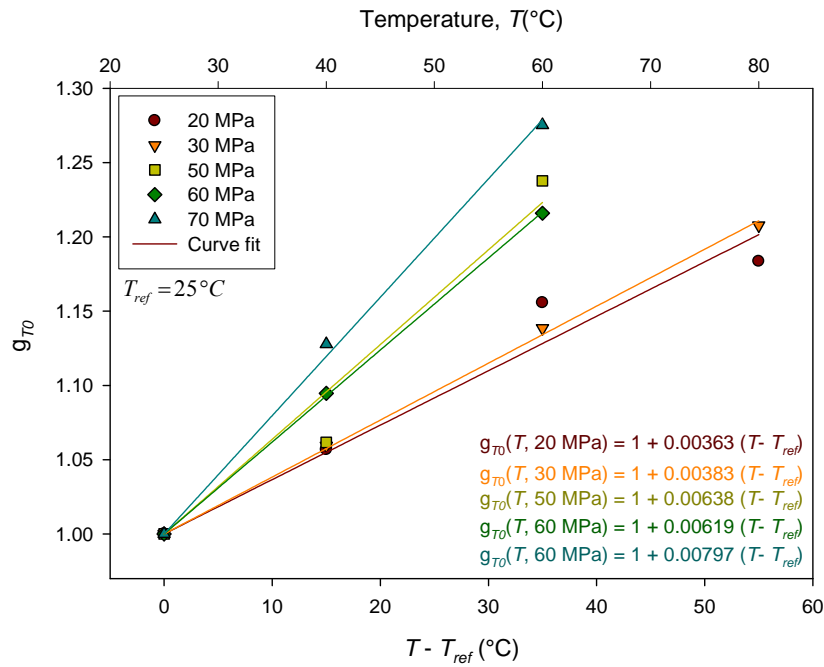
Figure 6.34 Variation of non-linear parameter g_{T0} with temperature at the various temperature levels and curve fit to equation $g_{T0} = 1 + k (T - T_{ref})$.

6.3.5 Non-linear viscoelastic-viscoplastic model

Non-linear viscoelastic model:

As mentioned above, the method provided in section 6.3.3 has been employed to determine the non-linear viscoelastic parameters while the viscoplastic model has been obtained using method provided in section 6.3.4. The parameters of the non-linear viscoelastic model at room temperature from section 5.3.4 and the Prony series parameters given in Table 5.3 have been adopted to determine the temperature dependence of the non-linear viscoelastic parameters at the various stresses.

From Figure 6.26, it is clear that the creep rate at 50 and 60 MPa (at 80°C) are very high. Comparing these curves with those at 70 MPa and 80°C in Figure 6.27, the material can be expected to exhibit tertiary creep followed by failure under these conditions. Also, the viscoplastic strains at 50 and 60 MPa at 80°C is very high. It is suggested that the long fiber GMT composite should not be used at these stresses and temperatures as the material is expected to fail over short durations when exposed to these conditions. Hence the data at these stresses and temperature is not considered in the model.

From an initial curve fit to the creep data obtained using the method in section 6.3.3, the non-linear parameter g_{T2}, modelling the transient creep was found to vary randomly with no-obvious trend. This is because the variations in the transient creep are small (compared to the instantaneous) and is further amplified by the noise in the creep-recovery strain data at higher temperatures, especially at lower stresses (20 and 30 MPa). However, from the creep curves, a reduction in the transient creep (after separating the viscoplastic strains) is observed with temperature at 20 MPa while it is almost constant at the other stress levels. In order to obtain a general creep model, the non-linear parameter g_{T2} has been considered as one. Thus $g_2 = g_{\sigma2}(\sigma)$ (obtained at room temperature given in equation (76)) has been employed at all temperatures.

The variation of non-linear parameter $g_0(\sigma,T) = g_{\sigma0}(\sigma)g_{T0}(T)$ with temperature at the various stress levels is plotted Figure 6.33. It can be seen that the slope of the curves at 20

164

and 30 MPa are very similar while the slope of the curves increases at stresses beyond 30 MPa. The variation of the non-linear parameter g_{T0} with temperature (absolute and relative) at the various stress levels is plotted in Figure 6.34. The g_{T0}-temperature curves at the five stresses has been fit to an equation of the form $g_{T0} = 1 + k\,(T\text{-}T_{ref})$ as shown in the figure. The parameter 'k' which is the slope of the g_{T0}-temperature curve has been found to be dependent on stress as shown in Figure 6.35. This indicates that the non-linear parameter g_{T0} is dependent on stress due to interaction between non-linear effects of stress and temperature, (i.e., the temperature dependence of the instantaneous response varies with stress). To obtain a final general model, the slope 'k' has been fitted as a linear function of stress. The final model obtained for the non-linear parameter 'g_0' is given in equation (94).
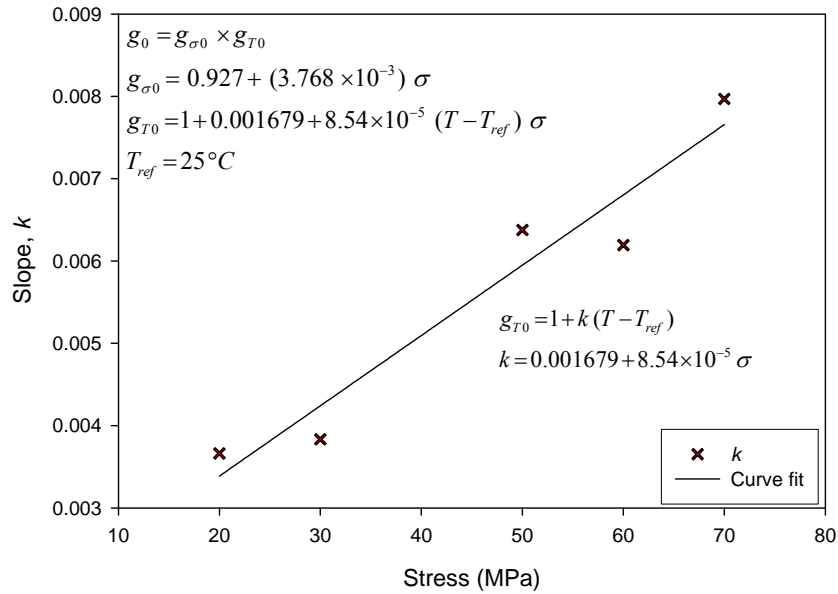
Figure 6.35 Variation of the slope 'k' of the g_{T0}-temperature curves at the various stresses.

$$g_{\sigma 0} = 0.927 + (3.768 \times 10^{-3})\,\sigma$$
$$g_{T0}(T) = 1 + k\,(T - T_{ref})$$
$$where,\ T_{ref} = 25\,^{\circ}C \ and \ k = 0.001679 + 8.54 \times 10^{-5}\,\sigma \tag{94}$$
$$g_2 = g_{\sigma 2}(\sigma) = \begin{cases} 1, & \sigma \leq 30\,\text{MPa} \\ 0.752 + (8.1811 \times 10^{-3})\,\sigma, & \sigma > 30\,\text{MPa} \end{cases}$$

Viscoplastic model:

The model for viscoplastic strains obtained at room temperature given by equation (77) was found to be in good agreement with that at 40°C. This is because the viscoplastic strains at room temperature (25°C) and 40°C vary similarly with stress as shown in Figure 6.30. The variation of the parameter 'n' of the viscoplastic model with stress at 60°C is shown in Figure 6.36. The parameter 'n' of the viscoplastic model has been fit as a linear function of stress. Although using a higher order function for 'n' provided better fits, the linear function has been used to simplify the final model. Further, the model for 'n' obtained at 60°C was found to agree well with that at 80°C for stresses 20 and 30 MPa. This can be seen by the similar values of viscoplastic strains at 20 and 30 MPa over all temperatures. The final model for viscoplastic strains is given equation (95).
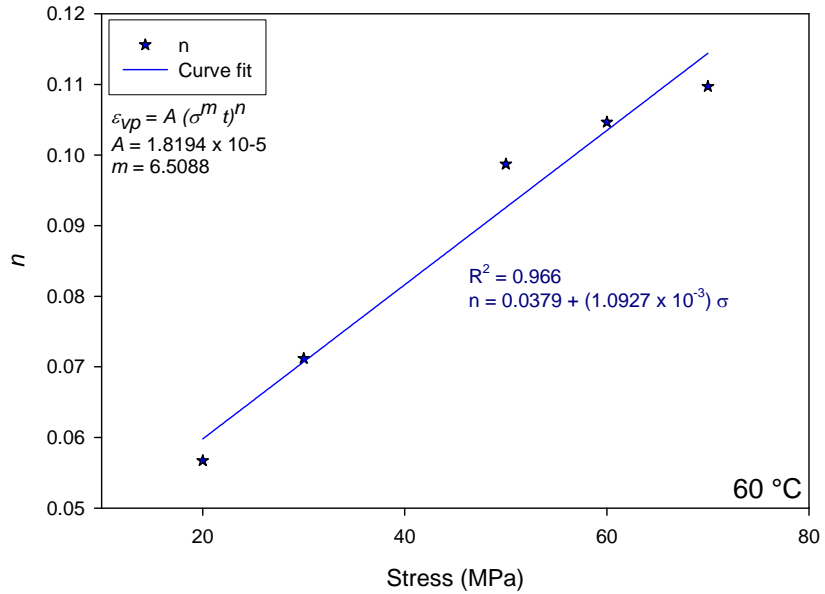
Figure 6.36 Viscoplastic strain parameters at 60°C.

$$A = 1.8194 \times 10^{-5}$$
$$m\ 6.5088$$

$$n = \begin{cases} 0.0420 + (8.7003 \times 10^{-4})\sigma, & 25°C \le T \le 40°C, \ 20 \le \sigma \le 70 \\ 0.0379 + (1.0927 \times 10^{-3})\sigma, & 40°C < T \le 60°C, \ 20 \le \sigma \le 70 \\ 0.0379 + (1.0927 \times 10^{-3})\sigma, & 60°C < T \le 80°C, \ 20 \le \sigma \le 30 \end{cases}$$

(95)

166

6.3.6 Complete non-linear viscoelastic viscoplastic constitutive model

Finally, the complete non-linear viscoelastic viscoplastic model over the entire stress and

$$20\,MPa \leq \sigma \leq 30\,MPa,\ 25°C \leq T \leq 80°C$$

temperature range of the material, i.e., $30\,MPa < \sigma \leq 60\,MPa,\ 25°C \leq T \leq 60°C$ is given

$$\sigma = 70\,MPa,\qquad\qquad 25°C \leq T \leq 40°C$$

below. It is suggested that the material should not be used at conditions exceeding the above range in both stress and temperature.

Viscoelastic model:

$$\varepsilon_c(t) = g_0 D_0 \sigma + \int_0^t \Delta D(\psi - \psi')\frac{dg_2\sigma}{d\tau}d\tau$$

where, $\quad \Delta D(t) = \sum_{i=1}^{N} D_i (1 - e^{-t/\tau_i})$

$$g_0(\sigma, T) = g_{\sigma 0}(\sigma) g_{T0}(T, \sigma),$$

$$g_2 = g_{\sigma 2}(\sigma)$$

with $\quad g_{\sigma 0}(\sigma) = 0.927 + (3.768 \times 10^{-3})\,\sigma$

$$g_{T0}(T, \sigma) = 1 + \left(0.001679 + 8.54 \times 10^{-5}\,\sigma\right)(T - T_{ref})\ ,\ T_{ref} = 25°C$$

$$g_2 = g_{\sigma 2}(\sigma) = \begin{cases} 1, & \sigma \leq 30\,MPa \\ 0.752 + (8.1811 \times 10^{-3})\,\sigma, & \sigma > 30\,MPa \end{cases}$$

And D_0, D_i and τ_i are given in Table 5.3 $\qquad\qquad$ (96)

Viscoplastic model:

$$\varepsilon_{vp} = A\left(\sigma^m t\right)^n$$

where, $\quad A = 1.8194 \times 10^{-5}$

$$m = 6.5088$$

$$n = \begin{cases} 0.0420 + (8.7003 \times 10^{-4})\sigma, & 25°C \leq T \leq 40°C, \quad 20 \leq \sigma \leq 70 \\ 0.0379 + (1.0927 \times 10^{-3})\sigma, & 40°C < T \leq 60°C, \quad 20 \leq \sigma \leq 70 \\ 0.0379 + (1.0927 \times 10^{-3})\sigma, & 60°C < T \leq 80°C, \quad 20 \leq \sigma \leq 30 \end{cases}$$

$$(97)$$

6.3.7 Model predictions
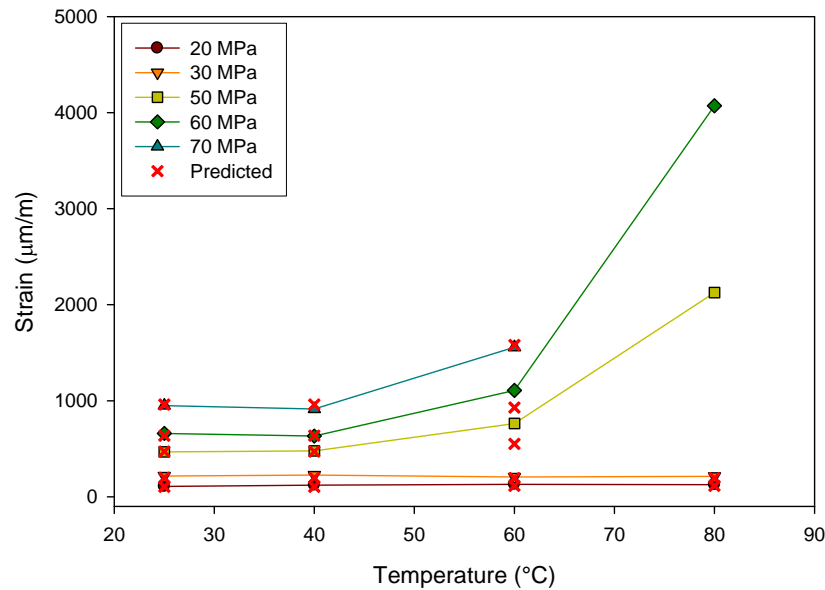
Figure 6.37 Comparison of predicted viscoplastic strains with experimental data after 1 day creep.

The viscoplastic strains after 1 day creep predicted using the model in equation (97) is compared with the experimental results in Figure 6.37. Only the experimental viscoplastic strains are plotted for 50 and 60 MPa at 80°. Overall, the predicted viscoplastic strains at all stresses and temperatures agree very well with experiments. The viscoplastic strains at 60°C for stresses 50 and 60 MPa are slightly under predicted due to the difference in parameter 'n' predicted used in equation (97) as can be seen in Figure 6.36. The viscoplastic strains during creep and recovery at the five stresses considered at 60°C are plotted in Figure 6.38. The predictions show that a large portion of the viscoplastic strain is developed upon loading with rate of viscoplastic strain evolution

decreasing with time. As expected, there is no viscoplastic strain development during recovery as the stress is removed.
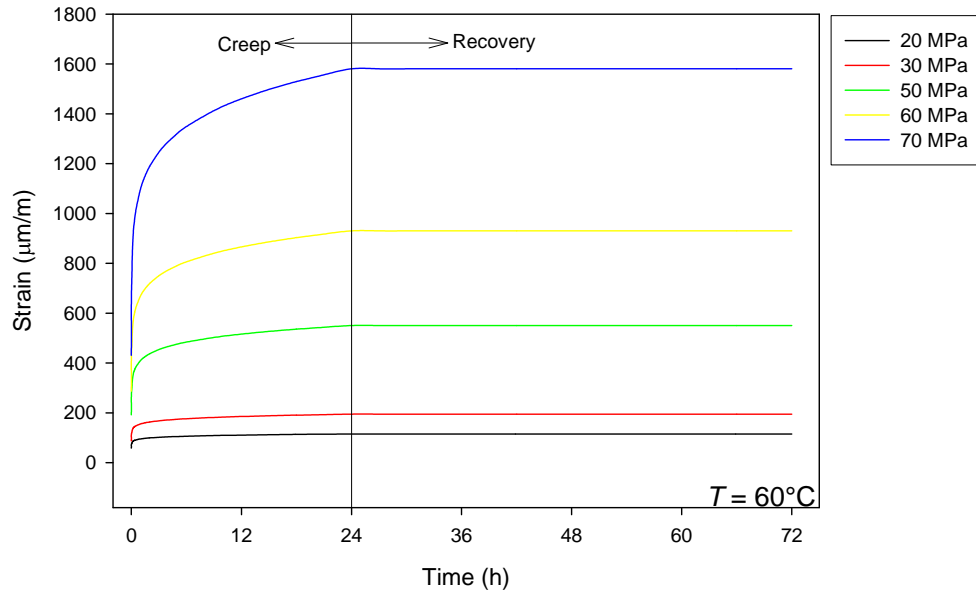
Figure 6.38 Predicted viscoplastic strains during creep and recovery at 60°C.

The creep curves predicted using models in equations (96) and (97) at the various stress levels at temperatures 40°C, 60°C and 80°C are compared with the experimental results in Figures 6.39, 6.40 and 6.41, respectively. Overall, the creep curve predictions are very good, with slight differences in the shape of the curves. Further, some of the creep curves are slightly over- or under-predicted due to the variations in the non-linear viscoelastic parameters, particularly g_{T0}, obtained using the respective model. g_{T0} is the non-linear parameter modelling the instantaneous response which is rather high. If g_{T0} is slightly over/under-predicted, so are the overall creep strains. However, this over/under-prediction due to g_{T0} is limited to a vertical shift of the creep curves since transient creep depends on g_2 and the Prony series parameters in Table 5.3.
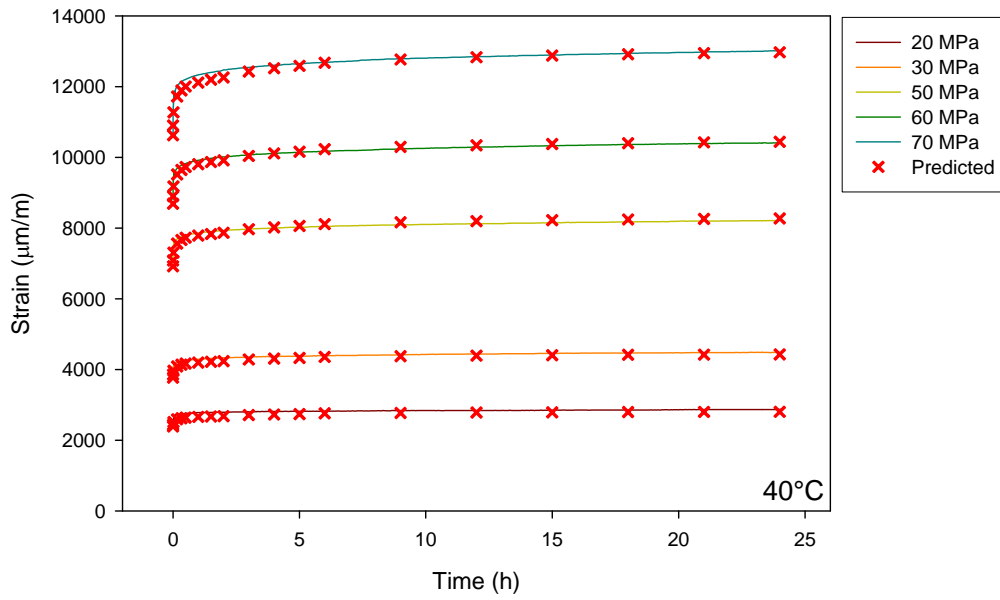
Figure 6.39 Comparison of the predicted creep curves with the experimental at 40°C.
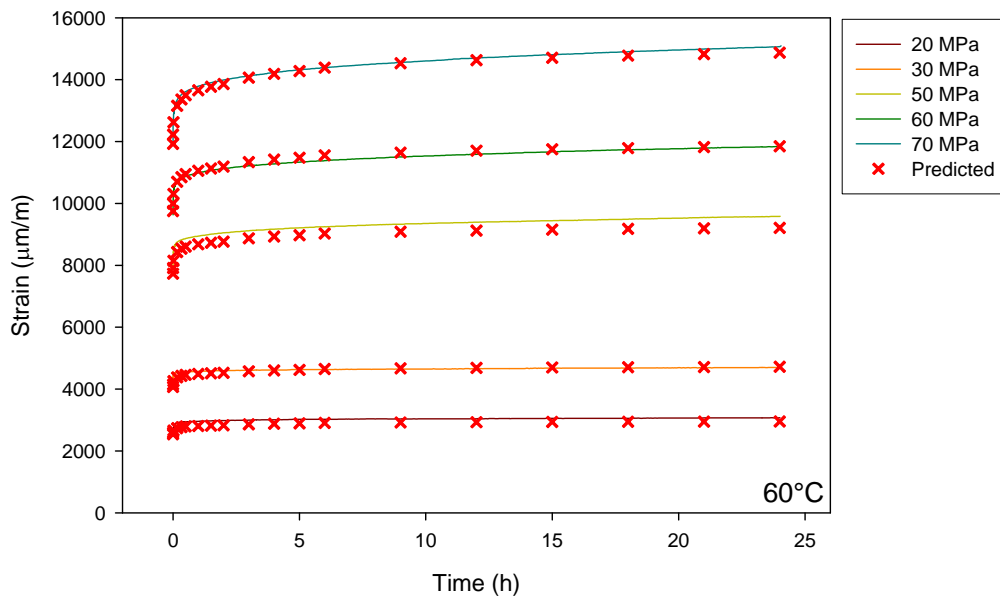
Figure 6.40 Comparison of the predicted creep curves with the experimental at 60°C.
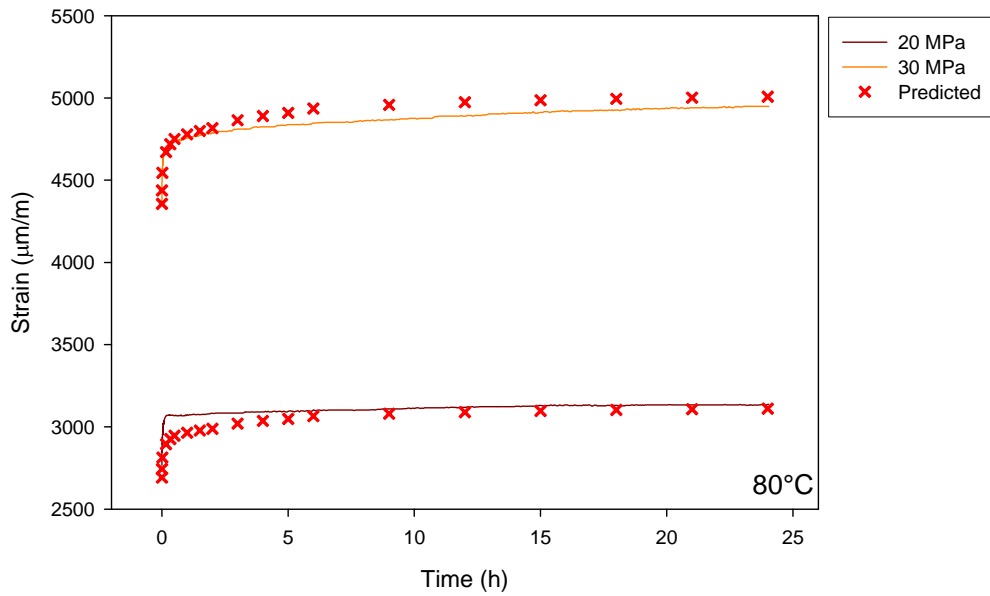
Figure 6.41 Comparison of the predicted creep curves with the experimental at 80°C.
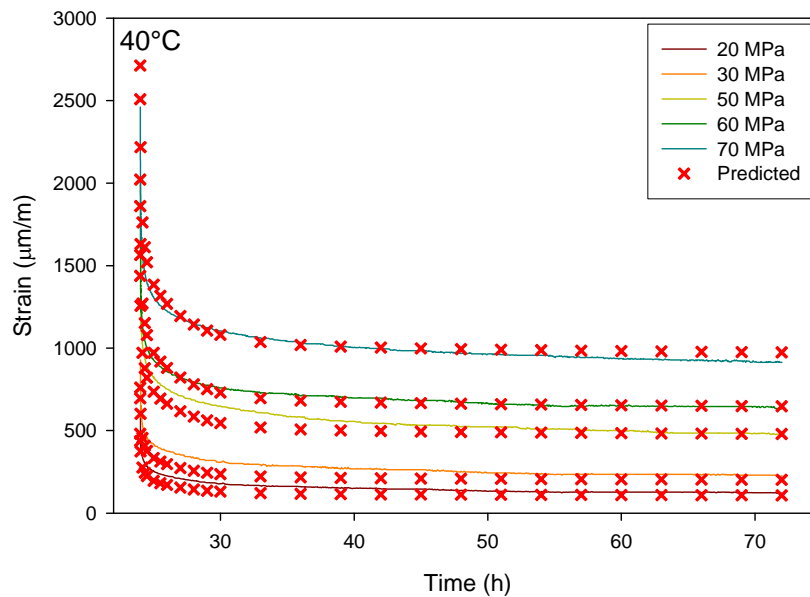
Figure 6.42 Comparison of the predicted recovery curves with the experimental at 40°C.

Finally, the recovery strain predictions at the various stresses for temperatures 40°C, 60°C and 80°C are compared with the experimental in Figures 6.42, 6.43 and 6.44 respectively. The recovery strain predictions at 40°C and 80°C are in good agreement with the experimental with slight variation in the initial time dependence. The predictions

at 50 and 60 MPa for 60°C in Figure 6.43 are slightly under-predicted due to the under-prediction of the viscoplastic strains as mentioned earlier.
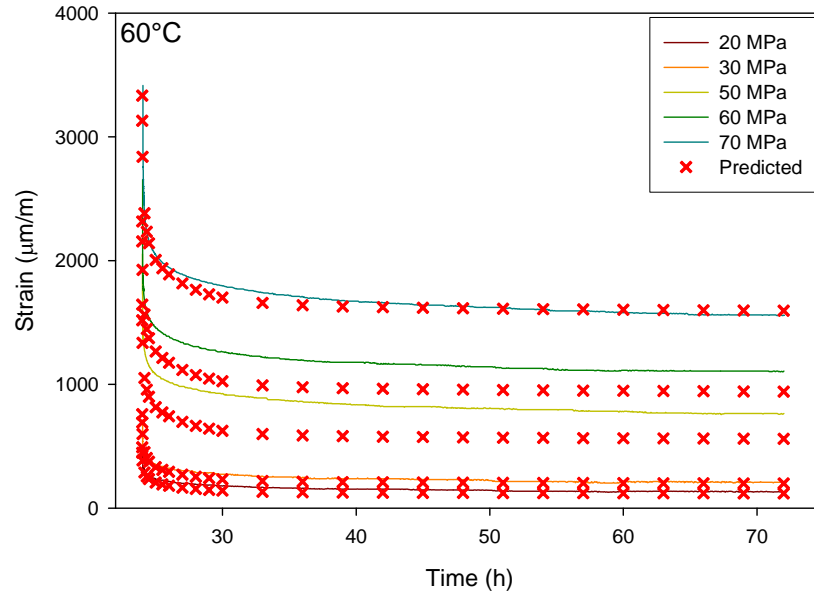
Figure 6.43 Comparison of the predicted recovery curves with the experimental at 60°C.
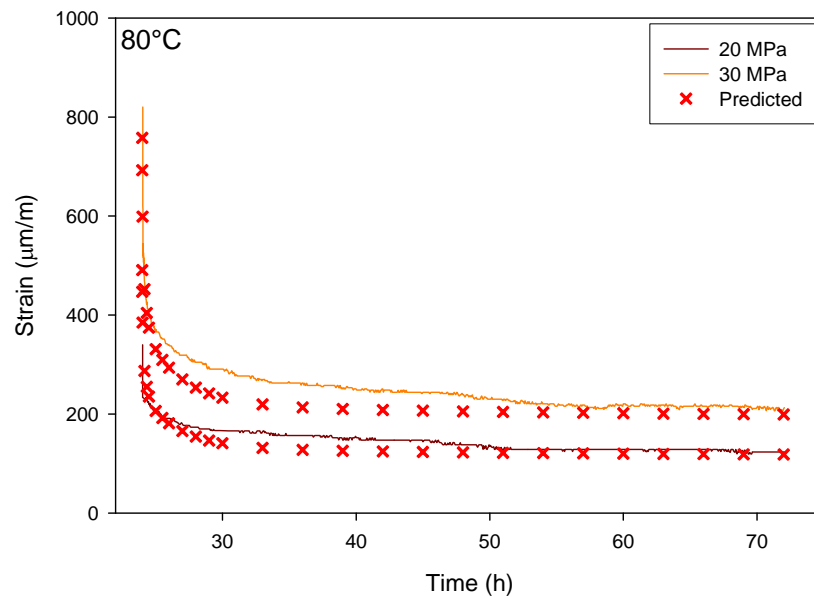
Figure 6.44 Comparison of the predicted recovery curves with the experimental at 80°C.

6.4 Chapter conclusions

In this chapter, the temperature dependence of the creep behaviour has been presented. The conclusions from the tests conducted are as follows:

- ***Short term creep tests:***

Short-term creep tests consisting of 30 minutes creep followed by 1 hour recovery have been conducted over a wide range of stresses from 20 to 60 MPa in increments of 10 MPa and temperatures from 25 to 90 °C, covering the service temperature range of the material. Time-temperature Superposition (TTS) has been carried out on data within the linear viscoelastic region which is at 20 MPa to obtain a long term master curve at 25°C. A 9-term Prony series has been curve fitted to this master curve of duration of more than 185 years. The creep tests showed that the material is non-linear viscoelastic with both stress and temperature. However, the non-linear behaviour with temperatures up to 50 MPa can be modeled using just the shift factors from the TTS. The non-linear parameters $g_{\sigma 0}$ and $g_{\sigma 2}$ below 50 MPa were found to vary linearly with stress. At 60 MPa, the non-linear parameters g_0 and g_2 have been modeled as a product of temperature and stress-dependent functions. The model predictions are in good agreement with the experimental at most stress and temperature levels. However, the creep curves predicted at higher temperatures especially at 60 MPa are in good agreement at shorter times while tending to underestimate over time. The model predictions are well within the material scatter of about 8 %. Finally, these tests infer that the continuous fiber GMT material should not be used at stresses above 60 MPa especially if the service temperature is higher than 45°C.

- ***Long term creep tests:***

Long term creep tests consisting of 1 day creep followed by 2 day recovery have been conducted over three temperatures, 40, 60 and 80°C, and five stresses, 20, 30, 50, 60 and 70 MPa, to obtain a general non-linear viscoelastic viscoplastic constitutive model. The creep tests suggest that the material should not be used at temperatures greater than 60°C when the stresses are over 50 MPa. The material exhibited similar variation in the viscoplastic strains with stress at room temperature and 40°C. Also the viscoplastic

173

strains are independent of temperature at stresses below 30 MPa. The method to estimate the non-linear parameters provided in the previous chapter has been extended to enable determination of temperature dependence of the non-linear parameters. Furthermore, a method to accurately separate the viscoplastic strains by assuming the viscoelastic behaviour at each stress level to be linear with respect to its own stress level has been developed. Finally, the creep and recovery strain predictions obtained from the model have been found to be generally in good agreement with the experimental.

CHAPTER 7

RESULTS AND DISCUSSION: VISCOPLASTIC STRAINS

7.1 Overview

From the results presented in chapters 5 and 6, it is clear that viscoplastic strains are developed during creep in long-fiber GMT composite materials. Moreover, the magnitude of the viscoplastic strains is significant and has to be accounted for in the constitutive model. In order to further understand the viscoplastic strains in long fiber GMT composites, an additional set of creep-recovery tests has been carried out. These tests consisting of multiple creep-recovery tests of increasing duration on a single specimen at seven stress levels were carried out to,

- experimentally determine the time and stress dependence of viscoplastic strains,

- validate the numerical method to obtain the viscoplastic strains provided in the previous chapters,

- validate the experimental method proposed by Nordin *et al*. [61],

- determine the effect of employing multiple loading cycles in determining the viscoplastic strains,

- determine the effects of the assumptions in equation (52),

- correlate the viscoplastic strains with the underlying damage mechanisms observed from in-situ microscopy and

- determine the effect of viscoplastic strains on the viscoelastic response of the material

The creep tests conducted consisted of 6 creep-recovery cycles of increasing duration carried out consecutively on a single virgin specimen. The durations of the creep cycles applied were 1, 3, 3, 6, 12 and 24 hours with each creep cycle followed by recovery of duration 3 times that of creep, i.e., 3, 9, 9, 18, 36 and 72 hours, respectively. The total creep duration was 49 hours with the total test (including recovery) lasting 196 hours

(8.17 days). The stress history during each test is as given in Figure 7.1. Tests at 7 stress levels between 20 and 80 MPa in increments of 10 MPa were carried out. Considering the scatter expected in these materials, all tests were replicated four times on separate strain-gauged virgin specimens. The models were developed from average curves obtained from these four replicates. The set of experiments conducted is very similar to that carried out by Nordin *et al.* [61] and Marklund *et al.* [62] but this work is more comprehensive in that the evolution of plastic strains with time at all the stress levels have been determined. Typically, such comprehensive sets of experiments are not necessary to model the viscoelastic and viscoplastic behavior of polymeric materials as illustrated in chapters 5 and 6 (numerically) and by Nordin *et al.* [61] (experimentally). But since the purpose of this study is to better understand the behavior of the viscoplastic strains, an extensive experimental investigation becomes necessary.
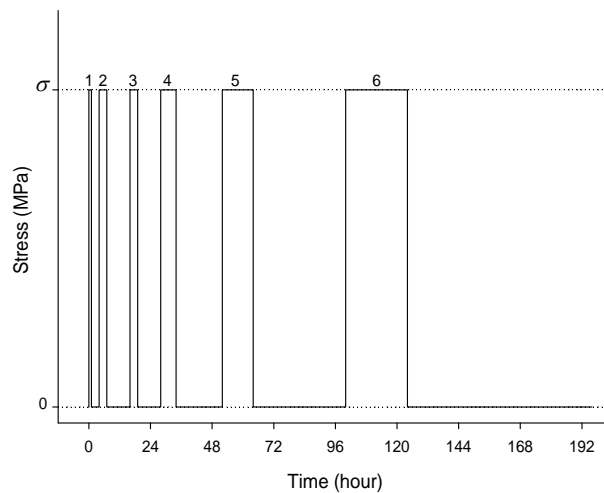
Figure 7.1 Stress history during the test.

7.2 Results and discussions

7.2.1 Creep test results

Figure 7.2 shows the average creep-recovery curves obtained at the seven stress levels between 20 and 80 MPa. Since two of the four specimens tested at 80 MPa failed – one during the fifth cycle and the other during the first cycle, the 80 MPa curve shown in Figure 7.2 was thus obtained as an average of two curves. Furthermore, the data at 80

176

MPa was not included in subsequent analysis. The total instantaneous creep strains obtained from cycle 1 for the four trials are plotted against applied stresses shown in Figure 7.3. Correspondingly, the average creep compliances are cross-plotted in the figure. As shown, the increase in compliance with stress indicates non-linear viscoelastic behavior.
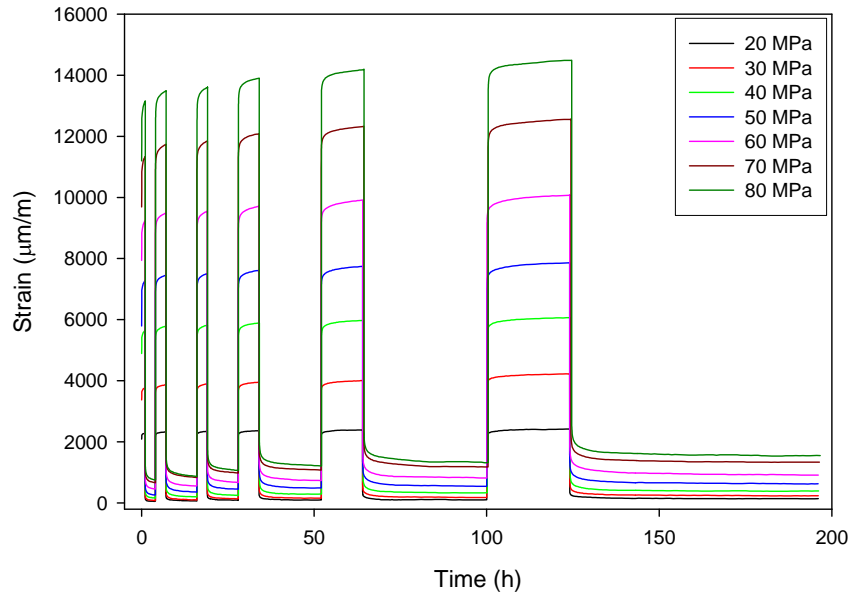
Figure 7.2 Average creep-recovery cycles at the seven stress levels.
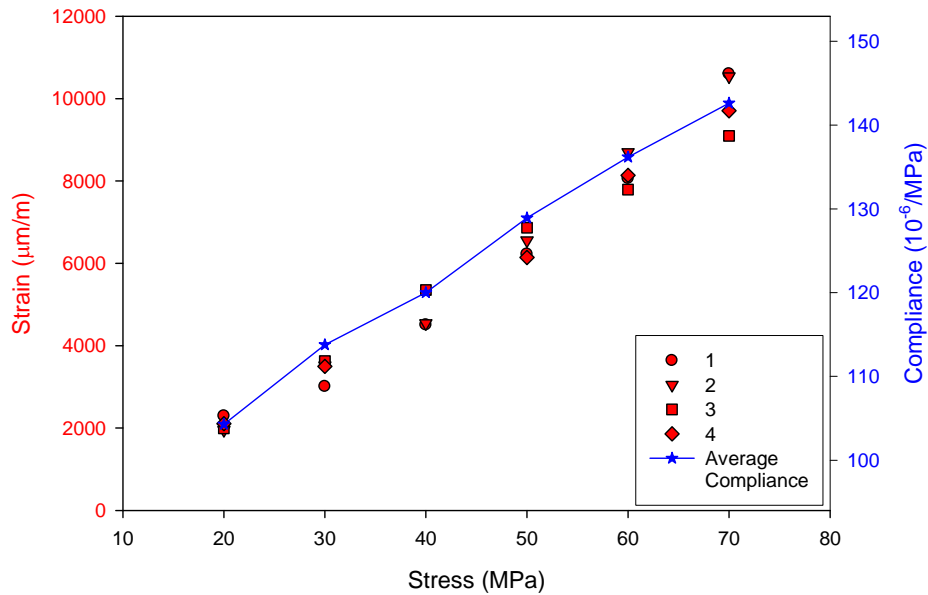
Figure 7.3 Instantaneous strains (four trials) and average compliance from cycle 1.
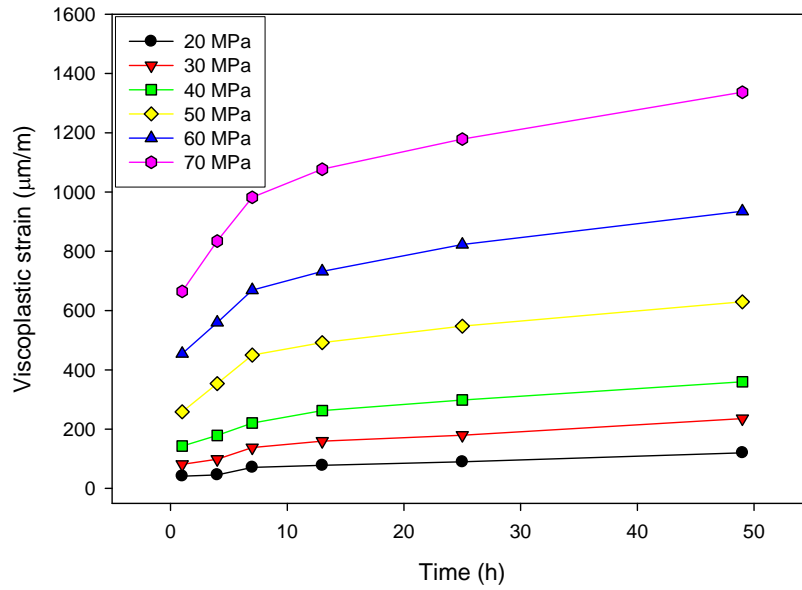
(a)
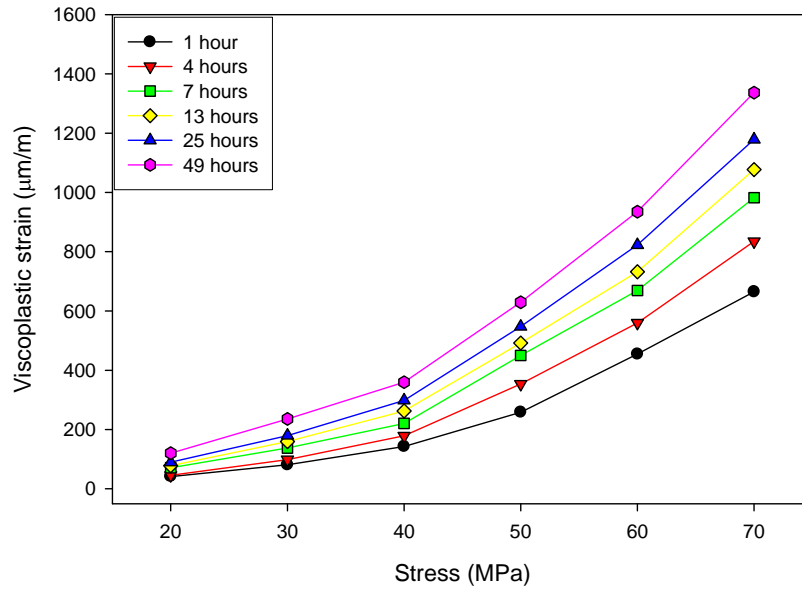
(b)

Figure 7.4 Plot of viscoplastic strains with (a) time at various stresses
(b) stress at various times.

The presence of viscoplastic strains is evident from the un-recovered strains at the end of
each cycle in Figure 7.2 and a trend of increasing viscoplastic strains with both time and
stress is observed. Following unloading, the magnitude of strains recovered after
durations equal to that of creep is negligible. However, in order to ensure maximum
recovery of viscoelastic strains developed during creep of one cycle before the start of

178

next cycle (creep), the specimens were recovered (under no load) for a duration equal to three times that of creep duration. The un-recovered strains at the end of recovery also provide a good estimate of the viscoplastic strain.

Figure 7.4 (a) shows the non-linear evolution of plastic strains with time at all of the six stress levels. Each point in Figure 7.4 (a) was obtained as the un-recovered strain at the end of recovery and will be referred to as the "experimental viscoplastic strain" henceforth. A large portion of the plastic strains are developed in the first cycle, for example, nearly 50 % of the total viscoplastic strains accumulated over 49 hours at 70 MPa is developed during the first hour (first cycle). The non-linear variation of viscoplastic strains with stress is shown in Figure 7.4 (b). The plot shows the increase in the non-linearity of the viscoplastic strain–stress curves with time, especially at stresses higher than 40 MPa. Thus, the viscoplastic strains are non-linear with both stress and time. The variation of viscoplastic strain rate with time for the various stress levels is shown in Figure 7.5. It can be seen that the viscoplastic strain rate reduces rapidly over the first 24 hours and then levels off approaching a constant value eventually. The viscoplastic strain rate over the first hour of the experiment is not plotted because the value is very large and lies outside the scale (due to its very high magnitude).
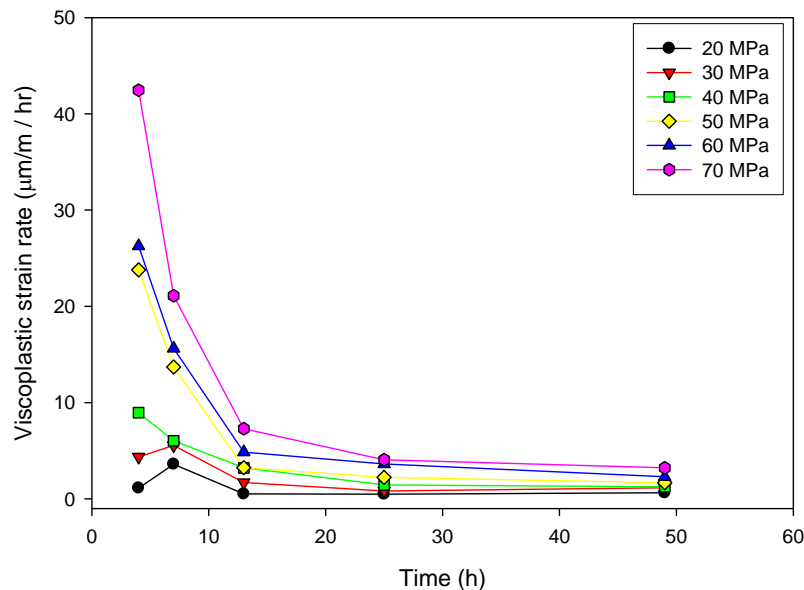
Figure 7.5 Variation of viscoplastic strain rate with time at various stresses.

7.2.2 Viscoplastic model development
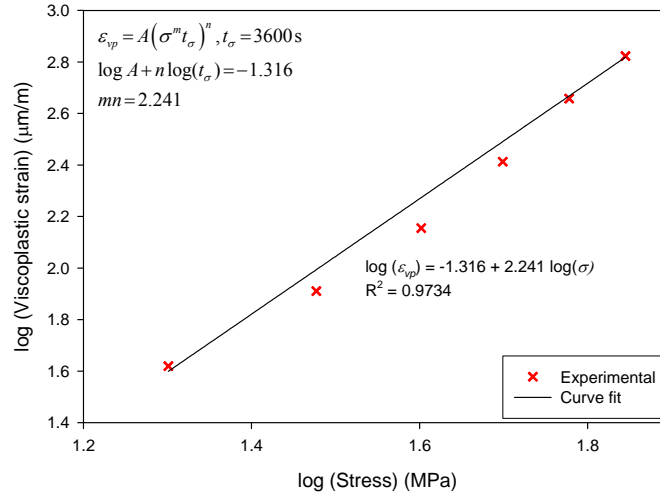
(a)
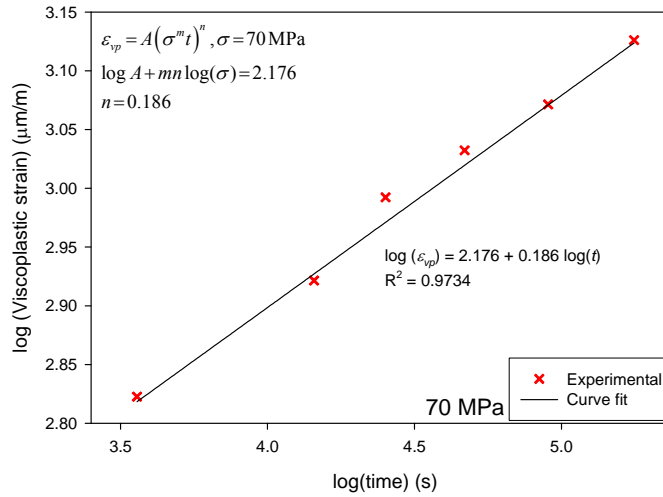
(b)

Figure 7.6 Curve fit of Viscoplastic strains (a) with stress at the end of 1 hour creep at 70 MPa on a log-log scale (b) with stress at the end of 1 hour creep on a log-log scale.

Although the stress- and time-dependence of the viscoplastic strains in the material have been determined experimentally (at all stresses and times considered), the method proposed by Nordin *et al.* [61] which requires only a portion of the data, will be applied here. The intent is to validate Nordin's method detailed in section 2.8. To determine stress-dependence, the viscoplastic strains at the various stress levels at the end of 1 hour creep plotted in Figure 7.6 (a) on a log-log scale has been employed. Fitting the data in

Figure 7.6 (a) to a linear function of log(stress) $\left(\log(\varepsilon_{vp}) = \left(\log A + n \log t_\sigma \right) + mn \, \log(\sigma) \right)$ gives the values $mn = 2.241$ and $\log A + n \log(t_\sigma) = -1.316$. To determine time-dependence, the viscoplastic strains over the 6 durations considered in the test at 70 MPa plotted in Figure 7.6 (b) on a log-log scale has been employed. By fitting the data in Figure 7.6 (b) to a linear function of log(time) $\left(\log(\varepsilon_{vp}) = \left(mn \, \log(\sigma) + \log A \right) + n \log t_\sigma \right)$, $n = 0.186$ and $\log A + mn \log(\sigma) = 2.176$ was obtained. Using these expressions, the parameters of the viscoplastic model have been determined as,

$$A = C^n = 11 \times 10^{-9}$$
$$m = 12.048$$
$$n = 0.186$$

(98)

It has to be noted that in the above procedure for determining the model parameters, the two curve fits yield distinct values of 'm' and 'n' directly while 'A' can be determined by using either $\log A + n \log(t_\sigma)$ value obtained from the first curve fit or using $\log A + mn \log(\sigma)$ value obtained from the second curve fit. From the values obtained from an initial curve fit of the viscoplastic strain-stress (Figure 7.6(a)) and strain-time curves (Figure 7.6 (b)), to the corresponding equations, it was found that the above two equations ($\log A + n \log(t_\sigma)$ and $\log A + mn \log(\sigma)$) did not result in distinct values of 'A', since the two curves were fit independently. However, after multiple iterations of imposing 'A' in the above equations during curve fitting, a unique value for 'A' could be obtained. Although this procedure indeed gave very good fits, it is possible that this would not always be the case. R^2 values of 0.9848 and 0.9923 were obtained for the initial curve fit to the viscoplastic strain-stress and strain-time curves, respectively, while the final curve fit yielded R^2 values of 0.9734 and 0.9887, respectively, showing slight decrease in the quality of the fits, although acceptable.

The viscoplastic strain predictions from the current model are compared with the experimental values in Figure 7.7. The model slightly underpredicts at 20 MPa but tends

to overpredict at 40 MPa especially at the shorter creep times. Overall, the model predictions are in excellent agreement with the experimental values. This provides strong evidence that the time- and stress-dependence of the viscoplastic strains can be accurately deduced using such reduced experimental schemes given by Nordin *et al.* [61]. Finally, it has to be noted that the tests conducted at the various stress levels (over a fixed creep duration) to determine the stress dependence of the viscoplastic strains have to be conducted on separate virgin specimens (one specimen per stress level). This is due to the fact that the maximum viscoplastic strains develop during the first loading cycle. If a single specimen is repeatedly tested at multiple stress levels, the measured viscoplastic strains at the end of subsequent tests after the first will be lower than actual values (that in a virgin specimen).
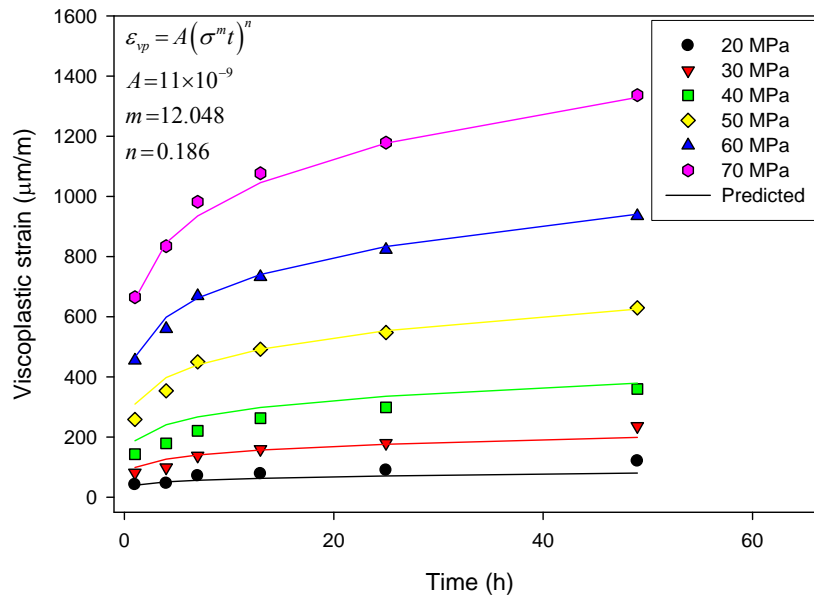
Figure 7.7 Comparison of the experimental and predicted viscoplastic strains at the various stress levels.

Note: Since the time dependence of the viscoplastic strains have been found at all stress levels, the viscoplastic model parameters can also be obtained by fitting the viscoplastic strain – time curves at the various stress levels given in Figure 7.4 (a) to the viscoplastic model i.e., $\varepsilon_{vp} = A\left(\sigma_0^{\,m} t\right)^n$. The parameters so obtained however, were found to vary with stress. This indicates that the time dependence of the viscoplastic strains varies with stress and is the reason for non-unique values of '*A*' obtained from the two curve fits

182

mentioned earlier. In the case of the long fiber GMT composite, the change in the time dependence was small and hence a reasonably good model could be obtained by imposing various values of 'A'. However, this might not be the case if the time dependence of the viscoplastic strains varies largely with stress and it might not be possible to obtain a unique value of 'A' from Nordin's experimental method and the method might not be applicable.

7.2.3 Evolution of viscoplastic strains

The viscoplastic model developed above is based on the assumption that the interruption between the tests (6 cycles) does not affect the viscoplastic strains, i.e., equation (52) is valid [61]. To check the validity of this assumption and to determine the underlying mechanisms in the development of viscoplastic strains and their evolution, the viscoplastic strains developed during each of the six creep cycles have been numerically separated. This can be done by either using the method for the non-linear model given in section 5.3.3 or can be achieved using the method outlined in section 6.3.4. While the former method yields the non-linear viscoelastic model, the latter method has been found to be better for separating the viscoplastic strains. Since the objective here is to accurately separate the viscoplastic strains, the method given in section 6.3.4 will be employed. This involves curve-fitting equations (90), (92) and (93) to creep, $\varepsilon_r(t) - \varepsilon_{vp}(t_r)$ and $\varepsilon_c(t_r) - \varepsilon_r(t)$ curves obtained for each cycle at all the stress levels considered. The method has been applied independently on the six creep-recovery cycles without considering the effect of one cycle on the next. This is justified by the long recovery durations in-between creep cycles. Considering the shorter durations of the cycles 1-5, a 4-term Prony series ($N = 4$) has been employed, while a 5 term Prony series ($N = 5$) was used for cycle 6. The time constants in both the cases were considered as $\tau_i = 10^i$.

The viscoplastic strains extracted at the 6 stress levels using the above procedure are plotted in Figure 7.8 (solid lines). The regions marked as C1 to C6 indicate that the portions of the viscoplastic strains between the vertical lines are obtained from cycles 1 – 6 respectively. The symbols ('x') in Figure 7.8 are the total experimental viscoplastic

strains at the end of each creep cycle. The viscoplastic strains obtained from the above method are slightly lower than the experimentally obtained viscoplastic strains for almost all of the cases. This is because a small portion of the un-recovered strains at the end of recovery process (estimates of viscoplastic strains) may in fact include un-recovered viscoelastic strains. The viscoplastic strains predicted using the model parameters in equation (98) obtained in the previous section are plotted as dotted lines (in Figure 7.8). While the viscoplastic strain predictions obtained from the model (equation (98)) are continuous and smooth over the entire time scale, the numerically extracted viscoplastic strains are intermittent with a rather large increase upon loading and subsequent time varying strain in most cases. The smooth nature of the model predictions is a consequence of the assumption in equation (52) that the interruption between creep-recovery cycles does not affect the viscoplastic strain development [61, 62]. It is clear that this is only partially true as there seems to be a loading effect.
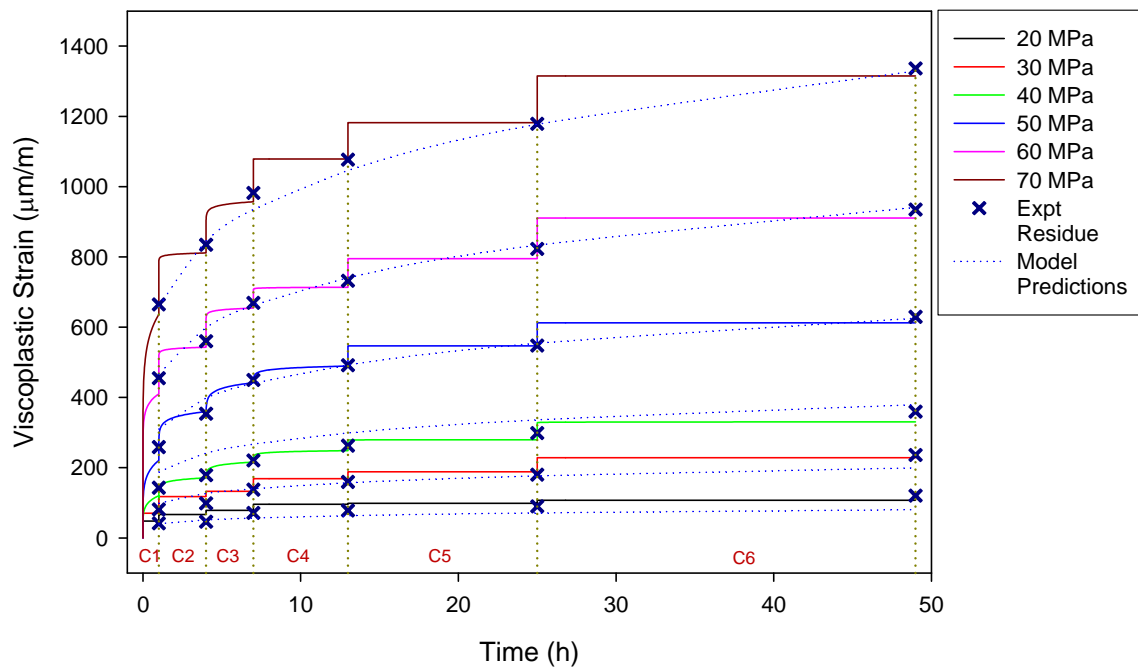
Figure 7.8 Numerically extracted viscoplastic strains (solid lines) at the various stress levels for the 6 creep-recovery cycles compared with the experimental ('**x**') and the model predictions (dotted lines).

7.2.4 Failure mechanisms underlying viscoplastic strains

Failure Observations

The viscoplastic strains in polymeric materials are usually attributed to cracks in matrix, fiber-matrix de-bonding, fiber rupture and matrix yielding. In order to investigate the deformation mechanisms underlying the viscoplastic strains during creep in the continuous fiber GMT, micrographs of the surface of specimens during creep were captured *in-situ* using optical microscopy [106, 107]. Creep tests were carried out using a Minimat 2000 miniature tensile machine on polished miniature size dog-bone shaped creep specimens prepared as per ASTM D-1078 standards with slight modifications to the gripping portion of the specimen.

(a)   (b)

(c)
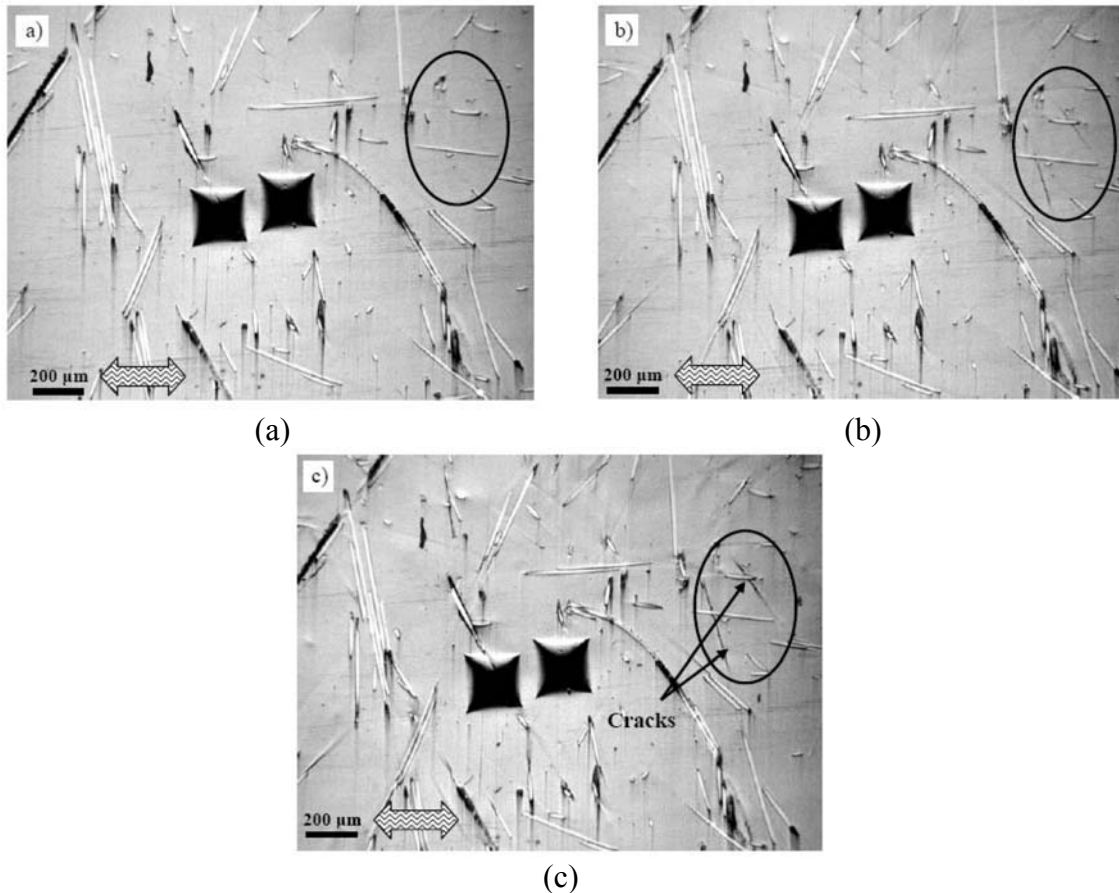
Figure 7.9 Micrographs of specimen (a) at no load (b) after 1 min of loading (c) after 1 day of loading [106, 107].

185

Figure 7.9 (a) shows the micrographs of the specimen before loading while Figures 7.9 (b) and (c) show the micrographs of the specimen obtained after 1 minute and 1 day of loading, respectively, at 62 MPa (about 67% of the ultimate tensile strength of the material). From Figures 7.9 (a) and (b) it is clear that cracks are initiated from the fiber-matrix interface upon loading. Figure 7.9 (c) shows transverse crack growth and an increase in crack width with time under load. Furthermore, no evidence of crack initiation during creep was found. Tests at a lower stress level of about 30 MPa showed negligible crack initiation or growth of existing cracks, however, fiber-matrix de-bonding was observed at multiple locations.

Damage accumulation and viscoplastic strains

As mentioned earlier, the magnitude of the viscoplastic strains decreases progressively with time and the maximum viscoplastic strains are developed during the first cycle although it is the shortest of the six cycles. To explain this, the observations from microscopy have to be considered. The *in-situ* micrographs obtained during creep in Figure 7.9 show that the viscoplastic strains in the continuous fiber GMT composite are due to a combination of matrix crack formation and fiber matrix debonding processes [106, 107]. Cracks are seen to originate from the fiber-matrix interface and usually crack growth terminates by either bridging of cracks or when the crack reaches the fiber-matrix interface of an adjacent fiber. Furthermore, the crack initiation usually occurs upon initial loading while increase in viscoplastic strain with time is due to multiple crack growth. Crack initiation typically occurs at weak sites such as defects along the fiber-matrix interface and voids in the material. Considering that there are a limited number of these defects (or crack initiation sites) along the fiber-matrix interface in the material and that maximum number of these sites is available before the first cycle or the virgin material, the largest viscoplastic strains must therefore occur during the first creep-recovery cycle. With multiple loading and unloading cycles, the number of the sites available for crack initiation also reduces, which explains the observed reduction in viscoplastic strains with time.

From Figure 7.8, the time-dependence of viscoplastic strains is obviously negligible at low stress levels (20 and 30 MPa) during all cycles, i.e., most of the viscoplastic strains are developed upon loading. This can be explained on the basis of the energy required for crack growth i.e., a minimum stress is required for crack propagation. Thus, considering the relatively low level of the applied stress, the crack initiation and/or growth is minimal and so is the time-dependence of viscoplastic strains. The increase in the viscoplastic strain upon loading may be mostly due to the rapid application of the load which provides the energy required to trigger crack initiation and/or growth, although the magnitude is quiet small.

At intermediate stress levels, 40 to 50 MPa, it is seen (in Figure 7.8) that the viscoplastic strains exhibit some time-dependence, although only during the first four cycles. During the last two cycles, the viscoplastic strains develop only upon loading with no time-dependence as there is no further accumulation of the plastic strains during creep. During the first four cycles, the cracks initiate upon loading and grow with time leading to a time varying viscoplastic strains. It should be noted that during instantaneous loading at all cycles, except the first, there could be both crack initiation and growth as the load is applied at a very rapid rate. The reduced or minimal time dependence during the last two cycles is due to a decrease in the number of sites for crack initiation and the measured plastic strains in these cycles are mostly due to crack growth. This is further supported by data at even higher stress levels (60 – 70 MPa). The viscoplastic strain is time-dependent for a shorter period, i.e., the first three cycles. Since the plastic strains at these stress levels are much higher than that at 40 - 50 MPa, the number of defect sites available for crack initiation is exhausted much earlier resulting in reduced time dependence after the third cycle.

7.2.5 Effect of loading and unloading on viscoplastic strains

The dotted lines in Figure 7.8 show the behavior of the viscoplastic strains predicted using the Zapas and Crissman model. However, these do not consider the loading effects (if any) especially when the viscoplastic strains are obtained from multiple creep-recovery experiments. To study the effect of loading on viscoplastic strains, the

viscoplastic data obtained from single duration creep-recovery tests (1 day creep followed by recovery) presented in section 5.3 can be used. The viscoplastic strains numerically extracted from these single creep-recovery experiments is compared with the experimental viscoplastic strains obtained from the multiple creep-recovery tests in Figure 7.10. For stresses up to 40 MPa, the viscoplastic strains obtained from both test schemes are very similar. At stresses above 50 MPa, however, they are similar only at initial creep i.e., up to about 5 hours, with the viscoplastic strains obtained from the multiple creep-recovery experiments accumulating at a higher rate than that obtained from single creep-recovery experiments. This can be attributed to the loading effects in the multiple creep-recovery experiments. Since the load is applied almost instantaneously at the start of creep, repeated loading causes an increase in the accumulated plastic strains. This suggests that the viscoplastic strains obtained from multiple creep-recovery experiments might be higher than the actual especially at higher stresses.
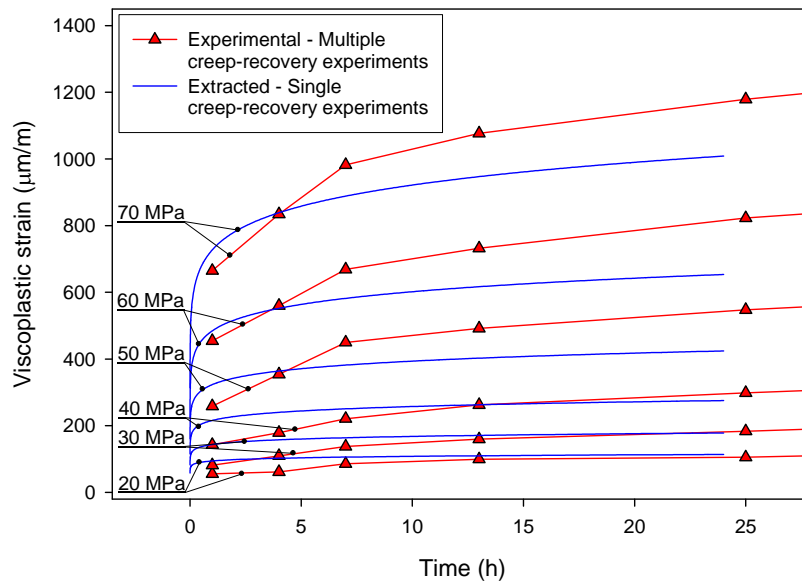
Figure 7.10 Comparison of viscoplastic strains numerically extracted from single creep-recovery test with that obtained experimentally from multiple creep-recovery experiments.

From Figure 7.10 it is clear that the numerically separated viscoplastic strains obtained from single duration creep-recovery tests are in good agreement with the experimental. This shows that the method proposed in section 5.3.3 to determine the non-linear

188

viscoelastic viscoplastic model indeed can provide a good estimate of the viscoplastic strains, thereby validating the method.

7.2.6 Use of pre-conditioning

The magnitude of the viscoplastic strains seen in most materials are relatively small in magnitude and constitute about 10 to 15% of the instantaneous or elastic strains. However, relative to the creep of the material, the viscoplastic strains are significant. In some of the earlier creep studies, such as that by Lou *et al.* [19] and Peretz *et al.* [3], pre-conditioned specimens were employed to reduce scatter in the experimental data. As mentioned earlier, pre-conditioning consisted of loading the specimen to about 60 – 70 % of its ultimate stress and unloading several times (8 – 10 times). This ensured that all viscoplastic strains developing during the creep tests are kept to a minimum. From Figure 7.8, it is evident that when the specimen is subjected to such high stresses (70 MPa = ~82 % of the Ultimate tensile strength), the time-dependence of the viscoplastic strains reduces with multiple loading cycles, with the viscoplastic strain rate reducing with each loading cycle. After about 10 cycles, it can be expected that the magnitude of the viscoplastic strains is very small and develops only upon loading (i.e., viscoplastic strains are not developed during creep). This explains the effectiveness of pre-conditioning in reducing viscoplastic strains during creep testing of polymeric materials.

7.2.7 Effect of viscoplastic strains on viscoelastic behavior

Following the above discussion on the use of pre-conditioned specimens, there has been speculation on whether the tests carried out using such pre-conditioned specimens can be used to represent viscoelastic behavior of a virgin specimen. Thus, in order to study the effect of viscoplastic strains on the creep behavior, the viscoelastic strains predicted (separated) for the six creep-recovery cycles in section 7.2.3 are plotted in Figures 7.11 for all the stress levels (Similar results were found when the viscoelastic strains were obtained by subtracting the viscoplastic strains predicted using the model parameters in equation (98) from the total). Although the change in the viscoelastic strains between the cycles is small, a distinct difference between the viscoelastic strains at 20 MPa and 70

MPa is observed. At 20 MPa, the viscoelastic strains reduce with repeated loading i.e., the creep curve for cycle six is lower than that at for cycle one. This implies a decrease in the creep-compliance of the material with repeated loading. Similar behavior up to 50 MPa is also observed. An opposite trend, however, is seen for 70 MPa stress, i.e., the viscoelastic strains increases with the cycles implying an increase in the creep compliance (modulus decreases) of the material. The increase in compliance is about 2%. At 60 MPa, the viscoelastic strain reduces up to cycle 3 and shows an increasing trend thereafter. Even though the magnitudes of the change in the viscoelastic behavior between the cycles are relatively small, three distinct behaviors are observed:

a. Stresses below 60 MPa – reduction in viscoelastic strains with the cycles.
b. At 60 MPa – initial reduction of viscoelastic strains followed by an increasing trend
c. Above 60 MPa – increase in viscoelastic strains with the cycles.

The change in the trend of the viscoelastic strains observed at 60 MPa can be associated with the viscoplastic strains. The magnitude of the viscoplastic strain after 1st cycle at 70 MPa (665 μm/m) is approximately equal to the magnitude of the viscoplastic strains after the 3rd cycle at 60 MPa and it is after the 3rd cycle that the magnitude of the viscoelastic strains starts increasing. This provides reasonable evidence that an increase in creep compliance is observed when the viscoplastic strain exceeds this magnitude (665 μm/m). An increase in creep compliance corresponds to a decrease in the modulus of the material. Thus, it can be concluded that when the accumulated viscoplastic strains exceeds this strain, there is a reduction in the creep resistance of the material.
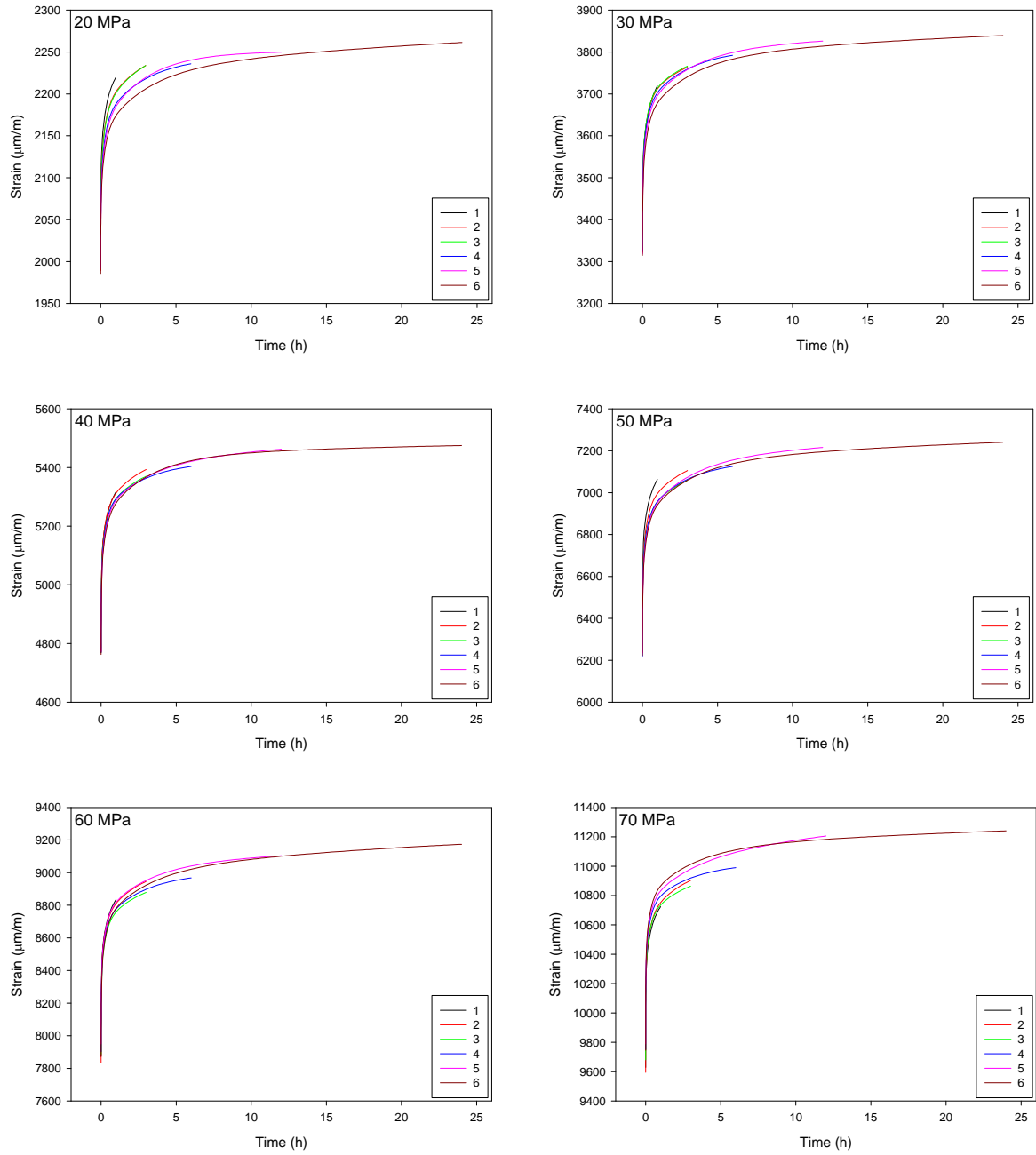
Figure 7.11 Viscoelastic strains separated for the six creep-recovery cycles at the six stress levels considered.

7.3 Chapter conclusions

The evolution of viscoplastic strains in long fiber GMT composites with both time and stress has been studied experimentally through multiple creep-recovery experiments of varying durations and stress. The viscoplastic strains in continuous fiber GMT composite vary non-linearly with both stress and time. Using a technique proposed by Nordin, a semi-empirical model for predicting viscoplastic strains has been developed using only a portion of the comprehensive data set generated in this experiment set. This viscoplastic model had excellent agreement with the experimental data, thereby validating Nordin's simplified method and its general applicability over all stresses and times considered. In retrospect, it is also possible to accurately model viscoplastic strains by numerical separation of strain data from single duration creep-recovery experiments without the need for a large experimental data set. Furthermore, this work has numerically separated the viscoplastic strain evolution during each of the creep cycles at all stress levels studied. The results showed that the Zapas and Crissman viscoplastic model is an approximation of the actual strain evolution. Numerical separation of strains offered an important advantage in that it provided insight into the underlying failure mechanisms associated with creep. The strain evolution corresponded with observed failure mechanisms namely, interfacial debonding and matrix cracking. Finally, it is proposed that a threshold viscoplastic strain exists, above which the creep rate increases due to the damaged state of the GMT material.

CHAPTER 8
MODEL VALIDATION

8.1 Overview

A relatively large number of creep tests have been carried out to determine the creep response in GMT composites subject to a wide range of stresses and temperature. For instance, the long-term master curve from TTS was obtained from short-term temperature tests while the complete non-linear viscoelastic viscoplastic model was obtained from the 1-day creep followed by 2-day recovery tests. Moreover, another set of tests consisting of multiple duration creep-recovery tests to determine the viscoplastic strains experimentally have also been carried out. It is encouraging to see that the data obtained from these different experimental sets are fairly similar (including variability in the data). In this chapter, the constitutive model in equation (96) and (97) will be validated for various test cases. Also, the long-term model obtained using TTS of the short-term temperature data will also be verified.

8.3 Case studies
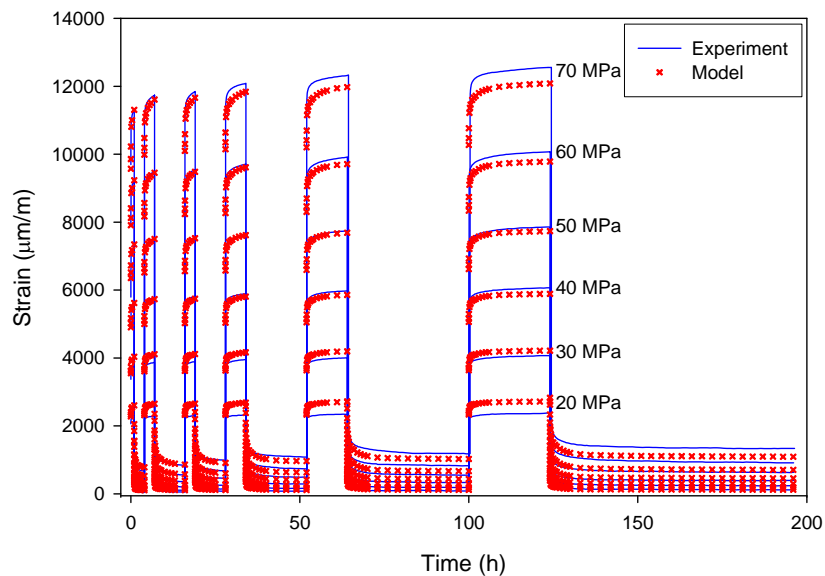
Figure 8.1 Comparison of predicted creep-strains with the experimental
(Viscoplastic strains predicted using equation (77)).

a. Multiple creep-recovery experiments
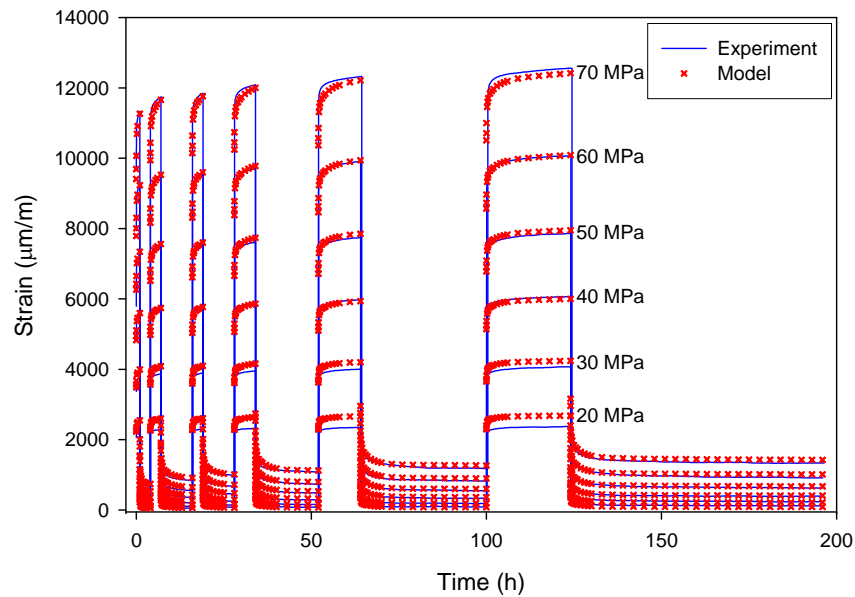
Figure 8.2 Comparison of predicted creep-strains with the experimental
(Viscoplastic strains predicted using equation (98)).

The model in equations (96) and (97) was developed using data from 1-day creep and followed by 2-day recovery tests. Another set of tests to determine the viscoplastic behaviour of the material has been carried out as mentioned in Chapter 7. The models developed were used to predict the total creep strains (viscoelastic + viscoplastic strains) subjected to the stress history given in Figure 7.1 i.e., six creep cycles of duration 1, 3, 3, 6, 12 and 24 hours with each creep load followed by recovery of 3 times the creep duration. The model predictions are compared with the experimental in Figure 8.1. The model over-predicts the strains at 20 and 30 MPa but underpredicts the strains at all the other higher stresses with the difference increasing with stress. It has to be noted that the viscoplastic model in equation (97) is developed from data for test durations up to 1 day creep and hence the viscoplastic strain predictions in Figure 8.1 for the last cycle are extrapolated data and are not accurate. As mentioned in section 7.2.5, the viscoplastic strains are affected by multiple loading cycles and result in a higher viscoplastic strains in the experimental data as shown in Figure 7.10. This difference is the cause of the under-prediction at stresses above 30 MPa. To illustrate this, the model predictions obtained using the viscoplastic model in equation (98), which include this effect, have been used to

194

predict the total creep and recovery strains in Figure 8.2. As can be seen the model predictions at most stress levels are in good agreement with the experimental. However, the model still over-predicts the strains at 20 MPa and slightly under-predicts at 70 MPa which is probably due to experimental scatter. Furthermore the recovery predictions are in excellent agreement with the experiments.
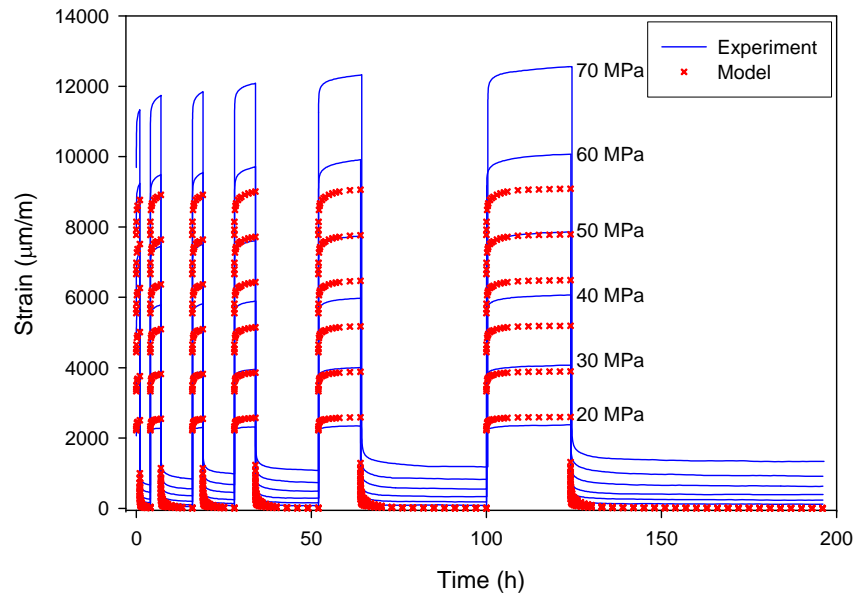
Figure 8.3 Comparison of predicted creep-strains using linear viscoelastic constitutive model with the experimental data.

Furthermore, to illustrate the importance of using a non-linear viscoelastic viscoplastic model rather than just a linear viscoelastic or a non-linear viscoelastic model, the predictions obtained from a viscoelastic model (model at 20 MPa described by a 5-term Prony series given in Table 5.3) and that from just a non-linear viscoelastic model (equation (96) and Table 5.3) are compared with the experimental data in Figures 8.3 and 8.4 respectively. The implications of employing just a linear viscoelastic model are rather large, with the difference between the predicted and experimental increasing drastically with stress (under-predicts by more than 25% at 70 MPa). Viscoplastic strains also have a similar impact as shown in Figure 8.4, where the predictions are obtained using the non-linear viscoelastic model. As expected, the recovery predictions in both Figures 8.3 and 8.4 differ from the experimental results by the magnitude of the viscoplastic strains.

195
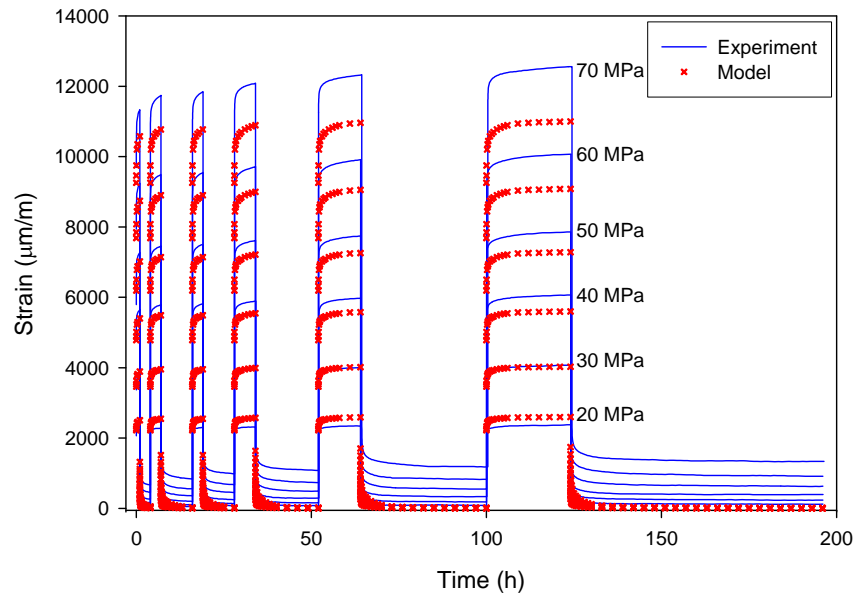
Figure 8.4 Comparison of predicted creep-strains using non-linear viscoelastic constitutive model with the experimental (viscoplastic strains not included).

b. Tapered bar
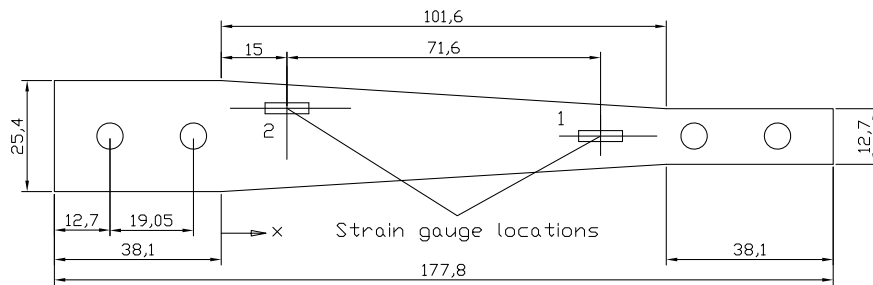
Figure 8.5 Tapered bar with strain gauge locations.

The developed constitutive model was also verified using a tapered bar experiment as shown in Figure 8.56. Two creep tests of 1-day duration were performed at a stress of 40 MPa applied at the narrow section. One of the specimens was strain gauged at location 1 while the other was strain gauged at two locations 1 and 2 as shown in Figure 8.5. Shorter strain gauges of length 5 mm were employed due to the change in the cross-sectional area (compared to 30 mm long strain gauges used for all the other creep tests). The approximate stresses at the center of strain gauges 1 and 2 are 34.85 and 21.59 MPa, respectively. The predictions obtained using these stresses at the two locations are compared with the experimental data in Figures 8.6 and 8.7. Although the model

196

predictions obtained here are fairly close to the experimental, larger differences can be expected especially when smaller strain gauges are used. It has been found that the gauge length over which the strains are measured does affect the variability [4, 86], with higher variation in case of shorter gauge lengths.
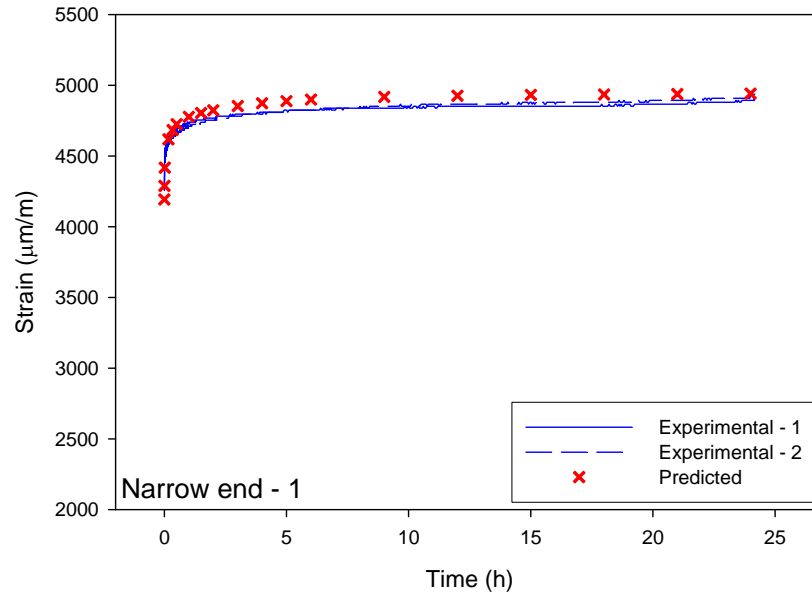
Figure 8.6 Comparison of the predicted strains with the experimental strains obtained using strain gauge at location 1 (Figure 8.5).
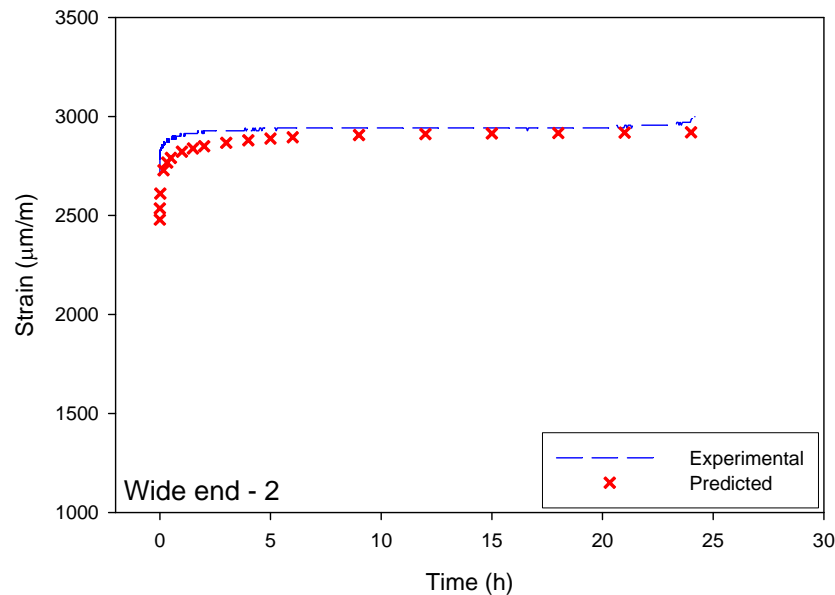
Figure 8.7 Comparison of the predicted strains with the experimental strains obtained using strain gauge at location 2 (Figure 8.5).

c. Long term model

The predictions from the long-term master curve-based model obtained using TTS from short-term tests presented in Section 6.2.4 are compared with the experimental data (1 day creep at 20 MPa – average of 4 trials) in Figure 8.8. The model consistently under predicts the experimental results by about 2% over the entire creep duration (1 day). Since the shape of the creep curve agrees very well with experiments, the difference must be due to the instantaneous response. It has to be noted that the short-term tests used for developing the master curve (TTS) were carried out on pre-conditioned specimens. As mentioned in section 7.2.7, the compliance reduces slightly with repeated loading cycles for stresses up to 50 MPa. Since the pre-conditioning was carried out at 50 MPa, the slightly lower strains obtained from the master curve may be attributed to this. However, the difference is well within the experimental scatter range of about 8 % which has been observed consistently in the entire experimental program.
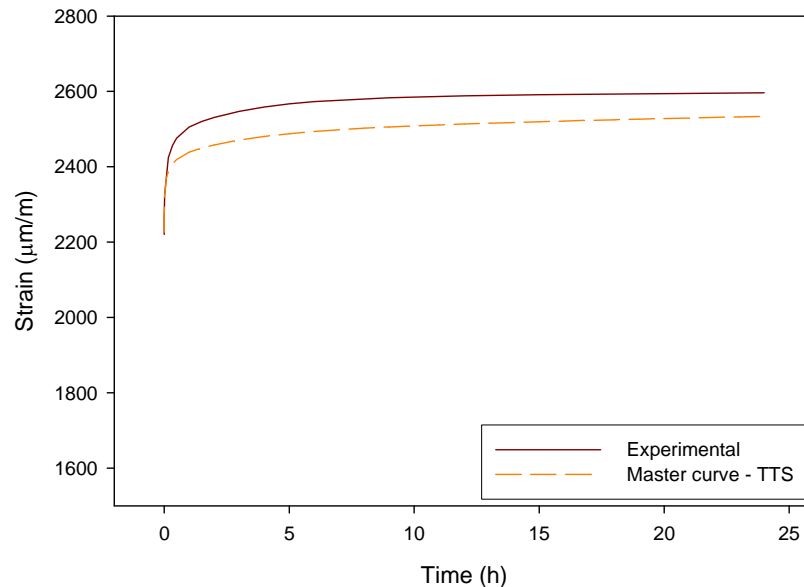
Figure 8.8 Comparison of the predicted strains obtained from TTS with the experimental data.

8.3 Chapter conclusions

Three verifications tests have been considered to validate the complete non-linear viscoelastic viscoplastic creep model developed in this test program. In the first test, the model was used to predict the creep-recovery behaviour during six loading and unloading cycles. The predictions at most stress levels were slightly under-predicted mostly due to the lower viscoplastic strains. This is attributed to the effect of multiple loading and unloading cycles on both the viscoplastic and viscoelastic strains. As a second test, a tapered bar strain gauged at two locations has been tested. The model predicted the strains rather well. Finally, the long-term model obtained from Time-Temperature superposition obtained from 30 minutes creep tests at the various temperatures was compared with the experimental data over 1 day. The model predictions, which were slightly lower than the experimental, was attributed to scatter in the data and also the effect of pre-conditioning on the long-term model obtained from the short term tests.

CHAPTER 9
CONCLUSIONS

From thermal analysis, tensile and creep tests performed in this work, the following conclusions related to the thermal and mechanical properties of the GMT composite can be drawn:

1. **Modulated Differential Scanning Calorimetry (MDSC):**

   Calorimetry showed that the melting point of the GMT composite is approximately 164.0°C and the crystallinity of the polypropylene matrix is between 49-54%. When the cooling rate was varied from 10 to 20°C/min, the crystallinity of the material decreased but the melting point increased. From the controlled cooling experiments, it can be estimated that the material was cooled at a rate between 15 to 20°C/min during moulding.

2. **Dynamic Mechanical Analysis (DMA):**

   DMA showed that the glass and secondary glass (α*) transitions for material occur at 3.49°C and 61.34°C respectively. The variation of the storage modulus with temperature has been determined. It was found that the storage modulus reduced by about 30% when heated from room temperature to 80°C. Further, there was 50% increase in the stiffness of the material as it was cooled from 25°C to -30°C.

3. **Tensile behaviour:**

   Tensile tests performed on 3-mm and 6-mm thick samples showed variability in the tensile properties of the 3-mm thick GMT to be lower than the 6-mm thick GMT. The mean tensile property variations between and within test plaques in both materials are statistically insignificant. Furthermore, the tensile properties of the 3-mm thick GMT showed lower directional dependence than the 6-mm thick GMT composite. The difference is due to the variation in the flow of the material during moulding between

the two materials. Finally, the tensile properties of the 6-mm thick GMT are higher than the 3-mm thick GMT due to higher fiber weight fraction in the former material.

4. Short-term Creep Modeling:

The creep behaviour in long fiber composites as a function of both stresses and temperature has been studied in great detail. Two sets of experiments consisting of short- and long- term creep tests have been performed. The short-term creep tests consisting of 30 minutes creep followed by recovery, enabled isolation of the stress and temperature effects on the creep behaviour by minimizing material response scatter. This was achieved by performing the creep tests at the various stress (and temperatures) levels on a single specimen. Short-term creep tests performed on the long fiber GMT composite showed that the material is non-linear viscoelastic at stresses above 20 MPa for the 3-mm thick GMT and above 25 MPa for the 6-mm thick GMT. Considerable non-linearity with temperature has also been observed. Time-Temperature Superposition was applied to creep curves at various temperature levels at 20 MPa to obtain a master curve which can predict compliance in the linear viscoelastic region up to 185 years at room temperature. Also, viscoplastic strains were observed during creep indicating that a non-linear viscoelastic-viscoplastic model is needed to accurately model the creep behaviour in the long fiber GMT material.

5. Long-term Creep Modeling:

Long-term tests consisting of 1 day creep followed by 2 day recovery were performed over a stress range of 20 to 70 MPa and a temperature range of 25 to 80°C to obtain a general non-linear viscoelastic-viscoplastic constitutive model. The material undergoes considerable creep at temperatures above 60°C especially when the stress is higher than 50 MPa. Furthermore, tertiary creep behaviour occurs at 80 MPa. The variation of the viscoplastic strains with stress was similar up to 40°C. In addition, the

viscoplastic strains at 20 and 30 MPa over all the entire temperature range considered have been found to be similar, indicating similar damage mechanisms.

The creep behaviour has been modeled using Findley's non-linear viscoelastic model (Reduced from of the Schapery non-linear viscoelastic model) and the Zapas and Crissman viscoplastic model. A numerical method to separate the viscoplastic and the viscoelastic strains from the total creep strains measured has been proposed. The method also provides the parameters of the non-linear viscoelastic model. To consider the stress and temperature effects on the creep behaviour, the non-linear parameters have been modeled as a product of stress and temperature dependent functions. The creep and recovery strain predictions obtained from the model generally agreed well with the experimental results. Moreover, the model predictions are well within the data scatter of about 7-8 %

6. Viscoplasticity in long fiber GMT composites:

The evolution of viscoplastic strains in long fiber GMT composites with both time and stress has also been studied experimentally through multiple creep-recovery experiments of varying durations and stress. The viscoplastic strains in continuous fiber GMT composite vary non-linearly with both stress and time. Using a technique proposed by Nordin, a semi-empirical model for predicting viscoplastic strains has been developed using only a portion of the comprehensive data set generated in this experiment set. This viscoplastic model had excellent agreement with the experimental data, thereby validating Nordin's simplified method and its general applicability over all stresses and times considered. Furthermore, the viscoplastic strain evolution during each of the creep cycles has been numerically determined at all stress levels studied. The results showed that the Zapas and Crissman viscoplastic model is an approximation of the actual strain evolution. Numerical separation of strains offered an important advantage in that it provided insight into the underlying failure mechanisms associated with creep. The strain evolution corresponded with observed failure mechanisms namely, interfacial debonding and matrix cracking.

Finally, it is proposed that a threshold viscoplastic strain exists, above which the creep rate increases markedly due to the damaged state of the GMT material.

Future work

The current work is the most comprehensive experimental study on creep of GMT composites. To advance the field, the following recommendations for future work are suggested:

1. Implementation of the viscoelastic-viscoplastic constitutive model to finite element codes.
2. Validation of the model under various loading conditions.
3. Validation of the model under stress and temperature variations.
4. Validation of the model in 3D has not been carried out in this work, which is a major issue during employing these models in finite element methods, and
5. As shown in this work, the viscoplastic strains are directly related to the failure in the material. By determining the viscoplastic strains before rupture (or even up to tertiary creep), the durability of composites can be fairly well predicted by using only viscoplastic strains.

REFERENCES

[1]   Ericson ML and Berglund LA, "Processing and mechanical properties of oriented preformed glass mat reinforced thermoplastics", *Composites Science and Technology*, Vol. 49, 1993, p. 121-130.

[2]   Berglund LA and Ericson ML, "Glass mat reinforced polypropylene, Polypropylene: structure, blends and composites-v3", Chapman & Hall, London, 1995.

[3]   Karger-Kocsis J, "Swirl mat and long discontinuous fiber mat reinforced polypropylene composites – Status and future trends", *Polymer composites*, Vol. 21, 2000, p. 514-522.

[4]   Tomkinson-Walles GD, "Performance of Random Glass Mat Thermoplastics", *Journal of Thermoplastic composite material,* Vol. 1, 1988, p. 94-106.

[5]   Wakeman MD, Cain TA, Rudd CD, Brooks R and Long AC, "Compression moulding of glass and polypropylene composites for optimised macro and micro mechanical properties II - Glass mat reinforced thermoplastics", *Composites science and technology*, Vol. 59, 1999, p. 709-726.

[6]   Quadrant Plastics, http://www.quadrantplastics.com/

[7]   Azdel Inc., Guide to Azdel Laminate, http://www.azdel.com

[8]   Dweib MA and Bradaigh CMO, "Compression moulding of Glass reinforced thermoplastics: Modelling and experiments", *Polymer composites*, Vol. 21, 2001, p. 832–845.

[9]   Ericson ML and Berglund LA, "Deformation and fracture of glass mat reinforced polypropylene", *Composites science and technology*, Vol. 23, 1992, p. 269-281.

[10]   Quadrant plastic composites AG, Processing guidelines.

[11]   Callister WD, "Materials science and engineering-an introduction", John Wiley & Sons Inc., Toronto, Canada, 1997.

[12]   Findley WN, James SL and Onaran K, "Creep and Relaxation of non linear viscoelastic materials", Dover Publications, Inc., New York, 1976.

[13]   Hopkins IL and Hamming RW, "On creep and relaxation", *Journal of applied physics*, Vol. 25, 1957, p. 906-909

[14]   Schapery RA, "Approximate methods of transform inversion for viscoelastic stress analysis", *Fourth U.S. National congress on Applied Mechanics*, ASME, 1962, p. 1075-1085.

[15]   Knoff WF and Hopkins IL, "An improved numerical interconversion for creep compliance and relaxation modulus", *Journal of applied polymer science*, Vol. 16, 1972, p. 2963-2972.

[16]   Macchetta A and Pavan A, "Testing of viscoelastic function interconversion methods for use in engineering design. II. Formulae to interconvert relaxation modulus and creep compliance", *Plastics, Rubber and composites processing and applications*, Vol. 17, 1992, p. 115-123.

[17]   Mead DW, "Numerical interconversion of linear viscoelastic material functions", *Journal of Rheology*, Vol. 38, 1994, p. 1769-1795.

[18]   Lakes RS and Vanderby R, "Interrelation of creep and relaxation: a modeling approach for ligaments", *Journal of Biomechanical Engineering*, Vol. 121, 1999, p. 612-615.

[19]   Park SW and Schapery RA, "Methods of interconversion between linear viscoelastic material functions. Part I - a numerical method based on Prony series", *International Journal of Solids and Structures*, Vol. 36, 1999, p.1653-1675.

[20]   Schapery RA and Park SW, "Methods of interconversion between linear viscoelastic material functions. Part I – an approximate analytical method", *International Journal of Solids and Structures*, Vol. 36, 1999, p.1677-1699.

[21]   Park SW, "Interconversion between relaxation modulus and creep compliance for viscoelastic solids", *Journal of materials in Civil Engineering*, Vol. 11, 1999, p. 76-82.

[22]   Bradshaw RD and Brinson LC, "A sign control method for fitting and interconverting material functions for linearly viscoelastic solids", *Mechanics of time-dependent materials*, Vol. 1, 1997, p. 85-108.

[23]   Sane SB and Knauss WG, "On interconversion of various Material Functions of PMMA", *Mechanics of time-dependent materials*, Vol. 5, 2001, p. 325-343.

[24]   Lakes RS, "Viscoelastic measurement techniques", *Review of scientific instruments*, Vol. 75, 2004, p. 797-810.

[25]   Schapery RA, "An Engineering theory of non linear viscoelasticity with applications", *International Journal of Solids and Structures*, Vol. 2, 1966, p. 407-425.

[26]   Schapery RA, "On the characterization of nonlinear viscoelastic materials", *Polymer Engineering and Science*, Vol. 9, 1969, p. 295-310

[27]   Howard CM and Holloway L, "The characterization of the non linear viscoelastic properties of randomly oriented fiber/matrix composite", *Composites*, Vol. 18, 1987, p. 317-323.

[28]   Xiao X, "Studies of the viscoelastic behavior of a thermoplastic resin composite", *Composite Science and Technology*, Vol. 34, 1989, p. 163-82.

[29]   Griffith WI, Morris DH and Brinson HF, "The accelerated characterization of Viscoelastic composite materials", VPI & SU Report, VPI-E-80-15, 1980.

[30]   Henriksen M, "Non-linear viscoelastic stress analysis – A finite element approach", *Computers & Structures,* Vol. 18, 1984, p. 133-139.

[31]   Chen T, "Determining the Prony series for a viscoelastic material form time varying strain data", NASA/TM-2000-210123 ARL-TR-2206, 2000.

[32]   Lou YC and Schapery RA, "Viscoelastic Characterization of a Non linear fiber reinforced plastic", *Journal of Composite Materials*, Vol. 5, 1971, p. 208-234.

[33]   Brueller OS, "On the non-linear characterization of the long term behavior of polymeric materials", *Polymer Engineering and Science*, Vol. 27, 1987, p. 144-148.

[34]   Willams ML, Landel RF and Ferry JD, "The temperature dependence of relaxation mechanisms in amorphous polymers and other glass forming liquids, *Journal of American Chemical Society*, Vol. 77, 1955, p. 3701-3707.

[35]   Ward IM and Sweeney J, "An introduction to the mechanical properties of solid polymers", John Wiley & Sons, Ltd, 2004

[36]   Struik LCE, "Physical Aging in Amorphous polymers and other materials", Elsevier, Amsterdam, 1978.

[37]   Struik LCE, "The mechanics and physical aging of semi-crystalline polymers: 1", *Polymer*, Vol. 28, 1987, p. 1521-1533.

[38]   Struik LCE, "The mechanics and physical aging of semi-crystalline polymers: 2", *Polymer*, Vol. 28, 1987, p. 1534-1542.

[39]   Struik LCE, "The mechanics and physical aging of semi-crystalline polymers: 3. Prediction of long term creep from short term tests", *Polymer*, Vol. 30, 1989, p. 799-814.

[40]   Struik LCE, "The mechanics and physical aging of semi-crystalline polymers: 4", *Polymer*, Vol. 30, 1989, p. 814-830.

[41]   Lai J and Bakker A, "Analysis of the non-linear creep of high density polyethylene", *Polymer*, Vol. 36, 1995, p. 93-99.

[42]   Ferry JD and Stratton RA, *Kolloid-Z*, Vol. 171, p. 107.

[43]   Brinson LC and Gates TS, "Effect of physical aging on long term creep of polymers and polymer matrix composites", *International Journal of Solids and Structures*, Vol. 32, 1995, p. 827-846.

[44]   Bradshaw RD and Brinson LC, "Physical aging in polymers and polymer composites: An analysis and method for time-aging time superposition", *Polymer Engineering and Science*, Vol. 37, 1997, p. 31-44.

[45]   Gates TS, Veazie DR and Brinson LC, "Creep and physical aging in a polymeric composite: Comparison of tension and compression", *Journal of Composite Materials*, Vol. 31, 1997, p. 2478-2505.

[46]   Skrypnyk ID, Spoormaker JL, Kandachar P, "A Constitutive Model for Long-Term Behavior of Polymers", Time Dependent and Non-linear Effects in Polymers and Composites, ASTM STP 1357, Schapery R.A and Sun C.T, Eds., American Society for Testing and Materials, West Conshohocken, PA, 2000, p. 70-82.

[47]   Peretz D and Weitsman Y, "The non-linear thermo-viscoelastic characterization of FM-73 adhesive", *Journal of Rheology*, Vol. 26, 1982, p. 245-261.

[48]   Peretz D and Weitsman Y, "The non-linear thermo-viscoelastic characterizations of FM-73 adhesives", *Journal of Rheology*, Vol. 27, 1983, p. 97-114.

[49]   Skrypnyk ID and Spoormaker JL, "Modeling of non linear viscoelastic behavior of plastic materials", 5th European conference on Advanced Materials/Euromat97/, Materials, Functionality and Design, Vol. 4, 1997, p. 491-495.

[50]   Aboudi J, "Micromechanical characterization of the non linear viscoelastic behavior of resin matrix composites", *Composites Science and Technology*, Vol. 38, 1990, p. 371-386.

[51]   Lai J and Bakker A, "A 3-D representation for non linear viscoelasticity and finite element implementation", *Computational Mechanics*, Vol. 18, 1996, p. 182-191.

[52] Tuttle ME, Pasricha A, Emery AF, "The Non-linear Viscoelastic-Viscoplastic behaviour of IM7/5260 Composites Subjected to Cyclic Loading" *Journal of composite materials*, Vol. 29, 1995, p. 2025-2046.

[53] Lai J and Bakker A, "An integral constitutive equation for nonlinear plasto-viscoelastic behaviour of high density polyethylene" *Polymer engineering and science*, Vol. 35, 1995, p. 1339-1347.

[54] Zaoutsos SP, Papanicolaou GC and Cardon AH, "On the non-linear viscoelastic behaviour of polymer matrix composites" *Computer Science and Technology*, Vol. 58, 1998, p. 883-889.

[55] Papanicolaou GC, Zaoutsos, SP and Cardon AH, "Prediction of the non-linear viscoelastic response of unidirectional fiber composites", *Composites Science and Technology*, Vol. 59, 1999, p. 1311-1319.

[56] Megnis M, Varna J, Allen DH, Holmberg A, "Micromechanical Modeling of Viscoelastic response of GMT composite", *Journal of Composite materials*, Vol. 35, 35, 849-882.

[57] Muliana A and Haj-Ali R, "A micromechanical model for the non linear viscoelastic behavior of laminated composites", 16th ASCE Engineering Mechanics Conference, 2003.

[58] Bocchieri RT and Schapery RA, "Time-dependent deformation and damage growth in a rubber-toughened fiber composite", *Mechanics of time dependent materials*, Vol. 8, 2004, p. 137-167.

[59] Zapas LJ and Crissman JM, "Creep and recovery behavior of ultra-high molecular weight polyethylene in the region of small uni-axial deformations", *Polymer*, Vol. 25, 1984, 57-62.

[60] Segard E, Benmedakhene S, Laksimi A and Lai D, "Influence of the fiber-matrix interface on the behaviour of polypropylene reinforced by short glass fibers above glass transition temperature", *Composites science and technology*, Vol. 62, 2002, p. 2029-2036.

[61] Nordin LO and Varna J, "Nonlinear viscoplastic and nonlinear viscoelastic material model for paper fiber composites in compression", *Composites Part A: applied science and manufacturing*, Vol. 37, 2006, p. 344-355.

[62] Marklund E, Varna J and Wallstorm L, "Nonlinear viscoelasticity and viscoplasticity of flax/polypropylene composites", *Journal of Engineering Materials and Technology*, Vol. 128, 2006, p. 527-536.

[63]   Chailleux E and Davies P, "Modeling the non-linear viscoelastic and viscoplastic behaviour of aramid fiber yarns", *Mechanics of time dependent materials*, Vol. 7, 2003, p. 291-303.

[64]   Perzyna P, "Fundamental problems in Viscoplasticity", *Advances in Applied mechanics*, Vol. 9, 1966, p. 243-377.

[65]   Schapery RA, "Non-linear viscoelastic and viscoplastic constitutive equations based on thermodynamics", *Mechanics of time dependent materials*, Vol. 1, 1997, p. 209-240.

[66]   Schapery RA, "Non-linear viscoelastic and viscoplastic constitutive equations with growing damage", *International Journal of Fracture*, Vol. 97, 1999, p. 33-66.

[67]   Megnis M and Varna J, "Non-linear viscoelastic viscoplastic characterization of unidirectional GF/EP Composite", *Mechanics of time dependent materials*, Vol. 7, 2003, p.269-290.

[68]   Karger-Kocsis J, "Swirl mat and long discontinuous fiber mat reinforced polypropylene composites – Status and future trends", *Polymer composites*, Vol. 21, 2000, p. 514-522.

[69]   Cantwell WJ, "The influence of stamping temperature on the properties of a glass mat thermoplastic composite", *Journal of composite materials,* Vol. 30, 1996, p. 1266-1281.

[70]   Wakeman MD, Cain TA, Rudd CD, Brooks R and Long AC, "Compression moulding of glass and polypropylene composites for optimized macro and micro mechanical properties II. Glass mat reinforced thermoplastics", *Composites science and technology*, Vol. 59, 1999, p. 709-726.

[71]   Zhao R, Zhou Z, Dai and Gance, "Effect of the microstructure of GMT on its Mechanical Properties", *Polymer composites*, Vol. 23, 2002, p. 1026-1035.

[72]   Nilsson G, Fernberg SP and Berglund LA, "Strain field in-homogeneities and stiffness changes in GMT containing voids", *Composites: Part A*, Vol. 33, 2002, p. 75-85.

[73]   Trende A, Astrom BT and Nilsson G, "Modeling of residual stress in compression moulded glass mat reinforced thermoplastics", *Composites: Part A*, Vol. 31, 2000, p. 1241-1254.

[74]   Kotsikos G, Bland JH, Gibson AG and Chandler HW, "Squeeze flow testing of glass mat thermoplastic material", *Composites Part A*, Vol. 27, 1996, p. 1195-1200.

209

[75]   Dweib MA and O Bradaigh CM, "Extensional and shearing flow of a glass-mat reinforced thermoplastic (GMT) material as non-Newtonian viscous fluid", *Composites Science and technology*, Vol. 59, 1999, p. 1399-1410.

[76]   Tornqvist R, Sunderland P and Manson JE, "Determination of the rheological properties of thermoplastic composites for compression flow moulding", *Polymer composites*, Vol. 21, 2000, p. 779-788.

[77]   Nilsson G, Ericson ML and Holmberg JA, "Flow induced fiber orientation in compression moulded glass mat thermoplastics", *Polymer composites*, Vol. 21, 2000, p. 1007-1013.

[78]   Lee NJ and Jang J, "The effect of fiber content on the mechanical properties of glass fiber mat/polypropylene composites", *Composites: Part A*, Vol. 30, 1999, p. 815-822.

[79]   Dasappa P, Zhou N and Sullivan PL, "Statistical analyses of Mechanical Property Measurements for two random glass mat reinforced thermoplastics", In: Proceedings of 5th International Canadian Composites conference (CANCOM), 2005.

[80]   Stokes VK, "Random Glass mat reinforced thermoplastic composites. Part I: Phenomenology of Tensile modulus variations", *Polymer composites*, Vol. 11, 1990, p. 32-44.

[81]   Stokes VK, "Random Glass mat reinforced thermoplastic composites. Part II: Analysis of model materials", *Polymer composites*, Vol. 11, 1990, p. 45-55.

[82]   Stokes VK, "Random Glass mat reinforced thermoplastic composites. Part III: Characterization of the tensile modulus", *Polymer composites*, Vol. 11, 1990, p. 342-353.

[83]   Stokes VK, "Random Glass mat reinforced thermoplastic composites. Part IV: Characterization of the tensile strength", *Polymer composites*, Vol. 11, 1990, p. 354-366.

[84]   Bushko WC and Stokes VK, "Random Glass mat reinforced thermoplastic composites. Part V: Statistical Characterization of the Tensile modulus", *Polymer composites,* Vol. 13, 1992, p. 295-308.

[85]   Bushko WC and Stokes VK, "Random Glass mat reinforced thermoplastic composites. Part VI: Methodology for predicting the stiffness of parts", *Polymer composites*, Vol. 13, 1992, p. 309-316.

[86] Bushko WC and Stokes VK, "Random Glass mat reinforced thermoplastic composites. Part VII: A statistical approach to strength", *Polymer composites*, Vol. 15, 1994, p. 359-366.

[87] Varna J and Berglund LA, "Specimen size effects on modulus of GMT and other inhomogeneous composites", *Journal of thermoplastic composite materials*, Vol. 5, 1992, p. 105-113.

[88] Allen DH, Holmberg JA, Ericson ML, Lans L, Svensson N and Holmberg S, "Modeling the viscoelastic response of GMT structural components", *Composites Science and Technology*, Vol. 61, 2001, p. 503-515.

[89] Zocher M A and Groves S E, "A three dimensional finite element formulation for thermo-viscoelastic orthotropic media", *International Journal for Numerical Methods in Engineering*, Vol. 20, 1997, p. 2267-2288.

[90] Wolfrath J, Michaud V and Manson JAE, "Deconsolidation in glass mat thermoplastic composites: Analysis of the mechanisms", *Composites: Part A*, Vol. 36, 2005, p. 1608-1616.

[91] Zampaloni MA, Pourboghrat F and Yu W, "Stamp thermo-hydroforming: A new method for processing fiber reinforced thermoplastic composite sheets", *Journal of Thermoplastic composite materials*, Vol. 17, 2004, p. 31-50.

[92] TA instruments manual for MDSC-2920.

[93] TA instruments manual for DMA-2980.

[94] Menard KP, "Dynamic Mechanical Analysis – A practical introduction", CRC Press, 1999, New York.

[95] Houston D and Hagerman E, "Test procedure to evaluate structural composites subjected to sustained loading", ACCM-T-03, July 2000.

[96] ASTM D2990-01, "Standard test method for tensile, compressive and flexural creep and creep rupture of plastics", *American Society of Testing Materials*, Philadelphia, United States.

[97] ASTM D638-03, "Standard test method for tensile properties of plastics", *American Society of Testing Materials*, Philadelphia, United States.

[98] Zhou. N., "Constitutive modeling of creep in a short fiber random mat GMT Composite", M.A.Sc. thesis, Department of Mechanical and Mechatronics Engineering, University of Waterloo, 2006.

[99]   Lee TH, Boey FYC and Khor KA, "On the determination of polymer crystallinity for a thermoplastic PPS composite by thermal analysis", *Composite science and technology*, Vol. 53, 1995, p. 259-274.

[100]   Mark JE, "Polymer Data handbook", Oxford University Press, 1999, New York.

[101]   Turi AT, "Thermal Characterization of Polymeric Materials", Academic press, 1981, New York.

[102]   Thomas. LC, "The best technique for measuring polymer crystallinity, Modulated DSC", TA instruments.

[103]   ASTM D638-93, "Standard test method for tensile properties of plastics", *American Society of Testing Materials*, Philadelphia, United States.

[104]   Findley WN and Lai JSY, "A modified superposition principle applied to creep of nonlinear viscoelastic material under abrupt changes in state of combined stress", *Transactions of the Society of Rheology*, Vol. 11, 1967, p. 361-380.

[105]   Law A, Lee-Sullivan P and Simon L, "Effects of thermal aging on isotactic polypropylene crystallinity", *Polymer Engineering and Science*, accepted and in press, 2008.

[106]   Law A, Lee-Sullivan P and Simon L, "In-situ observations of micro-damage accumulation during creep in glass mat reinforced polypropylene composites", submitted to *Journal of Composite Materials*, August 2008.

[107]   Law A, "Creep deformation and thermal aging of Random Glass-mat Polypropylene Composite", M.A.Sc. thesis, Department of Mechanical and Mechatronics Engineering, University of Waterloo, 2008.

RESEARCH CONTRIBUTIONS

a. Journal articles:

1. Dasappa P, Lee-Sullivan P, Xiao X and Foss HP, Tensile creep of a long-fiber glass mat thermoplastic (GMT) composite Part II: Viscoelastic-Viscoplastic constitutive modeling, Polymer composites, 2008, Accepted and in press.

2. Dasappa P, Lee-Sullivan P, Xiao X and Foss HP, Tensile Creep of a Long-Fiber Glass Mat Thermoplastic (GMT) Composite Part I: Short-term tests, Polymer composites, 2008, Accepted and in press.

3. Dasappa P, Lee-Sullivan P and Xiao X, Development of viscoplastic strains during creep in continuous fiber GMT composites, to be submitted.

4. Dasappa P, Lee-Sullivan P and Xiao X, Temperature effects on creep behaviour of continuous fiber GMT composites, to be submitted.

5. Dasappa P, Lee-Sullivan P, Cronin D and Xiao X, Modeling effect of temperature on viscoelastic and viscoplastic strains in a continuous fiber GMT composite, in preparation.

b. Conference proceedings:

1. Dasappa P, Zhou N, Lee-Sullivan P, Statistical analyses of Mechanical Property Measurements for two random glass mat reinforced thermoplastics, In: Proceedings of 5th International Canadian Composites conference (CANCOM-2005) 2005.

2. Dasappa P, Lee-Sullivan P, Creep in long-fiber random glass mat thermoplastic composite, In: Proceedings of 6th International Canadian Composites conference (CANCOM-2007) 2007.

3. Dasappa P, Lee-Sullivan P, Xiao X, Foss HP, Non-linear viscoelastic-viscoplastic constitutive modeling of creep in continuous fiber glass mat thermoplastic composites, In: Proceedings of 8th international conference on Durability of Composite systems (DURACOSYS 2008), 2008.

4. Dasappa P, Mui J, Lee-Sullivan P, Xiao X, Foss HP, Comparison of Creep response and damage accumulation between chopped and continuous glass fiber mat thermoplastic composites, In: Proceedings of the American Society for composites 23rd conference (ASC 2008), 2008.

c. **<u>Reports:</u>**

1. Dasappa P and Lee-Sullivan P, Review of Non-linear Viscoelastic constitutive modeling and finite element implementation, May 2005, GM report – CPRJ311196-#2.

2. Dasappa P, Zhou N and Lee-Sullivan P, Report on Creep testing for Quadrant GMT D100 and G100, June 2006, GM report – CPRJ311196-#3.

3. Dasappa P and Lee-Sullivan P, Report on constitutive modeling of Quadrant GMT D100 and G100, December 2006, GM report – CPRJ311196-#4.

4. Dasappa P and Lee-Sullivan P, Non-linear viscoelastic-viscoplastic constitutive modeling of a long fiber GMT composite, October 2007, , GM report – CPRJ311196-#5.

5. Mui J, Dasappa P and Lee-Sullivan P, Report on constitutive model development of quadrant GMT D100, February 2008, GM report – CPRJ311196-#6.

6. Dasappa P, Mui J and Lee-Sullivan, Final report on the constitutive modeling of GMT composites, August 2008, GM report – CPRJ311196-#7.

APPENDIX A
SPECIFICATIONS

A1. Material Data sheet for GMT – G100

QUADRANT
PLASTIC COMPOSITES

Product Data Sheet

G100 F40 F6

G100 F40 F6 is a endless fiber glass mat reinforced PP laminate with randomly oriented glass fibers. This product provides good flow properties and low warpage tendency. It is commonly used for large semi-structural applications, like front-end, backrest.

Properties		Standard	SI Units		Engl. Units	
Physical Properties						
Laminate Thickness*		Internal	3.8	mm	0.150	in
Area Weight*		Internal	4.6	kg/m^2	0.942	lb/ft^2
Fiber Content**		ISO 1172	40	%	40	%
Density (Laminate)*		ISO 1183	1.21	g/cm^3	0.0437	lb/in^3
Density (Molded)**		ISO 1183	1.22	g/cm^3	0.0441	lb/in^3
Mechanical Properties**						
Tensile Strength		ISO 527 / EN 13677	75	MPa	10879	psi
Tensile Elongation at Break		ISO 527 / EN 13677	1.76	%	1.76	%
Tensile Modulus		ISO 527 / EN 13677	5780	MPa	838	ksi
Flexural Strength		ISO 178 / EN 13677	135	MPa	19582	psi
Flexural Modulus		ISO 178 / EN 13677	5775	MPa	838	ksi
Impact Strength -	IZOD (4.0mm)	ISO 180/A	64	kJ/m^2	30	ft*lb/in^2
	IZOD (3.2mm)	ASTM D256 E	650	J/m	12.18	ft*lb(wt)/in
	Charpy (4.0mm)	ISO 179-1/2fn	70	kJ/m^2	33	ft*lb/in^2
Multiaxial Impact (4.0mm)						
Max. Load		ASTM D-3763	3267	N	734	lb(wt)
Energy @ Max. Load			16	J	12	ft*lb
Energy @ Failure			27	J	20	ft*lb
Max. Load		ISO 6603-2	4811	N	1082	lb(wt)
Energy @ Max. Load			19	J	14	ft*lb
Energy @ Failure			43	J	32	ft*lb
Processing Properties**						
Molding Shrinkage		ISO 2577	0.15 - 0.25	%	0.15 - 0.25	%
Special Properties**						
Heat Deflection Temperature		ISO 75-2	155	°C	311	°F
Coefficient of Thermal Expansion		EN ISO 11403-2	25 - 28	10^{-6}/K	25 - 28	10^{-6}/K
Burning Rate		ISO 3795 / FMVSS302	3 - 4	mm/min	0.12-0.16	in/min

1) = measured in longitudinal direction
2) = measured in transverse direction

* = Property was determined on the laminate
** = Property was determined on flat molded plaques

www.quadrantcomposites.com

Lenzburg, 04. August 2004

A2 Load cell specification

Precision Miniature Load Cells

Model 31 and 34

Model 31
(Tension/Compression)

Model 34
(Tension/Compression)

WELDED STAINLESS

RUGGED, SMALL SIZE

TENSION/COMPRESSION

Models 31 and 34, Precision Miniature load cells measure both tension and compression load forces of 50 grams to 10,000 lbs. These models are our highest accuracy, rugged miniature load cells. Model 31's welded, stainless steel construction is designed to eliminate or reduce to a minimum, the effects of off-axis loads. (The internal construction assures excellent long term stability for ranges 1000 grams and above.) A modification permits this model to be completely welded for underwater applications. The Model 31 tension/compression load cell has male threads while the Model 34 tension/compression load cell has female threaded load attachments. High accuracies of 0.15-0.25% full scale are achieved. Each bonded strain gage unit is built of welded 17-4 PH stainless steel for additional ruggedness. All load cells that have ranges ≤10 lbs. have a small electrical zero balance circuit board which is in the lead wire (approximately 1"x .087" thick). This balance board does not have to be the same temperature as the transducer. Applications include cable tension and electromechanical parts testing.

Dimensions

Model 31 (Order Code AL311)

Available Ranges*	T Thread	D"	H"	C"	F"	A"	B"
50; 150; 250 500; gm.	#6-32 UNC	1.00	.75	.25	.11	.50	.38
1000 gm.; 5; 10 lbs.	#6-32 UNC	.75	.45	.25	.05	.31	.19
25; 50; 100 lbs.	#10-32 UNF	1.00	.52	.25	.03	.50	.25
250; 500; 1000 lbs.	1/4-28 UNF	1.00	.52	.38	.03	.50	.25
2000; 3000 lbs.	3/8-24 UNF	1.00	.72	.50	.03	.50	.38
4000; 5000 lbs.	1/2-20 UNF	1.25	.94	.63	.03	.50	.38
7500; 10,000 lbs.	3/4-16 UNF	1.38	1.10	.88	.03	.50	.38

* Stocked ranges are in bold face print.
Notes: Model 31 load cells ≤ 250 grams have overload stops. For custom cells without overload stops consult SENSOTEC.
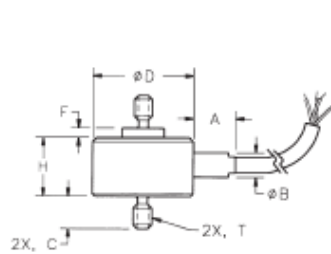
Model 31 Male Threads
(Tension/Compression)
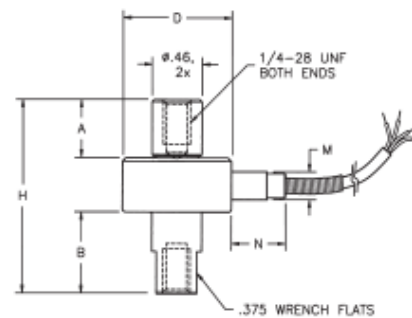
Model 34 Female Threads
(Tension/Compression)

Model 34 (Order Code AL312)

Available Ranges	D"	H"	A"	B"	M"	N"
50; 150; 250; 500 gm.	1.00	1.75	.52	.52	.38	.50
1000 gm.; 5; 10 lbs.	.75	1.75	.60	.72	.19	.31
25; 50; 100 lbs.	1.00	1.75	.52	.72	.25	.50
250; 500; 1000 lbs.	1.00	2.00	.75	.75	.25	.50

217

Options (See Appendix)

Temperature compensated 1b, 1c, 1f; Special calibration 30a, 30b
Premium Options: 1d, 1e, 1g, 1h (≥25 lb), 1i; 6d; 9a (≥5 lb.)
Accessories: Rod end attachments for Model 31

		Model 31 (Male Threads) (Tension/Compression) Order Code AL311	Model 34 (Female Threads) (Tension/Compression) Order Code AL312
PERFORMANCE	Load Ranges...............................	50 gms to 10,000 lbs.	50 gms to 1,000 lbs.
	Non-Linearity/Hysteresis (max)		
	50 gms to 1000 gms	±0.15% F.S.	±0.15% F.S.
	5 to 250 lbs.............................	±0.15% F.S.	±0.15% F.S.
	500 to 10,000 lbs.......................	±0.2% F.S.	±0.2% F.S.
	Non-Repeatability (max)		
	50 gms to 1000 gms	±0.1% F.S.	±0.1% F.S.
	5 to 10,000 lbs...........................	±0.05% F.S.	±0.05% F.S.
	Output (standard)		
	50 to 150 gms (semi)	.1mV/V/gm max	.1mV/V/gm
	250 to 500 gms (semi)	20mV/V	20mV/V
	1000 gms.................................	1.5mV/V (nominal)	1.5mV/V (nom)
	5 lbs. to 10,000 lbs. (foil)..........	2mV/V	2mV/V
	Resolution	Infinite	Infinite
ENVIRONMENTAL	Temperature, Operating...............	-65° F to 250° F	-65° F to 250° F
	Temperature, Compensated	60° F to 160° F	60° F to 160° F
	Temperature Effect		
	– Zero/Span (max)		
	50 gms to 500 gms	.015% F.S./° F	.015% F.S./° F
	1000 gms.................................	.005% F.S./° F	.005% F.S./° F
	5 to 10,000 lbs...........................	.005% F.S./° F	.005% F.S./° F
ELECTRICAL	Strain Gage Type..........................	Foil or Semiconductor	Foil or Semiconductor
	Excitation (Calibration)		
	50 gms to 10 lbs.......................	5.00VDC	5.00VDC
	20 lbs. to 10,000 lbs.................	10.0VDC	10.0VDC
	Insulation Resistance.....................	5000 megohm @ 50VDC	5000 megohm @ 50VDC
	Bridge Resistance		
	50 gms to 500 gms	500 ohm (semi)	500 ohm (semi)
	1000 gms.................................	350 ohm (foil)	350 ohm (foil)
	5 to 10,000 lbs...........................	350 ohm (foil)	350 ohm (foil)
	Shunt Calibration Data	Included	Included
	Wiring Code (std)	#1 (See Pg. AP-8)	#1 (See Pg. AP-8)
	Electrical Termination (std)...........	Teflon cable (5 ft.)	Teflon cable (5 ft.)
MECHANICAL	Overload, Safe	50% over capacity	50% over capacity
	Thread Size..................................	See table	See table
	Deflection – Full Scale	.0005"-.0020"	.0005"-.0020"
	Casing material	17-4 PH Stainless	17-4 PH Stainless
	Weight (nom).................................	1.6 oz.	2.5 oz.
IN-LINE AMPLIFIERS (Optional)	Outputs Available..........................	±5VDC, 4-20mA	±5VDC, 4-20mA

NOTES *Standard calibration for tension/compression load cells is in tension only.

General Information

How to order (See Pg. AP-19)
Load cell selection flow chart (See Pg. LO-1)
Installation Note: Maximum torque for installation of Model 31 in ranges less than 25 lbs. is 12 inch lbs.

A3 Strain gauge specification

Gages for General Stress Measurement

KFG

- ● Gage Factor — Approx. 2.1
- ● Applicable Linear Expansion Coefficients — 5, 11, 16, 23, 27
- ● Self-temperature-compensation Range — 10 to 100°C

Applicable Adhesives and Operating Temperature Ranges

CC-33A: −196 to 120°C
CC-35: −30 to 120°C
EP-34B: −55 to 150°C
PC-6: −196 to 150°C

Grid width
Grid length (Gage length)
Base length
Base width
Gage lead
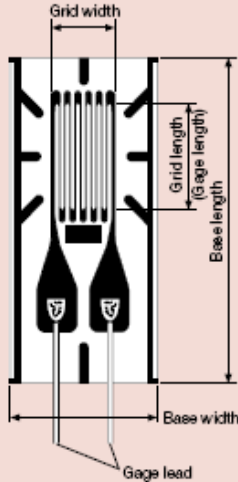
■General-purpose Foil Strain Gages
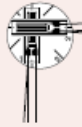
The KFG gages use polyimide resin for the base approximately 13μm thick, ensuring excellent flexibility. Besides indoor measurement, the outstanding moisture resistance lets them effectively perform outdoor measurement. Unless directly exposed to waterdrops, no coating treatment is required.

- ● Various lengths and patterns are available to cope with multiple applications.
- ● Excellent moisture resistance.
- ● The thin gage base provides less resiliency, and thus ensures excellent workability and easy bonding to curved surfaces.
- ● Compensated temperature range is as wide as 10 to 100°C and thermal effect in a range of 20 to 40°C is as small as $\pm 1\mu\varepsilon/°C$.
- ● Strain limit at room temperatures is approximately 5% and fatigue life is 1.2×10^7 times (uniaxial gages), making them suitable for material tests.
- ● The resistance, gage factor and leadwire cable are labeled.
- ● Delivered in an airtight package.
- ● Characteristic values are expressed in accordance with the OIML International Recommendation No. 62.
- ● Immediate delivery is ensured.

■Typical characteristic curve of thermally-induced apparent strain with KFG gage

Thermally-induced apparent strain output (μm/m)

$+1.8\mu\varepsilon/°C$
$+1\mu\varepsilon/°C$
$-1\mu\varepsilon/°C$
$-1.8\mu\varepsilon/°C$

Temp. (°C)

Adhesive: CC-33A

219

Pattern	Leadwire Cable – Type and Shape	Operating Temp. Range	Leadwire Length	Model
KFG-30-120-C1-11 16 23 27	Vinyl-coated flat 3-wire cable L-7 (L-10 for 6m or longer)	−10 to 80°C	1m	KFG-30-120-C1-11 L1M3R
			3m	KFG-30-120-C1-11 L3M3R
			5m	KFG-30-120-C1-11 L5M3R
	Vinyl-coated flat 2-wire cable L-6 (L-9 for 6m or longer)	−10 to 80°C	1m	KFG-30-120-C1-11 L1M2R
			3m	KFG-30-120-C1-11 L3M2R
			5m	KFG-30-120-C1-11 L5M2R
	Middle-temperature 3-wire cable L-12	−100 to 150°C	1m	KFG-30-120-C1-11 R1M3
			3m	KFG-30-120-C1-11 R3M3
			5m	KFG-30-120-C1-11 R5M3
	Middle-temperature 2-wire cable L-11	−100 to 150°C	1m	KFG-30-120-C1-11 R1M2
			3m	KFG-30-120-C1-11 R3M2
			5m	KFG-30-120-C1-11 R5M2
	3 polyester-coated copper wires 30cm 50cm·1m	−196 to 150°C	30cm	KFG-30-120-C1-11 N30C3
			50cm	KFG-30-120-C1-11 N50C3
			1m	KFG-30-120-C1-11 N1M3
Uniaxial	2 polyester-coated copper wires 30cm 50cm·1m	−196 to 150°C	30cm	KFG-30-120-C1-11 N30C2
			50cm	KFG-30-120-C1-11 N50C2
			1m	KFG-30-120-C1-11 N1M2
● Base Size 37 x 5.2 mm / ● Gage Length 30 mm / ● Gage Resistance 120Ω / ● Pieces per Pack 10	Silver-clad copper wires	−196 to 150°C	25mm	KFG-30-120-C1-11

Pattern	Leadwire Cable – Type and Shape	Operating Temp. Range	Leadwire Length	Model
KFG-5-120-D16-11 16 23 27	Vinyl-coated flat 3-wire cable L-7 (L-10 for 6m or longer)	−10 to 80°C	1m	KFG-5-120-D16-11 L1M3S
			3m	KFG-5-120-D16-11 L3M3S
			5m	KFG-5-120-D16-11 L5M3S
	Vinyl-coated flat 2-wire cable L-6 (L-9 for 6m or longer)	−10 to 80°C	1m	KFG-5-120-D16-11 L1M2S
			3m	KFG-5-120-D16-11 L3M2S
			5m	KFG-5-120-D16-11 L5M2S
	Middle-temperature 3-wire cable L-12	−100 to 150°C	1m	KFG-5-120-D16-11 R1M3
			3m	KFG-5-120-D16-11 R3M3
			5m	KFG-5-120-D16-11 R5M3
	Middle-temperature 2-wire cable L-11	−100 to 150°C	1m	KFG-5-120-D16-11 R1M2
			3m	KFG-5-120-D16-11 R3M2
			5m	KFG-5-120-D16-11 R5M2
	3 polyester-coated copper wires 30cm 50cm·1m	−196 to 150°C	30cm	KFG-5-120-D16-11 N30C3
			50cm	KFG-5-120-D16-11 N50C3
			1m	KFG-5-120-D16-11 N1M3
Biaxial, 0°/90° stacked rosette	2 polyester-coated copper wires 30cm 50cm·1m	−196 to 150°C	30cm	KFG-5-120-D16-11 N30C2
			50cm	KFG-5-120-D16-11 N50C2
			1m	KFG-5-120-D16-11 N1M2
● Base Size 11 mmφ / ● Gage Length 5 mm / ● Gage Resistance 120Ω / ● Pieces per Pack 10	Silver-clad copper wires	−196 to 150°C	25mm	KFG-5-120-D16-11

A4 Glue specification

Instruction Bulletin B-137-16
Vishay Micro-Measurements

Strain Gage Applications with M-Bond AE-10, AE-15 and GA-2 Adhesive Systems

GENERAL DESCRIPTION

The three adhesives described in this bulletin, M-Bond AE- 10, AE-15, and GA-2, are all 100%-solids epoxy systems for use with strain gages and special-purpose sensors. The gage installation procedure described is appropriate for each adhesive, the primary differences in the systems being in mixing instructions, pot life, cure cycles, and, to some extent, elongation properties. Each system is effective from the cryogenic region to +200°F [+95°C].

For proper results, the procedures and techniques presented in this bulletin should be used with qualified Vishay Micro-Measurements installation accessory products (refer to Vishay Micro-Measurements Accessories Catalog A-110). Accessories used in this procedure are:

- CSM Degreaser or
- CSP-1 Cotton Applicators
- GC-6 Isopropyl Alcohol
- PCT-2M Gage Installation Tape
- Silicon-Carbide Paper
- MJG-2 Mylar Tape
- M-Prep Conditioner A
- HSC Spring Clamp
- M-Prep Neutralizer 5A
- GT-14 Pads and
- GSP-1 Gauze Sponges
- Backup Plates

Handling Precautions

While these bonding agents are considered relatively safe to handle, contact with skin and inhalation of their vapors should be avoided. Immediate washing with ordinary soap and water is effective in cleansing should skin contact occur. For eye contact, rinse thoroughly with a copious amount of water and consult a physician. For additional health and safety information, consult the material safety data sheet, which is available upon request.

MIXING INSTRUCTIONS AND ADHESIVE CHARACTERISTICS

A. General

1. Each kit contains materials for mixing six batches of adhesive.

2. Any resin removed from refrigeration must be allowed attain room-temperature equilibrium before being opened.

3. Mix adhesives thoroughly for five minutes according to instructions. If a room-temperature cure is used, allow the freshly mixed adhesive to stand an additional five minutes before use.

4. The pot life for Systems AE-10 and GA-2 can be prolonged by occasionally stirring to prevent localized exotherm in the center of the resin system, or by pouring it out onto a chemically clean metal plate.

Note: During storage, crystals may form in the Resin AE. These crystals do not affect adhesive performance, but should be reliquefied prior to mixing by warming the resin jar to +120°F [+50°C] for approximately one-half hour. Allow the resin to return to room temperature before adding curing agent; excess heat will shorten mixed pot life.

B. M-Bond AE-10 Adhesive Kit

AE-10 will cure at +70°F [+20°C] in 6 hours, with approximately 6% elongation capability and essentially creep-free performance. Elongation capability of approximately 10% can be obtained by extending the cure time to 24 to 48 hours at +75°F [+24°C].* To mix, fill one of the calibrated droppers with Curing Agent 10 exactly to the number 10 and dispense the contents into the center of the jar of Resin AE. Immediately cap the bottle of Curing Agent 10 to avoid moisture absorption. Mix thoroughly for 5 minutes, using one of the plastic stirring rods. The pot life or working time after mixing is 15 to 20 minutes. Discard the dropper after use.

*Refer to Application Notes B-129 and TT-605 for discussions of high-elongation strain measurements.

APPENDIX B

PART DRAWINGS

B1 Cam attachment Drawings

B1.1 Holding Bar
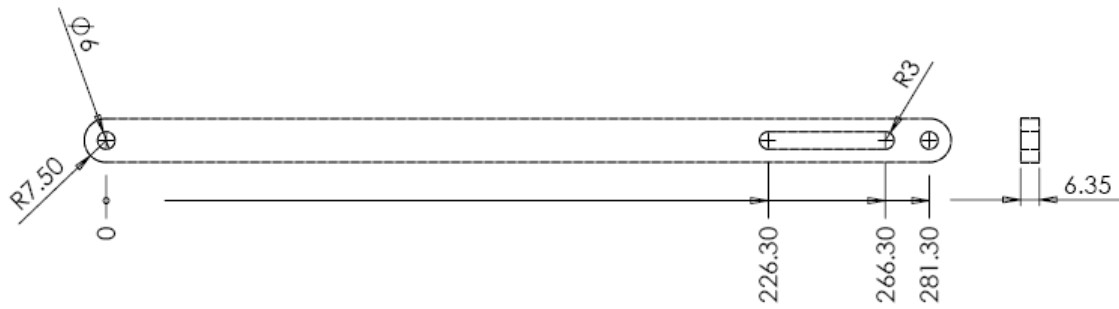
B1.2 Cam and handle
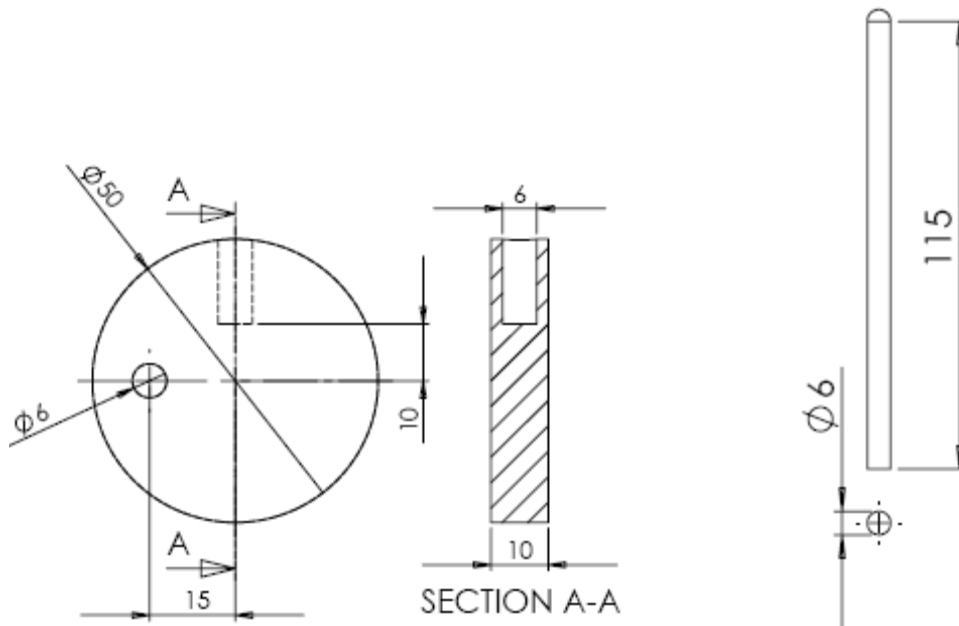
B2 Load cell Attachment

B2.1 Load cell attachment assembly
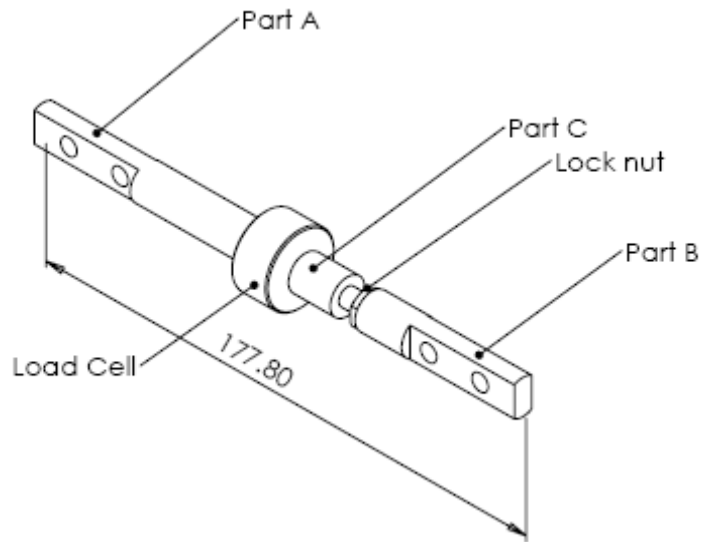
B2.2 Part A - Load cell attachment
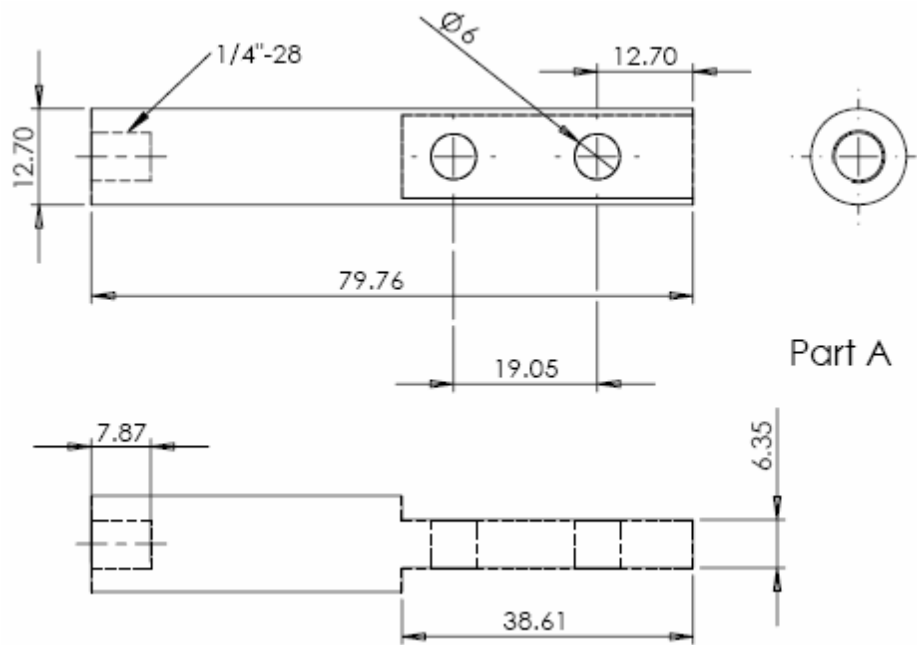
B2.3 Part B - Load cell attachment
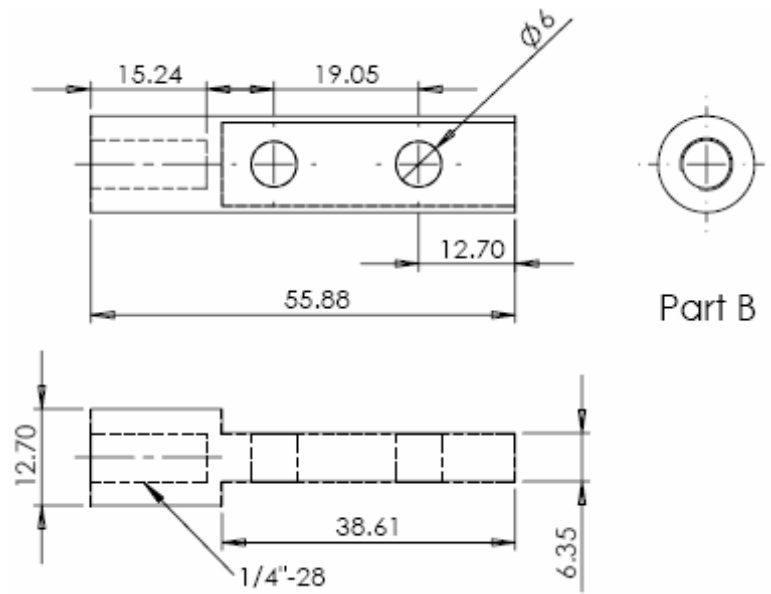
B2.4 Part C - Load cell attachment

224
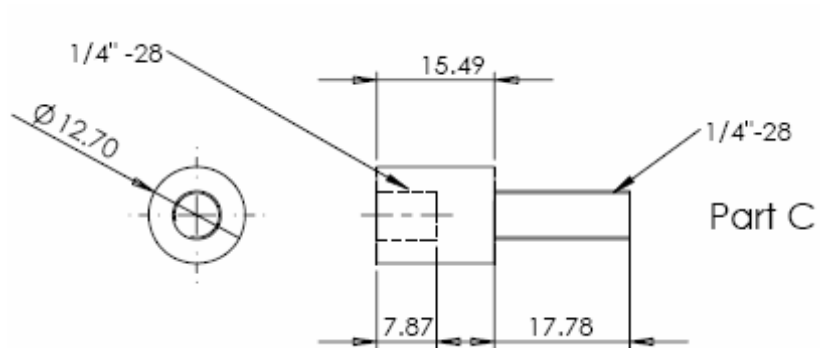
APPENDIX C

REVIEW OF STATISTICAL TERMS

C1 Some definitions

The three basic terms used in statistics are mean, variance and standard deviation which are given below.

a. Mean: It is a measure of the centrality of a data set. It is obtained by dividing the sum of all the samples by the number of samples. It is given by

$$\text{Mean, } \bar{y} = \frac{\sum_{i=1}^{n} y_i}{n}$$

b. Variance: It is a measure of the dispersion of a sample and is given by,

$$\text{Variance, } S^2 = \frac{\sum_{i=1}^{n} (y_i - \bar{y})^2}{n-1}$$

c. Standard deviation: It is measure of the spread of the sample. It is given by the square root of the variance.

d. Percentage relative standard deviation (%RSD): It is often considered as a measure of the variability in the data and is given by.

$$\% \, Relative \, Standard \, Deviation \, (\%RSD) = \frac{Standard \, Deviation}{Mean} \times 100$$

C2 Statistical Hypothesis

Two models which are commonly used to describe the results of an experiment are the means model and the fixed effects model which are given as follows.

Means model: $y_{ij} = \mu_i + \varepsilon_{ij}$

where, μ_i = mean of the factor level 'i'

ε_{ij} = Random error

Effects model: $y_{ij} = \mu + \tau_i + \varepsilon_{ij}$; where, $\mu = \mu_i - \tau_i$

where, μ is the overall mean

τ_i is the ith treatment effect

A statistical hypothesis is a statement about the parameters about a statistical model. The statement that the means at different levels are equal is called the null hypotheses (H_0) and the statement that the means are different is called the alternative hypotheses (H_1).

$H_0 : \mu_1 = \mu_2$
$H_1 : \mu_1 \neq \mu_2$

The hypothesis is usually tested at a particular level of significance (α) using a test statistic (t test, F test). Further, the p-value, which is the smallest level of significance at which the null hypotheses can be rejected, is often used to make statistical inferences.

C3 Analysis of Variance (ANOVA)

Consider a process (or experiment) which depends on a parameter 'X' with 'a' levels. Let y_{ij} be the output of the process from each of the 'n' tests carried out at each of the 'a' levels. If the means model is considered then the following hypotheses will be tested

$H_0 : \mu_1 = \mu_2 \ldots = \mu_a$

$H_1 : \mu_i \neq \mu_j$ for at least one pair

Further we have,

Mean at each level is given by $\bar{y}_{i.} = \dfrac{\sum\limits_{j=1}^{n} y_{ij}}{n}$

Overall mean is given by $\bar{y}_{..} = \dfrac{\sum\limits_{i=1}^{a}\sum\limits_{j=1}^{n} y_{ij}}{n \times a}$

Variance, $S^2 = \dfrac{\sum\limits_{i=1}^{a}\sum\limits_{j=1}^{n}(y_{ij} - \bar{y}_{..})^2}{na - 1} = \dfrac{SS_T}{n - 1}$

It can be shown that the sum of squares total (SS_T) can be expressed as the sum of two terms, the sum of squares treatments ($SS_{Treatments}$) and sum of squares error (SS_{Error}) with

$$SS_{Treatments} = n\sum_{i=1}^{a}(\bar{y}_{i.} - \bar{y}_{..})^2 \text{ and } SS_{Error} = \sum_{i=1}^{a}\sum_{j=1}^{n}(y_{ij} - \bar{y}_{i.})^2$$

Then the hypotheses can be tested by using the test statistic, F_0 which is given by,

$$F_0 = \frac{SS_{Treatments}/(a-1)}{SS_{Error}/a(n-1)}$$

If $F_0 > F_{\alpha, a-1, a(n-1)}$, then the null hypothesis can be rejected and it can be concluded that the there are differences in the means at the various levels.

Statistical softwares can be used to obtain F_0. The software also computes the p-value which can be used to draw inferences about the null hypotheses.

The assumption that the errors are normally and independently distributed (with $\mu = 0$ and constant variance, σ^2) have to be tested to determine the validity of the inferences drawn after ANOVA. The normality assumption can be checked by plotting the residuals on a normal probability plot. If the points lie along a straight line then the normality assumption is satisfied. Further, a plot of residuals vs. the fitted values has to be observed. If the points in this plot are randomly distributed, then the assumptions are correct. The residuals (at each level) mentioned above, can be obtained by the difference of the experimental and the estimated values.

APPENDIX D

STATISTICAL ANALYSIS (ANOVA)

The results of the statistical analysis (ANOVA) on the tensile and creep test data has been provided here. Analysis has been carried out using MINITAB®, a commercial statistical software. Inferences for all the tests are given at 95% level of significance (p-value = 0.05).

D1 Tensile tests

D1.1 Effect of location and plaque

ANOVA of Young's modulus and tensile strength obtained at various locations within a test plaque from 5 plaques for the 3- and 6-mm thick GMT composites are given below. Three locations (top, middle and bottom) shown in Figure 4.20 (b) were considered for the 3-mm thick GMT while only two locations (top and bottom) as shown in Figure 4.20 (c) has been considered for the 6-mm thick GMT.

3-mm thick GMT

The p-values for both Young's modulus and tensile strength are greater than 0.05 indicating no significant variation in the mean property values with both location and test plaque.

a. Young's Modulus

```
Factor      Type    Levels  Values
Location    fixed        3  Bot, Mid, Top
plaque      fixed        5  1, 2, 3, 4, 5

Analysis of Variance for modulus, using Adjusted SS for Tests

Source    DF   Seq SS   Adj SS   Adj MS     F      P
Location   2   784696   647464   323732  2.85  0.124
plaque     4   320515   320515    80129  0.71  0.613
Error      7   794920   794920   113560
Total     13  1900132
```

228

b. Tensile strength

```
Factor    Type   Levels  Values
Location  fixed       3  Bot, Mid, Top
plaque    fixed       5  1, 2, 3, 4, 5


Analysis of Variance for Tensile strength, using Adjusted SS for Tests

Source    DF  Seq SS  Adj SS  Adj MS     F       P
Location   2     3.8     9.3     4.7  0.04   0.960
plaque     4   404.3   404.3   101.1  0.89   0.515
Error      7   791.7   791.7   113.1
Total     13  1199.8
```

6-mm thick GMT

The p-values for both Young's modulus and tensile strength for the 6-mm thick GMT are greater than 0.05 indicating no significant variation in the mean tensile property values with both location and plaque. However, the p-value obtained from ANOVA of modulus is very close to 0.05 for location. It is to be noted that only two locations were considered for the 6-mm thick GMT.

a. Young's Modulus

```
Factor    Type   Levels  Values
Location  fixed       2  Bot, Top
Plaque    fixed       5  1, 2, 3, 4, 5


Analysis of Variance for Modulus, using Adjusted SS for Tests

Source    DF   Seq SS    Adj SS   Adj MS     F      P
Location   1  1527309  1527309  1527309  6.83  0.059
Plaque     4  1015877  1015877   253969  1.14  0.452
Error      4   894164   894164   223541
Total      9  3437350
```

b. Tensile strength

```
Factor    Type   Levels  Values
Location  fixed       2  Bot, Top
Plaque    fixed       5  1, 2, 3, 4, 5


Analysis of Variance for Tensile strength, using Adjusted SS for Tests

Source    DF  Seq SS  Adj SS  Adj MS     F      P
Location   1   131.8   131.8   131.8  1.03  0.368
Plaque     4   124.0   124.0    31.0  0.24  0.901
Error      4   512.4   512.4   128.1
Total      9   768.2
```

D1.2 Effect of Orientation

The results of ANOVA of Young's modulus and tensile strength from tensile tests of specimens machined in three directions – 0, 45 and 90° as shown in Figure 4.20 (a) are given below.

3-mm thick GMT

The p-values for both Young's Modulus and tensile strength are less than 0.05 indicating that the tensile properties in 3-mm thick GMT are dependent on direction.

a. Young's Modulus

```
Factor   Type    Levels  Values
Angle    fixed        3  0, 45, 90

Analysis of Variance for Modulus, using Adjusted SS for Tests

Source  DF    Seq SS     Adj SS    Adj MS     F       P
Angle    2   4078610    4078610   2039305   4.57   0.021
Error   23  10254378   10254378    445843
Total   25  14332988
```

b. Tensile strength

```
Factor   Type    Levels  Values
Angle    fixed        3  0, 45, 90

Analysis of Variance for Tensile strength, using Adjusted SS for Tests

Source  DF  Seq SS  Adj SS  Adj MS     F       P
Angle    2  1405.1  1405.1   702.6   6.47   0.006
Error   23  2496.6  2496.6   108.5
Total   25  3901.7
```

6-mm thick GMT

The p-value for Young's modulus with specimen orientation (angle) is less than 0.05 which shows that the Young's modulus is dependent on direction. However, the p-value obtained from ANOVA of tensile strength with specimen angle is greater than 0.05 indicating that tensile strength is independent of direction for the 6-mm thick GMT.

a. Young's Modulus

```
Factor  Type   Levels  Values
Angle   fixed       3  0, 45, 90


Analysis of Variance for Modulus, using Adjusted SS for Tests

Source  DF    Seq SS   Adj SS   Adj MS     F       P
Angle    2   3996320  3996320  1998160  5.44   0.013
Error   21   7720427  7720427   367639
Total   23  11716747
```

b. Tensile strength

```
Factor  Type   Levels  Values
Angle   fixed       3  0, 45, 90


Analysis of Variance for Tensile strength, using Adjusted SS for Tests

Source  DF    Seq SS   Adj SS   Adj MS     F       P
Angle    2    295.33   295.33   147.66  1.50   0.247
Error   21   2071.75  2071.75    98.65
Total   23   2367.08
```

D2 Creep tests

The results of ANOVA of compliance with stress and temperature extracted from the short and long term creep tests are given below.

D2.1 Short term creep tests: Stress (Section 5.2)

3-mm thick GMT

ANOVA of compliance after 30 minutes of creep obtained from short term tests at the various stress levels have been carried out. The tests were replicated 6 times. Test data at lower stress level (5 and 10 MPa) has not been included due to noise in the data (caused by fixture rigidity). The p-value obtained from ANOVA was lower than 0.05 indicating dependence of compliance on stress and hence non-linear viscoelastic behaviour with stress. Further, to determine the linear viscoelastic stress range, the ANOVA of compliance below 20 MPa has been carried out. A p-value of 0.744 which is greater than 0.05 has been obtained indicating equal compliances at stresses below 20 MPa for the 3-mm thick GMT. Hence, the 3-mm thick GMT is linear viscoelastic up to 20 MPa.

231

a. All stresses

```
Factor  Type   Levels
Stress  fixed     12

Factor  Values
Stress  12.5, 15.0, 17.5, 20.0, 22.5, 25.0, 30.0, 35.0, 40.0, 45.0, 50.0, 60.0

Analysis of Variance for End of creep Compliance

Source  DF        SS       MS      F      P
Stress  11    6238.49   567.14   7.19  0.000
Error   60    4733.22    78.89
Total   71   10971.71
```

b. Stresses below 20 MPa

```
Factor  Type   Levels  Values
Stress  fixed      4   12.5, 15.0, 17.5, 20.0

Analysis of Variance for End of creep Compliance

Source  DF        SS      MS      F      P
Stress   3     110.63   36.88   0.42  0.744
Error   20    1774.91   88.75
Total   23    1885.54
```

6-mm thick GMT

The p-value obtained from ANOVA was lower than 0.05 indicating dependence of compliance on stress for the 6-mm thick GMT as well. Further, to determine the linear viscoelastic region, the ANOVA of compliance at stresses below 25 MPa has been carried out. A p-value very close to 1 has been obtained indicating equal compliances at stresses below 25 MPa. Hence the 6-mm thick GMT is linear viscoelastic up to 25 MPa.

a. All stresses

```
Factor  Type   Levels  Values
Stress  fixed      9   15.0, 17.0, 18.0, 19.0, 20.0, 22.5, 25.0, 30.0, 40.0

Analysis of Variance for End of creep Compliance

Source  DF        SS      MS      F      P
Stress   8     796.62   99.58   2.18  0.048
Error   45    2058.82   45.75
Total   53    2855.44
```

b. *Stresses below 25 MPa*

```
Factor  Type   Levels  Values
Stress  fixed       7  15.0, 17.0, 18.0, 19.0, 20.0, 22.5, 25.0

Analysis of Variance for End of creep Compliance

Source  DF        SS     MS     F      P
Stress   6      5.53   0.92   0.03  1.000
Error   35   1179.15  33.69
Total   41   1184.67
```

D2.2 Short term creep tests: Temperature (Section 6.2)

ANOVA of the compliance obtained from short term creep tests over the 14 temperature levels at each of the 4 stresses have been carried out to determine the effect of stress and temperature. Although tests at 60 MPa have been carried out, the data has not been included in the analysis since only one trial has been carried out at this stress level. Compliance obtained at 2 time durations – Instantaneous and that after 30 minutes creep have been considered for the statistical analysis. The p-values obtained from ANOVA are very close to 0 (<0.05) indicating dependence of compliance on both stress and temperature. This shows that the 3-mm thick GMT composite is non-linear viscoelastic with both stress and temperature based on the short term creep test data.

a. *Instantaneous compliance*

```
Factor       Type   Levels  Values
Stress       fixed       4  20, 30, 40, 50
Temperature  fixed      14  25, 30, 35, 40, 45, 50, 55, 60, 65, 70, 75, 80, 85,
                            90

Analysis of Variance for Instantaneous Compliance, using Adjusted SS for Tests

Source        DF    Seq SS   Adj SS   Adj MS     F      P
Stress         3    7459.6   7459.6   2486.5  20.91  0.000
Temperature   13    7884.3   7884.3    606.5   5.10  0.000
Error        151   17959.3  17959.3    118.9
Total        167   33303.2
```

b. Compliance after 30 minutes creep

```
Factor        Type    Levels  Values
Stress        fixed        4  20, 30, 40, 50
Temperature   fixed       14  25, 30, 35, 40, 45, 50, 55, 60, 65, 70, 75, 80, 85,
                             90


Analysis of Variance for End of creep Compliance, using Adjusted SS for Tests

Source         DF    Seq SS   Adj SS  Adj MS      F       P
Stress          3   11505.7  11505.7  3835.2  25.79   0.000
Temperature    13    6539.4   6539.4   503.0   3.38   0.000
Error         151   22454.0  22454.0   148.7
Total         167   40499.1
```

D2.3 Long term tests: Stress (Section 5.3)

ANOVA of the compliance obtained from 1 day creep tests at the 6 stress levels tested have been carried out to determine the effect of stress. Compliance obtained at 2 time durations – Instantaneous (D_0) and that after 1 day creep have been considered for the statistical analysis. p-values obtained from the statistical analysis are less than 0.05 indicating strong dependence of compliance on stress. This shows that the 3-mm thick GMT composite is non-linear viscoelastic with stress from the long term creep test data.

a. Instantaneous compliance

```
Factor  Type   Levels  Values
Stress  fixed       6  20, 30, 40, 50, 60, 70


Analysis of Variance for Instantaneous Compliance

Source  DF       SS      MS     F       P
Stress   5  1986.22  397.24  5.50   0.003
Error   18  1301.08   72.28
Total   23  3287.30
```

b. Compliance after 1 day creep

```
Factor  Type   Levels  Values
Stress  fixed       6  20, 30, 40, 50, 60, 70


Analysis of Variance for End of creep Compliance

Source  DF      SS     MS     F      P
Stress   5  3855.5  771.1  5.97   0.002
Error   18  2323.7  129.1
Total   23  6179.2
```

D2.4 Long term tests: Temperature (Section 6.3)

The results of ANOVA of the compliance extracted from 1 day creep test results at the 5 stress levels: 20, 30, 50, 60 and 70 MPa obtained at 3 temperatures: 40, 60 and 80°C are given below. Compliance obtained at 2 time durations – Instantaneous and that after 1 day creep have been considered for the statistical analysis. The p-values obtained from the statistical analysis in all the cases are less than 0.05 which indicates dependence of compliance on stress at all three temperatures. This shows that the 3-mm thick GMT composite is non-linear viscoelastic with stress at the three temperatures considered.

D2.4.1 Effect of stress at 40 °C

a. Instantaneous compliance

```
Factor  Type   Levels  Values
Stress  fixed      5   20, 30, 50, 60, 70

Analysis of Variance for Instantaneous Compliance

Source  DF     SS      MS      F     P
Stress   4   4466.8  1116.7  9.95  0.002
Error    9   1010.4   112.3
Total   13   5477.2
```

b. *Compliance after 1 day creep*

```
Factor  Type   Levels  Values
Stress  fixed      5   20, 30, 50, 60, 70

Analysis of Variance for End of creep Compliance

Source  DF     SS      MS      F     P
Stress   4   6735.5  1683.9  9.20  0.003
Error    9   1646.6   183.0
Total   13   8382.2
```

D2.4.2 Effect of stress at 60 °C

a. Instantaneous compliance

```
Factor  Type   Levels  Values
Stress  fixed      5   20, 30, 50, 60, 70

Analysis of Variance for End of creep Compliance

Source  DF     SS      MS      F     P
Stress   4   6735.5  1683.9  9.20  0.003
Error    9   1646.6   183.0
Total   13   8382.2
```

b. Compliance after 1 day creep

```
Factor  Type   Levels  Values
Stress  fixed       5  20, 30, 50, 60, 70

Analysis of Variance for End of creep Compliance

Source  DF       SS      MS      F      P
Stress   4   8563.4  2140.9   6.93  0.008
Error    9   2779.3   308.8
Total   13  11342.7
```

D2.4.3 Effect of stress at 80 °C

a. Instantaneous compliance

```
Factor  Type   Levels  Values
Stress  fixed       4  20, 30, 50, 60

Analysis of Variance for End of creep Compliance

Source  DF     SS     MS      F      P
Stress   3  50610  16870   8.29  0.008
Error    8  16279   2035
Total   11  66889
```

b. Compliance after 1 day creep

```
Factor  Type   Levels  Values
Stress  fixed       4  20, 30, 50, 60

Analysis of Variance for Instantaneous Compliance

Source  DF     SS      MS      F      P
Stress   3  7072.1  2357.4   9.69  0.005
Error    8  1946.0   243.3
Total   11  9018.1
```

D2.5 Effect of stress and temperature (Sections 5.3 and 6.3)

ANOVA of the compliance obtained from the 1 day creep tests at the 5 stress levels: 20, 30, 50, 60 and 70 MPa and 4 temperature levels: 25, 40, 60 and 80°C have been carried out. Compliance obtained at 2 time durations – Instantaneous and that after 1 day creep have been considered for the statistical analysis. The p-values obtained from the statistical analysis in all the cases are less than 0.05 indicating dependence of compliance on stress and temperature at all three temperatures. This shows that the 3-mm thick GMT composite is non-linear viscoelastic with both stress and temperature over the respective ranges considered.

a. *Instantaneous compliance*

```
Factor        Type    Levels  Values
Stress        fixed        5  20, 30, 50, 60, 70
Temperature   fixed        4  25, 40, 60, 80


Analysis of Variance for Instantaneous Compliance, using Adjusted SS for Tests

Source        DF    Seq SS   Adj SS  Adj MS      F      P
Stress         4   10937.1  14958.9  3739.7  24.21  0.000
Temperature    3   17797.0  17797.0  5932.3  38.41  0.000
Error         52    8031.5   8031.5   154.5
Total         59   36765.6
```

b. *Compliance after 1 day creep*

```
Factor        Type    Levels  Values
Stress        fixed        5  20, 30, 50, 60, 70
Temperature   fixed        4  25, 40, 60, 80


Analysis of Variance for End of creep Compliance, using Adjusted SS for Tests

Source        DF   Seq SS  Adj SS  Adj MS      F      P
Stress         4    32919   44158   11039  12.08  0.000
Temperature    3    41023   41023   13674  14.96  0.000
Error         52    47527   47527     914
Total         59   121469
```